Methodologies for Obtaining Reliable Indicators for the Environmental Stress Cracking Resistance of Polyethylene

by

Amirpouyan Sardashti

A thesis
presented to the University of Waterloo
in fulfillment of the
thesis requirement for the degree of
Doctor of Philosophy
in
Chemical Engineering

Waterloo, Ontario, Canada, 2014

AUTHOR'S DECLARATION

I hereby declare that I am the sole author of this thesis. This is a true copy of the thesis, including any required final revisions, as accepted by my examiners.

I understand that my thesis may be made electronically available to the public.

ABSTRACT

Environmental stress cracking (ESC) is one of the main, and probably the most common, failure mechanisms involved in polymer fractures. This type of failure is critically important as it occurs suddenly, without any visible pre-fracture deformation. Such failure can be catastrophic and costly in cases where structural integrity is required. In polyethylene (PE), ESC occurs through a slow crack growth mechanism. Cracks initiate from stress-concentrated imperfections, propagate through the bulk of PE, and ultimately result in a brittle fracture. In order to predict the environmental stress cracking resistance (ESCR) of PE, it is necessary to fully understand the molecular structure of the resin. In this thesis, attempts were made to find relationships between molecular structure characteristics and material responses, mainly inter-lamellar entanglements and strain hardening behaviour of PE resins, through mechanical and rheological experiments. Inter-lamellar entanglements are believed to be the main factor controlling slow crack growth of PE. Extent of entanglements and entanglement efficiency were investigated by monitoring the strain hardening behaviour of PE resins in the solid state through a uniaxial tensile test, and in the melt state, through extensional rheometry.

ESCR is usually assessed by unreliable and time consuming testing methods such as the notch constant load test (NCLT) on notched PE specimens in the presence of an aggressive fluid and elevated temperatures. In this thesis, a practical, yet reliable, tensile test was developed for the evaluation and prediction of ESCR. The developed test offers a more reliable and consistent ESCR picture without the drawbacks of the subjective notching process and presence of aggressive fluids. Through this test, a factor called “corrected

hardening stiffness (cHS)" was developed, which can easily be used for a relative ranking of ESCR of different PE resins.

Studies were next extended to the melt state via shear and extensional rheometry. Through studies in the shear mode, a molecular weight-normalized average characteristic relaxation time (λ_N) was found to be efficient in predicting the extent of chain entanglements in resins. This provided a potential melt indicator for a relative measure of ESCR, for linear low density polyethylene (LLDPE), with different short chain branching levels. Extensional studies were conducted to evaluate the strain hardening behaviour in the melt state. An inverse correlation was obtained between ESCR and the melt strain hardening coefficient (MSHC), found from Sentmanat Extensional Rheometry (SER). This indicated an inverse relationship between ESCR and chain extensibility in the melt. In addition, a new factor called "melt hardening stiffness (mHS)" was developed from the slope of a stress-strain line, obtained from SER. This factor, analogous to cHS, can be used for a practical and reliable ranking of ESCR of PEs.

ESCR is usually associated with classical crystalline phase property indicators, such as crystallinity and lamella thickness. In this thesis, the effect of processing and post processing temperature on the extent of inter-lamellar entanglements were investigated, evaluated, and correlated to ESCR. Also, analysis of the lamella surface area (LSA) was pursued since LSA reflects changes in phase interconnectivity more precisely. The focus of this part of the study was on the effect of temperature on LSA to identify the optimum processing and post-processing conditions which yield a higher LSA. It was reasonable to presume that PE with larger lamella lateral surface areas will have more inter-lamellar entanglements, hence higher ESCR.

Finally, a well-controlled ultraviolet (UV) photoinitiated reactive extrusion (REX) process was developed for selective formation of long chain branches in the PE structure. This was conducted to impose restrictions against stretching of the polymer chain, which consequently enhanced ESCR.

ACKNOWLEDGEMENTS

I would like to express my sincere thanks and appreciation to my supervisor and mentor, Professor Alexander Penlidis, for his invaluable guidance and encouragement throughout the research, and also towards other aspects of my life. It was his involvement and instructions, through optimism and looking beyond the present, which made this research project possible.

I would also like to express my deepest gratitude to my co-supervisor, Professor Costas Tzoganakis, for all the insightful suggestions and guidance.

I wish to thank Professor Maria A. Polak, Department of Civil and Environmental Engineering, University of Waterloo, for all the instructive input and collaboration towards this project. I also like to thank Professor Martin Zatloukal, Polymer Centre, Faculty of Technology, Tomas Bata University in Zlin, Czech Republic, for considerable help with the rheological experiments.

I wish to gratefully acknowledge financial support from the Natural Sciences and Engineering Research Council (NSERC) of Canada, and the Canada Research Chair (CRC) program. Many thanks go to ExxonMobil Chemical Canada, Sarnia, ON Canada, for financial support and for providing resins for the study over many years. I would also like to thank the Borealis group, Linz, Austria, for providing additional resins.

Many thanks go to all my friends and coworkers in Waterloo for their invaluable friendship. I will always remember our many great adventures and fond memories.

Lastly, and most importantly, I would like to thank my parents, Mohammad Reza and Soudabeh Sardashti. Without their unconditional love, presence, and support, I would never be the person I am today.

TO MY PARENTS

MOHAMMAD REZA AND SOUDABEH

TABLE OF CONTENTS

LIST OF FIGURES

LIST OF TABLES

1 CHAPTER 1: INTRODUCTION AND OBJECTIVES

1.1 MOTIVATION AND OBJECTIVES

Brittle fractures are among the most common fracture mechanisms involved in plastic failure. This type of failure can be catastrophic and costly, specifically where structural integrity and long-term mechanical stability are important. In plastics, brittle fracture is mainly considered for amorphous (glassy) polymers. However, semi-crystalline polymers such as polyethylene (PE), with a relatively ordered and compact crystalline structure, can also exhibit a brittle fracture. A common type of brittle fracture in PE, known as Environmental Stress Cracking (ESC), occurs when PE is subjected to a low sustained mechanical stress. This type of fracture can be accelerated if PE is subjected to a chemical environment. The prolonged synergistic effect of a mechanical stress and a chemical component that can diffuse through a polymer, results in creep of the PE, where polymer chains deform by molecular disentanglement (1). For example, high density polyethylene (HDPE) pipe resins, for underground applications, predominantly fail by ESC due to the coexistence of the aforementioned stress and environmental conditions (2).

ESC in polyethylene takes place through a Slow Crack Growth (SCG) mechanism (3). In this mechanism, molecular deformation starts from existing microscopic inhomogeneities, introduced during production, processing, and installation of PE. The molecular deformation during SCG of PE includes craze initiation and propagation. This mechanism can be preceded by chemical diffusion and local plasticization of the inhomogeneous areas, if PE is subjected to an aggressive chemical environment. The collapse of crazes ultimately

introduces a crack surface, which then joins other microscopic crack surfaces, and causes a brittle failure.

ESC of PE is dependent mainly on three factors: molecular properties of the polymer, environmental conditions where it is exposed to, and type of applied stress. In general, PEs with high molecular weights (MW) and high short chain branching (SCB) contents are believed to have better Environmental Stress Cracking Resistance (ESCR). MW and short branches (both in content and length) can directly change the extent of formation of tie-molecules, which are considered to be the main property controlling ESCR. Tie-molecules are long PE chains anchored in two separate lamellae with their mid-section in the amorphous region. It has been shown that the rate of stress cracking can significantly be reduced with increasing the density of tie-molecules. Studies have been performed to indirectly estimate the tie-molecule density and its relationship with MW and SCB content (4-8).

Other molecular properties such as molecular weight distribution (MWD) and SCB distribution, can also affect ESCR of PE resins. Different production techniques including use of multiple reactors (cascade reactors in series), combination of catalysts, and co-immobilization of different catalysts on a single support, have been developed to create PEs with bi- or multimodal molecular weight distributions (9). Addition of co-monomers at different stages of these processes can further change the content and the distribution of short branches in PE's molecular structure. In general, in order to increase ESCR in PEs, bimodal structures comprising of a low molecular weight homo-polymer and a high molecular weight copolymer, with short branches distributed in the higher end of the molecular weight spectrum, are required. Environmental conditions can also change the ESCR of PEs. A low

molecular weight fluid (chemical environment) with moderate levels of hydrogen bonding is believed to be a more aggressive candidate for ESC in PEs. It should be noted that ESC in PE can only occur if the applied stress can orient chains to directions leading to molecular disentanglement (1).

In the recent literature, research on ESCR of PE resins has been limited to finding relationships between molecular structure (with a focus on MW and SCB content) and degree of tie-molecule formation. Most of these studies have been performed based on a single factor analysis, thus ignoring the possibility of the effect of interactions between molecular structure and ESCR. Moreover, these studies have been carried out in a relatively narrow property range. In a recent study, Cheng et al. (10) looked into the contribution of the inter-lamellar chain entanglements to ESCR, and found that PEs with a greater extent of physical chain entanglements have higher ESCR. The authors also studied the combined effects of MW and SCB content on ESCR. Then, they developed a uniaxial tensile test and found that the slope of the strain hardening line of a stress- strain curve can be used as a relative measure of ESCR.

This thesis aims to investigate and identify molecular properties which control the ESCR of PE resins. This work is a collaborative effort between the disciplines of Chemical and Civil engineering to study the ESCR of PEs. The principal objectives of this doctoral research were to conduct studies to identify, quantify, and improve ESCR of polyethylene resins. Several experimental stages were conducted in relation to molecular properties, extensional testing both in the solid and melt states, and the effect of temperature on crystalline phase properties during processing and post-processing. Moreover, reactive extrusion techniques were employed in order to enhance (in principle) the ESCR of polyethylene via the formation

of long chain branches (LCB). This modification was conducted through an ultraviolet (UV) photoinitiated reactive extrusion (REX) process in which a certain degree of long chain branching is achievable with minimum polymer degradation or crosslinking.

This study was designed to address the following objectives over different types of PEs with wide property ranges:

- Development of a potential standard test method for a quantitative estimation of ESCR in a timely and reliable fashion (a solid state investigation).
- Investigation of the effect of inter-lamellar links on ESCR through shear and extensional flow measurements (a melt state investigation).
- Examination of the relationships between crystalline state properties and ESCR.
- Identification of how temperature affects the lamellar structure of PEs of different molecular structures. This included the effect of cooling rate and annealing temperature rate on the lamellar structure.
- Evaluation of the effects of induced long chain branching (through a UV-photoinitiated reactive extrusion process) on the PE molecular structure.
- Finally, development of practical maps relating molecular properties to ESCR for a relative comparison between different PEs.

1.2 THESIS OUTLINE

A brief description of each chapter in this thesis is given below:

Chapter 2 summarizes relevant work presented in the literature in support of the motivation for this thesis research. Although each individual chapter will have its own more specific

literature review, Chapter 2 puts the problem investigated in context. This includes a brief review on the history and current state of the art with respect to PE, ESCR of PE, and methods for evaluation of ESCR. A review on extensional viscosity determinations through different mathematical and experimental techniques is introduced. Moreover, a brief review on UV photoinitiated crosslinking and long chain branching of PE resins is presented.

Chapter 3 presents the experimental methodologies that were used to investigate, identify, and improve ESCR of PE resins. Three main characterization classes, namely, molecular, rheological, and mechanical, were utilized in this work. A brief description of the materials and each characterization technique is presented.

Chapter 4 summarizes studies for verification and modification of a uniaxial tensile test, designed to estimate the ESCR of PEs. The validity of the test was extended to different grades of PE to determine the adaptability of the designed test. Furthermore, we identified optimal specimen dimensions and rate of testing for a more promising, practical, and conclusive prediction of ESCR. A factor called "corrected hardening stiffness (cHS)" was introduced by combining information obtained from the developed uniaxial tensile test and micromolecular properties of PEs. A correlation between cHS and ESCR was ultimately found for a more reliable ranking of PE resins with different structural characteristics.

Chapter 5 concentrates on rheological characterization of PEs in shear and extensional modes. In this chapter, linear viscoelastic (LVE) properties of PEs were determined from oscillatory shear measurements (frequency sweep and creep). Through these experiments, a correlation between a normalized characteristic relaxation time (λ_N), as a measure of network mobility, and the cHS was found for linear low density polyethylene (LLDPE) resins. Steady state and transient extensional viscosities were obtained using entry flow methodologies and

a Sentmanat extensional rheometer (SER), respectively. Entry flow methodologies were used to identify the steady state extensional viscosities from entrance pressure drops obtained from a dual-bore capillary rheometer. SER was used to investigate the extent of strain hardening of PEs in the melt state. A correlation was eventually developed between the extent of strain hardening, indicated by the strain hardening coefficient, and ESCR.

Chapter 6 is divided into two major sections. The first section presents a complete investigation of the crystalline structure to identify a potential correlation between ESCR and crystalline domain characteristics. Studies were performed to shed light on the existing ambiguity in the literature with respect to the relationship between crystalline domain properties and ESCR. The second section of this chapter includes studies performed to evaluate the degree of variability in the lamella surface area (LSA), as a measure of phase interconnectivity and ESCR. Different annealing and cooling conditions were employed to investigate the effect of temperature on LSA. A clear correlation between crystalline domain properties and ESCR was obtained only when polymers with similar molecular weights were compared. Both annealing conditions and cooling rate were found to affect LSA.

Chapter 7 summarizes the work from a series of designed experiments for developing a well-controlled photoinitiated reactive extrusion process for potential enhancement of ESCR. This was achieved by modifying the rheological properties of PEs by inducing different degrees of long chain branching, attained through controlling REX manipulated variables. These variables were the photoinitiator concentration, PE throughput, and the extruder screw speed.

Chapter 8 provides overview maps describing relations between key molecular properties and ESCR of PEs based on suggestions inferred from molecular, rheological and crystalline phase investigations (essentially, the culmination from all previous chapters). Based on these

instructions, a practical and reliable comparison can be made for selecting PE's with potentially higher ESCR.

Finally, Chapter 9 presents the conclusions and main contributions from this work. This summary is based on all the experimental and modelling attempts performed on different grades of PEs with a wide range of properties. Also included in this chapter are recommendations for future steps (immediate and longer-term) for identifying better indicators for and for more effective evaluation and ranking of ESCR of polyethylene resins.

2 CHAPTER 2: GENERAL LITERATURE BACKGROUND

2.1 POLYETHYLENE: PRODUCTION AND APPLICATIONS

Polyethylene (PE) is one of the most widely used thermoplastic polymers. It is chemically composed of only carbon and hydrogen atoms with the basic repeating unit ($-CH_2-CH_2-$), classifying the polymer in the polyolefin family. It is a semicrystalline polymer composed of ordered crystalline regions embedded in an amorphous phase. The semicrystalline structure gives PE its viscoelastic properties. The crystalline part of PE offers the strength and stiffness to the polymer, while the amorphous phase is responsible for its elastic properties. These morphological properties are mainly related to molecular characteristics of PE, namely molecular weight (MW), molecular weight distribution (MWD), and degree of branching.

PE was first developed in the 1930s and its properties have significantly improved since then. The first PE produced was the low density polyethylene (LDPE) with density between 0.912-0.925 g/cm^3. LDPE is usually manufactured through a free radical initiated polymerization process, conducted at high pressure (1000-3000 atm) and high temperatures (100-200 ºC). Two types of reactors, namely, continuous stirred autoclave and tubular reactors, have been used to produce LDPE. A highly branched polymer with both long and short chain branches, low crystallinity (45-55 %), low density, and low rigidity is obtained (see Figure 2.1). The structure of LDPE is usually altered by controlling polymerization conditions such as reaction pressure, temperature profile across the reactor, and addition of different chain transfer agents (1).

During the 1950s, the development of Ziegler Natta (ZN) and Phillips (chromium) catalysts made it feasible to manufacture linear PEs at low pressures and low temperatures. Reactions

at such conditions are conducted in three main processes: slurry, solution and gas-phase, which produce linear PEs through a coordination polymerization process. The catalysts consisted of an active transition metal compound (groups IV-VIII) or transition metal oxides (group V-VII) on a support, used with metal alkyls or hydrides as co-catalysts (2). The structural properties of the linear PEs are a reflection of the catalyst type and the specific process. Due to their multi-sited nature, these catalysts tend to form heterogeneous ethylene homo- and co-polymers with a polydispersity index (PDI) of above 4, and short branches distributed in the lower end of the molecular weight spectrum (1). The product of such processes is high density polyethylene (HDPE) with a more regular semicrystalline structure and density in the range of 0.940-0.975 g/mol. HDPE has a linear molecular structure imparting crystallisation to the polymer, thus resulting in a high density and a highly rigid material (see Figure 2.1). Inclusion of α-olefins as co-monomers was also possible in these low pressure processes, and this gave rise to the development of linear low density polyethylene (LLDPE) in the 1970s, with densities ranging between 0.915-0.930 g/mol. LLDPE has a linear molecular structure with short branches, imparting excellent properties to the material.

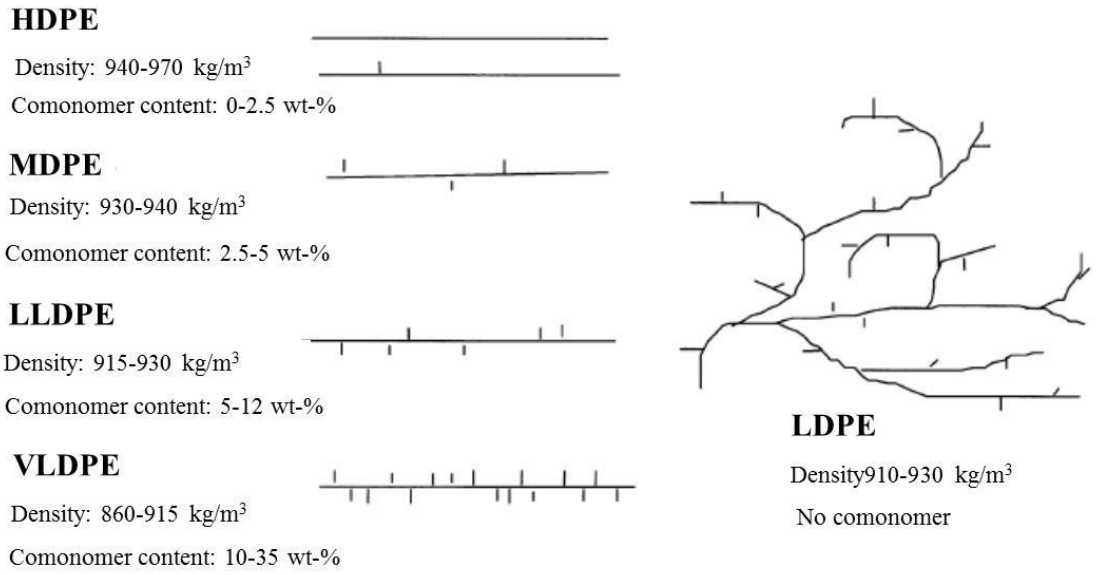

Figure 2.1: Molecular structure of different type of polyethylene (1)

The extent of branching in PE governs the polymer's density and rheological behaviour. Short chain branching (SCB) is introduced by copolymerization of PE with comonomers such as propylene, 1-butene, or 1-hexene, and long chain branching (LCB) is formed due to such reactions as transfer to polymer and terminal double bond polymerization (3). Branching tends to inhibit crystallinity since branches do not incorporate into the crystal lattice. The degree of inhibition depends on the length and frequency of the branching. LDPE has the highest number of short and long branches compared to HDPE or LLDPE. This results in a lower crystalline lamella formation for LDPE and consequently lower density. Other types of linear PEs such as medium density polyethylene (MDPE) with densities ranging between 0.926-0.945 g/mol, and very low density polyethylene (VLDPE) with densities ranging between 0.860-0.915 g/mol, have also been developed by controlling the extent of SCB in the polymer (see Figure 2.1). Density of PE is related to the crystallinity of the polymer. Higher crystallinity is an indication of existence of dense crystalline lamellae, thus suggesting a higher density. Many mechanical properties of PE such as yield strength,

stiffness and stress cracking resistance are affected by the crystallinity of polyethylene. Therefore, information in regards to the extent of chain branching and crystallinity are of great importance to predict the behaviour of PE resins.

A great deal of improvement in PE production has been achieved in the last 30 years. These accomplishments have been possible by development of new generations of ZN and Philips catalysts, along with use of single-sited metallocene and late transition metal catalysts. PEs with relatively narrower MWD (PDI below 4) and a more uniform SCB distribution can now be achieved. These PEs, in general, demonstrate better mechanical and thermal properties, but lack melt integrity and easy processing during manufacturing. Attempts were also made towards making PEs with tailored structural properties to meet requirements for applications where high performance is crucial. For example, development of bimodal PEs, mainly for the piping industry, through advancement in both catalysts and polymerization technologies has given rise to formation of PE-80 and PE-100 pipe resins. These PE resins are expected to withstand a minimum hoop stress of 8 and 10 MPa, respectively, for up to 50 years at 20 ºC (4). Production of bimodal PEs is mainly conducted in cascade reactors, with two reactors connected in series (5). In cases where a ZN catalyst is utilized, the fractions of the low molecular weight homopolymer and the high molecular weight copolymer can be controlled by the amount of hydrogen and the comonomer, added to each of the reactors. For cases where high mechanical and structural performance is needed, it is of common practice for SCB to be distributed in the higher end of the MWD spectrum (larger PE chains contain most of the short branches). For this reason, polymerization with high concentration of hydrogen is conducted in the first reactor to produce a low MW homopolymer. In the second reactor, polymerization is conducted in the presence of a comonomer and at lower levels of

hydrogen, to produce the high molecular weight copolymer. Other alternative techniques for the production of bimodal PEs, with both short and long chain branches, have also been developed. Most of these techniques include use of a single reactor with either combination of catalysts, or co-immobilization of different catalysts on a single support (4-8). Investigations on optimal operating conditions and the catalyst systems have enabled the development of both HDPE and LLDPE with multimodal structures and branching content (7, 9-11).

2.2 FAILURE MODES OF POLYETHYLENE

Polyethylene ruptures when subjected to loads. This failure generally involves micro-yielding of locally stress-concentrated defects, followed by fibrillation, cavitation (crazing), and fibril rupture. Lu and Brown (12) and Lu et al. (13) reported that PE goes through a ductile to brittle transition at room temperature and above, during which, ductile failure is promoted at higher stresses and brittle failure at low stresses. A typical ductile-brittle transition plot of PE exposed to stresses over sufficiently long time is shown in Figure 2.2. The strength of the polymer declines with time and temperature under load. A transition from a ductile yielding to a brittle failure is observed. Lu and Brown (12) and Lu et al. (13) further concluded that this transition region occurs because the creep strain which blunts the defect reduces the stress concentration so that crack growth is impeded. This indicates that given time, PE will eventually fracture even under low stresses.

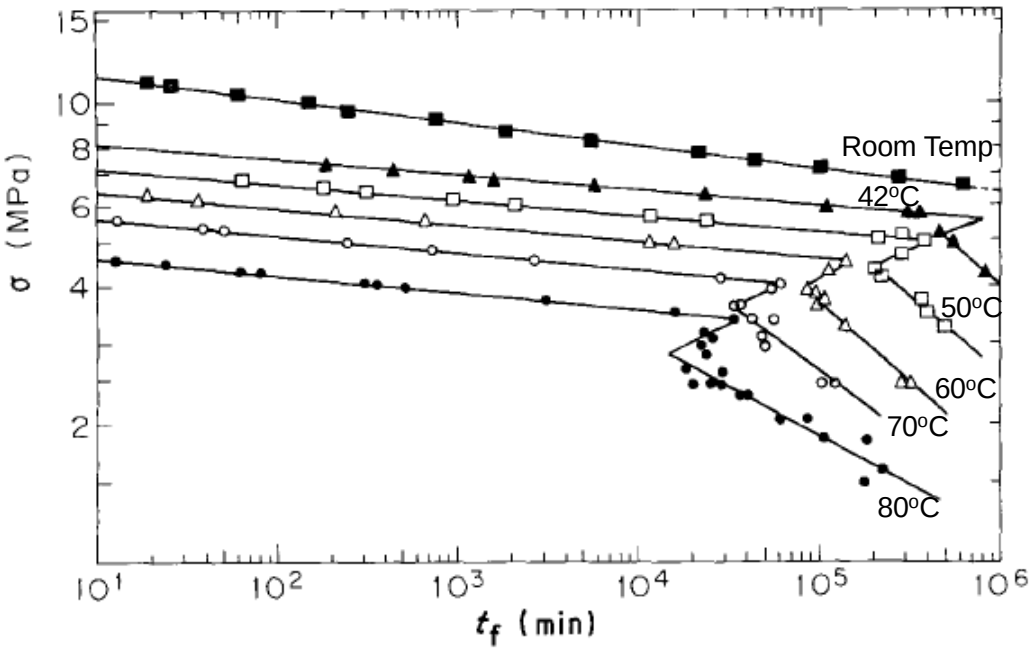

Figure 2.2: Polyethylene ductile-brittle transition behaviour recorded at different temperatures (12,14)

The transition to brittle fracture was found to be accelerated by factors such as temperature and contact with aggressive fluids. This transition is important because most materials are frequently subjected to low stresses (in order to have longer service lifetime). The sudden and catastrophic failure under low stresses makes brittle failure a more serious and less predictable event than ductile failure (15).

Ductile fracture of polymers occurs under constant loads after a certain amount of time, depending on the level of applied load and temperature. PE undergoes ductile failure (plastic deformation) when the level of stress is high (higher than yield stress) and the exposure time is low. As seen in all fracture processes, the crack starts from local stress concentration points. Therefore, when subjected to high levels of applied load, a high density of locally yielded sites will be generated, which consequently grow and multiply in time. This behaviour leads to the coalescence of yielded sites and eventual ductile yield fracture of the material. The ductile failure of PE results in large plastic deformation manifestations such as

necking and bulging, which are indications of both amorphous and crystalline phase deformation. In PE ductile deformation, the stress applied on the polymer stretches the tie-molecules until they cannot be pulled out any further. At this point the lamellae break into smaller chunks, called “mosaic blocks” (16), which consequently generate a rough and fibrous fracture surface.

On the other hand, PE brittle fracture will occur before the yield stress is reached. This is the case where stress-concentrating flaws are present. In the brittle region the failure is associated with the slow growth of a crack which is originated from a defect in the specimen. Polyethylene undergoes brittle fracture when it is exposed to low levels of stress over long periods of time. Brittle fracture surfaces have a clean break with little material deformation. Under an SEM, it can be seen that the surface actually consists of short random pullouts (3). In polyethylene, it is mainly the amorphous region that undergoes deformation upon brittle failure. Figure 2.3 presents the steps that are involved during brittle fracture of PE proposed by Lustiger and Markham (17). Initially, the amorphous region starts to stretch. Due to the longer time period, the tie-molecules under stress start to relax and untangle from each other until the number of remaining tie-molecules becomes very low. Once the remaining tie molecules are stretched to their limit, they break and brittle fracture occurs.

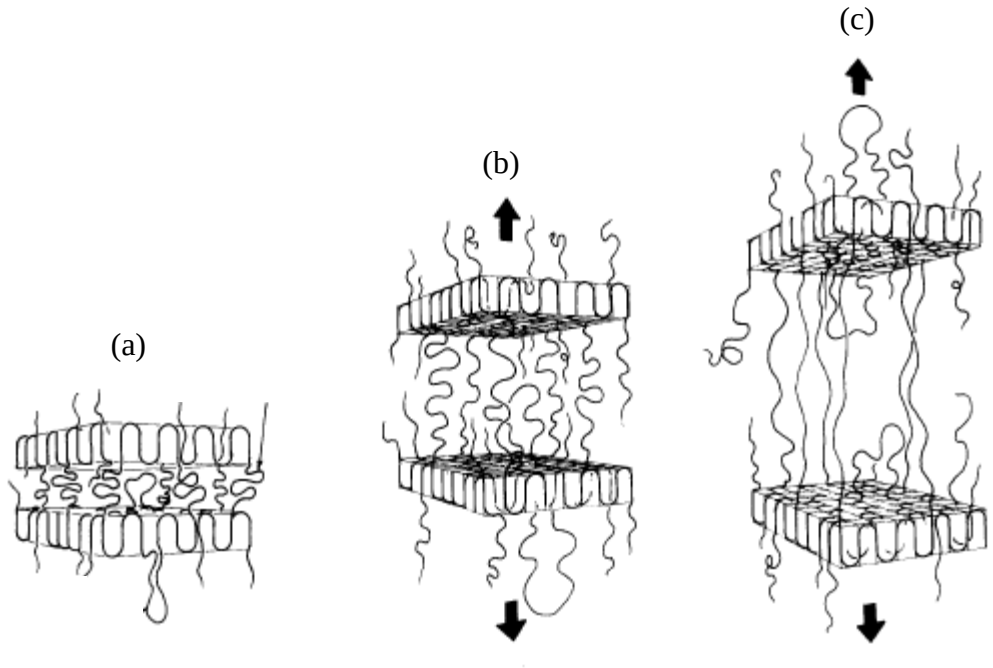

Figure 2.3: Brittle fracture of polyethylene; (a) Unstressed lamella structure (b) Stretch and break of tie-molecules (c) Seperation of lamellae (17)

2.3 ENVIRONMENTAL STRESS CRACKING (ESC) OF POLYETHYLENE

The term environmental stress cracking resistance (ESCR) was first used in the context of polyethylene cable insulation materials (15). ESC of polyethylene occurs when the polymer is subjected to low levels of mechanical stress (much lower than yield stress), over an extended period of time through a slow crack growth (SCG) mechanism. This failure mechanism is usually accelerated when PEs are subjected to an aggressive environment such as water, alcohol, detergents, and various oils. The failure of PE under such conditions is characterized by clean cracks, thus indicating a brittle fracture mechanism. The brittle cracks usually develop from a visible stress concentrator, such as system joints, nicks and cuts introduced during processing and installation (18).

This mode of failure is characterized by the presence of macroscopic cracks preceded by crazed fibrillar structures (19). Crazes are commonly found as a precursor to this type of fracture in PE (20). Due to surface and internal defects, PE under load contains a high density of local stress-concentration zones. At low levels of stress, only a few of these local points undergo yielding and slowly grow in a plane normal to the applied load with small chance of joining each other. As the load is constantly applied, these yielded zones cavitate and fibrillate to become crazes (15). Eventually crazes reach a critical length for fast and unstable crack growth, thus promoting a brittle fracture. A graphical representation of the brittle fracture process involved in ESC is shown in Figure 2.4. Therefore, it is confirmed that low levels of stress encourage brittle fracture; however, an accurate assessment of the craze behaviour at various rates and constraint levels is required to elucidate the damage and deformation mechanisms in polyethylene (21).

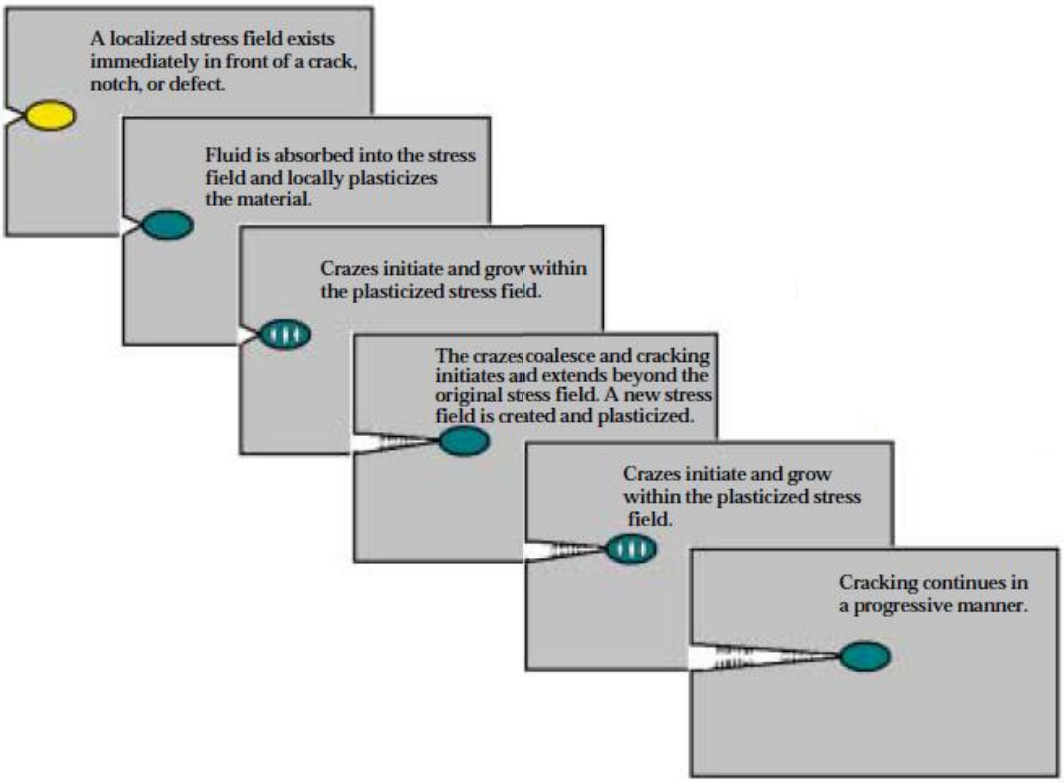

Figure 2.4: Gradual progress of ESC in polyethylene (22)

The aggressive environment involved in ESC does not structurally modify or degrade the polymer (no oxidation, chlorination, polymer chain scission or crosslinking). The role of the ESC fluid is to promote slow crack growth through a physical process which involves selective absorption of fluid in the micro-yielded zones. This local absorption reduces the local yield strength (plasticization) and consequently promotes embrittlement of the PE under stress. Surfactants are known to accelerate the process of void formation either by plasticizing the polymer chains, thus allowing easier chain motion, or by lowering the surface energy necessary for void formation (23). The "active environment" acts as lubrication for chain disentanglement, thus resulting in accelerated slow crack growth in PE (3). Ward et al. (24) proposed that the ESC fluid molecules have the ability to align themselves with the tie-molecules in the fibrils, thus easing the inter-lamellar disentanglements from the crystals.

The molecular structure of the ESC fluid is also important for the disentanglement process. In general, fluids with low molecular weights are more aggressive, as their smaller molecules can easily penetrate into the structure of the polymer (22). Moreover, fluids with a moderate hydrogen bonding are more aggressive ESC agents, compared to chemicals with high levels of hydrogen bonding (22).

2.3.1 MOLECULAR STRUCTURE CHARACTERISTICS AFFECTING ESCR

ESC of plastics including PE has been studied for over 30 years and a great deal of information has been obtained. However, there are many fundamental factors/variables along with their interactions which make it hard to predict the behaviour of PE environmental stress cracking with accuracy. Micromolecular properties, such as molecular weight, short chain branching content, and inter-lamellar links, including bridging tie-molecules and physical entanglements, have received most of the attention due to their closely associated relations with ESC (19, 25).

Tie-molecules, long polymer chains which connect crystal lamellae through the amorphous phase, have been linked to ESCR of PE. This idea was introduced by Huang and Brown (26, 27), who suggested models for formation of tie-molecules (probability of polymer chains becoming tie-molecules) with respect to the-end-to-end distance of the polymer chains. In this way, tie-molecules can be considered to act as linkages among different lamellae. As explained before, the brittle fracture of PE is related to its tie-molecules. As low stresses are applied, tie-molecules are stretched to their limit over time and ultimately break and cause brittle fracture.

Similarly, it is reported that separation of lamellae, either by disentanglement or rupture of the tie-molecules, is supposed to be the main molecular mechanism for ESC of polyethylene (23). The model developed by Huang and Brown (26) was further improved by Seguela (28) to calculate the overall area fraction of tie-molecules at the crystal–amorphous interface. Consequently, researchers used criteria related to the presence of tie-molecules to describe the effect of several polymer micromolecular variables on ESCR, mainly molecular weight, short chain branching, and processing conditions.

Huang and Brown (26) developed an equation to correlate the fraction of tie-molecule area in the amorphous region with the weight-average molecular weight of the polymer. The authors obtained a molecular weight critical value above which tie-molecule formation is possible. Similarly, another study by Lu et al. (29) concluded that a molecular weight greater than 1.5 x $l0^6$ is required to create the proper density of tie-molecules necessary to produce high resistance to slow crack growth. This means that the ESCR of PE increases as weight-average molecular weight of PE increases, since the tie-molecule concentration is increased (3).

Incorporation of a small amount of comonomers such as 1-butene or l-hexene gives rise to short chain branching in PE. Short chain branching tends to inhibit crystallinity since short branches do not incorporate into the crystal lattice. The existence of short chain branches in PE increases the density of tie-molecules, thus increasing the ESCR of PE. Researchers have investigated the effect of length and frequency of the SCB on ESCR. Yeh et al. (30) found an increase in the time of failure by 10,000 times when the short chain branch frequency was increased from 0 to 4.6 branches/1000 carbon atoms. Soares et al. (23) similarly reported that because SCB is responsible for the non-crystallizable sections of the polymer chains, an

increase in SCB will enhance the probability of tie-molecule formation. It was further reported that higher concentration and length of SCB provide better brittle fracture resistance since the portions of the polymer chains with the longer branches add to the formation of inter-crystalline tie-molecules (17). Presence/formation of SCB can further enhance the effectiveness of tie-molecule entanglements by inhibiting the ability of the tie-molecules to slip past one another.

Cheng et al. (16) in a detailed study on the effects of microstructure on creep characteristics have investigated the effect of crystallinity and lamella thickness on the ESCR properties of HDPE. They observed that both crystallinity and lamella thickness are inversely related to ESCR between PE samples that have similar MW. They also correlated the lamella surface area with ESCR of PE resins and found an increasing trend in ESCR with increasing (lateral) lamella surface area. They postulated that larger lamella surface area increases the occurrence probability of inter-lamellar linkages, hence improving the ESCR.

2.3.2 METHODS OF EVALUATION OF ESCR

Various types of techniques have been utilized to assess the ESCR of polymers. One major test category is the bending beam test which includes the application of a flexural load on the polymer samples in the presence of ESC fluids. The major tests under this category are the single cantilever test (rigid polymers), three-point bending test, shown in Figure 2.5 (a) (rigid polymers), and the bell telephone test, shown in Figure 2.5 (b) (flexible polymers). These test methods are rather ‘primitive’ nowadays as the assessment of failure is recorded by the naked eye. Therefore, these tests are recommended mainly for quick quality control or relative comparison purposes.

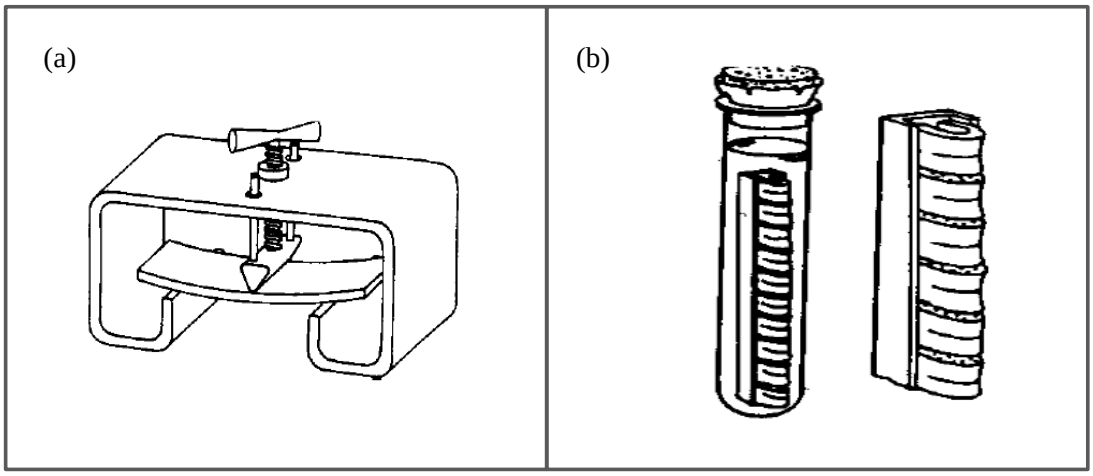

Figure 2.5: (a) The three-point bending test and (b) the Bell telephone test, used frequently to measure the ESCR of polymers (15)

Another ESCR test category is the tensile testing at constant loads. Tensile tests of creep rupture, creep, and monotonic creep are the main techniques under this category. These tests represent the most direct method of quantifying the effect of fluid on the durability of the polymers (15). The tests mainly involve the application of constant unidirectional tensile load and the recording of the time to failure. One major problem with these types of test is the long period of testing.

Accelerated tensile testing, such as the notch constant load test (NCLT), was developed to compensate for the long testing periods. In this technique, failure is accelerated to shorter times by introducing a notch in the test specimens, and by performing the test at elevated temperature. Other techniques such as the full notch creep test (FNCT), the Pennsylvania notch test (PENT), the notched pipe test (NPT), and the cone test were further introduced and used in industry (31).

The typical ESCR testing methods mentioned above are time consuming and rather unreliable. The difficulty involved with such testing methods is mainly the poor reproducibility and large subjective errors due to specimen preparation, notching process,

and surfactant quality. Consequently, development of alternative testing methods is required to overcome the aforementioned issues.

Kurelec et al. (32) and Cheng et al. (33) proposed new methodologies for evaluation of ESCR based on the "strain hardening" behaviour of PE resins under uniaxial tensile testing. During strain hardening, the inter-lamellar entanglements are fully drawn to their limit and the polymer hardens. This behaviour is quantified by the strain-hardening modulus, the slope of the line in the strain hardening section of the stress-strain curve during tensile testing. Polyethylene with a greater number of entanglements exhibits higher strain hardening and a higher ESCR.

Kurelec et al. (32) concluded that the creep of the fibrils within a craze is the determining factor for evaluation of the slow crack growth process involved in ESC of HDPE. They attempted to relate the ESCR to the slope of the strain hardening part of a stress–strain curve, at elevated temperature (80 ^{o}C). They demonstrated that the amount of strain hardening at elevated temperatures is highly sensitive to molecular differences (mainly SCBC and MWD), leading to variation in ESCR performance. The average slope of the strain hardening section, the so called "strain hardening modulus", obtained from true stress and strain values, was found to be sensitive to the same molecular differences that govern the slow crack resistance in HDPE. Therefore, it was concluded that comparison between the strain hardening modulus of PE resins is indicative of the long-term behaviour of PE. Through this technique, an easier and more reliable prediction of ESCR was obtained at relatively shorter periods of time. The complications involved with the notching process and the ESC surfactant were also eliminated; however, their proposed test is only possible at low strain rates (0.25 mm/min) and becomes less snsitive if performed at room temperature.

Cheng et al. (33) proposed a more practical test where uniaxial tensile tests were performed at room temperature and higher strain rate (7 mm/min). As compared to the Kurelec et al. (32) approach, where true stress and strain measurements were needed for evaluation of the strain hardening modulus, their method did not require any special equipment and could be readily carried out on any tensile tester (33). The measured slope from the strain hardening section of their test was called the "hardening stiffness (HS)", in order to distinguish the variable from the conventional definition of stiffness of the material (related to Young's modulus). They postulated that their strain hardening test method, which exhibited the lowest coefficient of variation among ESCR tests, had the potential to replace the conventional ESCR testing methods.

It should be noted that although the Cheng et al. (33) approach showed a proportional relationship between HS and ESCR of the PE resins tested, a gap was still left between HS and ESCR for high and low ESCR resins (since their resins did not cover the middle range). It is postulated that observing the behaviour of different types and grades of PEs will fill the gap and make it possible to determine the exact nature of the relationship between HS and ESCR. Further analysis is also required to identify the best specimen dimensions and rate of testing for a more promising and conclusive prediction of ESCR. These are aspects to be pursued further in the current thesis research.

2.4 EXTENSIONAL FLOW PROPERTIES OF POLYMERS

Cheng et al. (3, 33) showed that inter-lamellar entanglements, the most important micromolecular factor controlling the ESCR of PE, can be assessed by the extent of the strain hardening region from a simple tensile test at room temperature. They further provided

insight into the entanglement nature of PE resins through shear experiments (34). They were able to establish a method to predict the number of inter-lamellar entanglements from the molecular weight between entanglements (M_e) through oscillating shear experiments (parallel-plate rheometry). Rheological experiments in extensional flow could possibly provide additional information. It is believed that the strain hardening behaviour of the PE resins in extensional flow can be linked more reliably to inter-lamellar entanglements. Thus, a comparison between melt and solid strain hardening behaviour could provide new insight into the influence of chain entanglements on the mechanical behaviour of polymer.

It is well accepted that for a thorough rheological characterization of polymers, shear experiments are not sufficient (35, 36) and information in regards to extensional (elongational) flow behaviour is of critical importance. Polymer melts are frequently exposed to large strains and strain rates in rather complex fields under processing conditions (37), thus measurements obtained from shear and extensional flows should complement each other for a more accurate characterization of the rheological behaviour of the polymer. This is because polymers under extension are more sensitive to micromolecular and microstructural differences than under shear experiments. The knowledge obtained from extensional rheometry is of great importance in describing the stability of the polymer under various processing techniques, such as melt-spinning, blow-moulding, sheet and film drawing.

The main property measured through extensional rheometry is the extensional viscosity (η_{ext}). Extensional viscosity represents the resistance of a flow to extension controlled by molecular entanglements. Therefore, understanding the melt behaviour, mainly strain hardening behaviour, under extensional flow could shed light on the extent of entanglements and, consequently, the ESCR of a polymer. Strain hardening behaviour under extensional

deformation is caused by stretching of the polymer chains, similar to the behaviour of strain hardening in the solid state.

Due to the difficulties in generating a controlled extensional flow, experimental determination of extensional viscosity is not straightforward (38). Consequently, researchers have developed indirect methods to evaluate the extensional viscosity of polymers.

2.4.1 CONVERGING FLOW TECHNIQUES

The most frequently used technique for determination of extensional viscosity is the converging flow technique in which polymer flows from a large reservoir through a capillary die, where the entrance pressure drop is measured as a function of flow rate (38). Cogswell (39, 40) concluded that these converging flows can be analyzed in terms of their shear and extensional components to calculate the relationship between volume flow rate, pressure drop, and polymer melt swelling. He further derived a solution for the estimation of extensional viscosity from simple shear flow properties as shown in Equation 2-1 and Equation 2-2, for the extensional stress (σ_E) and extensional rate ($\dot{\varepsilon}$), respectively (40). Cogswell's analysis is based on the assumption that the flow is fully developed. The flow parameters are obtained by minimization of the local pressure gradient in the region.

$$\sigma_E = \frac{3}{8}(n+1)\ \eta_{ENT}\ \dot{\gamma}_{app} \qquad 2\text{-}1$$

$$\dot{\varepsilon} = \frac{4}{3(n+1)}\ \frac{\eta\ \dot{\gamma}_{app}}{\eta_{ENT}} \qquad 2\text{-}2$$

In the above equations, η_{ENT} is the entrance viscosity, η is the shear viscosity obtained from measurements at apparent shear rates ($\dot{\gamma}_{app}$), and "n" is the power law exponent of the PE resin. The value of entrance viscosity is related to the entrance pressure drop (P_o) and the apparent shear rate ($\dot{\gamma}_{app}$) according to Equation 2-3.

$$\eta_{ENT} = \frac{P_o}{\dot{\gamma}_{app}} \qquad 2\text{-}3$$

The apparent shear rate ($\dot{\gamma}_{app}$) is obtained for a pressure driven flow in a tube at steady state and fully developed conditions. The extensional viscosity is then defined as the ratio of the extensional stress to the extensional rate.

Cogswell's model was further improved by many researchers. Bersted et al. (41) relaxed the power law index assumption and found marginal improvement in predictions of extensional viscosity. Binding (42) further studied the converging flow field and developed a model. In his analysis, Binding used an energy minimization technique to minimize the viscous energy dissipation within the flow field. Binding's technique allows the extensional viscosity to vary with deformation rate and also includes a correction for the non-Newtonian behaviour of polymers (Weissenberg-Rabinowitch correction). Equations 2-4 to 2-7 were developed from Binding's analysis for the extensional rate and extensional stress, respectively (38).

$$\dot{\varepsilon} = \frac{(3n+1)(1+k^2)}{3k^2(1+n)^2} \frac{\eta\dot{\gamma}_{app}}{\eta_{ENT}} \left(\frac{3n+1}{4n}\right)^n \qquad 2\text{-}4$$

$$\sigma_e = \frac{2^{k-1}\, 3k\, (1+n^2)}{(3n+1)(1+k)^2} \frac{\eta_{ENT}\dot{\gamma}_{app}}{I_{nk}} \quad 2\text{-}5$$

I_{nk} and k are defined according to Equations 2-6 and Equation 2-7.

$$I_{nk} = \frac{n\, ((1+n)/n)^{k+1}}{2n + (1+n)(k+1)} \quad 2\text{-}6$$

$$k = \frac{t}{1+n-t} \quad 2\text{-}7$$

In the above equations, t is defined according to Equation 2-8.

$$t = \frac{dlog\, (\eta_{ENT})}{dlog(\dot{\gamma}_{app})} - 1 \quad 2\text{-}8$$

2.4.2 ELONGATIONAL RHEOMETERS

In the last 30 years, various instruments have been designed to evaluate the extensional behaviour of polymer melts. The extensional rheometers apply extension at a constant elongational rate on a stress-free polymer specimen. The most problematic aspects of extensional flow studies are supporting the sample and applying a tensile force without introducing strong end effects. Most of the earlier designs included uniaxial extension of polymer samples in the form of a rod (clamped in both sides) at elevated temperature in an oil bath. Meissner (43) introduced a new technique in which the moving clamps were replaced by two rotating wheels. This way, the elongation was not limited by the size of the equipment and the end effects caused by the moving clamps were removed.

Other researchers adapted the idea of Meissner's rotary clamp technique to measure transient uniaxial extensional properties (44). Connelly et al. (44, 45) reportedly improved the Meissner original design and employed extensional data to evaluate the performance of adhesives. Munstedt (46) also designed a rotating clamp rheometer along with sample preparation techniques based on Meissner's approach. This apparatus made it possible to perform elongational measurements on small samples at constant tensile stresses or constant strain rates. Sentmanat (47) developed a detachable fixture for a rotational rheometer, the Sentmanat Extensional Rheometer Universal Testing Platform. This platform applies a uniform extensional deformation on polymer melts using dual wind up drums (see Figure 2.6). TA Instruments also developed a similar design in which one drum stays stationary, while the second drum rotates the sample (48).

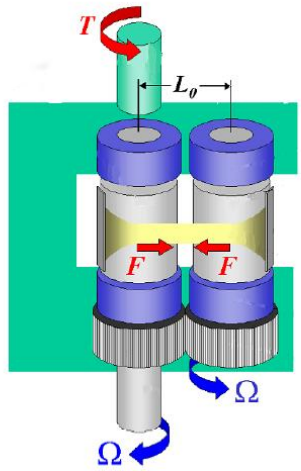

Figure 2.6: Miniature test platform designed by Sentmanat (47)

Finally, Rheotens was developed simultaneously with the uniaxial elongational rheometers (49). This instrument is designed based on the principle of two rotating wheels to draw polymer melt samples to generate extensional deformation. Rheotens performs the

elongational analysis on polymer melts that are under constant stress exiting from a capillary die as shown in Figure 2.7.

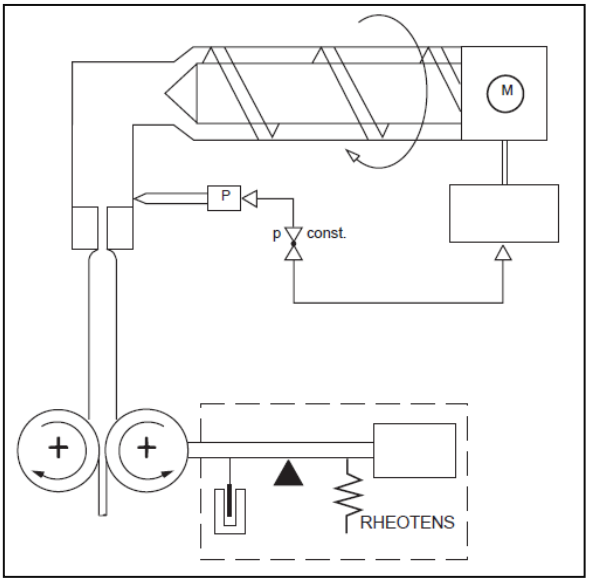

Figure 2.7: Experimental set up for Rheotens based on Meisner design (49)

2.5 FREE RADICAL MODIFICATION OF POLYETHYLENE

Structural and rheological modification of polymers through various techniques has always been of interest to both academic and industrial research. These techniques mainly involve the use of chemicals or application of some sort of energy which is capable of modifying the polymer structure. Free radical induced chain scission is one of the methods extensively employed to modify and control the rheology of polymers. Degradation due to polymer chain scission is achieved by generating free radicals either thermally or chemically, which further attack the polymer chains and cause chain scission. Through chain scission, polymer with shorter chain length (and hence lower molecular weight) is produced. This type of modification is generally used in cases where higher melt flows (lower viscosity) are required. An example would be modification of the flow properties of polypropylene (PP) by

chain scission to achieve a desirable flow range. The structurally modified PP is referred to as controlled-rheology polypropylene (CRPP) (50). Through chain scission, molecular weight and molecular weight distribution are tailor-made to fit the performance requirements. Molecular degradation in PE, however, is not very convenient as polyethylene has the tendency to crosslink in the presence of a free radical. Only a limited number of studies have been conducted to modify rheology and structure of PE through degradation. Degradation in PE has been possible mainly either by processing the polymer at extreme operating conditions (thermo-mechanical with temperatures above 290 ºC) (51), or exposing the polymer to irradiation over a prolonged period of time (24-48 h) (52). During these processes, careful control over processing temperatures is needed as a small change in the reaction temperature can change the degradation mechanism from chain scission to branching/crosslinking (reactions are not mutually exclusive but competitive (51)). At the same time, the reaction should be conducted under an oxygen-rich environment to avoid promotion of branching.

Free radical induced crosslinking is another method employed for modification of PE. In this method, free radicals are in charge of abstracting hydrogen molecules from PE chains. Abstraction of the hydrogen molecules enables other chains or bridging species to attach to the donor polymer chain and generate crosslinking. Crosslinks can occur at random intervals along the chains, from an average of only one crosslink per several thousand carbon atoms to one per few dozen (53).

Crosslinking of polyethylene has been a subject of interest and of great importance in improving the properties of the polymer. The main applications were to increase the thermal and creep resistance of high temperature pipe and cable insulations (54). ESCR is also

increased by crosslinking. This is due to the imposed restrictions against stretching of the polymer upon crosslinking. In crosslinked PE, extensibility of the material is controlled by the number of crosslinks. On the other hand, for PE without crosslinks, chain entanglements control the extensibility of the material (3). Therefore, it is postulated that ESCR of PE can be directly modified by introducing selective crosslinking. Reactions such as crosslinking and endlinking (branching) predominate over scission in PE at moderate temperatures (200 ^{o}C or lower) (55).

Different crosslinking techniques for polymers have been extensively used and investigated. Among these, high energy electron beams (γ-rays), thermo-chemical reactions involving aromatic peroxides and vinyl-silanes, and ultraviolet irradiation are the most preferred ones (55-59). These techniques have essentially been used in order to either induce crosslinking and grafting in polymers (e.g., PE (60), Polyvinyl Chloride (PVC) (61)), or modify the rheological properties of polymers (e.g., PP (50), Polystyrene (PS) (62)) by imposed chain scission, and production or removal of unsaturation (63).

The UV irradiation technique is preferred in many industries due to two main reasons. Firstly, UV irradiation is a one stage process in which polymer degradation is minimal. Secondly, UV light sources are readily available and easy to handle, which makes the process inexpensive and safer to operate.

2.5.1 ULTRAVIOLET (UV) PHOTOINITIATED BRANCHING AND CROSSLINKING OF POLYETHYLENE

Polymer structural modification by UV irradiation was first initiated by Oster and coworkers in the 1950s, where crosslinking of polyethylene was attempted. No great deal of success was

achieved until the late 1980s, due to poor penetration of the UV light into specimens and the slow reaction rates of the photocrosslinking (64). Therefore, the use of UV irradiation was limited to applications where post fabrication curing and thin specimens were of interest.

Detailed studies have been performed since the 1980s on UV initiated photocrosslinking of linear and branched polyethylene (64-70). These studies have given rise to highly effective and efficient methods for modification of polyethylene.

The process of photoinitiated modification (both crosslinking and branching) in PE takes place in three consecutive steps: initiation, propagation, and termination. Initiation involves the excitation of the photoinitiator upon irradiation. Excitation is further followed by hydrogen abstraction from the donor molecule of PE. In most of the studies performed, benzophenone and its derivatives were selected as the photoinitiator. It was found that irradiation at wavelengths of 340 nm or 254 nm excites the benzophenone molecule to an excited singlet state (S_1). The intersystem crossing (ISC) further excites the molecule to a tertiary state (T_1) very efficiently during 10^{-10} seconds (58). This mechanism is shown in Figure 2.8.

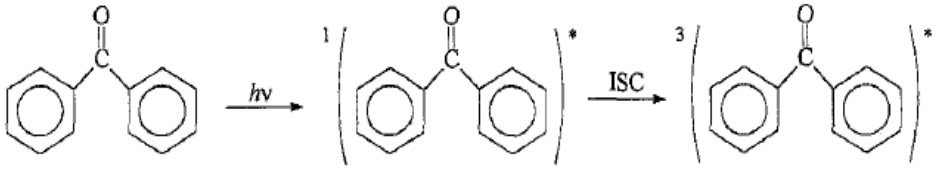

Figure 2.8: Benzophenone excitation reaction to primary and tertiary states upon irradiation and intersystem crossing (71)

The tertiary excited state of the photoinitiator can abstract a hydrogen from the hydrogen donor molecules (PE in this case). The reaction between excited benzophenone and polyethylene is shown in Figure 2.9. The product of such a reaction is a free radical called benzophenone ketyl ($K^{\bullet}$) and a reactive alkyl group ($P^{\bullet}$) (58). Propagation and termination steps promoting crosslinking (H-type branching) mainly involve the reaction of the alkyl groups ($\dot{P}$) with each other or with other bridging molecules such as crosslinking agents. For long chain branching (Y-type branching), the alkyl groups react with a vinyl end groups (unsaturated double bonds), which are either formed during polymer production, or by β scission during the photoinitiation process.

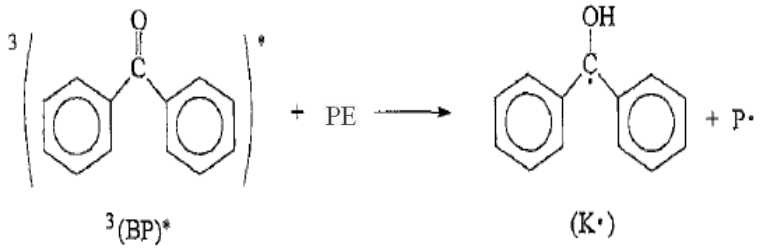

Figure 2.9 Hydrogen abstraction process from a hydrocarbon by tertiary state excited benzophenone (71)

Various UV photoinitiated processes have been designed to induce crosslinks in PE. In most of these processes, however, crosslinking is either achieved by passing the extrudate (melt exiting the die of an extruder) through a UV curing section placed right after the extruder, or by post-processing the extruded parts in a UV curing chamber. It should be noted that no

attempt has taken place to initiate crosslinking within the extruder. Consequently, it was decided to expand the investigation for better assessment of polymer modification through a reactive extrusion process in which crosslinking is induced. Information from such a study can shed light onto developing an appropriate process in which thermal and chemical degradation can be minimized (through fast reactions/ low residence time) along with selective extent of crosslinking.

Attempts have also been made to form long chain branches in PE though irradiation techniques (72-75). In these studies, high energy gamma rays and electron beams have been utilized, in an oxygen-free environment, to prevent crosslinking, yet promote branching. It should be noted that in these studies, a combination of crosslinks and long chain branches were found. The amount of different type of branching in these experiments was found to be related to processing variables such as irradiation dosage and operating temperature. Randal (76) was able to create a larger yield of Y-type branching in a polyethylene using high energy beams. The author justified his findings using C NMR and found that long branches can be formed, when there is a reaction between a terminal vinyl group and a secondary alkyl radical (i.e., disappearance of terminal vinyl groups, with formation of long branches). This reaction is shown in Figure 2.10.

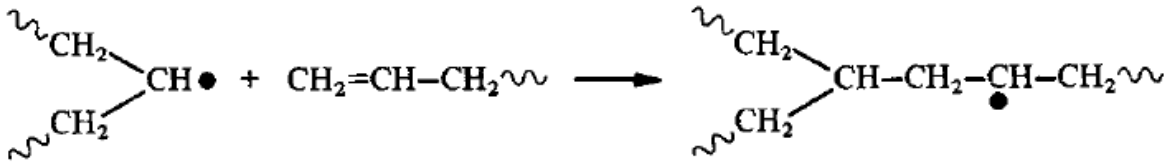

Figure 2.10: Reaction involved in Y-type branching (76)

2.5.2 REACTIVE EXTRUSION (REX)

The demand for application of extruders as continuous processing reactors to produce high performance products is increasing especially in the field of polymerization and polymer modification. Compounding by extrusion has long been used due to the high levels of consistency in the final product. Compounding usually includes feeding the raw material followed by applied shear and heat within the extruder. Due to high shear, agglomeration of raw materials is inhibited and melt mixing takes place, which in turn creates a homogenized melt.

In a reactive extrusion (REX) process, the synthesis or modification of a polymeric material takes place simultaneously with its processing and shaping into a finished plastic product. Consequently, reaction extrusion is now being viewed as an efficient means of continuously polymerizing monomers as well as chemically modifying polymers. It is defined as the engineering specialty that combines two traditionally separate operations: the chemical reactions for the formation or modification of polymeric macromolecules and the processing of the polymer for the purpose of structuring it into shaped plastic products (77). Therefore, REX processes are means for modification of commodity polymers to produce and shape new specialty resins (60).

Different types of REX process have been reported in the literature. The following have been widely used: free radical, anionic, cationic, condensation, and coordination polymerization of monomers, controlled degradation and crosslinking of polymers by means of a free radical initiator, functionalization of commodity polymers for the purpose of producing materials to be used in grafting applications, and polymer modification by grafting of monomers or

mixtures of monomers onto the backbone of existing polymers for the purpose of improving various properties.

3 CHAPTER 3: EXPERIMENTAL METHODOLOGIES

3.1 THERMAL AND MOLECULAR PROPERTIES

ESCR of PE is dependent on different molecular properties. ESCR performance is usually dictated by a combination of many structural properties such as MW, MWD, and branching content. Other structural characteristics such as density, percentage crystallinity, and crystalline lamella thickness, can also influence ESCR. In order to have a more clear understanding of the individual and the combined effects of these properties on ESCR, complete molecular and thermal characterization is essential. Hence, we aimed to investigate major molecular properties, such as average molecular weights, molecular weight distribution, and branching content and branching distribution, through chromatography and magnetic resonance techniques. X-ray and Differential Scanning Calorimetry were further conducted to identify potential crystalline structures, affecting ESCR. A detailed summary of the principles behind each test, and additional details about each characterization methodology used in this work are presented below.

3.1.1 DIFFERENTIAL SCANNING CALORIMETRY (DSC)

Information in regards to resin crystallinity and lamella dimensions was investigated by differential scanning calorimetry (DSC). In DSC, the energy required to establish a nearly zero temperature difference between the polymer and a reference material is measured, as the two samples are subjected to identical temperature in an environment heated at a controlled rate. The result obtained from a DSC experiment is a curve of heat flux versus temperature or time (see Figure 3.1). The DSC curves can be used to evaluate the enthalpies of transition by

integrating the peaks. These peaks identify the thermal transitions (due to changes in enthalpy) in a sample as the temperature is increased. At the glass transition temperature (T_g), the material changes from the brittle to the rubbery state, as shown by a drop in the heat flow (endothermic behaviour). The exothermic crystallization process, indicated by an increase in the heat flow, is due to generation of crystals. Finally, the endothermic melting, indicated by the convex peak, represents the change from a rubbery state to a liquid state (melting of crystallites).

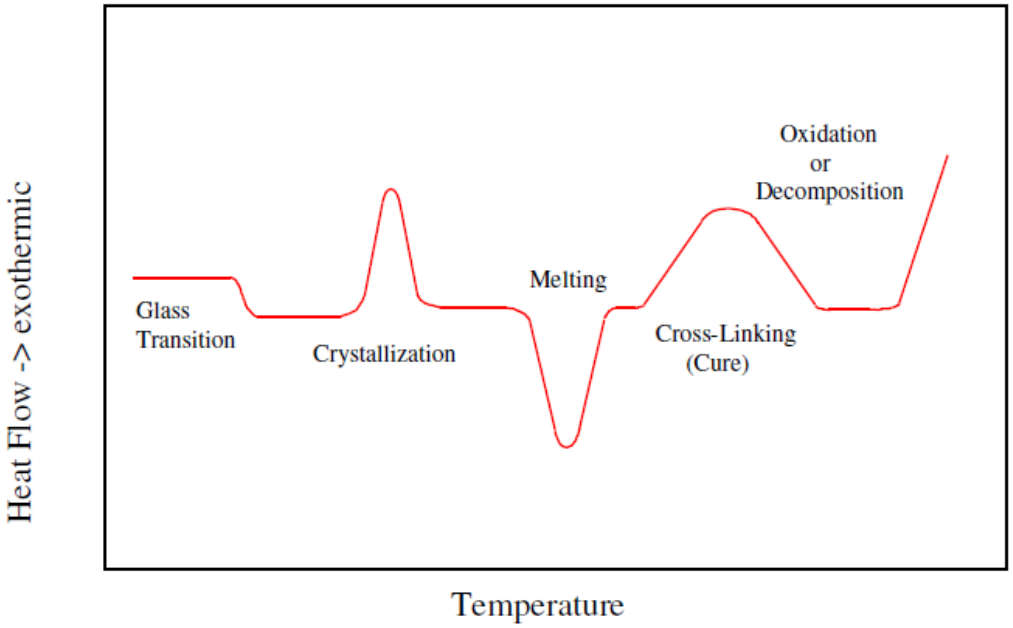

Figure 3.1:Thermal events recorded by DSC (1)

The enthalpies obtained from integration of the DSC peaks can be used to evaluate the percentage crystallinity (X_c) (Equation 3-1), and the lamella thickness (l) based on the Gibbs-Thompson correlation (Equation 3-2). In these equations, ΔH_c is the enthalpy of the 100% crystalline material (293.6 J/g in the case of PE), and T_m is the melting point obtained from

the melting peak of the DSC curve. The Gibbs-Thompson correlation parameter values for polyethylene resins are based on the work of Wlochowics et al. (2). $T_m^o = 415\,K$ is the equilibrium melting point of an infinite crystal; $\sigma_e = 60.9 \times 10^3\ \left(\frac{J}{m^2}\right)$ is the surface free energy of the basal plane, and $\Delta h_m = 2.88 \times 10^8\ \left(\frac{J}{m^3}\right)$ is the enthalpy of fusion per unit volume.

$$\%\ Crystallinity, X_c = \frac{\Delta H}{\Delta H_c \times 100} \qquad 3\text{-}1$$

$$T_m = T_m^o\left(1 - \frac{2\sigma_e}{\Delta H_m l}\right) \qquad 3\text{-}2$$

In this work, DSC analysis was performed with a Q2000 DSC controlled by a TA processor.

3.1.2 GEL PERMEATION CHROMATOGRAPHY (GPC)

Molecular properties, namely, average molecular weights and molecular weight distribution, were evaluated by GPC. GPC is a type of size-exclusion chromatography (packed bed column of porous material) in which the dissolved polymer molecules are fractionated based on their retention time (see Figure 3.2). The larger molecules are mainly excluded from the pores of the packing particles (gel beads), and consequently elute before the smaller molecules. A GPC is usually composed of a large solvent reservoir, a high pressure (precise flow) pump, an injection device, and a different number of packed columns (3). Once the injected sample is fractionated based on its molecular size, the eluted fractions are passed through a series of different detectors to measure specific molecular properties of the polymer, including, MW, MWD, and branching content. Some common detectors used in

GPC are differential refractive index (RI) detectors, differential viscometers, ultraviolet, infrared (IR), and light scattering (LS) detectors.

A differential refractive index detector is a polymer concentration detector and is the most common detector, present in almost any GPC set up. It can be combined with other detectors that will offer information about specific molecular weight averages. The detector responses are eventually converted into a molecular weight distribution curve, using a calibration curve based on known polymer standards. Molecular weight averages and polydispersity index values, then, are extracted from the MWD curve.

Differential viscometers are also quite common nowadays, to quantify the amount of long branches in a polymer. A differential viscometer provides the intrinsic viscosity (η_{int}) of a polymer. The principle involved in viscometers is monitoring the pressure drop across different capillary tubes with differential pressure transducers. Pressure drop values are converted into specific viscosities, from which an accurate measure of intrinsic viscosity is obtained. Intrinsic viscosity is used to obtain a contraction factor (g), suggested by Zimm and Stockmayer (4), from a ratio between intrinsic viscosities of a branched polymer to its linear parent of the same molecular weight (see Equation 3-3). "ε" in this equation is a parameter dependent on the GPC solvent and structure of LCB (5). "g" can be used to identify long chain branching content for a variety of polymers with different branching structures (6).

$$g^{\varepsilon} = g' = \left| \frac{[\eta_{int}]_{branched}}{[\eta_{int}]_{linear}} \right|_{MW} \qquad 3\text{-}3$$

In order to identify the comonomer distribution (short chain branching distribution), a GPC is usually coupled with an IR detector. The fractionated polymer passes through an IR detector,

where a distribution of chemical groups is identified based on their absorption characteristics (7). This distribution is converted into a comonomer content distribution by using an IR calibration curve, based on a polymer of known methyl content.

In the case of PE, high temperature GPC should be used to overcome the difficulty in dissolving the polymer. The most common GPC solvent and operating temperature used for PE are 1, 2, 4 trichlorobenzene (TCB) at 140 ºC. In this work, GPC analysis was performed on a high speed GPC from Polymer CHAR (Spain), with a viscometer, and a light scattering detector. The GPC was also equipped with an infra-red detector (GPC-IR5) for determination of short branching content and branching distribution.

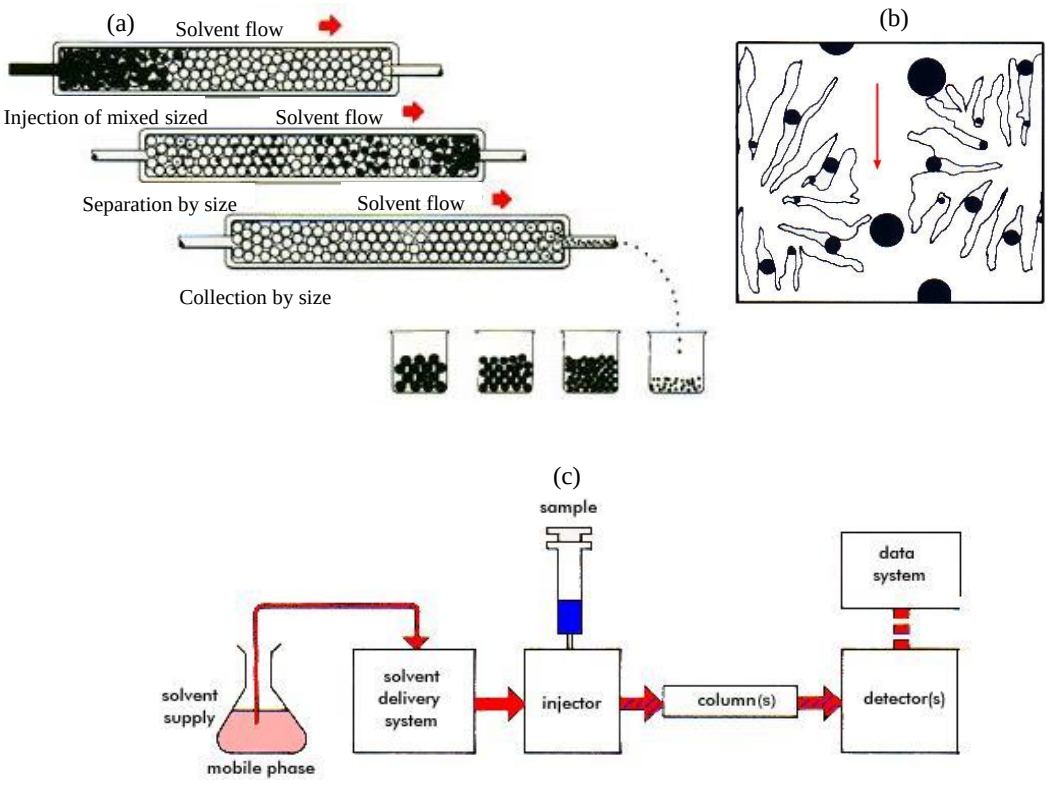

Figure 3.2: (a) Fractionation of polymer molecules of different sizes in a GPC column, (b) cross sectional view of porous GPC packings and flow of molecucles, (c) schematic of steps involved in a conventional GPC (18)

3.1.3 CARBON-13 NUCLEAR MAGNETIC RESONANCE (^{13}C NMR)

^{13}C NMR spectroscopy has been extensively used to quantify branching content in polymers. When polymers are placed under a magnetic field, the ^{13}C and other active magnetic nuclei become excited and shift to higher energy levels, creating magnetic resonances at specific resonance frequencies. Therefore, it is possible to identify various chemical compounds by comparing the NMR of the compound to that of a standard reference material (chemical shift of branching points differ from the main polymer chain). Figure 3.3 represents a typical ^{13}C-NMR spectrum for PE. The frequencies shown above the spectrum for each peak are a representation of the abundance of the nuclei; hence, the largest peak represents the backbone C-C bonds. The NMR spectrum along with Equation 3-4 are used in order to identify the short chain branching content in the PE resins. The area under the branching peak divided by

the area under the backbone peak represents the number of branches per thousand carbon atoms. The inability of measuring the length of a branch longer than 6 carbons is a disadvantage of ^{13}C NMR. In this work, ^{13}C NMR was mainly used to identify the extent of short chain branches in the polymer. An AVANCE 500 Bruker NMR was utilized to investigate the short chain branching content of the PE resins at 120 ºC. The solvent of choice was deuterated TCB.

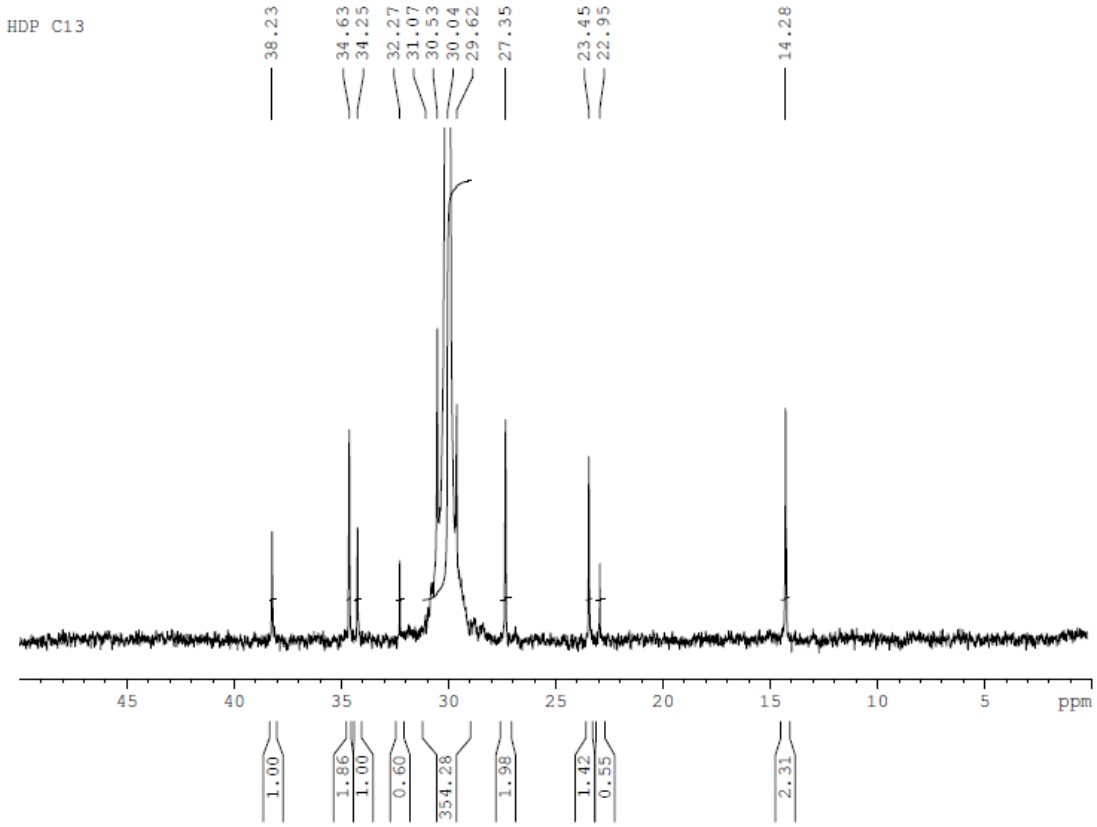

Figure 3.3:Typical ^{13}C NMR spectrum of a PE sample

$$\frac{Branch\ type}{1000\ carbons} = \frac{Area\ under\ branch\ peak}{Area\ under\ backbone\ peak} \times 1000 \qquad 3\text{-}4$$

3.1.4 X-RAY DIFFRACTION

X-Ray methodologies including, wide angle X-ray scattering (WAXS) and small angle X-ray scattering (SAXS), have been extensively employed to study the crystalline structure and morphological behavior of polymers. WAXS spectra include peaks representing the molecular structure of a crystal. In a semi-crystalline polymer such as PE, the scattered X-ray peaks consist of peaks, reflecting effects of both the crystalline and amorphous domains of the polymer. Figure 3.4 is a typical WAXS spectrum for different types of PE, and a

polypropylene resin (8). There is a steady decrease in the sharpness of the crystalline peaks (peak broadening) with an increase of the amorphous region.

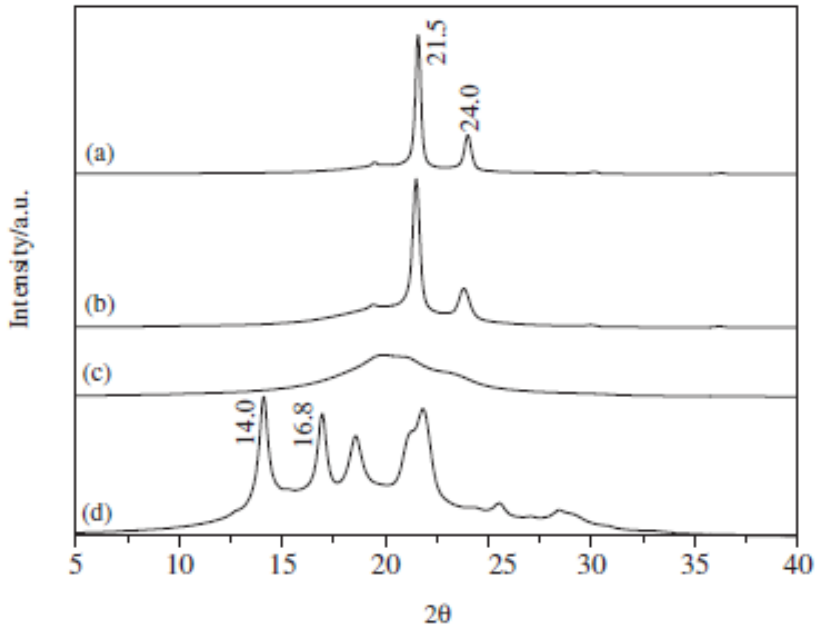

Figure 3.4: WAXS specrtrum for differnet types of PE (a) HDPE (b) LLDPE (c) Metallocine PE (with low percentage crystallinity), and (d) polypropylene (8)

The ratio of the area under the crystalline peak to the total area of the X-ray scan, obtained from a WAXS spectrum, provides information about the percentage crystallinity of the polymer, according to Equation 3-5. In this equation, I_c and I_a represent the areas of the crystalline and amorphous regions, and hence, they are related to the scattering intensities of the crystalline and amorphous regions, respectively.

SAXS is commonly used to find the long spacing (L) and, consequently, the lamella thickness (*l*) of the resins. Long spacing is calculated using the Bragg formula (shown in Equation 3-6) from the peak position of the first maximum (ε) in the SAXS pattern. In Equation 3-6, "*n*" represents the level of scattering and λ is the wavelength of the X-ray.

Ultimately, the lamella thickness (l) can be found using the relationship shown in Equation 3-7.

$$Crystallinity\ (\%) = \frac{\int_0^\infty I_C}{\int_0^\infty I_C + \int_0^\infty I_a} \times 100 \quad 3\text{-}5$$

$$L\varepsilon = n\lambda \quad 3\text{-}6$$

$$Lamella\ thickness\ (l) = Crystallinity\ (\%) \times L \quad 3\text{-}7$$

In this work, WAXS patterns were measured in a STOE two-circle goniometer using Cu Kalfa radiation from an ENRAF NONIUS FR 571 rotating anode generator. To minimize the background level, the X-rays were detected with a MOXTEK energy sensitive Si-detector, connected to single channel analyzers that selected photons corresponding to the Cu Kalfa radiation (Lambda (λ) = 1.54178 Å). The SAXS patterns were measured in a Bruker NANOSTAR using Kalfa radiation. For both techniques, bars 25 mm in length and 10 mm in width were compression-molded at 190 ºC and 44.5 kN, followed by quenching in cold water.

3.2 MECHANICAL PROPERTIES

ESCR is a long-term mechanical property. In order for a polymer to go through ESC, a mechanical stress, acting only under conditions of a tensile stress, should be present (9). This tensile stress is required for the disentanglement process involved in ESC. In this work, a conventional mechanical testing methodology, the Notch Constant Load Test (NCLT), was conducted to measure ESCR of PEs. Also conducted was a uniaxial tensile test to identify the strain hardening behavior of PEs under tensile conditions, performed at room temperature.

3.2.1 TENSILE TEST

A uniaxial tensile test is employed to identify the elongational behaviour of the PE resins in the solid state according to the American Society of Testing and Materials (ASTM) D638 (10). In this test, uniaxial load (stress) is applied to sample specimens and the percentage elongation of the samples, the increase in the length of the sample divided by its original length, is measured. A typical stress-strain curve of semicrystalline PE under uniaxial tension is shown in Figure 3.5. Three distinctive regions can be observed, representing the behaviour of the polymer at different levels of applied load. In the first region, the strain is linearly increased as the stress increases, a behaviour known as the Hookean elastic behavior. The slope of the line obtained from the first region is called the Young's modulus and represents the stiffness (resistance to deformation) of the material. The behaviour of the material in this region is primarily governed by the crystallinity and the crystal structure of the polymer. The elastic behaviour changes at yield point where unrecoverable plastic deformation (cold drawing) starts. In this region additional strain is possible without increase of stress. This additional strain is permanent and will remain when the stresses are removed. In the third stage, the strain hardening stage, polymer chains are reoriented and can bear higher applied loads. Hence, the stress level increases until the material fails.

The tensile test was performed at a deformation rate of 10 mm/min at room temperature on an Instron 3365 machine. The tensile specimens were prepared by punching compression-moulded plaques. Plaques were prepared by compression moulding at 190 ºC+5 ºC and 44.5 kN.

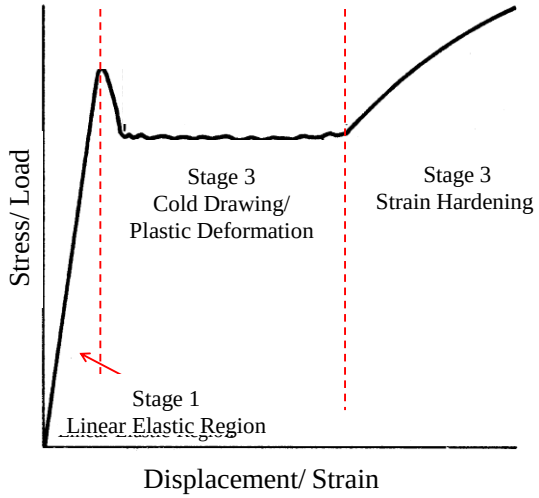

Figure 3.5:Typical elongation behaviour of semicrystalline PE

3.2.2 NOTCH CONSTANT LOAD TEST (NCLT)

The NCLT was utilized to identify the ESCR properties of the PE resins. In this test, specimens are subjected to a constant load under an aggressive environment. A notch is introduced in the sample and the test is performed at elevated temperatures to accelerate the failure processes/mechanisms involved in the slow crack growth of PE.

ASTM D5397 (11) was employed to perform the test. A notch is introduced to the dogbone samples prepared from compression moulding. The depth of the notch should produce a ligament thickness of 60 % of the nominal thickness of the specimens. The notched specimens are suspended in 10 % surface-active agent (surfactant) with 90 % water in the apparatus shown in Figure 3.6 (a) at 50 ^{o}C. The dogbone samples (Figure 3.6 (b)) are attached from the top to the end of a loaded lever, and from the bottom to the base of the apparatus. The time of failure is recorded by an automatic timing device attached to the loaded lever. The surfactant in this test is Igepal (nonyl phenol ether glycol, $C_{19}H_{19}$-C_6H_4-O-

($CH_2CH_2O)_8$-CH_2CH_2OH). In order to guarantee a brittle fracture, the stress is 15 % of the yield stress of the PE resins.

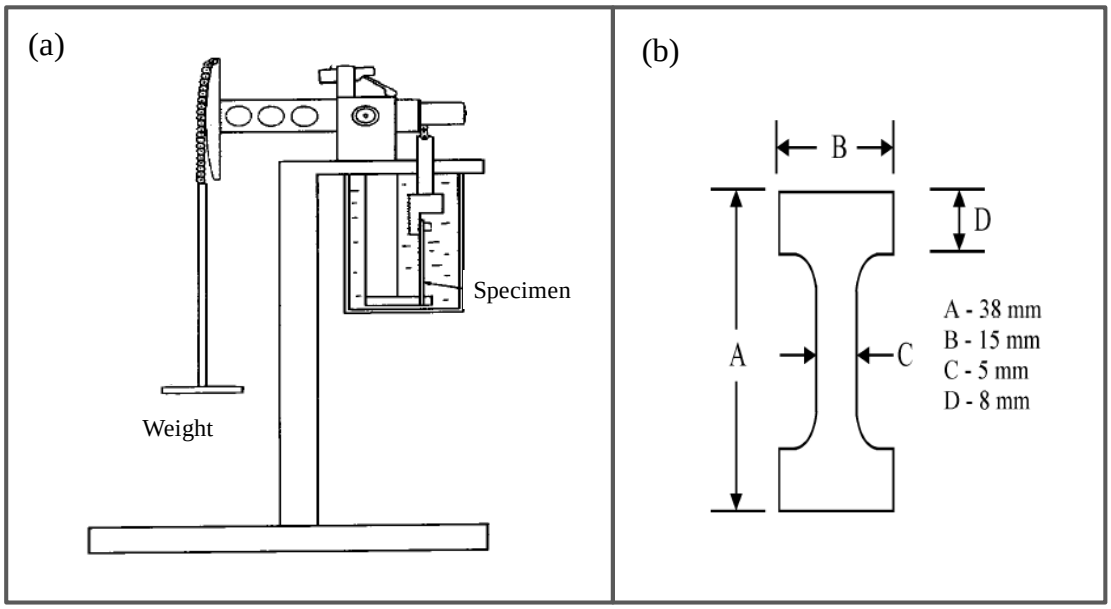

Figure 3.6: (a) NCLT apparatus schematic (12) (b) Specimen dimensions used for the NCLT (7)

3.3 RHEOLOGICAL PROPERTIES

Rheological properties are valid indicators of the molecular structure of polymers. These properties are extremely useful for cases where subtle structural differences (such as branches) between polymers are not distinguishable with conventional techniques (i.e., GPC). In this work, rheological properties of PEs were obtained, through different rheological methodologies, to identify melt indicators for an indirect measure of the extent of entanglements, responsible for ESCR. Rheological characterizations were conducted in shear, using an oscillatory rheometer, and extension, using an extensional rheometer. Specific attention was given to the average characteristic relaxation time (λ) from shear measurements, and extensional viscosity (η_{ext}) found from extensional measurements.

3.3.1 OSCILLATORY SHEAR TECHNIQUES

Oscillatory shear is a common characterization technique to measure linear viscoelastic (LVE) properties of polymers. An oscillatory rheometer applies a sinusoidal shear strain (γ) with amplitude of γ_o, according to Equation 3-8, and causes a sinusoidal shear stress (σ) with amplitude σ_o, that leads the strain by a phase angle (δ), as shown in Equation 3-9. In these equations, "ω" represents frequency.

$$\gamma(t) = \gamma_o \sin(\omega t) \tag{3-8}$$

$$\sigma(t) = \sigma_o \sin(\omega t + \delta) \tag{3-9}$$

A material is called a Hookean solid, if the phase angle between the dynamic stress and strain is zero (stress is in phase with strain). On the other hand, a material is called a Newtonian fluid if the phase angle is 90 º (stress is in phase with strain rate). The stress in oscillatory measurements can be expressed by the material's dynamic moduli, storage (G´) and loss (G´´) modulus, according to Equation 3-10. The storage module represents the elasticity of a polymer and is a measure of the ability of the polymer to store energy. The loss modulus represents the viscous behaviour of a material and is related to the ability of a polymer to dissipate energy. Addition of the dynamic moduli defines a complex modulus (G*), shown in Equation 3-11, which includes both effects of the viscous and elastic parts of the material. "i" in this equation is the imaginary number, which indicates that the storage modulus is out of phase with the loss modulus. The ratio between the loss and storage moduli is called the damping factor (or loss factor), with the usual symbol tan (δ). This ratio is a representation of the viscous and elastic portions of the viscoelastic deformation. For a perfectly elastic (viscous) material, G´´ (G´) is zero.

$$\sigma(\omega,t) = \sigma'(\omega,t) + \sigma''(\omega,t) = G'\gamma_o \sin(\omega t) + G''\gamma_o \cos(\omega t) \quad 3\text{-}10$$

$$G^* = G' + iG'' \quad 3\text{-}11$$

Other material properties such as zero shear viscosity (η_o) (Equation 3-12) and steady state compliance (Equation 3-13) can also be obtained from the dynamic moduli, as shown in the following equations.

$$\eta_o = \lim_{\omega \to 0}\left(\frac{G''(\omega)}{\omega}\right) \quad 3\text{-}12$$

$$J_{eq}^o = \frac{1}{\eta_o^2}\lim_{\omega \to 0}\left(\frac{G'(\omega)}{\omega^2}\right) \quad 3\text{-}13$$

One of the advantages of using oscillatory rheometry is the ability to obtain information about the rheological behavior of the material under different oscillatory modes. Temperature sweep measurements can be conducted over a wide range of temperatures and frequencies to provide information about the stability of the polymer. Strain sweep measurements, at a specific frequency, can also be performed to identify the linear viscoelastic region of the test. Furthermore, dynamic moduli, at a specific frequency, can be measured from a temperature sweep test (temperature changes at a specific rate). This provides moduli over a range of temperature. Utilizing the time-temperature superposition principle (13), the temperature value can be converted to a frequency domain. This is extremely helpful for cases where measuring the dynamic moduli at low frequencies are not possible.

In this work, oscillatory shear experiments and dynamic shear creep tests were performed on a TA Instruments AR2000 rheometer with parallel plate geometry. Samples were

compression-molded into 25 mm disks at 190 ºC and 44.5 kN, followed by quenching in cold water. Prior to frequency sweeps, strain sweeps between 0.1-100 % strains were performed at 100 Hz and 190 ºC to identify the linear viscoelastic region of the PE samples. Furthermore, time sweeps were conducted in order to identify any degradation or crosslinking during the frequency sweeps. The time sweeps were performed for 3 hours at 1 Hz and 1 % strain. A series of frequency sweep shear experiments were carried out at frequencies (ω) between 0.01-100 Hz under nitrogen to avoid any possible polymer degradation or crosslinking. Shear creep tests were also conducted at 190 ºC on compression-molded disks. Creep experiments were conducted at 10 Pa (linear viscoelastic region) for 3 hours. It should be noted that all the rheological experiments were independently replicated at least 3 times to ensure good reproducibility in the results. Independent replication is not frequently conducted in the literature.

3.3.2 CAPILLARY RHEOMETRY

One of the most common methods to characterize polymer behaviour at high shear rates is capillary rheometry. Traditionally, capillary rheometers have been used to determine shear viscosity and elasticity characteristics of viscous materials at high shear rates (14). This was more recently complemented with extensional viscosity through the work of Cogswell (15). The achievable high shear rates enable one to identify the polymer behaviour subjected to real processing conditions under extrusion or injection moulding. The design and operational principle of a capillary rheometer are conducive to providing rheological data under these unique processing conditions. The capillary rheometers are mainly composed of a capillary tube (die) of certain diameter and length connected to the bottom of a reservoir. Usually, a

piston (driven by a ram) is used to generate pressure on the polymer melt in the reservoir. Pressure drop and volumetric flow rate in the region of fully developed flow are used to determine the shear viscosity of the polymer. The polymer melt flow inside the capillary die is essentially identical to a simple pressure driven flow inside a tube (Poiseuille flow), as shown in Figure 3.7.

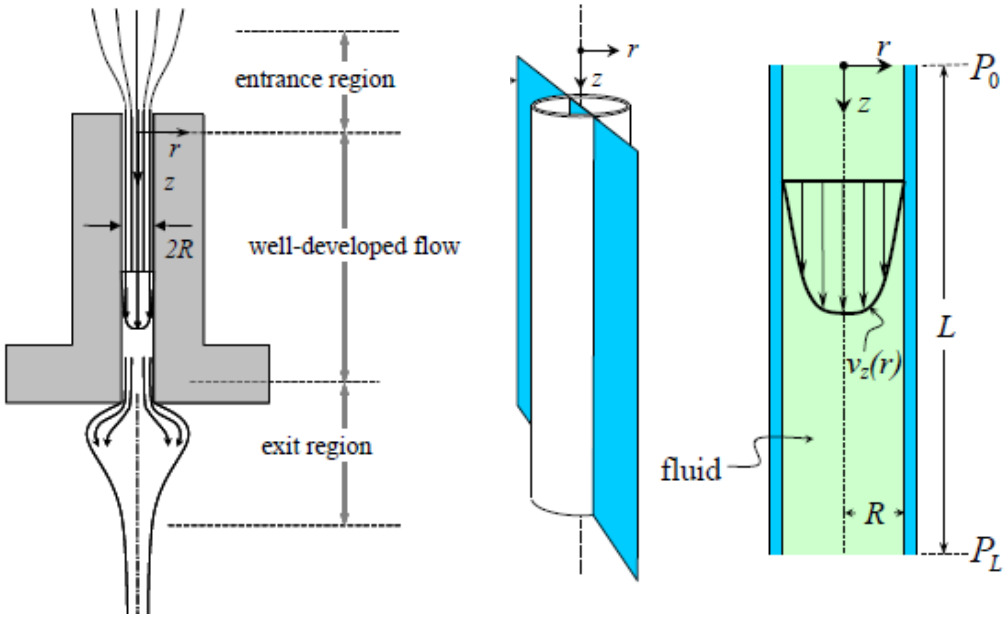

Figure 3.7: Fully developed fluid flow behaviour in a capillary die (16)

If it is assumed that the flow is laminar, fully developed, and at steady state conditions, Equation 3-14 can be developed for the velocity profile ($u(r)$) of a Newtonian fluid inside a tube as a function of "r" (obtained from the Navier-Stokes equations). In this equation, R is the radius of the capillary die, L is the length of the die, ΔP is the pressure drop, and η is the viscosity of the polymer. If it is further assumed that the fluid has constant viscosity (η), the shear stress at the tube wall (τ_W) is obtained by differentiating Equation 3-14 with respect to the radius of the tube (R), and multiplied by the viscosity (η) of the fluid, as shown in

Equation 3-15. The shear rate ($\dot{\gamma}$) in a capillary rheometer for a Newtonian fluid is further related to the volumetric flow rate (Q) and the radius of the tube as shown in Equation 3-16.

$$u(r) = \frac{(\Delta P)R^2}{4\eta L}\left(1 - \left(\frac{r}{R}\right)^2\right) \quad 3\text{-}14$$

$$\tau_W = \frac{(\Delta P)R}{2L} \quad 3\text{-}15$$

$$\dot{\gamma} = \frac{4Q}{\pi R^3} \quad 3\text{-}16$$

The pressure drop (ΔP) is found from the Hagen-Poiseuille law for pressure driven flow of Newtonian fluids inside a tube according to Equation 3-17.

$$\Delta P = \eta L \, \frac{8Q}{\pi} \, R^{-4} \quad 3\text{-}17$$

The non-Newtonian behaviour of polymer melts in the capillary experiments requires corrections to the aforementioned equations. Entrance and exit pressure drops, wall slip, and a non-parabolic velocity profile are mainly the reasons for the need of such corrections. When capillaries are relatively short (L/R < 40), the Bagley correction (n_B) is necessary to account for the excess pressure drop (ΔP_e) at the capillary entry. Therefore, a Bagley corrected stress (true shear stress,$\tau_{W,true}$) at the capillary tube wall would have the form presented in Equation 3-18. A Rabinowitsch correction will further be applied to correct for the shear thinning behaviour of the polymer. The true shear rate ($\dot{\gamma}_{true}$) is related to the power law index of the polymer (n) and the apparent shear rate ($\dot{\gamma}_{apparent}$), according to Equation 3-19. In this equation, Q and R are the fluid volumetric flow rate and the tube

radius, respectively. The viscosity of the polymer is subsequently found by dividing the true shear stress by the true shear rate.

$$\tau_{W,true} = \frac{\Delta P + \Delta P_e}{2\left(L/R\right) + n_B} \quad 3\text{-}18$$

$$\dot{\gamma}_{true} = \left(\dot{\gamma}_{apparent}\right) \times \frac{3n+1}{4n} = \left(\frac{4Q}{\pi R^3}\right) \times \frac{3n+1}{4n} \quad 3\text{-}19$$

A bench top twin bore Rosand capillary rheometer (RH2200 series) manufactured by Malvern was used to measure the shear viscosity and entrance pressure drop. Due to the twin bore option, simultaneous measurements were made using a long die and a zero length die. The long die was used to determine shear properties, while the zero length die provided the entrance pressure drops due to the sudden barrel contraction (between the capillary reservoir and capillary die). In order to identify the entrance pressure drop at various shear rates, three different pressure transducers were used. A 250 psi and a 1500 psi transducer were separately attached to the bore (reference bore) equipped with the zero length die (orifice) to measure the entrance pressure drops. A 5000 psi transducer was attached to the sample bore, equipped with the long die to measure the shear viscosities at various shear rates. Ultimately, the entrance pressure drops obtained from the reference bore were used to correct the applied stress data (reflected on the viscosity measurements).

3.3.3 SENTMANAT EXTENSIONAL RHEOMETRY

A Sentmanat extensional rheometer (SER) is composed of many parts, including paired equal-dimension wind up drums, with intermeshing gears (17). The rotation of the drum shafts causes the drums to rotate in opposite directions. The ends of a sample are secured to

the drums using clamps. For a constant rotation rate (Ω), the Hencky strain rates obtained from the rheometer are found from Equation 3-20 (17). In this equation, R is the radius of the drums, and L_o is the unsupported gauge length of the sample, being stretched. The instantaneous area of the sample can also be measured from the applied Hencky strain rate, according to Equation 3-21 (17). A_o in this equation is the initial cross sectional area of the un-stretched specimen. Finally, the stress growth function (transient extensional viscosity) can be calculated from the ratio shown in Equation 3-22 (17). F(t) in this equation is the instantaneous force exerted by the sample as it is stretched (recorded by the torque transducer).

$$\dot{\varepsilon}_H = \frac{2\Omega R}{L_o} \qquad 3\text{-}20$$

$$A(t) = A_o exp(-\dot{\varepsilon}_H t) \qquad 3\text{-}21$$

$$\eta_{ext} = \frac{F(t)}{\dot{\varepsilon}_H A(t)} \qquad 3\text{-}22$$

In this study, the transient uniaxial extensional viscosity, η_{ext}, was determined at 150 ^oC and 190 ^oC on a Sentmanat Extensional Rheometer SER-HV-A01 model attached to an ARES 2000 rotational rheometer. The extensional rheology specimens were prepared by compression molding PE pellets to create thin sheets. The sample width was fixed at 12.7 mm (prepared by a calibrated dual blade cutter) and the thickness was 0.65 mm (measured precisely before each test by a micrometer). Maximum Hencky strains of up to 5.6 can be achieved with this instrument.

3.4 TYPES AND PROPERTIES OF RESINS

A total of 18 polyethylene resins were selected for this research project. These resins included four rotational molding grade LLDPE type resins, and fourteen HDPEs. Selected HDPE resins consisted of three rotational molding grades, one injection molding grade, four blow molding, and six pipe resins (two PE 80, and four PE 100 type pipe resins). These resins were selected in order to cover a wide range of molecular structures and ESCR values, to develop a more clear understanding of potential relationships between important molecular structural characteristics and ESCR.

Table 3.1 lists a number of resin properties obtained from the resin manufacturers. The pieces of information given in this table are typical values reported for commercially available resins. This information is limited and needs major updates for a better understanding of the effect on ESCR of resin molecular (microstructural) properties. Throughout this thesis, Table 3.1 will be progressively updated in order to have a better understanding of the relationships between major molecular properties and ESCR. Eventually, a complete mapping of molecular structure vs. ESCR through different practical prescriptive tips will be presented in Chapter 8, where a relative comparison of ESCR values among different resins is available. “Blind tests” will be conducted on unknown resins to show and confirm the validity and the extent of the work done in this research project.

Table 3.1: PE resins used in this research project

Polymer ID	PE grade	Density (kg/m^3)	MFI[a] (g/10min)	Tensile Y.S.(MPa)	Elongation at yield (%)	ESCR[b] (h)
LLDPE 1	R.T.[1]	936	6.8	17.2	18.0	60
LLDPE 2	R.T.	938	3.3	18.0	20.0	150
LLDPE 3	R.T.	937	5.0	18.0	20.0	190
LLDPE 4	R.T.	932	5.2	15.0	20.0	650
HDPE 1	R.T.	948	5.0	23.4	15.0	8
HDPE 2	R.T.	942	2.0	20.3	16.0	50
HDPE 3	Pipe-100[2]	958	---	29.9	---	1000
HDPE 4	Pipe-100	955	---	29.9	---	3000
PE 4	I.M.[3]	948	5.0	23.3	48.0	18
PE 8	Pipe-80[4]	958	---	30.2	---	>500
P1	B.M.[5]	948	7.0**	24	10.0	500
P2	B.M.	957	0.2	29	8.0	40
P3	B.M.	954	0.3	25	9.0	300
P4	B.M.	965	0.7	32	7.0	15
P5	Pipe-100	959	0.25*	25	2.0	>1000
P6	Pipe-100	948	0.25*	25	2.0	>5000
P7	Pipe-80	951	0.85*	19	---	2000
P11	R.T.	---	---	---	---	21***

a: Melt flow index measured at 190 ºC and 2.16 kg (unless otherwise specified), * MFI measured at 190 ºC and 21.6 kg, ** MFI measured at 190 ºC and 5.0 kg, b: ESCR reported from a Bent Strip Test (BST) according to ASTM D1693A,*** ESCR measured from a Notch Constant Load Test according to ASTM D5397, 1: Rotational molding grade PE, 2: PE100 grade pipe resin, 3: Injection molding grade PE, 4: PE80 grade pipe resin, 5: Blow molding grade PE.

4 CHAPTER 4: INFLUENCE OF MOLECULAR PROPERTIES ON ESCR THROUGH A MODIFIED TENSILE TEST

4.1 INTRODUCTION

The term environmental stress cracking resistance (ESCR) was first used in the context of polyethylene cable insulations (1). Environmental stress cracking (ESC) of polyethylene occurs when the polymer is subjected to an aggressive environment (fluids such as water, detergents, and oils) under stresses much lower than the polymer yield stress. The failure of PE under such conditions is characterized by clean cracks, indicating involvement of a brittle fracture mechanism. The brittle fracture mechanism starts from defects (stress concentrating points), introduced during processing and installation, followed by a slow crack growth mechanism which consequently gives rise to premature catastrophic failure. This mode of failure is characterized by the presence of macroscopic cracks preceded by crazed fibrillar structures (2).

Micromolecular properties such as molecular weight (MW), molecular weight distribution (MWD), short chain branching (SCB) content and inter-lamellar links, including the bridging tie-molecules and physical entanglements, have received the most attention due to their closely associated relations with ESC (3). Tie molecules, long polymer chains which connect crystal lamellae through the amorphous phase, have been linked to ESCR of PE. This idea was introduced by Brown and Ward (4-5) where they theorized models for formation of tie-molecules with respect to the end to end distance of the polymer chain. Similarly, it has been reported that separation of lamellae, either by disentanglement or rupture of the tie molecules, is the main molecular mechanism for ESC of polyethylene. Sharif et al. (2) used a

model developed by Huang and Brown (17) for evaluation of slow crack growth in PE based on the density of tie-molecules. This model was further improved by Seguela (6) to calculate the overall area fraction of tie-molecules at the crystal–amorphous interface. Consequently, researchers used criteria related to the presence of tie-molecules to describe the effect of several polymer micromolecular variables on ESCR, mainly molecular weight, short chain branching, and processing conditions.

Huang and Brown (7) developed an equation to correlate the fraction of tie-molecules area in the amorphous region to weight-average molecular weight of the polymer. They obtained a molecular weight critical value above which tie-molecule formation is possible. Similarly, in another study by Lu et al. (8) it was concluded that a molecular weight greater than $1.5 \times l0^6$ is required to create the proper density of tie-molecules necessary to produce high resistance to slow crack growth. This means that the ESCR of PE increases as weight-average molecular weight of PE increases, since the tie-molecule concentration is increased (9).

Incorporation of small amounts of comonomers such as 1-butene or l-hexene creates short chain branching in PE. Researchers have investigated the effect of length and frequency of the SCB on ESCR. Yeh et al. (10) found an increase in the time of failure by 10,000 times when the short chain branch frequency was increased from 0 to 4.6 branches/1000 carbons. Several others have similarly reported that because SCB is responsible for the noncrystallizable sections of the polymer chains, an increase in SCB will enhance the probability of tie-molecule formation. It is further reported that higher concentration and length of SCB provide better brittle fracture resistance since the portions of polymer chains with the longer branches add to the inter-crystalline tie-molecules (11).

Cheng et al. (12) in a detailed study on the effects of microstructure on creep characteristics have investigated the effect of lamella thickness on the ESCR properties of high density polyethylene (HDPE). They observed that lamella thickness is inversely related to ESCR between PE samples that have similar MW. They also correlated the lamella surface area with ESCR of PE resins and found an increasing trend in ESCR with increasing lamella lateral surface area. They postulated that larger lamella surface area increases the probability of occurrence of more inter-lamellar linkages, hence improving the ESCR.

Various types of techniques have been utilized to assess the ESCR of polymers. The bending beam test and other tensile tests such as creep rupture and monotonic creep have been extensively used in industry (1). These tests mainly involve the application of constant flexural and unidirectional tensile loads to polymer specimens and the time to failure is recorded. One major problem with these types of test is the long period of testing. Accelerated tensile testing such as the notch constant load test (NCLT) and best strip tests (BST) were developed to compensate for the long testing periods. In these techniques, failure is accelerated to shorter times by introducing a notch in the test specimens, and by performing the test at elevated temperature. Other techniques such as the full notch creep test (FNCT), the Pennsylvania notch test (PENT), and the notched pipe test (NPT), were further introduced and used in industry (13). The typical ESCR testing methods mentioned above are time consuming and rather unreliable. The difficulty involved with such testing methods is mainly the poor reproducibility and large subjective errors due to specimen preparation, notching process, and surfactant quality. Consequently, development of alternative testing methods is required to overcome the aforementioned issues.

Kurelec et al. (14), first, and subsequently Cheng et al. (15) proposed new methodologies for evaluation of ESCR based on the "strain hardening" behaviour of PE resins under uniaxial tensile testing. Both groups were inspired by the work of O'Connell et al. (16) where a uniform relationship between the creep rate deceleration and growth of fibrillar crazes in fully drawn polymer was obtained. This relationship indicated that the creep of fibrils within the craze is the determining factor in slow crack growth (SCG) of PE resins (14). During strain hardening, the polymer chain entanglements are fully drawn to their limit and the polymer hardens. This behaviour is quantified by the strain-hardening modulus, the slope of the line in the strain hardening section of the stress-strain curve during tensile testing. It has been shown that PE with a greater number of entanglements exhibits higher strain hardening and has a higher ESCR.

Kurelec et al. (14) attempted to relate the ESCR of HDPE to the slope of the strain hardening part of a stress–strain curve, at elevated temperature (80 ^{o}C). They demonstrated that the amount of strain hardening at elevated temperatures is strongly dependent on molecular differences, leading to variation in ESCR performance. The average slope of the strain hardening section, the so called "strain hardening modulus", obtained from true stress and strain values, was found to be sensitive to the same molecular differences that govern the slow crack resistance in HDPE. Therefore, it was concluded that comparison between the strain hardening modulus of PE resins is indicative of the long term behaviour of PE.

Cheng et al. (15) proposed perhaps a more practical test where uniaxial tensile tests were performed at room temperature. As compared to the Kurelec et al. (14) approach, where true stress and strain measurements were needed for evaluation of the strain hardening modulus, their method does not require any special equipment and can be readily carried out on any

tensile tester (9). The measured slope from the strain hardening section of their test was called the "hardening stiffness (HS)", in order to distinguish the variable from the conventional definition of stiffness of the material (related to Young's modulus). They postulated that their strain hardening test method is more reliable and could potentially replace the noisier conventional ESCR testing methods.

In this chapter, it is attempted to extend the validity of HS to linear low density polyethylene (LLDPE) and other grades of HDPE to determine the adaptability of the HS test to different grades of PE with various levels of ESCR. It was postulated that selecting a wider range of PE will make it possible to determine the exact nature of the relationship between HS and ESCR. Further, it is attempted to identify optimal specimen dimensions and rate of testing for a more promising, practical, and conclusive prediction of HS, and hence, ESCR. Specimens from different PE resins with different width, thickness, and gauge length were tested at various strain rates. It is intended to identify the test specimen dimensions and rate which amplify the effect of molecular structure (mainly molecular weight and short chain branching) on hardening stiffness, increase sensitivity, and reduce variability of the test for better reflection of ESCR of PE resins.

4.2 EXPERIMENTAL

4.2.1 MATERIALS

In this study, a range of commercially available rotomolding and pipe grades of LLDPE and HDPE were selected. These resins were selected according to their ESCR values, reported in their product data sheets. The ESCR values were reported from a bent strip test (BST) according to ASTM D 1693A (10 wt-% Igepal, 50 ^{o}C). The objective was to select resins that

offered ESCR values between 8 and ≥1000 hours. The resin material properties are summarized in Table 4.1.

Table 4.1: PE resin properties used in this study

PE ID	Type	Density (kg/m^3)	MI (g/10 min)[a]	Mn (kg/mol)	Mw (kg/mol)	Mz (kg/mol)	PDI	SCB[b]
LLDPE 1	R.M*	936	6.8	15.4	71.8	252.0	4.65	4.2
LLDPE 2	R.M	938	3.3	20.8	82.0	232.0	3.94	7.5
LLDPE 3	R.M	937	5.0	18.0	74.6	191.0	3.98	13.3
LLDPE 4	R.M	932	5.2	15.1	76.6	286.0	5.08	22.3
HDPE 1	R.M	948	5.0	18.7	77.9	349.0	4.17	1.6
HDPE 2	R.M	942	2.0	25.24	118.5	336.0	4.70	2.4
HDPE 3	Pipe	958	----	10.4	217.9	1244.2	20.90	7.0
HDPE 4	Pipe	955	----	5.9	315.4	2129.3	53.30	11.8

*: Rotational moulding, a: Melt index at 190 ºC, 2.16 kg, b: Short chain branching (per 1000 carbon atoms)

4.2.2 MOLECULAR CHARACTERIZATION

Chemical properties of molecular weight averages and molecular weight distribution were evaluated by gel permeation chromatography (GPC) in a high speed GPC from Polymer CHAR (Spain), equipped with an Agilent injection pump. The solvent and operating temperature were 1, 2, 4 trichlorobenzene (TCB) and 140 ºC, respectively. An AVANCE 500 Bruker NMR was utilized to investigate the short chain branching content of the PE resins at 120 °C. The solvent of choice was deuterated TCB

4.2.3 TENSILE TEST

The tensile tests were performed at room temperature on an Instron 3365 machine. The specimens were prepared by punching compression moulded plaques prepared at two different processing conditions:

Condition 1: Compression molding at 195 ºC±5 ºC and 44.5 kN. The plates were allowed to cool down in the mold at room temperature over a period of 24 hours.

Condition 2: Compression molding at 195 ºC±5 ºC and 44.5 kN, followed by cooling to room temperature at a rate of 1 ºC/min, while increasing the pressure to 89 kN.

The HS was obtained by measuring the slope of the strain hardening section of the load-displacement curve. The test specimens were extended until complete failure was obtained.

4.2.3.1 EXPERIMENTAL DESIGN FOR TENSILE TEST

Two experimental designs were adopted in this study. The first experimental design, a D-optimal factorial design, was selected to investigate the significance of specimen dimensions, strain rate, and the molecular weight of PE resins on HS (D-optimal designs are mainly used to fraction general factorial experiments (lower number of experiments)). The algorithm selects points that minimize the volume of the confidence ellipsoid (joint confidence region (JCR)) for the model coefficients by maximizing the determinant of the X´X matrix (X being the process matrix), in order to provide the most accurate estimates. Three levels of strain rate, specimens' thickness, gauge length and width were selected and tensile tests were performed on three different HDPE resins, as indicated in Table 4.2. A total of 60 uniaxial tensile experiments according to the D-optimal design were performed on a variety of specimen's dimension of which, 50 were used for model prediction, and 10 for evaluation of residuals (lack of fit and pure error).

Table 4.2: Experimental design to investigate Mw, specimen's dimension, and strain rate effect on HS1

Study Type: Factorial Design Model: 2FI[a]	Design Type: D-optimal Runs: 60		
Factor	Levels		
Mw[b] (kg/mol)	118	218	315
Strain rate (mm/min)	0.5	5	10
Gauge Length (mm)	16	33	60
Width (mm)	3	6	12
Thickness (mm)	0.6	1.8	3

1: HDPE 2-4 were used for this analysis, a: two factor interaction, b: weight-average molecular weight

The second experimental design included a completely randomized central composite design (no blocks, face centered) on three LLDPE resins to investigate the sensitivity of HS to short chain branching content. The tensile tests were performed at different strain rates according to Table 4.3.

Table 4.3: Experimental design to investigate the significance of SCB on HS[1]

	Type	SCB[a]	Strain Rate (mm/min)	SCB/ 1000 C	Strain Rate (mm/min)
1	Center	0	0	13.25	2.55
2	Axial	0	0	13.25	0.1
3	Factorial	+1	+1	22.3	5
4	Center	0	0	13.25	2.55
5	Axial	+1	0	22.3	2.55
6	Factorial	+1	-1	22.3	0.1
7	Factorial	-1	+1	4.2	5
8	Axial	0	+1	13.25	5
9	Center	0	0	13.25	2.55
10	Center	0	0	13.25	2.55
11	Factorial	-1	-1	4.2	0.1
12	Axial	-1	0	4.2	2.55
13	Center	0	0	13.25	2.55

1: LLDPE 1, 3-4 were selected for this analysis, a: short chain branching per 1000 carbon atoms

4.2.4 NOTCH CONSTANT LOAD TEST (NCLT)

The NCLT was utilized to identify the ESCR properties of the PE resins according to ASTM D5397 58. In this test, specimens were subjected to constant load under an aggressive environment. A notch was introduced in the sample and the test was performed at elevated temperature to accelerate the failure mechanism involved in the slow crack growth of PE. The depth of the notch should produce a ligament thickness of 60 % of the nominal thickness of the specimens. The notched specimens were suspended in 10 % surface-active agent (surfactant) with 90 % water at 50 ºC. The time of failure was recorded by an automatic timing device attached to the loaded lever. The surfactant in this test was Igepal nonyl phenol ether glycol ($C_{19}H_{19}$-C_6H_4-O-$(CH_2CH_2O)_8$-CH_2CH_2OH) purchased from Sigma Aldrich. In order to guarantee a brittle fracture, the stress was 15 % of the yield stress of the PE resins.

4.3 RESULTS AND DISCUSSION

4.3.1 EFFECT OF MOLECULAR PROPERTIES ON ESCR OBTAINED BY NCLT AND BST

ESCR results obtained from the NCLT and BST are shown in Table 4.4 (other columns of this table will be discussed in later subsections). The ESCR values reported in Table 4.4 for NCLT are mean values over several replicates (15-20 independent replicates). Although both NCLT and BST tests are used to measure the failure time of plastics under an aggressive environment, they are fundamentally different from each other. During an NCLT experiment, a constant load (15 % of resin's yield strength) is applied to notched samples, and time to a complete failure is measured. On the other hand, BST applies a constant deformation to notched polymer samples and time to failure (50 or 100 % failure or creation of crack) is recorded. As a result, deviations in reported ESCR values from both tests were expected. In this study, however, the deviations between the measured ESCR from the two tests were large. This deviation was clearly obvious for LLDPE resins, especially for resins with higher SCB content, but considerably lower for HDPE, especially for resins experiencing either very high or very low ESCR. Figure 4.1 and Figure 4.2 represent the effect of Mw and SCB on ESCR of HDPE resins obtained from both NCLT and BST. Despite the differences between the reported ESCR values by the two tests, ESCR of HDPE showed the expected (correct) trend and increased with Mw. On the other hand, no correlation between the SCB content and the ESCR of the resins was obtained as shown in Figure 4.2, alluding to the domination of Mw on the ESCR of HDPE. This behaviour was completely reversed for LLDPE as shown in Figure 4.3 and Figure 4.4. No correlation between Mw and ESCR was found as ESCR of LLDPE 2 was lower than LLDPE 3-4. A trend between the SCB and ESCR of the LLDPE

resin obtained from the BST was found, indicating the dominance of SCB of the LLDPE when relatively similar LLDPE (in terms of Mw) are compared. The inconsistency in Figure 4.4 between the ESCR values of BST and NCLT suggested the lack of sensitivity of the NCLT to subtle differences in molecular structure such as SCB and molecular weight differences (especially Mz). Further, it was suggested that the test condition for the NCLT may have been too harsh (notch depth of 40 % of nominal thickness) for the LLDPE resins and thus caused premature failure. Because of the constant applied strain in BST, HDPEs with various densities (as a result of different crystallinities) and hence different stiffness can be subjected to much higher applied loads than needed for the test. This tends to develop heterogeneous crack initiation and propagation, resulting in a premature failure of the HDPE (as was the case for HDPE 2). LLDPE on the other hand, due to lower stiffness, performs well when subjected to BST as crack initiation and growth are relatively smoother and more homogeneous. Therefore, NCLT should be considered for HDPE and BST for LLDPE, when ESCR conventional testing methods are required. It should be noted that the aforementioned suggestions need to be confirmed by performing through microscopic methodologies on the fracture surface of the resins. This however, was not performed in this study as it was not the main focus of this work.

Table 4.4: PE molecular characteristics used in this study

PE ID	ESCR by NCLT (h)[a]	St. Dev (h)[b]	ESCR by BSR (h)[c]	HS (N/mm)	St. Dev (N/mm)	cHS (N/mm)[d]
LLDPE 1	12.00	1.53	60	0.249	0.012	2.68
LLDPE 2	57.10	6.73	150	0.336	0.007	7.38
LLDPE 3	22.63	3.96	190	0.269	0.001	9.53
LLDPE 4	180.00	67.20	650	0.300	0.005	18.3
HDPE 1	8.36	2.09	8	0.214	0.002	0.95
HDPE 2	27.19	9.30	50	0.352	0.002	1.34
HDPE 3	872.10	338.00	1000	0.536	0.009	29.20
HDPE 4	3000	---	1000	0.550	0.015	73.11

a: Notch constant load test (performed in our laboratories, sample preparation according to condition 1), b: Standard deviation, c: Bent strip test (performed by industrial partner), d: Corrected HS

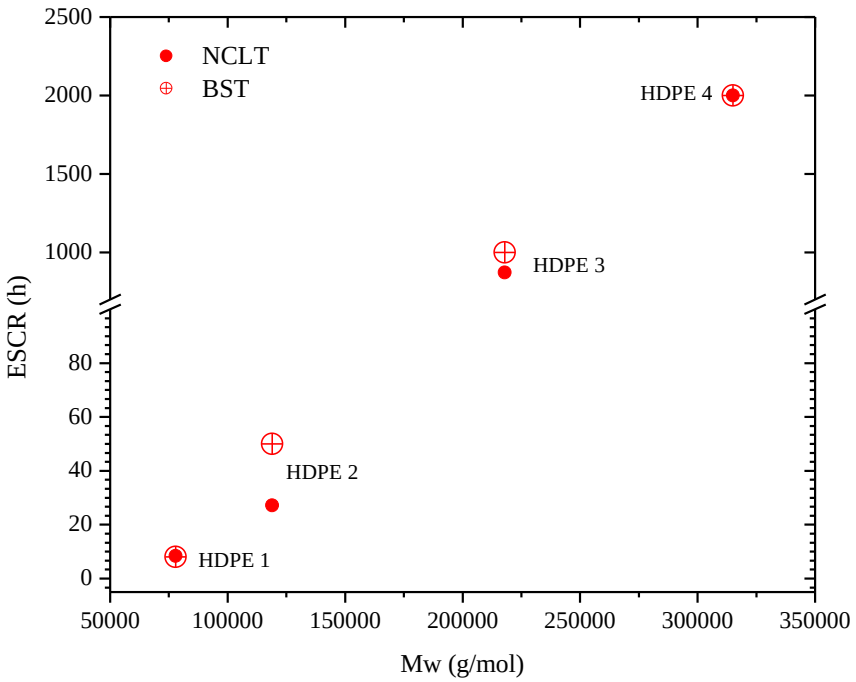

Figure 4.1 Effect of Mw on ESCR obtained from both NCLT and BST

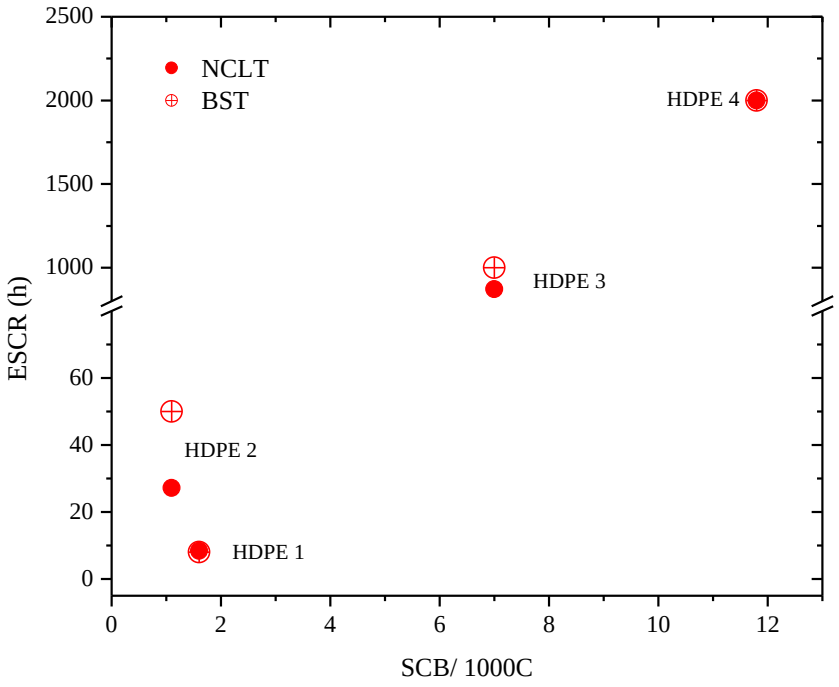

Figure 4.2: Effect of SCB on ESCR obtained from both NCLT and BST

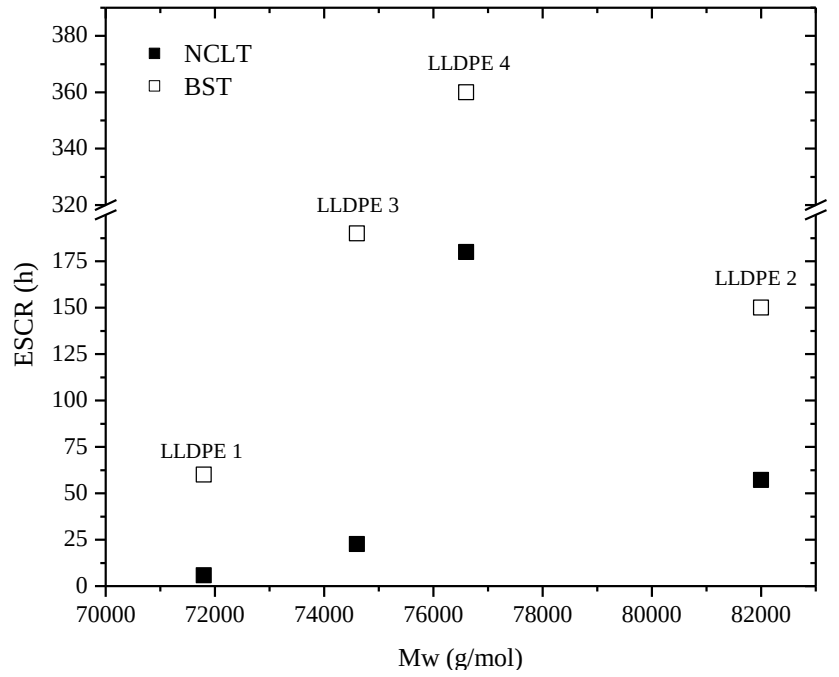

Figure 4.3: Effect of Mw on ESCR of LLDPE resins

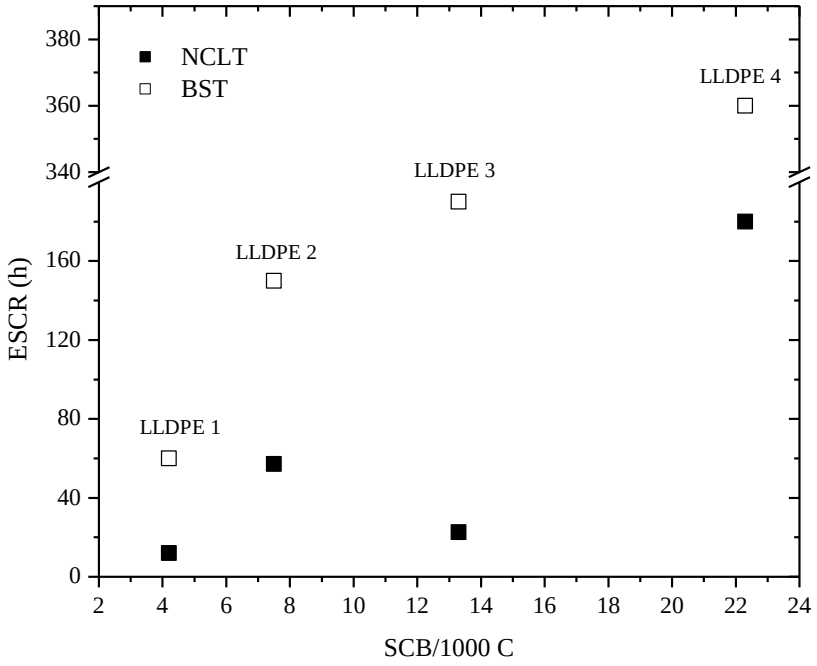

Figure 4.4: Effect of SCB on ESCR of LLDPE resins

4.3.2 EVALUATION OF SPECIMEN'S DIMENSIONS AND STRAIN RATE ON HARDENING STIFFNESS

In this study, it was intended to identify the effects of specimen's dimension and strain rate on hardening stiffness of the PE resins. This was done in order to create a more practical and informative tensile test for the evaluation of HS. An experimental design according to the factors of Table 4.2 was constructed and tensile tests at different strain rates were performed on specimens with different dimensions and molecular weights. It should be noted that the lower range of gauge length was limited to the lowest possible distance between the tensile tester grips. Similarly, the range of thickness was limited to the availability of the molds. These selected ranges, however, cover most of the ASTM allowable dimensions for tensile testing, and hence were selected in this study. Results from the tests were analyzed using DesignExpert8 software to identify the significance of the design variables and their possible

interactions. Table 4.5 shows the ANOVA (Analysis of Variance) for this factorial design (only the significant terms are shown). The model F-value was 162.48 implying that the model is significant. P-values less than 0.01 indicated that the model terms are significant. In this case, Mw (A), strain rate (B), width (D) and thickness (E), along with some of their interactions (AE, DE) were found to be the significant factors. Gauge length had no significant effect on the HS. This was anticipated as dog bone shaped specimens that are subject to uniaxial load have uniaxial stress normal to the cross-sectional plane (thus verifying the significance of width and thickness). The width and thickness used in this study refer to the original dimensions of the specimens before loading begins. All significant main factors had a positive relationship with HS, from which, molecular weight, thickness, and width were the most significant ones. It was postulated at this point that in order to amplify the effect of molecular structure (Mw, SCB, etc.) on HS, the effect of specimen's dimensions, namely, thickness and width, should be minimized. Further, the strain rate and gauge length should be properly selected to make the test easier, faster, and more practical. The effect of thickness and width (the interaction plot obtained at highest Mw and strain rate) on HS is shown in Figure 4.5. As the thickness of the specimens increases, the effect of width on HS becomes more pronounced. This trend suggested that a thickness of 0.6 mm should be selected in order to minimize the effect of width on HS, for widths between 3-6 mm (slope of the line represents the effect on HS). If the width of the specimen is selected between 6-12 mm, then thicknesses between 0.6-1.8 mm should be selected to minimize the effect of width on HS (where slope is the lowest). Figure 4.6, similarly shows the relationship between HS and Mw at various specimens' widths (the figure was constructed at highest strain rate, and lowest thickness and gauge length). The idea was to select the condition at which the

effect of Mw on HS is maximized. The slope of the lines for widths of 6-12 mm is very similar, suggesting that any width selected in that range would maximize the effect of Mw on HS, however, for simplicity and practicality of the test it is recommended to use lower values. Widths below 6 mm also reflect the effect of Mw on HS, however to a smaller extent. It should be noted that a minimum width to thickness ratio of 8 is recommended when constructing dog bone shaped specimens. In this study, it was decided to keep the thickness to its lowest value of 0.6 mm (to minimize the effect of width) and width to a value of 5 mm. Further, for practicality and ease of testing, it was decided to keep the gauge length at 16 mm (lowest value), and strain rate at 10 mm/min (highest rate). Figure 4.7 is a representation of this finalized test specimen. It should be mentioned that any width and thickness selection that follows the above mentioned criteria can be used (although it is recommended to use thinner specimens).

Table 4.5: ANOVA of effect of Mw, specimen's dimensions and strain rate on HS

Source	Sum of Squares	df[a]	Mean Square	F value	p-value	
Model	3.330	16	0.208	162.48	< 0.0001	Sig.*
A-MW	0.984	2	0.492	384.08	< 0.0001	
B-Strain rate	0.049	2	0.024	19.04	< 0.0001	
D-Width	0.956	2	0.478	373.27	< 0.0001	
E-Thickness	1.013	2	0.507	395.52	< 0.0001	
AE	0.024	4	0.006	4.76	0.0029	
DE	0.032	4	0.008	6.31	0.0004	
Residual	0.055	43	1.28E-03			
Lack of Fit	0.054	39	1.38E-03	4.93	0.0647	not sig.
Pure Error	0.001	4	2.81E-04			
Total	3.385	59				

a:degree of freedom, * Significant

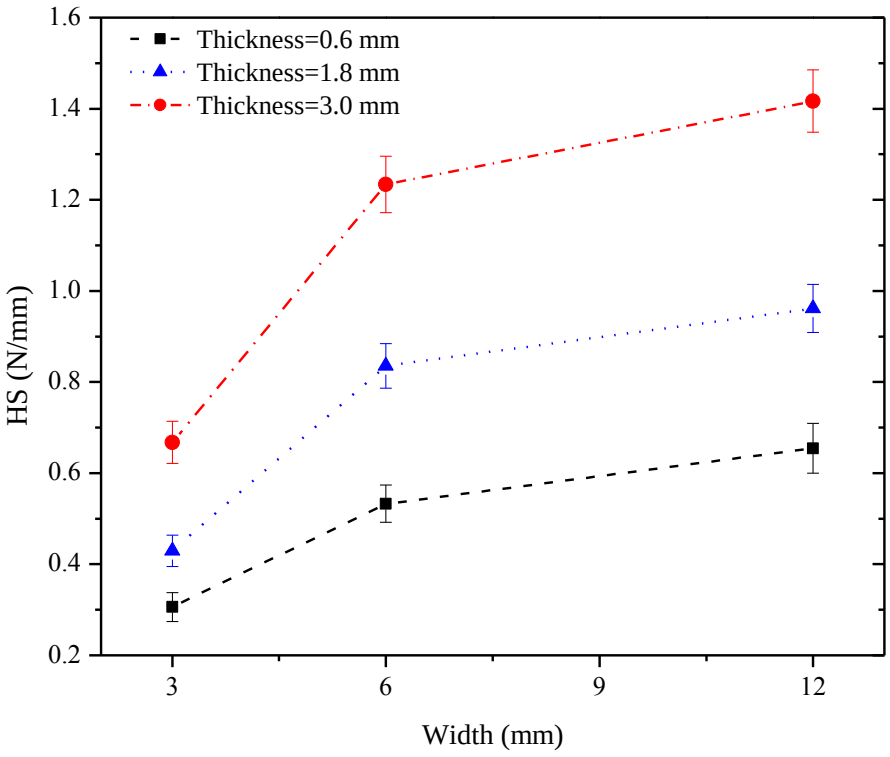

Figure 4.5: Effect of width on HS at various thicknesses (factor levels: Mw=218 kg/mol, strain rate= 10 mm/min, gauge length= 16 mm)

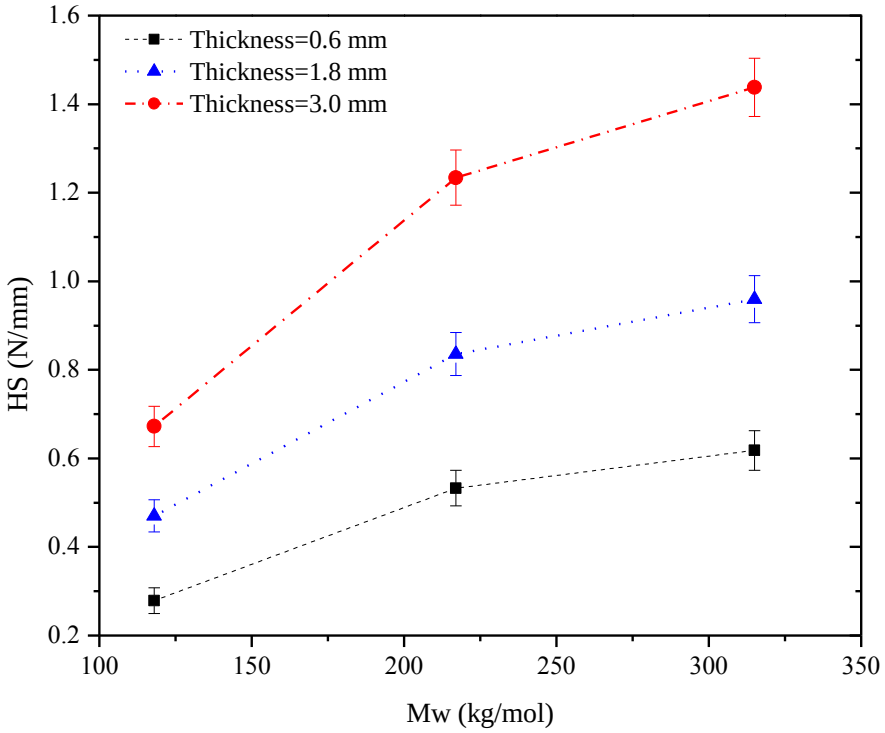

Figure 4.6: Effect of Mw on HS at different widths (factor levels: strain rate= 10 mm/min, gauge length= 16 mm, width= 6 mm)

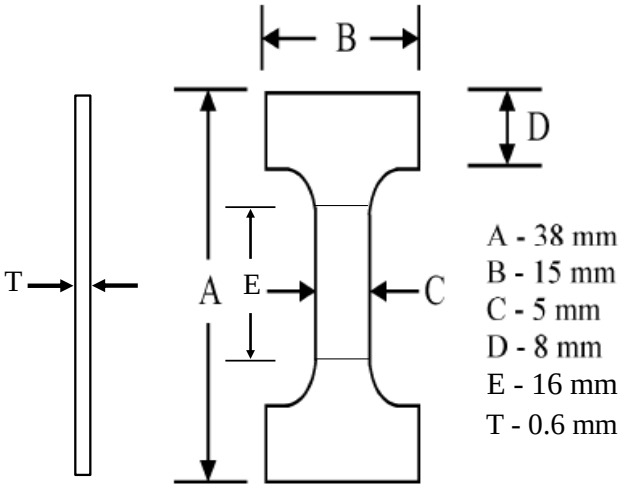

Figure 4.7: Specimens' dimensions used in this study

4.3.3 HARDENING STIFFNESS AND ESCR OF RESINS

Cheng et al. (9, 15) performed studies on different HDPE resins and developed a correlation between the ESCR obtained from NCLT and HS. In their study, higher HS (as a result of higher Mw, SCB, PDI, etc.) corresponded to a higher ESCR. ESCR was further related to the existence of a larger extent of inter-lamellar chain entanglements which have a direct relationship with the aforementioned molecular properties. In this study, HS data obtained from tensile testing on specimens designed in the previous section of this study (Figure 4.7 at a strain rate of 10 mm/min) are shown in Table 4.4. In Figure 4.8, the HS values are plotted against the corresponding ESCR values of the HDPE resins. As expected, there exists an increasing trend in HS as ESCR values increase, representing a higher resistance of the polymer in question towards slow crack growth. This trend verified, once again, that the hardening stiffness can be used as a measure of ESCR of HPDE resins. Compared to Cheng et al. (15), HS values obtained in this study were recorded in a more practical, reproducible, and reliable fashion (low standard deviations as reflected in Table 4.4 and Figure 4.9). It is also believed that the effect of molecular structure is more readily reflected on HS due to the previously established minimization of the effect of specimens' dimension (shape) on HS.

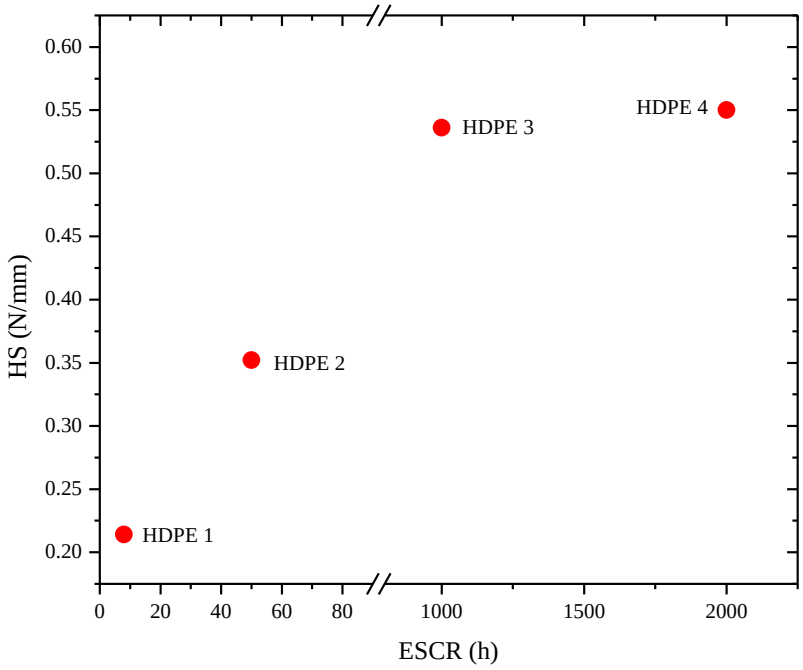

Figure 4.8: HS versus ESCR for HDPE resins

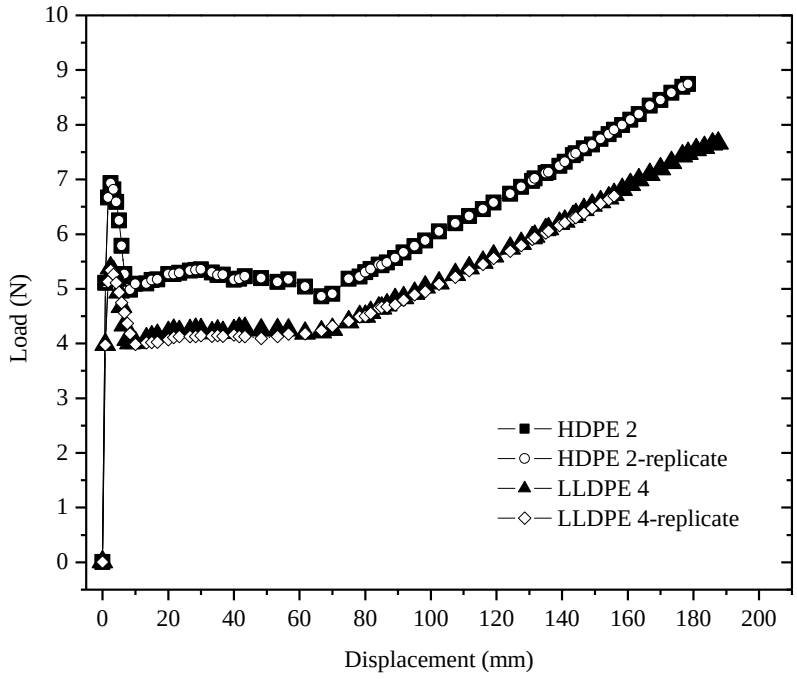

Figure 4.9: Load vs. displacement graph showing the reproducibility of the test (performed on specimens shown in Figure 4.7, at 10 mm/min strain rate)

The analysis was further applied to LLDPE. It was speculated that the values of HS for LLDPE resins are very similar to each other. For this reason, Fisher's least significant difference (LSD) test was performed to look into the minimum difference between the HS means, which represent a significant difference. The LSD was found to be 0.045 N/mm. This meant that there was no significant difference between the HS values of LLDPE 1, 3, and 4. This result triggered speculations that HS is mainly a reflection of the Mw of LLDPE, rather than a combination of other molecular structural characteristics (Mw, SCB, etc.). Since these three resins have very similar molecular weight properties, their HS was found to be indistinguishable, thus raising a possible caution with the HS test. It was further postulated that the selected test condition (mainly strain rate), was not properly selected to identify the effect of SCB on HS, and hence on ESCR. For this reason, it was decided to perform another experimental design according to Table 4.3 to investigate the effect of strain rate and SCB on HS. The main reason for selecting these two factors was to see if there exists an interaction effect between them which would result in a better reflection of SCB on the HS behaviour. Resins with similar Mw (LLDPE 1, LLDPE 3-4) were selected for this study in order to prevent any possible Mw-SCB interaction. Sample specimens were prepared according to condition 2 and tensile tests were performed at various rates of 0.1, 2.55, and 5 mm/min. It was speculated that performing the tensile test at lower strain rates would resemble performing the tensile test at higher temperatures, hence creating a more suitable condition for the polymer chains to relax and fully extend. Table 4.6 represents the ANOVA, and Figure 4.10 the contour plot for this response surface reduced linear model (backward elimination at a 95 % confidence level). The model F-value of 15.45 implies that the model is significant. In this case, only the strain rate was found to be the significant term and both

SCB content and its interaction with the strain rate were non-significant. Information obtained from this analysis confirmed the speculation that HS is mainly a reflection of Mw of the LLDPE resins and the effect of SCB content cannot be detected. Therefore, HS values for different types of PE cannot be used as a relative measurement of ESCR, unless the resins contain roughly the same SCB and hence they are compared within the same category of PE grade. In such a case, the ESCR is mainly dictated by the Mw characteristics and will reliably be detected by HS.

Table 4.6: ANOVA of effect SCB and strain rate on HS

Source	Sum of Squares	df[a]	Mean Square	F value	p-value	
Model	6.1440E-03	1	6.14400E-03	15.45565	0.0023	Significant
Strain rate	6.1440E-03	1	6.14400E-03	15.45565	0.0023	
Residuals	4.3728E-03	11	3.97524E-04			
Lack of Fit	2.4356E-03	7	3.47938E-04	0.718436	0.6711	not significant
Pure Error	1.9372E-03	4	4.84300E-04			
Total	1.0517E-02	12				

a: degree of freedom

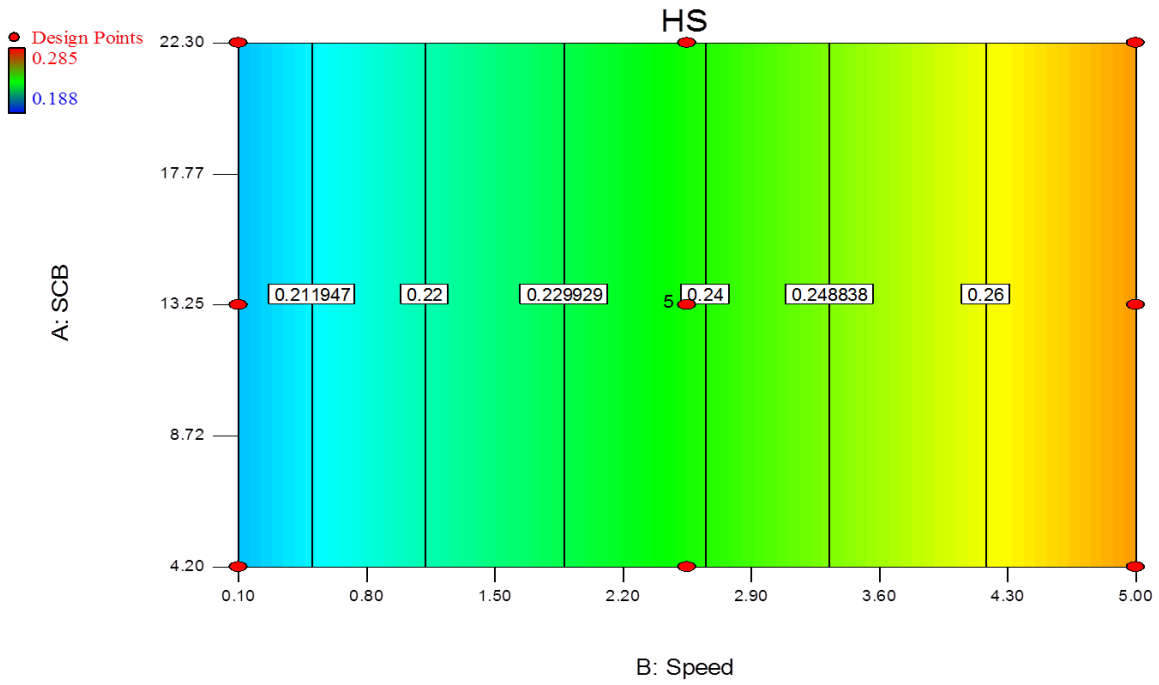

Figure 4.10: Contour plot representing the relationship between speed, SCB and HS

Comparing the ESCR values obtained from the NCLT and also taking into account the corresponding HS values, it could be concluded that both NCLT and HS tests should mainly be used for HDPE resins. Both NCLT and HS are not sensitive enough to detect the enhancement of SCB content on ESCR. In order to take into account both Mw and branching effects (SCB) on HS, it is proposed that a new factor be used along with HS. This factor should capture the effects of both Mw and SCB properties of the resin. It is proposed to use a dimensionless factor, termed the "weight-average number of branching (m)", which is found directly from the measured weight-average molecular weight (Mw), the measured short chain branching content (SCB, in short chain branches per 1000 carbon atoms), and the monomer molecular weight (M_m), as shown in Equation 4-1. Factor "m" is then basically the number of

branching points present per molecule in the PE resin, a reflection of both the Mw and branching content of the polyethylene in question.

$$Number\ of\ branching\ points\ (m) = \frac{SCB\ \times Mw}{M_m} \qquad 4\text{-}1$$

It is suggested that HS should be multiplied by m (hence forming a 'corrected HS' value or cHS in Table 4.4). This cHS is believed to be a better indicator of the ESCR of bulk PE resins as it takes both Mw and branching effects into account. The ratio between Mw and Mm in Equation 4-1 represents the degree of polymerization (DP, number of monomer repeating units) of resins, hence the number of monomer units. SCB is expressed in number of branches (i.e., branching points) per 1,000 carbon atoms. Since there are two carbon atoms per monomer unit, the right-hand side of Equation 4-1 should be multiplied by a factor of 2 for unit consistency, i.e., for "m" to be the number of branch points (alternatively, the NMR measurement that gives SCB can be expressed in number of branches per 500 carbon atoms). It should be noted that throughout this study, this factor of 2 (2 carbons per repeating monomer unit (C_2H_4)) was eliminated from Equation 4-1 (as it would not change the trends of the plots, but only the scales). As a result, factor "m", for all practical purposes; represents one half of the total number of branching points in the polymer molecule.

The ESCR values obtained from the BST for all HDPE and LLDPE resins in this work, were graphed vs. cHS and are shown in Figure 4.11. As shown, ESCR values of all PE resins increase with cHS, a trend that was only seen earlier for HDPE. It should also be noted that the development and use of the cHS indicator has several distinct advantages over HS. Firstly, a clear comparison between ESCR values of different types of PE resins is now possible, secondly, the effects of Mw and branching are both better reflected in the value of

cHS, and thirdly, the mapping between ESCR and cHS seems more universal (with all different resins in Figure 4.11 falling onto a “master” curve).

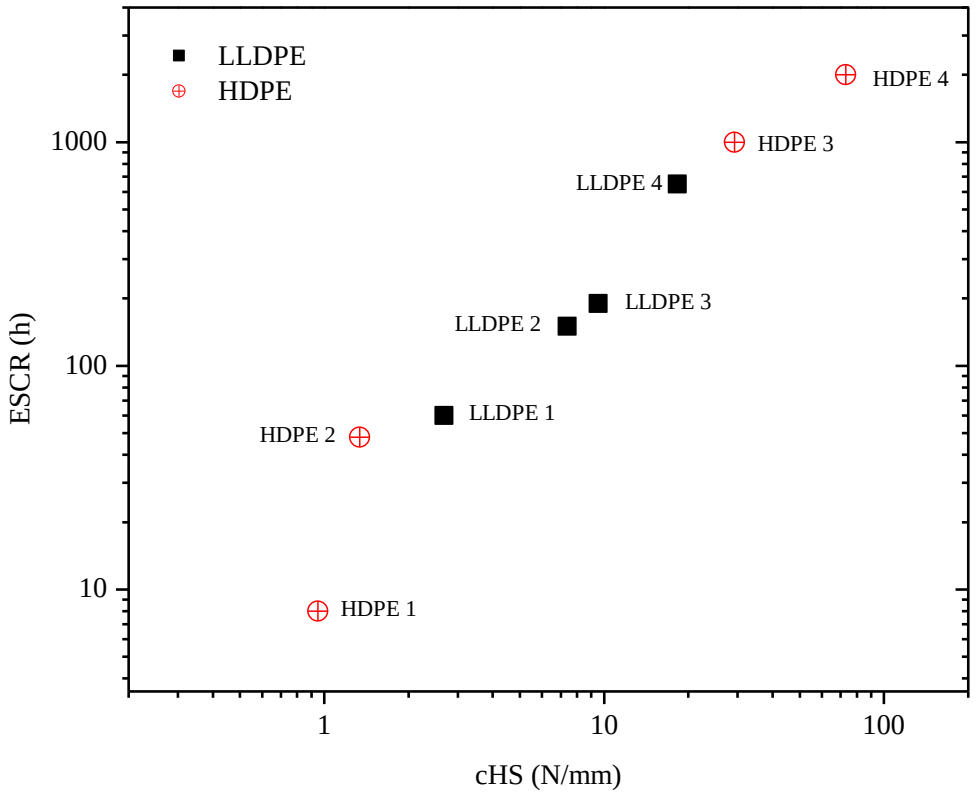

Figure 4.11: ESCR vs cHS graph

An extension of the developed master curve, based on all the resins shown in Table 3.1, can be found in Appendix A. Using the developed master curve, a reliable and practical measure of ESCR is offered, probably for the first time in the literature.

4.4 CONCLUDING REMARKS

The objective of this work was to conduct an investigation on the relationships between micromolecular structural characteristics and long term mechanical properties of PE resins with a focus on ESCR of LLDPE and HDPE for rotational moulding and pipe applications. The first contribution from this study was to predict and evaluate ESCR from a simple characterization test in a timely and reliable fashion. The second contribution was to refine and improve the hardening stiffness (HS) test proposed by Kurelec et al. (14) and Cheng et al. (15). The third major contribution of the study was to clarify the nature of the relationship between hardening stiffness and ESCR over a larger range of PE resins (and, hence, micro-structural properties), and establish the universality and generality (and relative flexibility and ease of use) of a modified HS indicator, the cHS. The cHS captures both molecular weight and short chain branching effects, and thus provides a reliable measure for ranking PE resins with different structural characteristics.

5 CHAPTER 5: RHEOLOGICAL INDICATORS FOR ENVIRONMENTAL STRESS CRACKING RESISTANCE

5.1 INTRODUCTION

It is well accepted that for thorough rheological characterization of polymers, shear experiments are not sufficient (1) and information about extensional (also called elongational) flow behaviour is of critical importance. This is because the behaviour of a polymer subjected to extensional deformation is more sensitive to molecular and microstructural differences than that under shear deformation. This information is needed as polymer melts are frequently exposed to large strains and strain rates in rather complex fields (2). This knowledge is of great importance in describing the performance of the polymer under various processing techniques, such as melt-spinning, blow-moulding, and film drawing, where polymer chains are highly stretched and oriented. The main property measured through extensional rheometry is extensional viscosity. Extensional viscosity represents the resistance of a fluid to extension, controlled by polymer chain entanglements, a property that is a reflection of several molecular features such as polymer molecular weight, molecular weight distribution, and branching content. Therefore, knowing the melt behaviour under extensional flow could improve understanding of the characteristics of chain entanglements, a molecular property that controls many of the critical aspects of the mechanical behaviour of a polymer. This information can lead to advances in grasping structure-property relationships and aid the proper material selection for various industrial applications.

Due to difficulties in generating a controlled extensional flow, experimental determination of extensional viscosity is not straightforward (3). Consequently, researchers have developed indirect methods to evaluate the extensional viscosity of polymers. The most frequently used technique for determination of extensional viscosity is the converging flow technique, in which polymer flows from a large reservoir through a capillary die, where the entrance pressure drop is measured as a function of flow rate (3-4). Cogswell (5-6) concluded that these converging flows can be analyzed in terms of their shear and extensional components to calculate the relationship between volumetric flow rate and pressure drop. He further derived a solution for the estimate of extensional viscosity from simple shear flow properties. Various extensional rheometers have also been designed to evaluate the extensional behaviour of polymer melts. These rheometers apply extension at a constant rate on a polymer specimen. The most problematic aspects of extensional flow studies were supporting the sample and applying a tensile force without introducing strong end effects. Most of the earlier designs included uniaxial extension of polymer samples in the form of a rod, clamped on both sides, in an elevated temperature oil bath or inert gas. The sample specimens were either mounted vertically (Münstedt type rheometer (7)) or horizontally (Meissner type rheometers (8)). These techniques were further improved by replacing the moving clamps with rotating wheels or rotating belts. This way, the elongation was not limited by the size of the equipment, and the end effects caused by the moving clamps were removed. Other researchers adapted the idea of rotary clamp techniques to measure transient uniaxial extensional properties (9-10). Most of the techniques included stretching polymer samples between counter-rotating drums at a constant rate. Sentmanat (11-12) developed a detachable fixture for a rotational rheometer, the Sentmanat Extensional Rheometer Universal Testing

Platform. This platform applies a uniform extensional deformation on polymer melts using the dual wind up drums. TA Instruments also developed a similar design in which one drum stays stationary, while the second drum rotates the sample (13).

In this chapter, we looked into the entanglement behaviour of polyethylene (PE) through rheological experiments in shear and extensional flow. Investigations were carried out to identify the feasibility of a correlation between shear and extensional viscosity, as a measure of polymer chain entanglements, and the environmental stress cracking resistance (ESCR) of the PE resins. ESCR in PE resins occurs through a slow crack growth (SCG) mechanism under low applied stresses and long periods of time. This property is usually assessed by unreliable and time consuming testing methods in the presence of an aggressive fluid at elevated temperatures. Cheng et al. (14) showed that the extent of inter-lamellar entanglements can be assessed by the degree of the strain hardening region from a simple tensile test at room temperature. This idea was recently modified and further advanced by Sardashti et al. (15), in which the extent of entanglements was investigated by monitoring the strain hardening behaviour of PE resins from a reliable and practical uniaxial tensile test. Measurements were made through a modified tensile test, called the "tensile strain hardening test". Through this test, the slope of the strain hardening region of a load-displacement curve, called hardening stiffness (HS) was found to correlate with ESCR of the PE resins (a steeper line represented higher ESCR). The observed correlation was related to the fact that the deformation mechanism involved in the strain hardening region of the tensile test is similar to the mechanism involved in the slow crack growth of the PE resins. The prediction of ESCR was further refined and improved to cover a broader range of PE resins, along with easier sample preparation, and faster testing. Furthermore, a correction factor for the HS values was

developed to enhance the effect of extent of short chain branches on the ESCR of the resins, hence enabling the prediction of ESCR for other types of PE (see Figure 4.11) (15). Cheng et al. (16) also provided insight into the entanglement nature of PE resins through shear experiments. They were able to establish a method to predict the number of inter-lamellar entanglements from the molecular weight between entanglements through oscillating shear experiments. In their study, they related melt entanglement indicators to entanglement effects on the environmental stress cracking resistance of PE.

Initially, it was intended to look into melt properties through shear studies, with a focus on linear low density polyethylene (LLDPE) resins with different short chain branching content, in order to identify a potential factor for estimation of the extent of chain entanglement, responsible for ESCR. Extensional properties of polymer melts were also investigated to identify the influence of chain entanglements on the extensional viscosity and the degree of strain hardening. The main purpose of this chapter then was to compare these melt state properties with solid state properties (obtained from the HS test (15)), in order to provide new insight into the influence of chain entanglements on the mechanical behaviour of polymer resins. This work was also essential in rationalizing the newly developed HS test and a considerable improvement on the prior state of the art, as described in Sardashti et al. (15).

5.2 EXPERIMENTAL

5.2.1 MATERIALS

Various types and grades of polyethylene resins were selected for this study (supplied by ExxonMobil Chemical Canada, and Borealis group, Lind, Austria). The resins were selected

according to their ESCR values, according to ASTM D 1693A (10 wt-% Igepal, 50 ºC), in order to cover a broad range of ESCR. The resin material properties are summarized in Table 5.1. In this table, Mn, Mw, and Mz represent number-average, weight-average and z-average molecular weight, respectively. PDI is the polydispersity index representing the breadth of the molecular weight distribution of the resins (Mw/Mn). ESCR is reported from a Bent Strip Test (BST) performed by our industrial partner, and it shows the time required for at least 50 % of all notched samples to fail.

Table 5.1: Molecular properties of the PE resins

Polymer ID	PE grade	Density (kg/m^3)	Mn (kg/mol)	Mw (kg/mol)	Mz (kg/mol)	PDI (Mw/Mn)	SCB[a] (/1000C)	ESCR[b] (h)
LLDPE 1	R.T.[1]	936	15.4	71.8	252.0	4.7	4.2	60
LLDPE 2	R.T.	938	20.8	82.0	232.0	3.9	7.5	150
LLDPE 3	R.T.	937	18.0	74.6	191.0	4.0	13.3	190
LLDPE 4	R.T.	932	15.1	76.6	286.0	5.1	22.3	650
HDPE 1	R.T.	948	18.7	77.9	349.0	4.2	1.6	8
HDPE 2	R.T.	942	25.2	118.5	336.0	4.7	2.4	50
HDPE 4	Pipe-100[2]	955	5.9	315.4	2129.3	53.3	11.8	>3000
PE 8	Pipe-80[3]	958	14.0	202.1	1398.4	14.4	4.5	>500
P1	B.M.[4]	948	14.8	258.3	2176.6	17.5	3.0	500
P2	B.M.	957	12.5	193.3	1779.2	15.4	1.2	40
P3	B.M.	954	10.8	209.2	1617.0	19.4	4.0	300
P4	B.M.	965	10.4	182.0	1591.0	17.5	2.6	15
P5*	Pipe-100	959	---	260.3	---	---	5.6	>1000
P6*	Pipe-100	948	---	301.5	---	---	11.9	>5000
P7*	Pipe-80	951	---	168.7	---	---	11.3	2000
P11	R.T.	---	18.0	126.5	905.3	7.0	2.2	21

*: PE with pigments (No GPC was performed, MW averages were not measured, the reported Mw was found from rheological methodologies (32), a: Short chain branching per 1000 carbon atoms, b: ESCR reported from a Bent Strip Test (BST) according to ASTM D1693A, 1: Rotational molding grade PE, 2: PE100 grade pipe resin, 3: PE80 grade pipe resin, 4: Blow molding grade PE

5.2.2 MOLECULAR CHARACTERIZATION

PE resin molecular weight averages and molecular weight distributions were evaluated by high temperature gel permeation chromatography (GPC) in a high speed GPC from Polymer CHAR (Spain). The solvent and operating temperature were 1, 2, 4 trichlorobenzene (TCB) stabilized with 300 ppm of butylhydroxytoluene (BHT) and 140 ºC, respectively. Calibration for MW averages and MWD were based on a conventional narrow polystyrene standard which was ultimately converted to PE using a transformation factor. An AVANCE 500 Bruker ^{13}C NMR was utilized to investigate the short chain branching content of the PE resins at 120 ºC. The solvent of choice was deuterated TCB. ^{13}C NMR chemical shifts were

used to identify the types of branching structures in the resins. Quantitative estimation of the content of branches was obtained from the ratio between the areas under a specific peak (representative of the branching type) to the area under the backbone peak. These results are shown in Table 5.1.

5.2.3 HARDENING STIFFNESS (HS) TEST

The hardening stiffness tests were performed at room temperature on an Instron 3365 machine. The specimens were prepared by punching compression moulded plaques prepared at the following condition: compression molding at 190 ºC ± 5 ºC and 44.5 kN, followed by air cooling to room temperature at a rate of 1 ºC /min, while increasing the applied force to 89 kN. The principle involved in the selection of the sample dimensions is the same as that described (in detail) in Chapter 4, section 4.3.2 (15). The HS was obtained by measuring the slope of the strain hardening section of the load-displacement curve. The test specimens were extended until complete failure was obtained at a rate of 10 mm/min.

5.2.4 RHEOLOGICAL CHARACTERIZATION

5.2.4.1 OSCILLATORY SHEAR RHEOMETRY

A TA Instruments AR2000 rheometer with parallel plate geometry was used to measure the shear properties. Both oscillatory shear experiments and shear creep tests were performed to measure the linear viscoelastic properties of the polymers. All PE resins were compression molded into 25 mm disks at 190 ºC and 44.5 kN, followed by quenching in cold water. Prior to frequency sweeps, strain sweeps between 0.1-100 % strains were performed at 100 Hz at 150 ºC and 190 ºC, to identify the linear viscoelastic region of the PE samples. Further, time

sweeps at the specified temperatures were conducted in order to identify any degradation or crosslinking during the frequency sweeps. Then a series of frequency sweeps were carried out at frequencies (ω) between 0.01-100 Hz under nitrogen. Shear creep tests were also conducted at 150 ºC and 190 ºC on compression molded disks. Creep experiments were conducted at 10 Pa (linear viscoelastic region) for 3 hours. It should be noted that all the rheological experiments were independently replicated at least 3 times to ensure good reproducibility in the results.

5.2.4.2 EXTENSIONAL RHEOMETRY

The transient uniaxial extensional viscosity, η_E, was determined at 150 ^oC and 190 ^oC on a Sentmanat Extensional Rheometer SER-HV-A01 model (11) attached to an ARES 2000 rotational rheometer. The extensional rheology specimens were prepared by compression molding PE pellets to create thin sheets. The sample width was fixed at 12.7 mm (prepared by a calibrated dual blade cutter) and the thickness was 0.65 mm (measured precisely before each test by a micrometer). Maximum Hencky strains of up to 5.6 can be achieved with this instrument. Note that the steady state extensional viscosity data were taken from the peaks appearing on the transient viscosity curves for the corresponding extensional strain rates.

5.3 RESULTS AND DISCUSSION

5.3.1 RHEOLOGICAL CHARACTERISTICS UNDER SHEAR

The initial objective of this work was to identify potential melt properties that are affected by the extent of short chain branching, responsible for enhancement of ESCR. Short chain branches are incorporated in the structure of polymers by introduction of small amounts of

comonomers, such as 1-butene or l-hexene. In general, it is well accepted that presence of SCB (content and length) improves the long-term mechanical properties of PE resins (17), as reflected on ESCR (and, similarly, on cHS values) of different linear and short chain branched PE (15). The enhancement in resistance to initiation and propagation of premature cracking in PE is due to the increase of interlamellar tie-molecules, as a result of direct incorporation of non-crystallizable SCB.

To identify the effect of short branches on rheological behavior, LLDPE 1-4, and HDPE 1 were selected for the first stage of study. These resins have a relatively similar MWD, but differ significantly in degree of short chain branching content (same comonomer type (1-hexene), but different frequencies (see Table 5.1)). It should be noted that rheological properties are mainly a reflection of MW, MWD and long chain branching (18-19). Since the selected PEs in this stage of the study have the same MWD, and no LCB content, any deviation in the rheological properties can be attributed to MW and short branches. Ultimately, a normalization technique is needed in order to outweigh the effect of MW, for a better understanding of the effects of SCB on rheological properties.

For a complete range of viscoelastic data over a large frequency range, results from a time-dependent creep analysis were converted into frequency-dependent data, and were subsequently combined with oscillatory measurements. A nonlinear regression analysis program (NLREG) (20) was used to convert the creep data, in the form of compliance (J(t)), to a retardation spectrum. The retardation spectrum was then utilized to estimate the compliance as a function of frequency (21). Ultimately, other viscoelastic properties such as storage (G') and loss (G'') moduli were obtained. Figure 5.1 shows the moduli for LLDPE 1 and LLDPE 2 by converting the time-dependent creep data to frequency data (represented by

lines). Also shown in Figure 5.1 are moduli obtained from the oscillatory measurements (shown by symbols). There is a good connection between the two data sets, verifying the validity of the transformation. Combination of the data sets extended the frequency range by three decades, which ultimately provided melt behavior in the terminal region of the PEs. Using the NLREG software, zero shear viscosity (η_o) and equilibrium compliance (J_e^o) of all PEs were also estimated (according to Equation 5-1 and Equation 5-2, respectively). These values are reported in Table 5.2. Due to the polydisperse nature of the PEs (no clearly defined plateau region, or a sharp transition to the terminal zone was observed), estimation of the plateau modulus (G_e^o) was not possible. Moreover, to verify results obtained from NLREG and also to identify other melt flow properties, the Carreau-Yasuda (CY) model (22-23) (shown in Equation 5-3) was fit to the experimental data. In this equation, ω is the angular frequency, and λ and "a" are parameters which control the shape of the viscosity curve. λ is the average characteristic relaxation time, "a" controls the width of the transition region between the terminal and shear thinning region (24), and "n" is the power-law index obtained from the slope of the shear thinning region (logarithmic scale). Estimates of these parameters are summarized in Table 5.3.

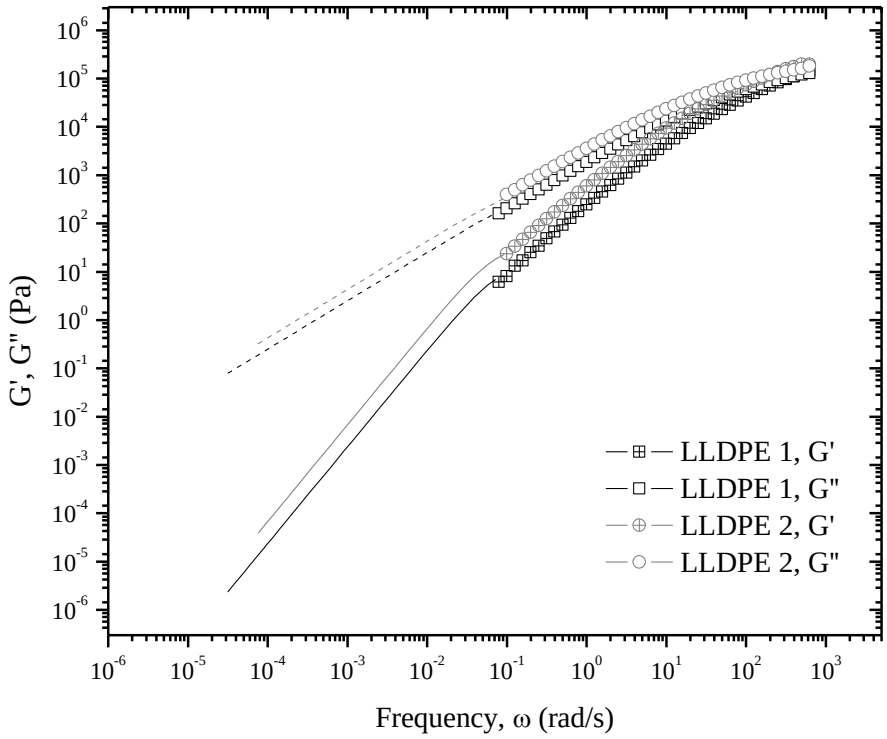

Figure 5.1: Combined storage and loss moduli from creep and dynamic data

$$\eta_o = \lim_{\omega \to 0} \frac{G''(\omega)}{\omega} \tag{5-1}$$

$$J_e^o = \lim_{\omega \to 0} \frac{G'(\omega)}{{\eta_o}^2 \omega^2} \tag{5-2}$$

$$\eta^* = \eta_o[1 + (\lambda\omega)^a]^{(n-1)/a} \tag{5-3}$$

Table 5.2: Values for zero shear viscosity (η_o) and equilibrium compliance (J_e^o) obtained from the combined data and NLREG

	Creep/ NLREG	
PE ID	η_o (Pa.s)	J_e^o (1/Pa)
LLDPE 1	2257	4.89E-04
LLDPE 2	4252	4.63E-04
LLDPE 3	2900	4.82E-04
LLDPE 4	2975	6.19E-04
HDPE 1	3180	5.13E-04

Table 5.3: Model parameters obtained from fitting the CY model

	Carreau-Yasuda (CY) model			
PE ID	η_o (Pa.s)	λ (s)	a	n
LLDPE 1	2180	0.01608	0.5257	0.31
LLDPE 2	4247	0.03360	0.5584	0.34
LLDPE 3	2941	0.03538	0.5719	0.40
LLDPE 4	3000	0.06025	0.6167	0.46
HDPE 1	3265	0.00679	0.4459	0.10

The estimated zero shear viscosities from NLREG (see Table 5.2) are very similar to the values obtained by fitting the CY model to the dynamic data (Table 5.3). Since the selected PEs in this stage of study were linear polymers, it is valid to assume that zero shear viscosity scales with weight average molecular weight (Mw) to the power of 3.6 ($\eta_o = KM_w^{3.6}$). Since the MWD does not significantly change the zero shear viscosity (25), the ratio $(\eta_o)_{NLREG}/(\eta_o)_{Mw}$, taken between the estimated zero shear viscosities obtained from NLREG, and the zero shear viscosities obtained from the η_o- Mw relationship, can normalize the effect of MW on zero shear viscosity. It should be noted that a ±5 % error in the GPC measurements has been employed in this work (an error of 5-10 % for GPC measurements are typically expected). Based on a ±5 % error in the values of Mw, a ratio close to unity was

obtained, indicating that the estimated zero shear viscosities are mainly a reflection of MW, and not of short chain branches as expected. Similar to η_o, equilibrium compliance values (see Table 5.2) obtained from NLREG did not show any significant dependence on the SCB content.

NLREG was further utilized to estimate relaxation spectra of the PEs. Storage and loss moduli obtained from combing dynamic and creep measurements were used as input data into the software. Relaxation spectra of the PEs are shown in Figure 5.2. The results plotted in Figure 5.2 are in the form of a dimensionless relaxation strength ($\tau.H(\tau)/\eta_o$) versus relaxation time (τ) for PEs shown in Table 5.2. All the PEs have the same relaxation distribution breadth, corresponding to a similar MWD. At small relaxation times, all PEs have the same relaxation strength except LLDPE 2, owing to its slightly higher Mw. In the mid relaxation region, LLDPE 4, which has the highest SCB content, has a different behavior. The relaxation strength for LLDPE 4 in the mid relaxation region is shifted towards higher relaxation times, indicating a slight (but still noticeable) change in the relaxation behavior. In order to have a better understanding of the effect of short branches on the relaxation spectrum, the dimensionless relaxation strength was plotted against a molecular weight normalized relaxation time (τ/η_o), using zero shear viscosities. The results are plotted in Figure 5.3. One interesting observation is that all PEs have a similar relaxation behaviour at both extreme ends of the spectrum (low and high relaxation times), but can differ in the mid relaxation region. This difference is more obvious for LLDPE 4 and HDPE 1, which have the highest and lowest content of short branches, respectively. LLDPE 1-3 had the same relaxation behavior and no differences between their relaxation spectra were observed. Also, it should be noted that short branches in LLDPE 4 are mainly distributed in the low and mid

ranges of the molecular weight distribution. Hence, changes in the relaxation behavior, in the mid relaxation time region, can be expected. This observation led to the postulation that when the relaxation characteristics of PEs with similar MW and MWD (and no long chain branches) are compared, a normalized average characteristic relaxation time (λ_N) can be used as a measure of molecular structure differences.

To verify this postulation, the average characteristic relaxation times (λ), obtained from the CY model (see Table 5.3) were revisited. An increasing trend with increasing short chain branching is observed, even prior to normalizing the data, however, the differences are negligible. In order to normalize λ, an established correlation between relaxation time and molecular weight, developed by Stadler and Mahmoudi (24), was utilized. The authors observed changes in the relaxation time behavior of LLDPE and HDPE resins, having different comonomer length and comonomer frequency. In their study, they found that λ followed a similar dependence to molecular weight as found for zero shear viscosity ($\lambda \propto Mw^{3.6}$). In this study, a similar analogy was adopted and the molar mass normalized relaxation times were obtained by dividing λ values obtained from the CY model, by the developed universal power-law relationship (based on a prefactor of 0.85×10^{-21}) (24).

The estimated λ_N can be taken as an indicator of the degree of network mobility in the polymer system. Therefore, the higher the determined λ_N (higher mobility in melt state, indicating a higher branching content, and consequently a less entangled melt (25)), the higher will be the possibility of creation of effective tie-molecules and physical chain entanglements in the solid state. Therefore, a plot of λ_N versus SCB or cHS (or ESCR, for all practical purposes, see Chapter 4, section 4.3.3) should indicate an increasing trend. This behaviour is shown in Figure 5.4, where an increase in λ_N represents an increase in ESCR of

PE. Stadler and Ruymbeke (26) similarly observed a broadened relaxation time upon increasing comonomer content (and length). The authors claimed that short branches reduce the number of chain entanglements in the melt, due to their unentangled nature, increase the molecular weight between entanglement (M_e), and ultimately reduce the plateau modulus (G_N^0).

Another interesting behavior observed was the dependence of a certain factor "a" on SCB content. Factor "a" controls the transition region between terminal and shear thinning regions. A higher "a" represents a sharper/ faster transition to shear thinning. A similar observation was reported by Stadler et al. (24), where an increase in factor "a" was related to a decrease in complex modulus (G*), upon introduction of short branches. This observation also indicated another potential melt indicator for ESCR of PEs resins with similar MW structures.

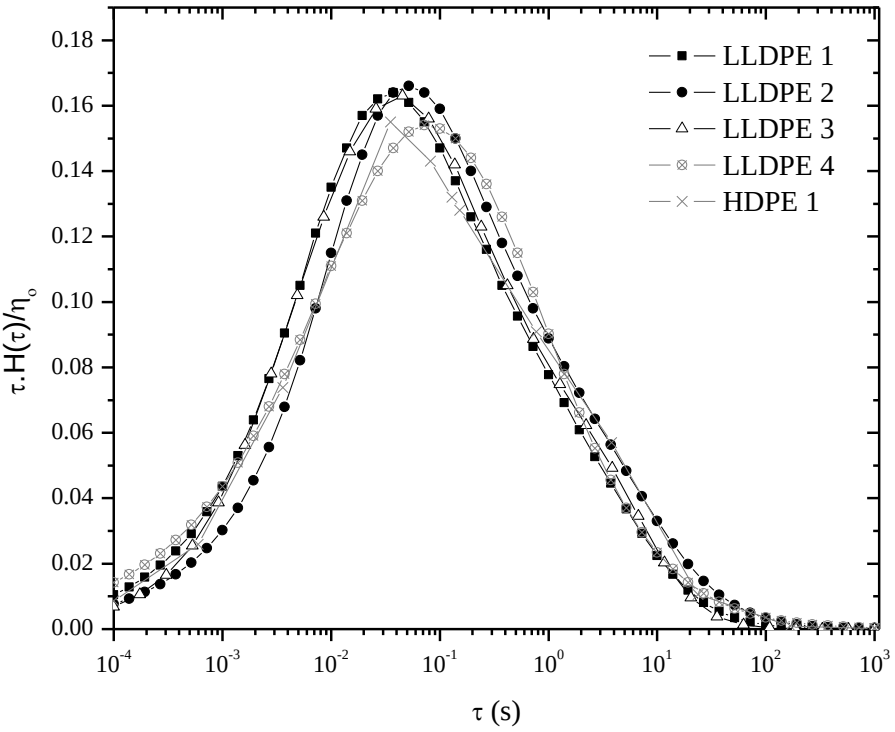

Figure 5.2: Relaxation spectra obtained from NLREG

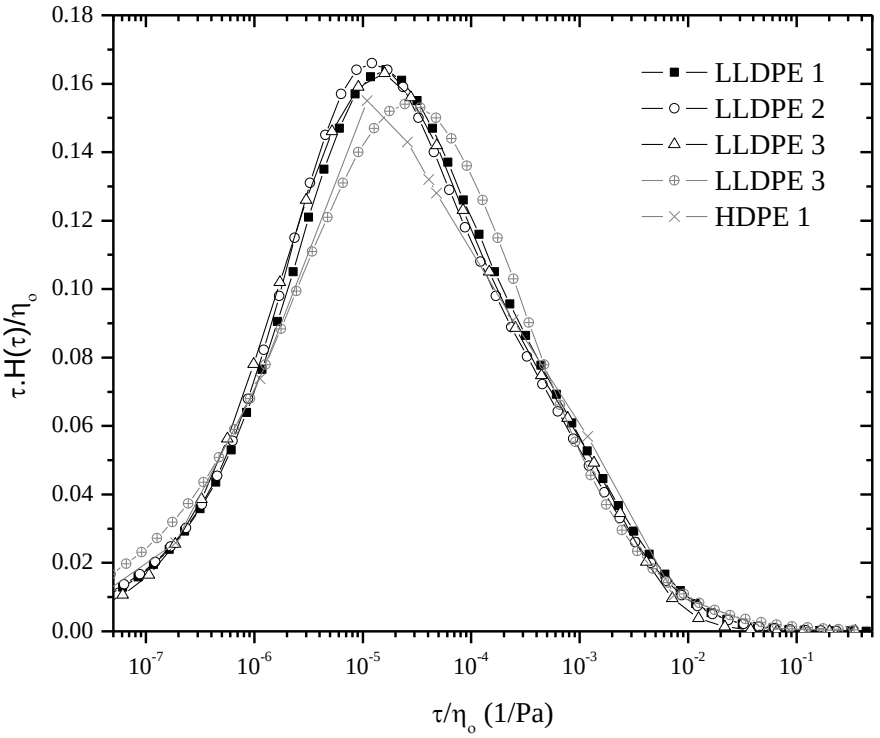

Figure 5.3: Molecular weight normalized relaxation spectra

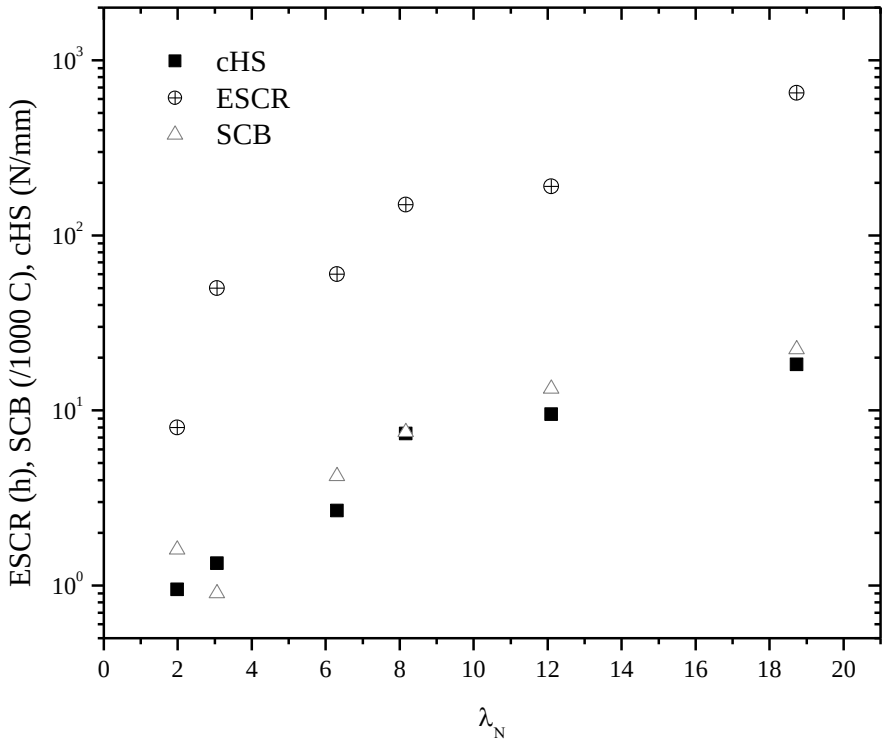

Figure 5.4: ESCR, SCB and cHS vs. normalized average relaxation time

In the second stage of this work, studies were extended to the other HDPEs (HDPE 2, P 1-7, and P 11). These resins are high density PEs with relatively higher MW and broader MWD, and different short chain branching contents (see Table 5.1). In an analogous way, results obtained from creep and dynamic experiments were combined to produce dynamic moduli master curves, from which zero shear viscosity and equilibrium compliance were obtained. These values are tabulated in Table 5.4. Moreover, in order to find average relaxation times and also to verify the measured zero shear viscosities, the Cross model (27), shown in Equation 5-4, was fit to the dynamic data. Prior to fitting the Cross model, the CY model and a generalized Cross-Carreau model (28) were fitted to the data, but both models showed a lack of fit. Parameter estimates obtained from the Cross model are shown in Table 5.5. In this table, also included are Cross model parameter estimates for PE 8 and HDPE 4. Zero shear

viscosity data obtained from creep analysis and the Cross model are similar and show the same trend, except for P 3 and P 6. PEs at this stage of the study have relatively high MW and broad MW distributions. Since the underlying data from the dynamic measurements do not always approach the constant low shear rate asymptote (for a proper estimation of η_o), the parameter estimates for zero shear viscosity using the Cross model can be misleading. For this reason, throughout this work, zero shear viscosity data obtained from creep analysis are only used.

Table 5.4: Viscoelastic properties obtained from combining creep and dyanmic data

	Creep/ NLREG	
PE ID	η_o (Pa.s)	J_e^o (1/Pa)
HDPE 2	8180	4.99E-04
P1	355614	6.06E-03
P2	111606	1.11E-02
P3	33900	1.34E-02
P4	44714	9.95E-02
P5	258983	1.08E-02
P6	432356	1.17E-02
P7	69221	1.13E-02
P11	81097	9.86E-02

$$\eta^* = \frac{\eta_o}{(1 + (\lambda\omega)^{1-n})} \qquad 5\text{-}4$$

Table 5.5: Cross model parameter estimates

	Cross Model		
PE ID	η_o (Pa.s)	λ (s)	n
HDPE 2	7370	0.109	0.44
P1	298500	33.12	0.44
P2	110600	19.10	0.47
P3	58280	6.44	0.47
P4	30190	5.01	0.50
P5	214000	8.66	0.37
P6	259200	10.18	0.36
P7	67300	3.99	0.43
P11	83890	43.08	0.50
PE 8	110500	12.53	0.38
HDPE 4	1014000	31.78	0.28

The dependence of zero shear viscosity on the number and length of branching has been extensively studied (19, 29-31). In general, low levels of long chain branches, increase zero shear viscosity. On the other hand, a decrease in zero shear viscosities is expected at high levels of branching (for both long chain branches and crosslinks). A graph of zero shear viscosity (η_o) vs. weight average molecular weight (Mw) was developed in this work to identify any possible branching in the structure of the PEs. Figure 5.5 shows the zero shear viscosity data obtained from creep measurements as a function of weight average molecular weight. The straight line represents the general relationship of $\eta_0 \propto Mw^{3.6}$ for a linear PE (32). Again, a 5-10 % error in the values of Mw, determined from GPC measurements, was assumed. It can be seen that most of the resins are located on the straight line, representing a linear structure. PE 11 and HDPE 4 are located above the reference line, indicating the possibility of presence of long chain branches in their structure. P 3-4, on the other hand, are located slightly below the straight line. It was postulated that these resins may include a crosslinking agent in their formulation. Similar to short branches (refer to discussions on λ_N,

presented earlier in this section), high branching densities due to crosslinking, reduce the overall extent of entanglement density. Comparing a linear PE of the same Mw to a branched counterpart, a higher extent of entanglements for the linear PE, and hence a higher η_o , is expected.

To verify this postulation, Soxhlet extraction experiments in xylene were conducted according to ASTM D2765-11 on P 3-4 to determine the levels of gel content. It was found that the resins have insignificant amount of gel (less than 2 % gel content) in their structure. This observation then led to the conclusion that the deviations from the linear reference line, demonstrated by P 3-4, must be attributed to a combination of very low degrees of crosslinking and experimental error , involved in the GPC measurements.

Due to differences in the molecular structures of the PEs in this stage (different MW, MWD, SCB content and distribution, and LCB content), it was not possible to draw any conclusions about the ESCR of the resins, based on shear (creep and dynamic) analyses. Developing a molecular weight normalized relaxation time λ_N (as discussed earlier in this section) did not seem feasible as both LCB and MWD have a similar effect on polymer relaxation behavior. Similarly, a mass normalized zero shear viscosity would also not provide any information about ESCR, since short chain branches do not have a significant effect on η_0. Also, variability in the measured Mw, and possible crosslinking (even to a very small extent, yet potentially effective) limited the amount of information for developing a potential melt indicator of ESCR through shear measurements.

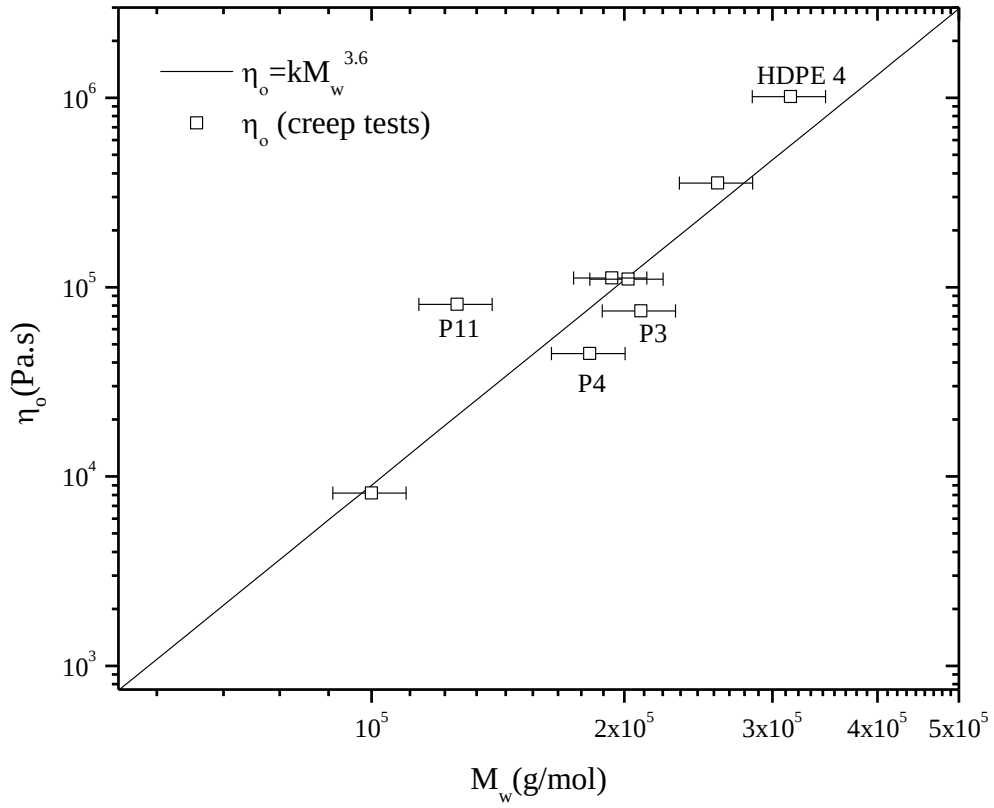

Figure 5.5: Zero shear viscosity vs. Mw

5.3.2 RHEOLOGICAL CHARACTERISTICS UNDER EXTENSION

5.3.2.1 ENTRY FLOW METHODOLOGIES

A dual bore capillary rheometer, equipped with different pressure transducers, an orifice (zero length die) and a capillary die (see Appendix B for a full description of the equipment and the capillary dies), was utilized to measure the entrance pressure drops of the PEs at different shear rates. Cogswell, Binding and Gibson methodologies (see Appendix C for more details on these techniques) were utilized to estimate the extensional viscosity of the PEs, from the measured entrance pressure drop. Results from these methodologies are summarized in Appendix B.

5.3.2.2 EXTENSIONAL RHEOMETRY

In order to obtain a potential melt indicator for estimation of ESCR, rheological experiments under extensional flow were conducted on a Sentmanat extensional rheometer (11-12). It was intended to study the melt behavior of the resins under extension, with an interest in finding a possible correlation between melt strain hardening behavior and ESCR. Extensional measurements were conducted at two different temperatures of 150 ºC (for LLDPE 1-4, and HDPE 1-2) and 190 ºC (the rest of the PEs). LLDPE 1-4 and HDPE 1-2 samples were uniaxially stretched at strain rates of 0.1, 0.32, 1.0, and 3.2 s^{-1} at 150 ºC. All the other PEs were stretched at strain rates of 0.05, 0.5, and 5 s^{-1} at 190 ºC. Experiments continued until an unstable deformation started and eventually led in total filament breakage, indicated by a reduction in the viscosity values. The values of the transient stress growth coefficient (η_E^+) (i.e. transient extensional viscosity) versus time of LLDPE 1-4 and HDPE 1-2 are shown in Figure 5.6. The dotted lines in this figure represent the linear viscoelastic (LVE) profile, representing three times the shear viscosity obtained from dynamic measurements (i.e., $3\eta_o^+$, based on the Trouton's law). Any upward deviation from the LVE profile (dotted line) is an indication of melt strain hardening (33), representing molecular orientation due to the applied uniaxial stress. The LLDPE 1-4 and HDPE 1-2 resins exhibited the expected behaviour. At all extensional rates, the transient extensional viscosities increased with time, and eventually reached equilibrium (plateau region). The plateau behaviour was obtained from the low extensional rate experiments, whereas the initial jump and the slope of the extensional viscosity curves were obtained from the higher extensional rate experiments. No significant strain hardening behaviour was seen, something that was expected from linear PEs, with relatively low MW and narrow MWD. This observation indicated that extensional rheometry

cannot be used as an indicator for the estimation of ESCR of LLDPE and HDPE resins that are used for rotational or injection molding applications (low MW, narrow MWD, different short branches, and no LCB content). For such PEs, it is recommended to conduct shear analysis, as shear experiments in this chapter, showed higher sensitivity to the content of short branches (see section 5.3.1). The mass normalized average relaxation time, discussed earlier in section 5.3.1, can predict the effect of such subtle structural differences more readily, compared to extensional experiments.

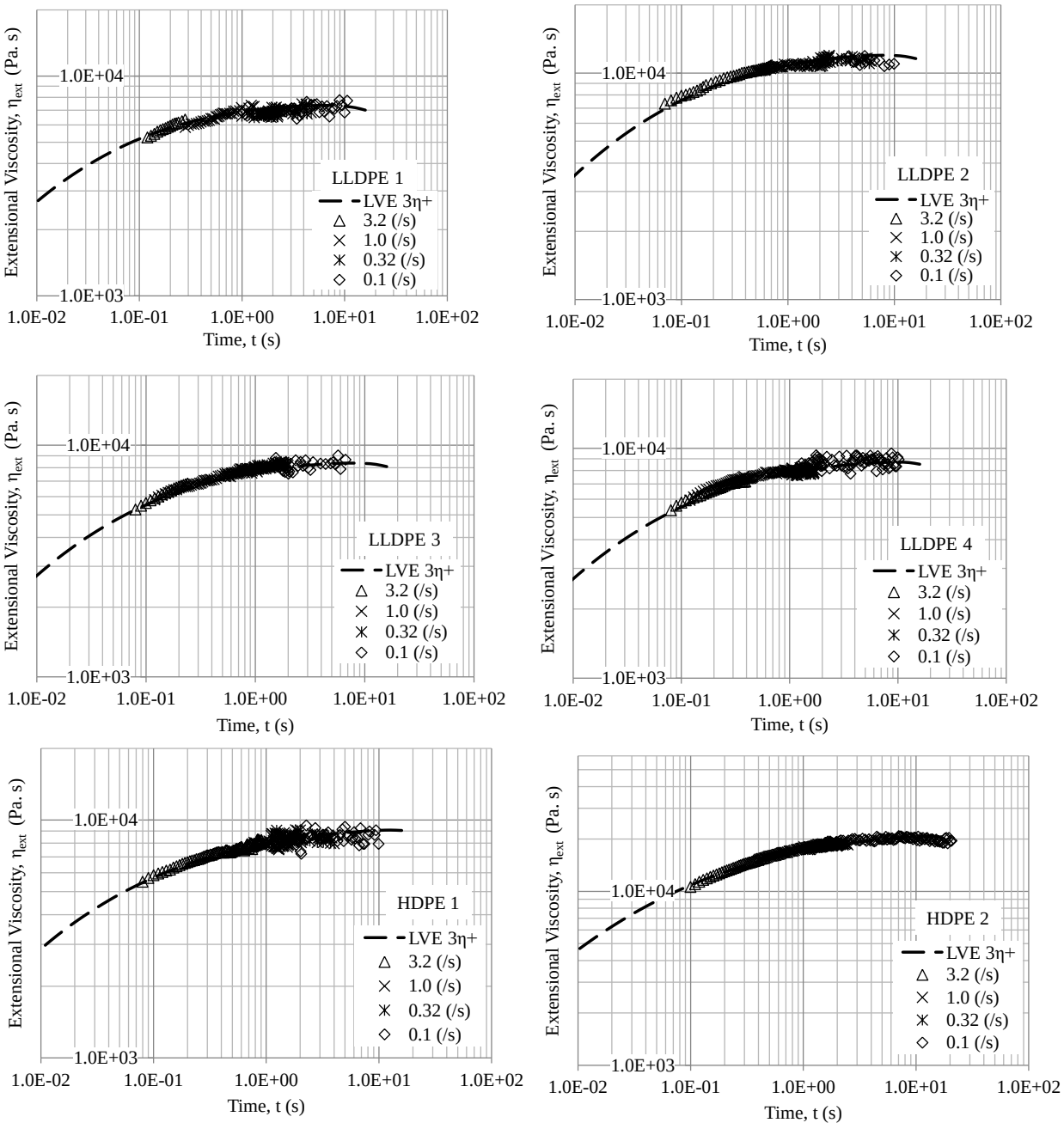

Figure 5.6: Transient extensional viscosity of LLDPE 1-4, and HDPE 1-2

Extensional experiments were conducted for the other resins of this work (P 1-7, PE 8, HDPE 4, and P 11). Shear experiments, performed earlier on these PEs, did not find any correlation between ESCR and shear melt behavior due to the large differences in their molecular structures. The values of the transient stress growth coefficient (η_E^+) for P 1-4 are

shown in Figure 5.7, and for the rest of the PEs in Figure 5.8. All PEs indicated strain hardening, almost at all strain rates. A melt strain hardening coefficient (MSHC) (34), according to Equation 5-5, was determined for all PEs in order to compare their degree of strain hardening. In this equation, $\eta_E^+(t,\dot{\varepsilon})$ is the stress growth coefficient at the Hencky strain of 2.65, and $\eta_0^+(t)$ is the shear stress growth coefficient. It was postulated that the MSHC can provide insight about ESCR, as both properties are related to the extent of chain entanglements. The stress coefficient factors for P 1-4, P 6, and HDPE 4, at Hencky strain rates of 0.05, 0.5, and 5 s^{-1}, are shown in Figure 5.9. This figure indicated the following trend between the MSHC of the selected PEs: P 4 > P 2 > P 3 > P 1 > P 6 ≥ HDPE 4. This trend indicated an inverse correlation between the ESCR and MSHC of PEs (see Table 5.1). Chain entanglements in a polymer affect its extensibility. The degree to which extensibility is affected, is related to the number of joints (or entanglements for a linear PE and crosslinks for a crosslinked PE) in the structure of the polymer. A polymer of high ESCR has a high content of chain entanglements, which can reduce its extensibility significantly. A reduction in extensibility is represented by a reduction in the values of MSHC obtained in this section. Although the obtained MSHC can be used as a possible indicator of ESCR of PEs, extra care should be given when measuring extensional behavior and LVE profiles of the PEs. A small amount of deviation between these properties can result in an inaccurate estimation of MSHC (as was the case, for example, for P 11 and PE 8 in this study).

$$Melt\ Strain\ hardening\ coefficient, MSHC = \frac{\eta_E^+(t,\dot{\varepsilon})}{3\eta_0^+(t)} \qquad 5\text{-}5$$

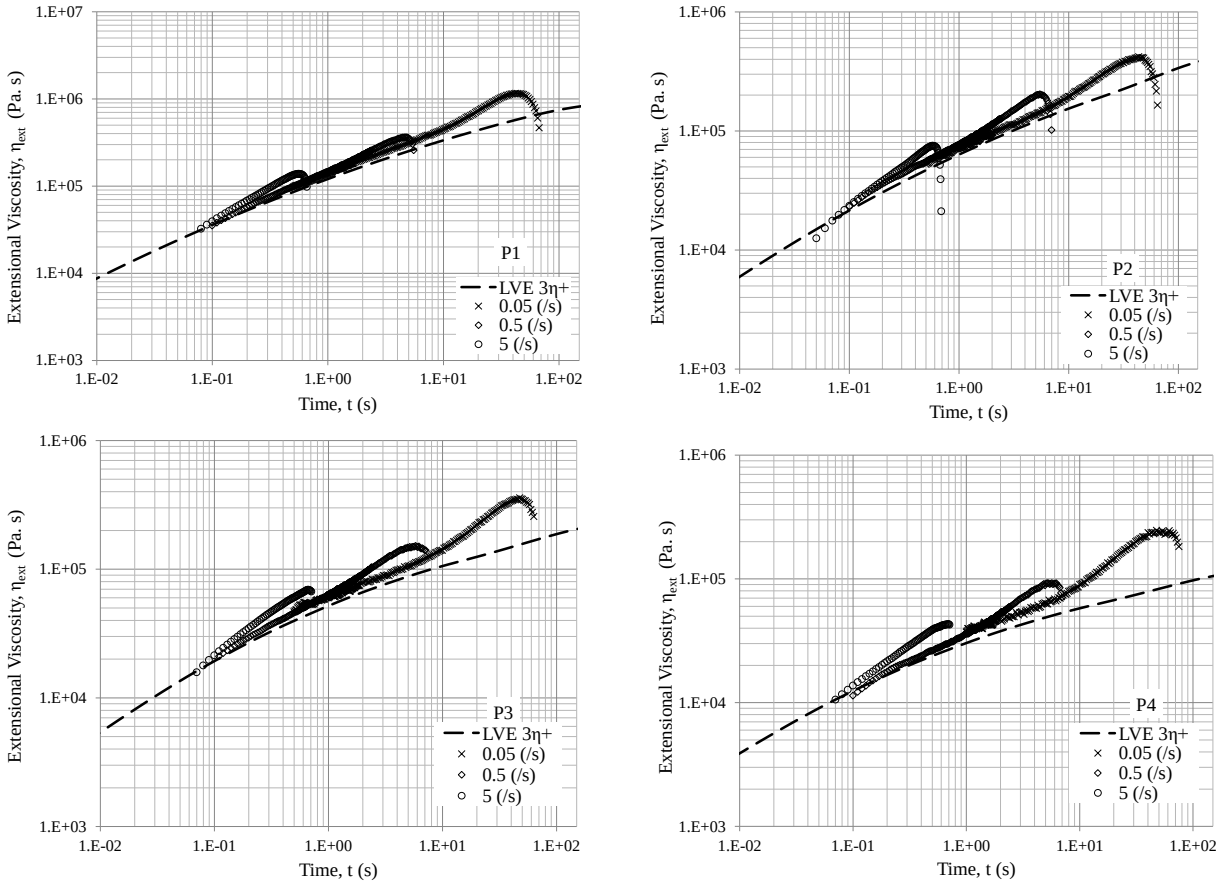

Figure 5.7: Transient extensional viscosity of P1-4

.

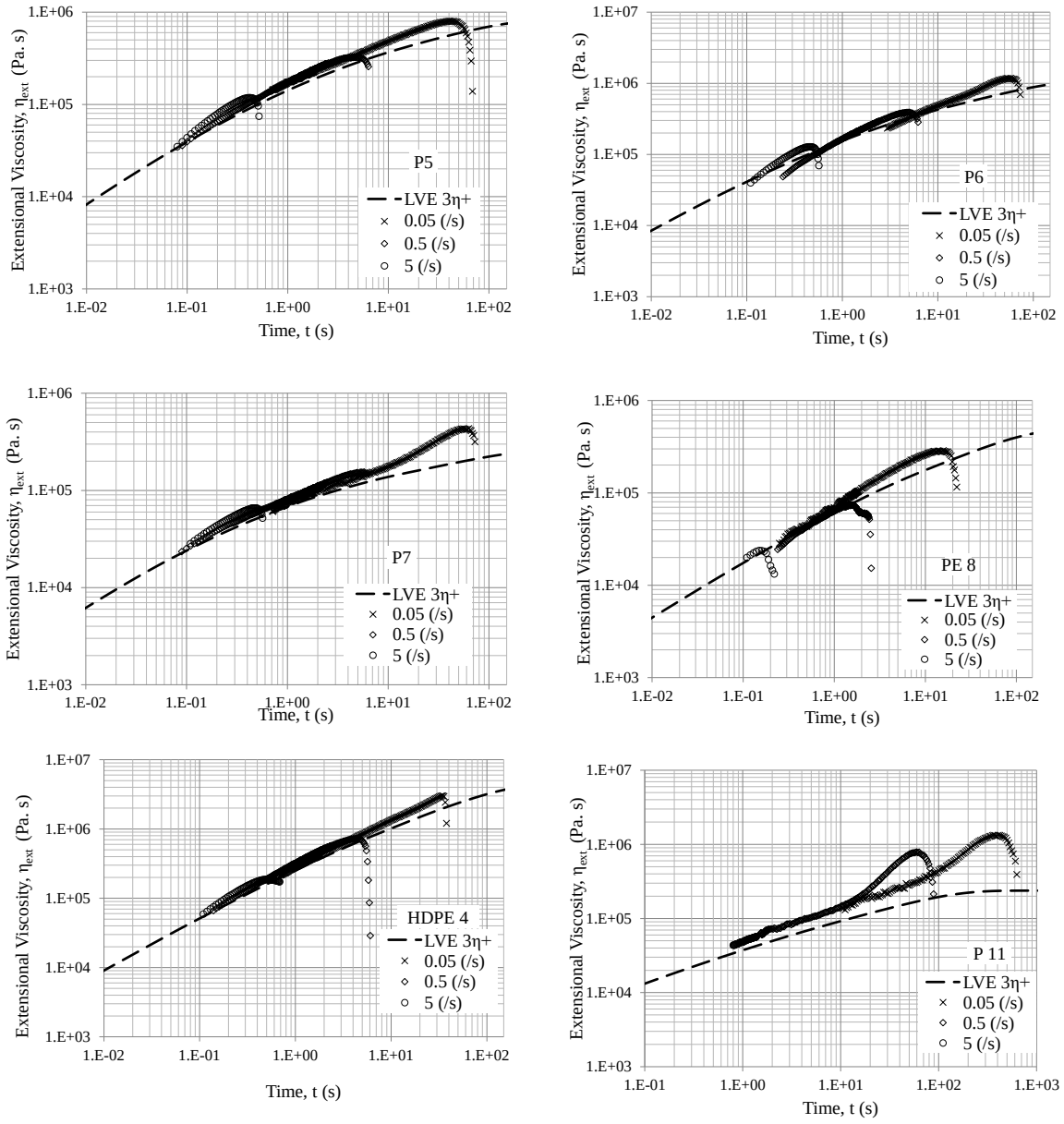

Figure 5.8: Transient extensional viscosity of different PEs

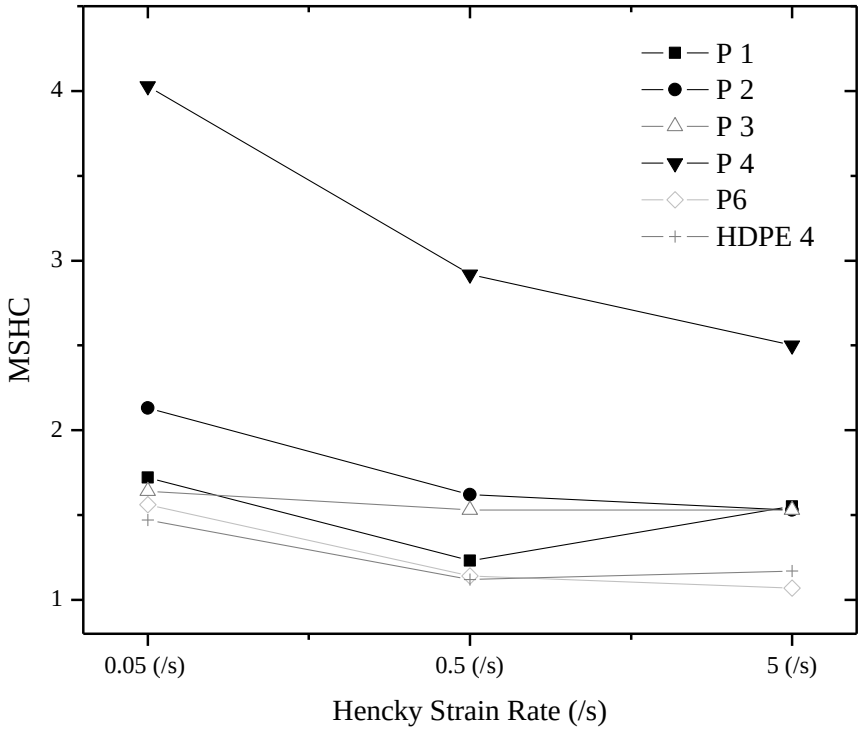

Figure 5.9: Melt strain hardening coefficient vs. Hencky strain rate

5.3.2.3 THE STRAIN HARDENING SLOPE AND ESCR

In recent work performed in our laboratory (see Chapter 4 and reference (15)), the hardening stiffness (HS) test was shown to be a reliable tool for measuring the entanglement characteristics of PE resins. A correlation between molecular structure, namely, weight average molecular weight and short chain branching content, in relation to strain hardening behaviour (in the solid state) was established. This correlation shed more light on the dependence of ESCR of PE resins to the inter-lamellar entanglements, which are the main factor controlling the slow crack growth in PE resins. This correlation was developed by monitoring the strain hardening behaviour of PE resins in the solid state through a uniaxial tensile test. The scaling of hardening stiffness (slope of the strain hardening region) with molecular weight was indicated by the test. The short chain branching effect on HS,

however, was very subtle and not easily discernible. For that reason, a correction factor was developed and used with the measured HS to reflect the effect of branching (presented by cHS, see Chapter 4, section 4.3.3). This behaviour indicated that the HS test can be readily used for a relative 'measurement' of ESCR of HDPE resins (and hence a ranking of HDPE resins with respect to ESCR) without knowing much about the properties of the resin (similar to a blind characterization test).

A similar analogy was adopted in this work to identify a possible correlation between the slope of the strain hardening region (extensional stress vs. Hencky strain), obtained from the extensional measurements, and ESCR of the PEs. It was postulated that differences in molecular structure can be better indicated via rheological characterization, hence providing better prediction of ESCR, particularly between PEs with different MWDs. Figure 5.10 presents the extensional stress plotted against the Hencky strain, obtained from the SER, performed at different strain rates for P 1 (ESCR: 500 h), P 3 (ESCR: 300 h), P 4 (ESCR: 15 h), and HDPE 4 (ESCR: above 3000 h). The strain hardening curves are well-defined, hence, an average characteristic slope can be determined for the resins. The slope is determined from the linear section of the curve, prior to the plateau behavior and filament breakage, as shown in Figure 5.7 and Figure 5.8. Figure 5.11 illustrates ESCR vs. mHS values (see immediately below for a definition), obtained at different extensional Hencky strain rates. The scaling of ESCR with mHS is observed, indicating a potential correlation between the slope of the extensional stress-strain curve and ESCR of the PEs. This correlation verified the adaptability of the developed HS test, even in extensional flows. The slope of the extensional stress-strain curve, which is now called the "melt Hardening Stiffness (mHS)", can be used as another potential indicator of ESCR for PE resins. P 11

(indicated by circles in Figure 5.11, at the three rates), however, showed a deviation from the established trend. As it was mentioned earlier, P 11 contains long chain branches. The long braches increase both the zero shear viscosity and strain hardening behavior of the PE, which ultimately increases the slope of the extensional stress-strain line. On the other hand, ESCR is not as sensitive to long chain branches (a characteristic of mechanical behavior). The different effect of long branches on ESCR and mHS of P 11, resulted in a deviation from the established trend between the two measured properties (ESCR vs. mHS).

In Figure 5.12, cHS values obtained from the HS tests (Chapter 4, section 4.3.3), and mHS values obtained from the extensional measurements are plotted against each other. It can be seen that both types of measurements indicate the same trend. This once again verified the potential of using either of these properties for the estimation of ESCR. It should be noted that P 4 and P 11 did not show any strain hardening behavior in the solid state, hence, their cHS values are not reported (another indication of their low ESCR).

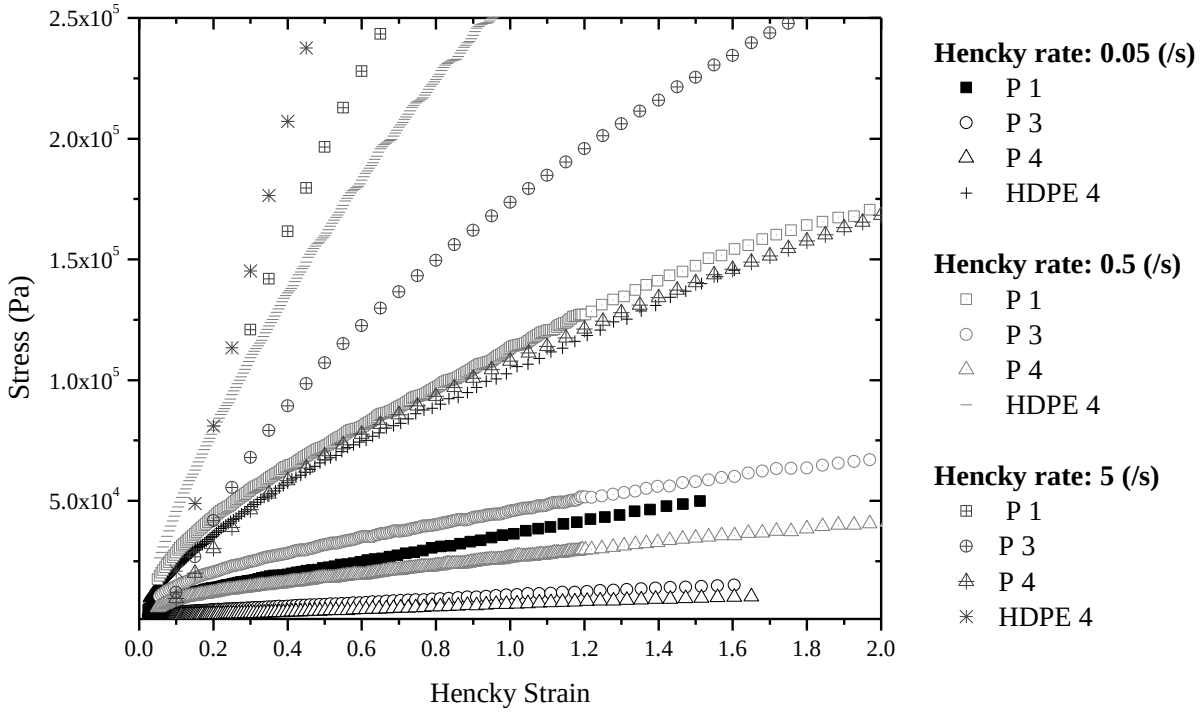

Figure 5.10: Stress vs. strain curves obtained from extensional measurements

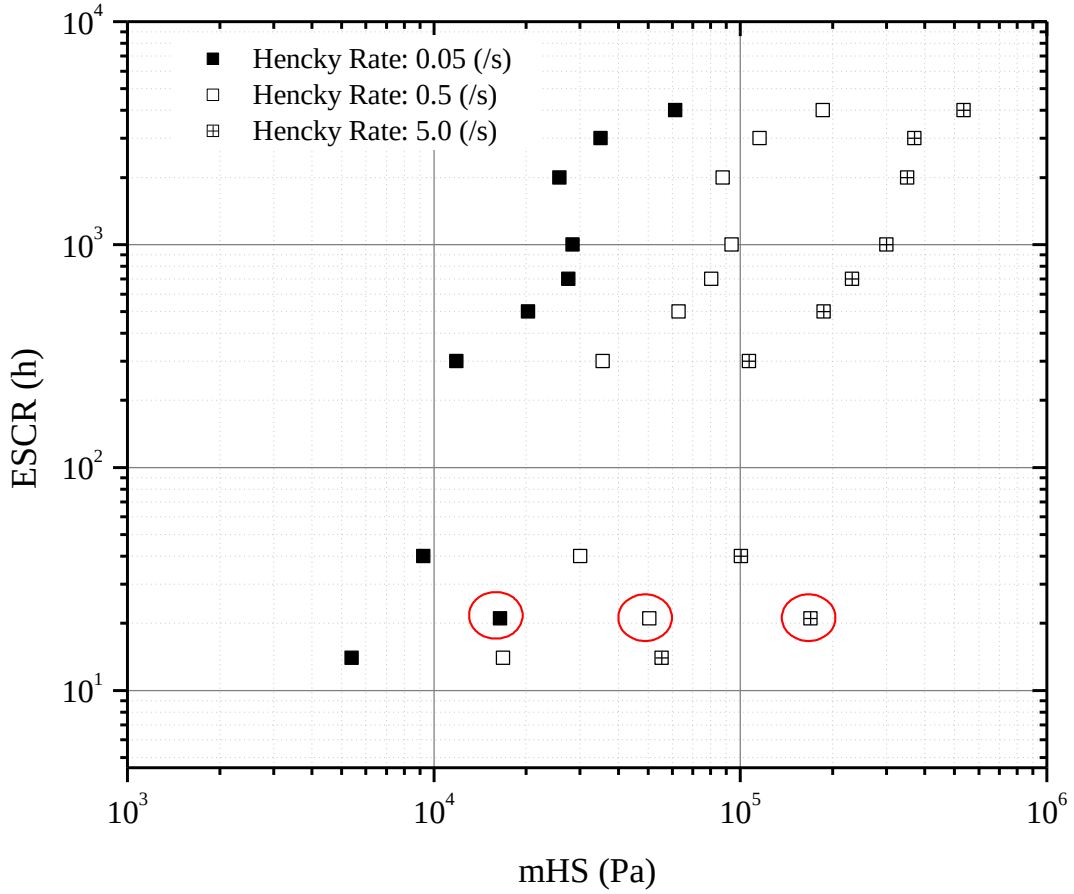

Figure 5.11: ESCR vs. mHS for all PEs

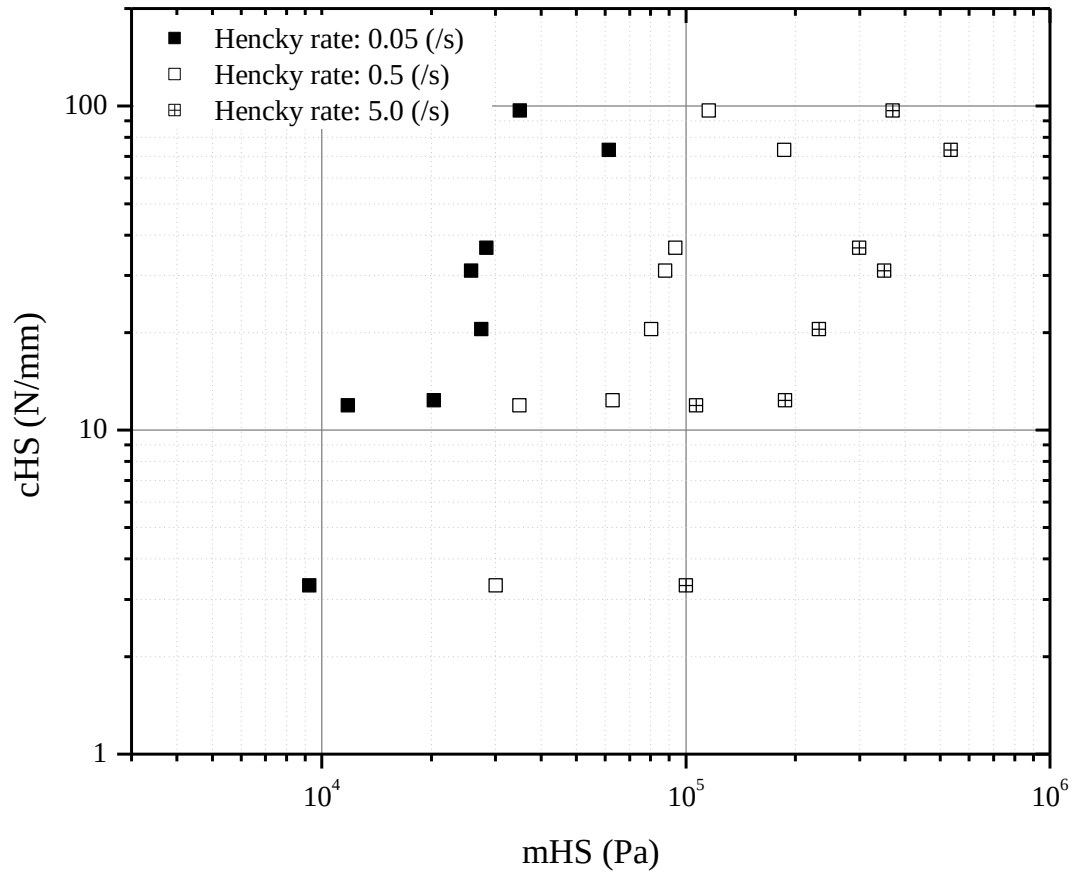

Figure 5.12: cHS vs. mHS trend

5.4 CONCLUDING REMARKS

Rheological tests both in shear and extensional modes were conducted to investigate the melt state chain entanglement behaviour of linear and short chain branched PE. PE chain entanglements are believed to be the main factor controlling the long-term resistance of polymer towards cracking. The outcome of the rheological studies was compared to findings from tensile strain hardening behaviour in the solid state to shed more light on the structure of chain entanglements. Experimental results in shear mode revealed that the normalized characteristic relaxation time (λ_N) can be used as a relative measure of ESCR, as it mainly represents the effect of branching content on ESCR. This outcome is very useful in the case

of LLDPE resins, where the similarity between molecular structures (both molecular weight and molecular weight distribution) restricts the evaluation of ESCR by extensional methodologies.

Extensional viscosities were evaluated using Sentmanat extensional rheometry. Experimental results revealed that the strain hardening behavior in extensional experiments can differentiate between molecular structures. An inverse correlation between the coefficient of strain hardening and ESCR was obtained, indicating the inverse relationship between polymer extensibility and ESCR. Furthermore, a factor called "average melt hardening stiffness (mHS)" was developed from the slope of the strain hardening section of a stress-strain line, obtained from SER experiments. mHS was found to be an indirect measure of chain entanglements in PE and was found to correlate well with both cHS and ESCR, obtained from a uniaxial tensile tests in the solid state.

6 CHAPTER 6: EFFECT OF TEMPERATURE AND CRYSTAL STRUCTURE ON ENVIRONMENTAL STRESS CRACKING RESISTANCE OF POLYETHYLENE

6.1 INTRODUCTION

Environmental stress cracking (ESC) is one of the most common failures in plastics, in which a brittle fracture takes place through a slow crack growth (SCG) mechanism. Usually, this type of fracture is preceded by formation of stress-localized microscopic crazes from existing inhomogeneities in the bulk, as a result of polymer production or processing methodologies. These highly stressed-localized areas eventually collapse and give rise to cracks, which ultimately propagate and cause a sudden catastrophic brittle fracture. A great deal of interest has been given to ESC of many polymers for which structural and long term integrity is of importance. Among these polymers, polyethylene (PE) has been extensively studied due to its versatile commercial applications. ESC in PE is believed to involve extension and consequent disentanglement of load bearing inter-lamellar chains that exist between PE crystal domains. These entanglements have been shown to include both tie-molecules (large PE chains anchored in between two or more adjacent crystals with their mid-section in the amorphous domain) and physical chain entanglements (cilias, loose loops, etc.). Therefore, it is believed that the availability and extent of such entanglements are indeed critical in enhancing the environmental stress cracking resistance (ESCR) of polymers.

ESCR has been shown to be a function of different molecular properties, among which molecular weight (MW) and short chain branching (SCB) content are more critical (1-3). A polymer of high molecular weight consists of relatively long polymer chains. These long chains can form tie-molecules more readily and span the inter-lamellar distance; they

consequently increase the overall chain entanglements (there is a relatively higher chance for longer chains to become tie-molecules). SCB has also been shown to increase the ESCR of PE (1, 4). The enhancement in resistance to brittle fracture is due to the increase of interlamellar tie-molecules, as a result of direct incorporation of non-crystallizable SCB (exclusion of the branches from the crystalline lamellae). These short branches tend to push the polymer chains into the amorphous region by disrupting the chain folding process. This leads to random chain folding, which eventually increases both the physical entanglements and the degree of tie-molecule formation. Other molecular properties such as the distribution of molecular weights and branches, and the morphology of the polymer have also been shown to affect ESCR (2, 5-6). A broader molecular weight distribution (MWD) represents a greater extent of large molecules in the higher (molecular weight) end of the MWD spectrum. The presence of such large molecules (as indicated by higher order molecular weight averages such as M_z and M_{z+1}) enhances many mechanical properties, including ESCR. In general, it is acceptable to say that in order to have a high ESCR, high MW and SCB are necessary. The probability of creating tie-molecules is higher if SCB is distributed along the higher end of the MWD spectrum.

Most studies performed on ESCR in the past have focused on the amorphous phase of the material, and significant progress was made by Lustiger & Markham (7) and Huang & Brown (3) who looked into the effect of molecular structure on the extent of formation of tie-molecules. Other studies considered the effect of the crystalline phase (crystallinity, crystal thickness) on ESCR, mainly as a consequence of different processing conditions. Hittmair and Ullman (8) studied the effect of cooling rate on the size of individual crystallites and reported an increase in ESCR with slow cooling. On the other hand, Sharif et al. (9) reported

that increasing the cooling rate from the melt increases the ESCR due to a lower crystallinity. Similarly, in a recent study, Nie et al. (10) reported that air cooling can delay the crack initiation time and lower the crack growth rate, hence enhancing the ESCR. Strebel and Benson (11) investigated the effect of processing factors on blow-molded PE bottles. They claimed that ESCR of the bottles can be enhanced by decreasing mold temperature, die temperature, and molding time.

In a detailed study, Cheng et al. (12) tried to find a correlation between phase interconnectivity and ESCR, mainly as a consequence of resin properties rather than processing factors. The authors found no clear relationship between percentage crystallinity or lamella thickness and ESCR, which may have been due to large MW differences between their resins. The authors, however, reported that a correlation can exist between crystallinity or lamella thickness and ESCR, if the comparison is made between PE resins with relatively similar molecular weights. They confirmed that lower percentage crystallinity and thinner lamellae can result in a larger extent of interlamellar linkages, which ultimately increase the ESCR of PE. Cheng et al. (12) further extended their studies to investigate relationships between lamella surface area (LSA) and ESCR. They postulated that LSA can be a better indicator of ESCR as it represents effects of both MW and SCB.

Most studies in the past on phase interconnectivity and ESCR focused on the effect of processing temperature on the lamella thickness of the polymer (13-17). However, no literature regarding the temperature effect on the LSA was found. In general, research showed that lamella thickness increases with increasing crystallization and annealing temperature. The change in lamella thickness was small at temperatures lower than 85°C. On the other hand, sharp increases of lamella thickness with temperature were observed at

temperatures above 85°C. In annealing experiments, it was also noted that lamella thickness increased with increasing annealing time.

Therefore, the next logical step in studying the effect of phase interconnectivity is to investigate how processing conditions (e.g. processing temperature) affect LSA and subsequently the ESCR of PE. In order to study the effect of processing temperature on the lamella crystal, some researchers (14-15, 17) chose to study single solution-grown crystals of PE. ESC is a characteristic related to the macro-mechanical behaviour of polyethylene, and this makes the investigation of the bulk polymer necessary. In addition, there is considerable dispute about whether crystallization of PE occurs in the same way when it happens in solution and in the melt. Based on the reasons stated above, it makes sense to use bulk PE to carry out a study on the relationship between LSA and processing temperature.

This study was initiated to address the ambiguity associated with the influence of crystallinity and crystal structure on ESCR. Furthermore, studies were performed to find relationships between processing (different cooling rates) and post-processing (annealing temperature and time) conditions that can enhance ESCR by improving phase interconnectivity. Additionally, the intent was to address the following questions, if possible:

1. Which of the two methods, different cooling rate or different annealing temperature/time, causes larger differences in the LSA of PE?
2. Do changes in LSA/ESCR with temperature follow the same trends for all resins?
3. What are the effects of MW and SCB content (individually and via interactions) on the LSA vs. temperature relationship?

6.2 EXPERIMENTAL

6.2.1 MATERIALS

A wide range of commercially available PE resins (linear low density PE (LLDPE) and high density polyethylene (HDPE) with unimodal and bimodal molecular weight distributions), as shown in Table 6.1, were selected for this study. In order to reflect molecular properties on the crystalline structure and phase interconnectivity, PE resins were carefully chosen to cover a large range of MW, MWD and branching content. All PEs shown in Table 6.1 were characterized in detail in order to clarify the ambiguity regarding the relationship between crystalline structure and ESCR (initial stage of the study). For the second stage of the study, LSA investigations were carried out on four of the HDPE resins (HDPE 1-2, PE 4, and PE 8). These four PE resins were good candidates for such a study, as they provided a proper spectrum of MW and SCB (both low and high), which allowed for the identification of the effect on ESCR of material properties in combination with processing factors.

Table 6.1: Molecular properties of PE resins

PE ID	PE grade	Density (kg/m^3)	Mn (kg/mol)	Mw (kg/mol)	Mz (kg/mol)	PDI (Mw/Mn)	SCB[a] (/1000C)	ESCR[b] (h)
LLDPE 1	R.T.[1]	936	15.4	71.8	252.0	4.7	4.2	60
LLDPE 2	R.T.	938	20.8	82.0	232.0	3.9	7.5	150
LLDPE 3	R.T.	937	18.0	74.6	191.0	4.0	13.3	190
LLDPE 4	R.T.	932	15.1	76.6	286.0	5.1	22.3	650
HDPE 1	R.T.	948	18.7	77.9	349.0	4.2	1.6	8
HDPE 2	R.T.	942	25.2	118.5	336.0	4.7	2.4	50
HDPE 3	Pipe-100[2]	958	10.4	217.9	1244.2	20.9	7.0	1000
HDPE 4	Pipe-100	955	5.9	315.4	2129.3	53.3	11.8	3000
PE 4	I.M.[3]	948	19.7	79.4	239.3	4.0	3.8	18
PE 8	Pipe-80[4]	958	14.0	202.1	1398.4	14.4	4.5	>500
P1	B.M.[5]	948	14.8	258.3	2176.6	17.5	3.0	500
P2	B.M.	957	12.5	193.3	1779.2	15.4	1.2	40
P3	B.M.	954	10.8	209.2	1617.0	19.4	4.0	300
P4	B.M.	965	10.4	182.0	159.1	17.5	2.6	15
P5*	Pipe-100	959	---	260.3	---	---	5.6	>1000
P6*	Pipe-100	948	---	301.5	---	---	11.9	>5000
P7*	Pipe-80	951	---	168.7	---	---	11.3	2000
P11	R.T.	---	18.0	126.5	905.3	7.0	2.2	21

*: PE with pigments (no GPC was performed, MW averages were not measured, the reported Mw was determined from rheological methodology (18)), a: Short chain branching (number of short branches) per 1000 carbon atoms, b: ESCR reported from a Bent Strip Test (BST) according to ASTM D1693A, 1: Rotational molding grade PE, 2: PE100 grade pipe resin, 3: Injection molding grade PE, 4: PE80 grade pipe resin, 5: Blow molding grade PE.

Note: Resins with a unimodal MW distribution: LLDPE 1-4, HDPE 1-2, P 1-3, PE 4 and PE 11; Resins with a bimodal MW distribution: HDPE 3-4, PE 8, and P 4-7.

6.2.2 MOLECULAR CHARACTERIZATION

High temperature gel permeation chromatography (GPC) experiments were conducted at Polymer Char, Spain, to identify MW and MWD of the resins. The GPC was equipped with an infra-red detector (GPC-IR) for determination of short branching content and branching distribution. The solvent and operating temperature were 1, 2, 4 trichlorobenzene (TCB)

(stabilized with 300 ppm of butylhydroxytoluene (BHT)) and 140 ºC, respectively. Calibration was based on a conventional narrow polystyrene standard which was ultimately converted to PE using a transformation factor. An AVANCE 500 Bruker NMR was utilized to investigate the short chain branching content of the PE resins at 120 ºC. The solvent of choice was deuterated TCB.

6.2.3 DIFFERENTIAL SCANNING CALORIMETRY (DSC)

Information regarding resin crystallinity and lamella dimensions was investigated by DSC. DSC analyses were performed with a Q2000 DSC controlled by a TA processor. In order to clear their thermal history, samples were heated at a rate of 10 ºC/min from room temperature to 240 ºC, followed by a 3 min isothermal step under a nitrogen environment. Ultimately, samples were subjected to a cooling cycle and a second heating cycle, both at a rate of 10 ºC/min, to obtain the DSC peaks. The enthalpies (ΔH) obtained from integration of the DSC peaks were used to evaluate the percentage crystallinity (X (%)) according to Equation 6-1, and the lamella thickness (*l*) based on the Gibbs-Thompson correlation, shown in Equation 6-2. In these equations, ΔH_c is the enthalpy of the 100% crystalline material (293.6 $\left(\frac{J}{g}\right)$ in the case of PE), and T_m is the melting point obtained from the melting peak of the DSC curve. The Gibbs-Thompson parameter values for polyethylene resins are based on the work of Wlochowicz and Eder (19). $T_m^o = 415\ K$ is the equilibrium melting point of an infinite crystal; $\sigma_e = 60.9 \times 10^3\ \left(\frac{J}{m^2}\right)$ is the surface free energy of the basal plane, and $\Delta H_m = 2.88 \times 10^8\ \left(\frac{J}{m^3}\right)$ is the enthalpy of fusion per unit volume.

$$Crystallinity, X(\%) = \frac{\Delta H}{\Delta H_c \times 100} \quad 6\text{-}1$$

$$T_m = T_m^o \left(1 - \frac{2\sigma_e}{\Delta H_m l}\right) \quad 6\text{-}2$$

6.2.4 X-RAY DIFFRACTION

Two types of X-ray diffraction (XRD) techniques were used in this work. The first technique was wide-angle X-ray scattering (WAXS), in which the scattering angles were from 6-34 º. WAXS patterns were measured in a STOE two circle goniometer using Cu Kalfa radiation from an ENRAF NONIUS FR 571 rotating anode generator. To minimize the background level, the X-rays were detected with a MOXTEK energy sensitive Si-detector, connected to single channel analyzers that selected photons corresponding to the Cu Kalfa radiation (Lambda (λ) = 1.54178 Å). WAXS was conducted to identify the X-ray percentage crystallinity of the PE resins (ratio of the area under the crystalline peak to the total area of the X-ray scan) as shown in Equation 6-3. In this equation, I_c and I_a are the scattering intensities of the crystalline and amorphous regions, respectively. The second technique was small-angle X-ray scattering (SAXS), which was used to find the long spacing (L) and, consequently, the lamella thickness (*l*) of the resins. The SAXS patterns were measured in a Bruker NANOSTAR using Kalfa radiation. Long spacing was calculated using the Bragg formula (Equation 6-4) from the peak position of the first maximum (ε) in the SAXS pattern. In Equation 6-4, "*n*" represents the level of scattering and λ is the wave length of the X-ray. Ultimately, the lamella thickness (*l*) was found using the relationship shown in Equation 6-5.

For both techniques, bars 25 mm in length and 10 mm in width were compression-molded at 190 ºC and 44.5 kN, followed by quenching in cold water.

$$Crystallinity\ (\%) = \frac{\int I_C}{\int I_C + \int I_a} \times 100 \quad \text{6-3}$$

$$L\varepsilon = n\lambda \quad \text{6-4}$$

$$Lamella\ thickness\ (l) = Crystallinity\ (\%) \times L \quad \text{6-5}$$

6.2.5 NOTCH CONSTANT LOAD TEST (NCLT)

The NCLT according to ASTM D5397 was utilized to identify the ESCR of the resins. In this test, specimens were subjected to constant load under an aggressive environment at elevated temperatures. A notch was introduced in the compression-molded dog-bone samples that had been prepared at 190 ºC, producing a ligament thickness of 60 % of the nominal thickness of the specimens. The notched specimens were suspended in a solution of water and 10 % surfactant (Igepal) under an applied stress equivalent to 15 % of the yield stress. The time of failure was recorded and reported as the ESCR of the resins. It should be mentioned that NCLT was used to selectively verify the ESCR reported from a Bent Strip Test (BST, which is one of the preferred conventional methodologies to evaluate ESCR), provided by the resin manufacturer.

6.2.6 HARDENING STIFFNESS (HS) TEST

The hardening stiffness test was performed at room temperature on an Instron 3365 machine. The specimens were prepared by punching compression-molded plaques prepared at the

following conditions: compression-molding at 195 ºC ± 5 ºC and 44.5 kN, followed by cooling to room temperature at a rate of 1 ºC/min, while increasing the applied force to 89 kN. The principles involved in the selection of sample dimensions were the same as those described in Sardashti et al. (20). The HS was obtained by measuring the slope of the strain hardening section of the load-displacement curve. The test specimens were extended until complete failure was obtained at a rate of 10 mm/min.

6.2.7 EXPERIMENTAL DESIGN

In this work, two experimental designs were utilized. The first design was a D-optimal response surface design, used to identify the significance of annealing temperature and annealing time of different PE resins on the following material properties (responses): percentage crystallinity, lamella thickness, LSA, and ESCR (determined from the HS test). Four levels of PE resins (each having different Mw and branching content), two levels of annealing temperature, and three levels of annealing time were selected, as indicated in Table 6.2. A total of 29 experimental runs were performed for each response, according to the D-optimal design.

The second experimental design was a D-optimal factorial design, used to identify the effect of cooling type on the same response variables. In this design, three different types of cooling rate were used, including quenching (rapid cooling in cold water), air cooling at a rate of 5 ºC/min, and slow cooling (over a period of 3 hours).

Table 6.2: Experimental design to investigate the effects of annealing time and temperature on different PE resins

Study Type: Response surface	Design Type: D-optimal			
Design Model: Reduced cubic	Runs: 29			
Factor	Levels			
PE Type	HDPE 1	PE 4	HDPE 2	PE 8
Annealing Temperature (°C)	90	100		
Annealing Time (h)	1	5	10	

6.3 RESULTS AND DISCUSSION

6.3.1 CRYSTALLINE PROPERTIES AND ESCR

6.3.1.1 CRYSTALLINITY AND ESCR

In this part of the study, the crystalline phase properties of all PEs, namely percentage crystallinity (X (%)), lamella thickness (*l*), and lamella surface area (LSA), were evaluated by DSC. The results are summarized in Table 3. Also reported in this table are HS and cHS (corrected HS) values, which are the hardening stiffness values measured from the HS test (see section 6.2.6, and also Chapter 4 of this thesis), evaluated from a uniaxial tensile test as per our earlier work (20). ESCR (from Table 6.1) vs. measured percentage crystallinity (X (%), from Equation 6-1 and Table 6.3) are plotted in Figure 6.1 (log scale was used on the y-axis due to the large ESCR values). In earlier studies, no clear trend between ESCR and percentage crystallinity had been established. Cheng et al. (12) attributed this lack of a clear trend to major differences between the molecular weights of the selected resins. Both ESCR and crystallinity are highly influenced by MW and SCB content of the resins. That being said, ESCR is primarily controlled by the MW of the PE resin and only secondarily affected by SCB. On the other hand, percentage crystallinity is highly sensitive to SCB content, and a

slight change in the comonomer content can significantly change crystallinity. As a result, PE resins in this study were divided in two groups: the low MW group (PE resins with Mw around or below 120 kg/mol), and the high MW group (PE resins with Mw above 170 kg/mol). The low MW group includes all of the LLDPE resins, HDPE 1-2, PE 4, and P 11. On the other hand, the high MW group consists of HDPE 3-4, P 1-7, and PE 8. Once the resins are separated according to the aforementioned criterion, a clear trend can be seen between ESCR and percentage crystallinity: there is a steady decrease in ESCR with increasing percentage crystallinity. Investigating the crystallinity of the resins in the low MW group, it is clear that decreasing percentage crystallinity is primarily dictated by short chain branches, as these resins have very similar MW and MWD (also indicated by the density values of Table 6.1).

The high MW group showed a similar decreasing trend in ESCR as crystallinity increased; however, this trend is a bit more complicated to explain than the former case. Additional information is needed in order to identify the molecular difference causing this complication. P 4-7 are bimodal HDPEs. P 4 is a blow molding grade, whereas P 5-7 are pipe resins (P 5-6 are PE 100, P 7 is PE 80). High ESCR values (and, consequently, lower percentage crystallinity) were expected for P 5-7, as these resins have a relatively high MW ethylene-α-olefin (hexene) component, a low MW homo-polymer component, and a relatively higher SCB content. The SCB content in P 5-7 is expected to be at the higher end of the molecular weight spectrum. On the other hand, while P 4 is a bimodal PE resin, it is mostly composed of a homo-polymer component, and consequently exhibits poor ESCR and higher percentage crystallinity.

More attention was given to P 5 and P 6. These PEs have a similar percentage crystallinity (Table 6.3), yet they differ significantly in the ESCR values (Table 6.1). This was found to be related to the larger number of short chain branches in P 6, which are believed to be distributed at the higher end of the molecular weight distribution. Due to their large sizes, the chains located at the higher end of the MWD of P 6 do not fit into the crystal lamella structure, and are consequently placed in the non-crystalline amorphous phase. Therefore, adding SCB to these chains does not affect the overall percentage crystallinity of the polymer. However, it adds to the overall chain entanglement in the amorphous domain, which is subsequently reflected on its ESCR value (highest ESCR among the selected PEs, Table 6.1).

Additional investigations also indicated that when PE resins have a relatively high MW, an increase in the percentage crystallinity is not necessarily going to reduce the ESCR (Figure 6.1, P 7 and PE 8 vs P 6). On the contrary, a higher crystallinity level can enhance ESCR, given that PE chains are long enough to generate a sufficient number of tie-molecules to resist SCG. A similar observation has been reported by Cheng et al. (12) and Lu et al. (21).

Focusing now on the unimodal high density resins (P 1-3), the results showed a clear dependence of crystallinity on SCB content. P 2 had the highest percentage crystallinity level due to its lower SCB content. On the other hand, P 3 showed a higher percentage crystallinity compared to P 1, although it had a higher SCB content. These observations suggest that when PE resins with a similar molecular structure (unimodal) and SCB content are compared, the resins with a higher MW tend to have a lower crystallinity. A similar observation has been reported by Tung and Buckser (22). Secondly, it is believed that the short chain branches in P 3 are located at the higher end of the MWD (this was subsequently verified from GPC-IR

measurements, but chromatograms/traces are not shown here for the sake of brevity), hence, they do not affect the overall crystallinity of the polymer (as per earlier discussion on P 6).

In brief, examining the crystalline structure and ESCR showed that, for a unimodal PE resin in the low MW group, ESCR increases with increasing molecular weight and SCB content. This consequently lowers the crystallinity of the polymer. Therefore, one could expect a decrease in the rate of slow crack growth with a decrease in crystallinity (density). On the other hand, for the high MW group, if the molecular weight is high enough to produce a large number of tie-molecules, or if the PE of choice has a bimodal molecular structure, no definite correlation can be found between crystallinity/density and ESCR. In this case, additional details regarding the MW, SCB, and their respective distributions are needed to make a selection.

Table 6.3: Crystalline properties and hardening stiffness values

Polymer ID	X (%)	*l* (nm)	LSA (nm^2/mol)	HS (N/mm)	cHS (N/mm)
LLDPE 1	49.41	10.86	3.3	0.249	2.68
LLDPE 2	48.90	11.15	3.7	0.336	7.38
LLDPE 3	46.90	10.76	3.3	0.269	9.53
LLDPE 4	42.38	10.77	3.1	0.3	18.3
HDPE 1	59.69	13.71	3.4	0.214	0.95
HDPE 2	55.19	12.87	5.2	0.352	3.55
HDPE 3	61.5	14.6	9.3	0.536	29.2
HDPE 4	51.5	11.7	14.1	0.55	73.11
PE 4	58.4	13.16	3.6	0.22	2.37
PE 8	58.1	13.52	8.8	0.38	12.34
P1	64.4	15.44	10.9	0.74	20.48
P2	72.7	18.09	7.8	0.40	3.31
P3	70.8	15.97	9.3	0.40	11.92
P4	80.6	20.48	7.2	---	---
P5	63.0	14.15	11.4	0.70	36.46
P6	62.3	14.34	13.3	0.75	96.74
P7	55.9	12.98	11.4	0.46	30.99
P11	66.3	15.07	5.6	---	---

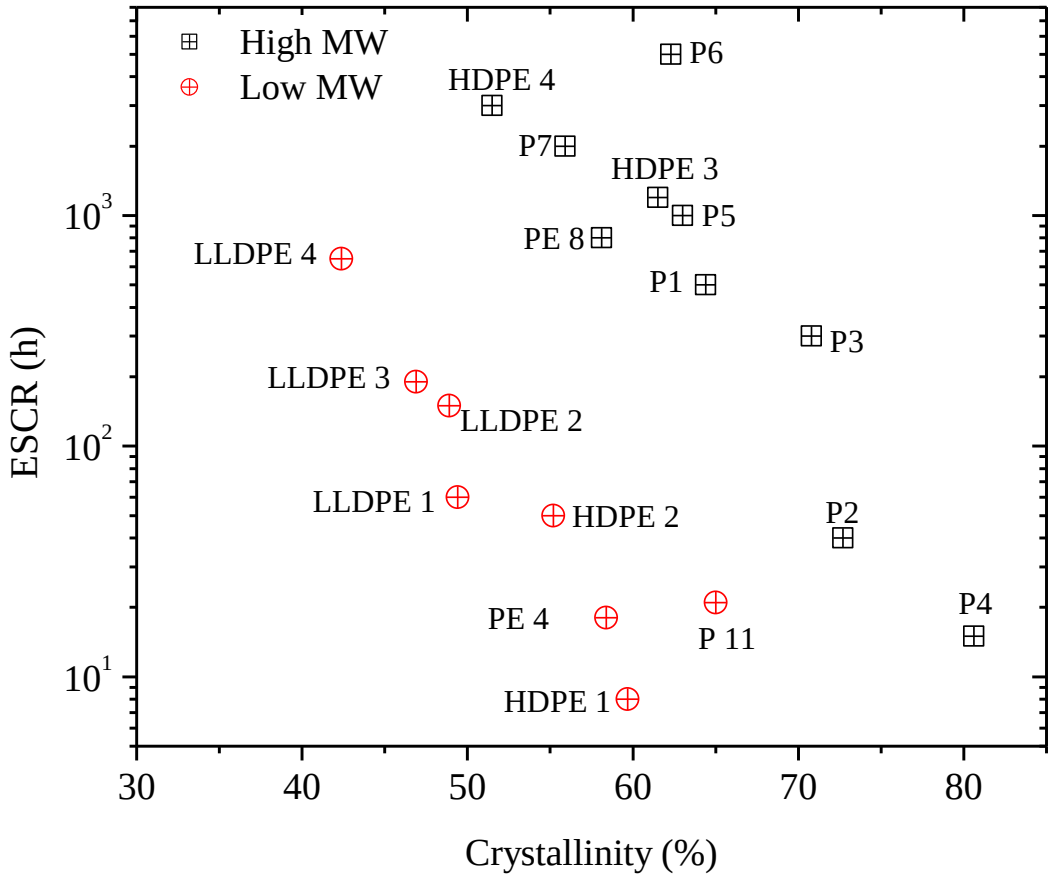

Figure 6.1: ESCR vs. percentage crystallinity

6.3.1.2 LAMELLA THICKNESS AND ESCR

Lamella thicknesses of all PE resins in this study were obtained by DSC (see "*l*" in Equation 6-2) and the results are tabulated in Table 6.3. Figure 6.2 shows ESCR values (Table 6.1) vs. the calculated lamella thickness. A similar analogy was adopted to separate resins into two groups based on their weight average molecular weights (as was the case earlier with crystallinity). It has been shown in the literature (10, 12) that there is an inverse relationship between ESCR and lamella thickness. The probability for a long molecule to become a tie-molecule is higher when the lamella thickness is lower (i.e., thinner lamella). Examining Figure 6.2, it can be seen that the LLDPE resins, due to their high SCB content,

exhibit significantly lower lamella thickness values (and a higher ESCR) compared to the other resins in the low MW group. That being said, it is not possible to distinguish differences in ESCR of different LLDPE resins by solely inspecting their lamella thickness. LLDPE 1 and LLDPE 3-4 have a relatively similar MW and MWD, but different SCB content. Increasing SCB from 4 to 13 /1000 C units lowered the lamella thickness only slightly. A further increase in SCB, however, had no significant effect on the lamella thickness (see LLDPE 3-4). This observation suggests that short chain branching in such low molecular weight PE resins changes the lamella thickness only slightly, in contrast to crystallinity, and no clear correlation between ESCR and lamella thickness can be made. On the contrary, many studies have illustrated a large dependence of lamella thickness on the SCB content (12, 23). It was postulated that the SCB content in the LLDPE resins may not change the lamella thickness obtained from Equation 6-2 (mean lamella thickness obtained at the melting point), but may affect the lamella thickness distribution (LTD) in the polymers. For this reason, LTDs for the LLDPE resins were calculated based on the work of Alberola et al. (24), as shown in Equation 6-6. In this equation, M ($M = M_T X$) is the mass of the total crystalline domain obtained by multiplying the total mass of the polymer (M_T), used in the DSC measurements, by its degree of crystallinity (X (%)). dE/dT is the amount of energy required to melt M (obtained from DSC). Finally, T_m and T^o_m are the melting point and the equilibrium melting point of an infinite crystal, and σ_e is the surface free energy of the lamella (all three as presented earlier in the discussion around Equation 6-2).

$$\frac{1}{M}\frac{dM}{dl} = \frac{\left(dE/dT\right)(T_m^o - T_m)^2}{2\sigma_e T_m^o} \qquad 6\text{-}6$$

Figure 6.3 illustrates the lamella thickness distribution of the LLDPE 2-4 resins (in Figure 6.3 and in similar figures that follow, the Y-axis has units of m^{-1}). The lamella thickness values reported in Table 6.3 (third column) are determined from the measured melting point (DSC melting peak) of the resins. This thickness value is related to the "most available" lamella dimension, due to the nature of the DSC measurement. The values in Table 6.3 indicate that all LLDPE resins have lamellae with comparable thickness values measured at their melting points. The lamella thickness distributions (LTD), however, shown in Figure 6.3, tell a much more interesting story. The LTDs of the LLDPE 2-4 showed that as the SCB content increased (see the 8th column of Table 6.1, rows 2-4), a narrower LTD was obtained (higher number of thinner lamellae). This observation showed that LTD is a better indicator of the effect of short branches (and ultimately of ESCR), compared to only a single lamella thickness value (which includes an averaging effect), for LLDPE resins with low MW. On the other hand, extending the study on the other resins in the low MW group (HDPE 1-2, PE 4) showed a clear decreasing trend in ESCR with increasing lamella thickness (see relevant entries in Table 6.1 and Table 6.3). Similarly, the lamella thickness distributions for all these resins were determined and are summarized in Figure 6.4. The contrast between the lamella thickness distributions, along with shifts towards thicker/thinner lamellae, seems to be a more promising tool for prediction of ESCR, for cases where the established decreasing trend (ESCR vs. lamella thickness) does not hold valid.

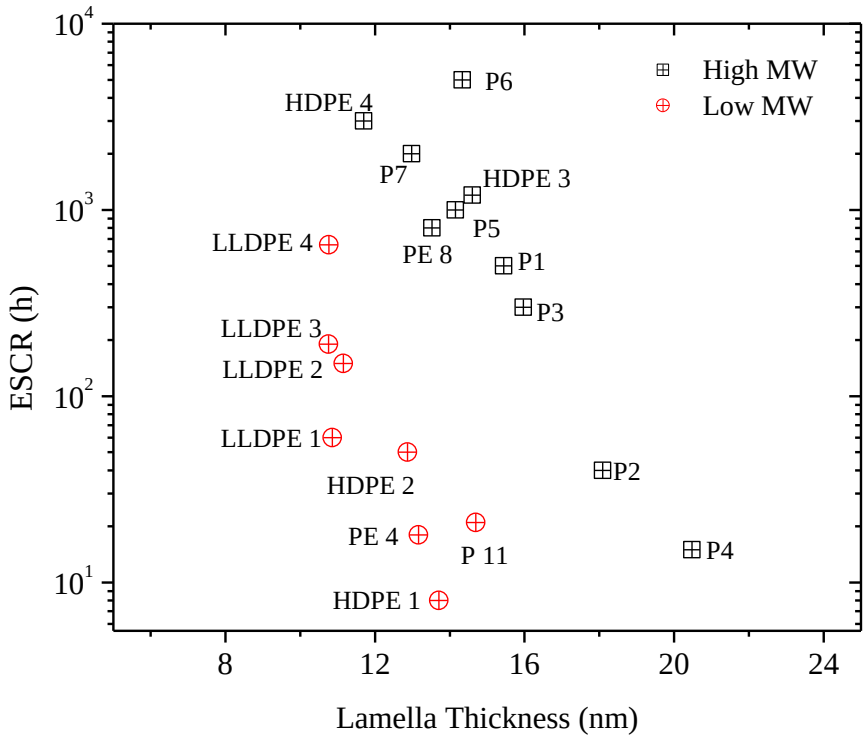

Figure 6.2: ESCR vs. lamella thickness

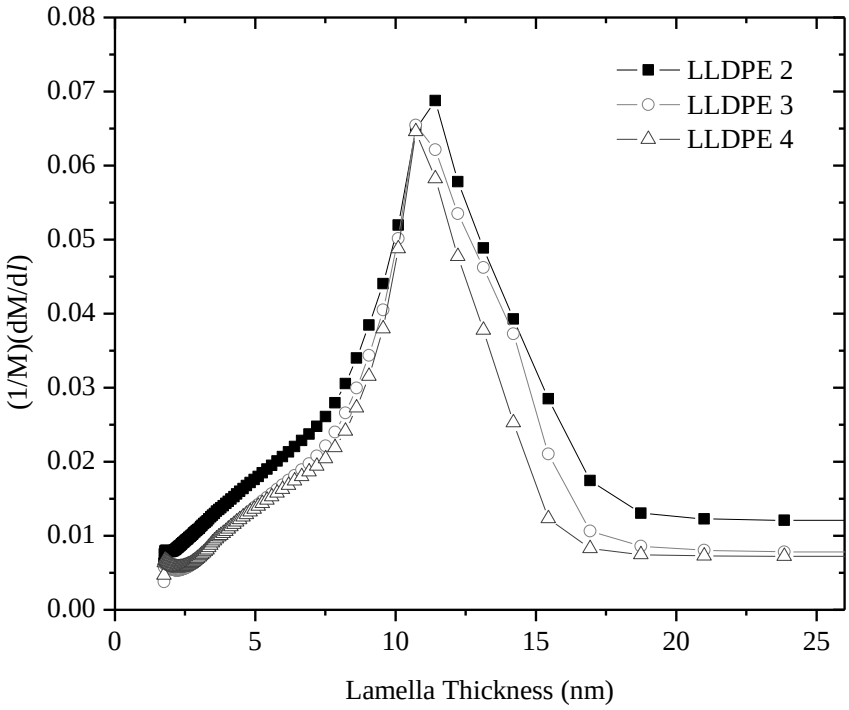

Figure 6.3: Lamella thickness distribution of LLDPE 2-4 resins

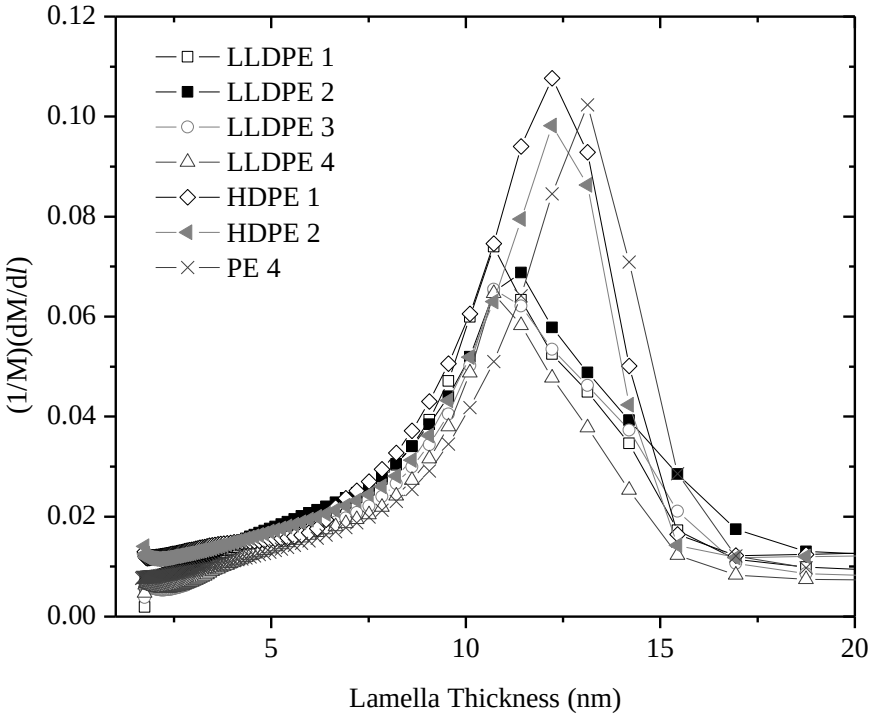

Figure 6.4: Lamella thickness distribution of low MW PE resins

Similarly, the high MW group showed a decrease in ESCR with increasing lamella thickness. All bimodal HDPE resins (P 4-7, HDPE 3-4), excluding P 6, followed this trend. Lamella thickness distributions (shown in Figure 6.5) for the bimodal P 4-7 were scrutinized further in an attempt to identify the reason for the deviation of P 6 from the norm. It was speculated that the LTD of P 6 was relatively narrower than P 5 and P 7, offering a range of thinner lamellae, however, no clear differences in the LTD of P 5 and P 6 were observed. The lack of consistency in the observed trend pointed to the fact that a more subtle molecular difference should exist between P 6 and the other bimodal PE resins. The deviation exhibited by P 6 is postulated to be due to a different methylene sequence length of the short branches. It has been shown that longer SCB tends to increase the lamella thickness (25), and this would explain the deviation in the behaviour of P 6.

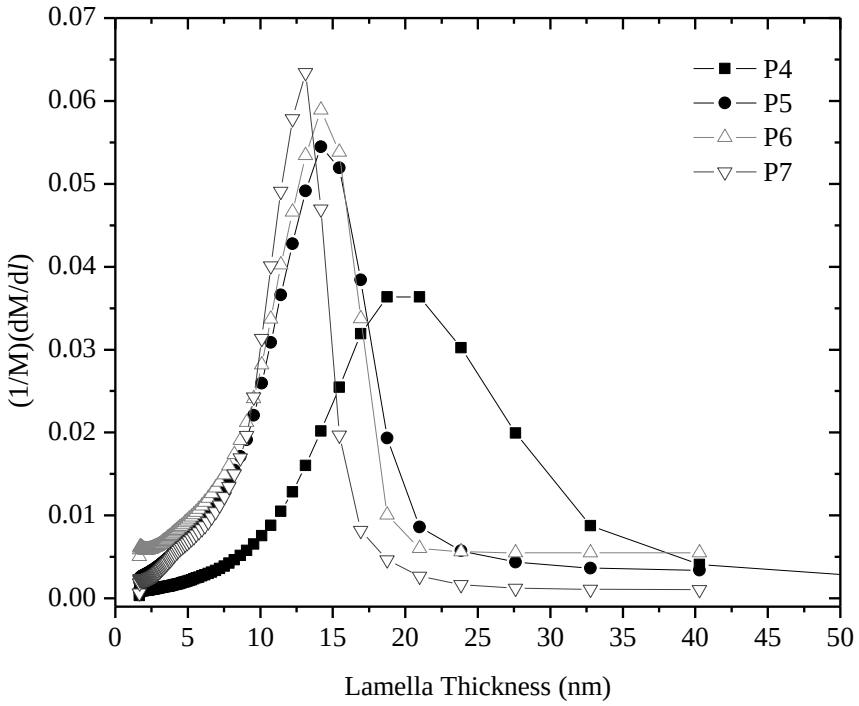

Figure 6.5: Lamella thickness distribution of bimodal P4-7

The next step in the study involved determining the lamella surface area (LSA in Table 6.3) of the resins, which is believed to be an indicator of phase interconnectivity between crystalline and amorphous regions. A strong interconnectivity between regions of polymer can properly transfer an applied stress to various lamellar regions and prevent possible deformation. Melt crystallization in PE is believed to occur in two main stages (26). Stage one involves heterogeneous nucleation and growth of crystalline spherulites, which are made of flat lamellae, arranged in a radial direction from the nucleus (see Figure 6.6). The lamellae have a rectangular structure with lateral dimensions X and Y, and a significantly smaller thickness (*l*) in the range of 10-20 nm. The difference between the length of PE chains and the lateral dimensions of the lamellae alludes to the chain folding process in the PE crystalline lamellae. PE chains fold back and forth with their chain axis perpendicular to the

crystal basal plane. The surfaces with dimensions X and Y (which contain the folded chains) are called the "fold surfaces", and the surfaces with X and "*l*" dimensions are called the "lateral surfaces". The second stage of crystallization involves lamellae thickening, or further formation of new lamellae in between the existing ones (26). During these crystallization stages, molecular defects in the PE chains can hinder the regular chain folding process and give rise to formation of tie-molecules and other interlamellar entanglements. These entanglements can be anchored from one end to the crystal lamella (cilias), or anchored from two ends to either the same lamella (loose loops), or an adjacent lamella (tie-molecules). As these chains contribute to the overall interconnectivity of the semicrystalline PE, one can argue that an increase in the area of the "fold surface", which contains all these chains, can increase the overall chain extensibility and subsequently the ESCR of the polymer. There have been a very limited number of attempts in the literature to measure the "fold surface" area of the PE lamellae. In one such attempt, Cheng et al. (12) found the lamella surface area by simplifying the microstructure of the crystals. They assumed a thin flat rectangular prism structure for a single PE lamella, whose area can be found from the ratio of its specific volume to its height (thickness). Equation 6-7, adopted from Cheng et al. (12), was used to obtain a measure of the LSA for all the PE resins in this study, with a slight change. The specific volume of the crystal of PE resins in Cheng et al. (12) was assumed to be equal to 1 m^3/kg. In this work, an approximate value of the specific volume of the crystal (V_C) in the numerator of Equation 6-7 was estimated using Equation 6-8 (27). In Equation 6-8, V_W is the van der Waals molar volume (V_C = 1.435 V_W), and X is the percentage crystallinity (from DSC). The values for the specific volume of all PEs (V_{PE}, from DSC) and the specific volume of the crystalline region of the PEs (V_C) were in line with literature data. The MW

weight of a crystal (in Equation 6-7) was estimated by multiplying the Mw of a PE resin (Table 6.1) with its corresponding percentage crystallinity (Table 6.3). The lamella thickness values were obtained from DSC endotherms and Equation 6-2, as described earlier.

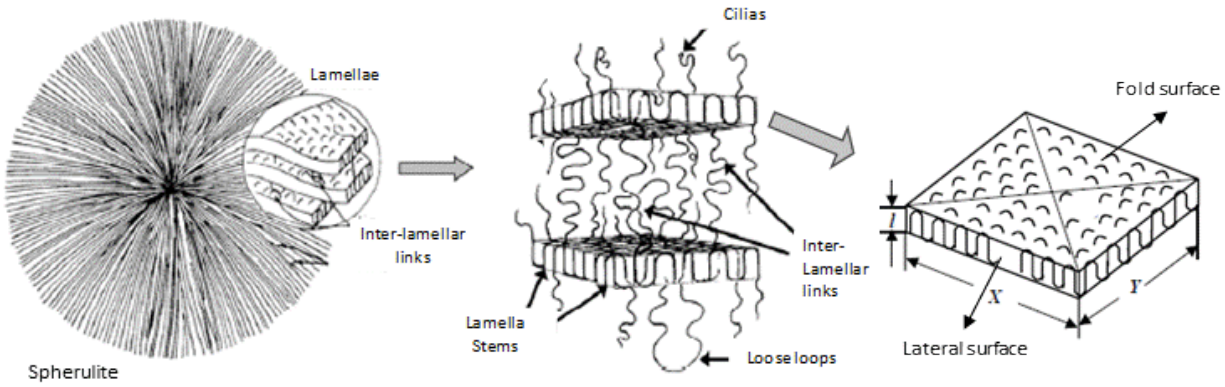

Figure 6.6: Spherulitic and lamellar structure of melt crystallized PE, adapted from (7, 26)

$$LSA\left(\frac{m^2}{mole}\right) = \frac{specific\ volume\ of\ crystal, V_C\ (m^3/kg)}{lamella\ thickness, l\ (m)} \times MW\ of\ crystal \qquad 6\text{-}7$$

$$Specific\ volume\ of\ PE, V_{PE}\left(\frac{m^3}{kg}\right) = 1.43\,XV_W + 1.6\,(1-X)V_W \qquad 6\text{-}8$$

Figure 6.7 illustrates ESCR vs. LSA results. As in earlier sections, PE resins were separated into two groups. The unimodal HDPE resins (P 1-3) in the high MW group showed a clear increase in ESCR with LSA, as a result of their low lamella thickness, which was directly affected by the SCB content. The bimodal PE resins in the high MW group, again excluding

P 6, also showed an increasing trend in ESCR with LSA, verifying the earlier statement that a larger LSA can lead to a higher ESCR. A closer inspection of HDPE 4 and P 6 showed that the reported lamella area estimates were highly sensitive to the SCB content. No correlation between ESCR and LSA was obtained for the low MW group, if the LLDPE resins (which fall within the elliptical region in Figure 6.7) are taken into consideration. It is believed that these PE resins, due to their relatively low MW and high SCB content, do not produce lamellae with significantly different surface areas. Differences in molecular properties of these resins are mainly reflected on their crystallinity and lamella thickness distribution, and any suggested relationship to ESCR should only be based on those properties.

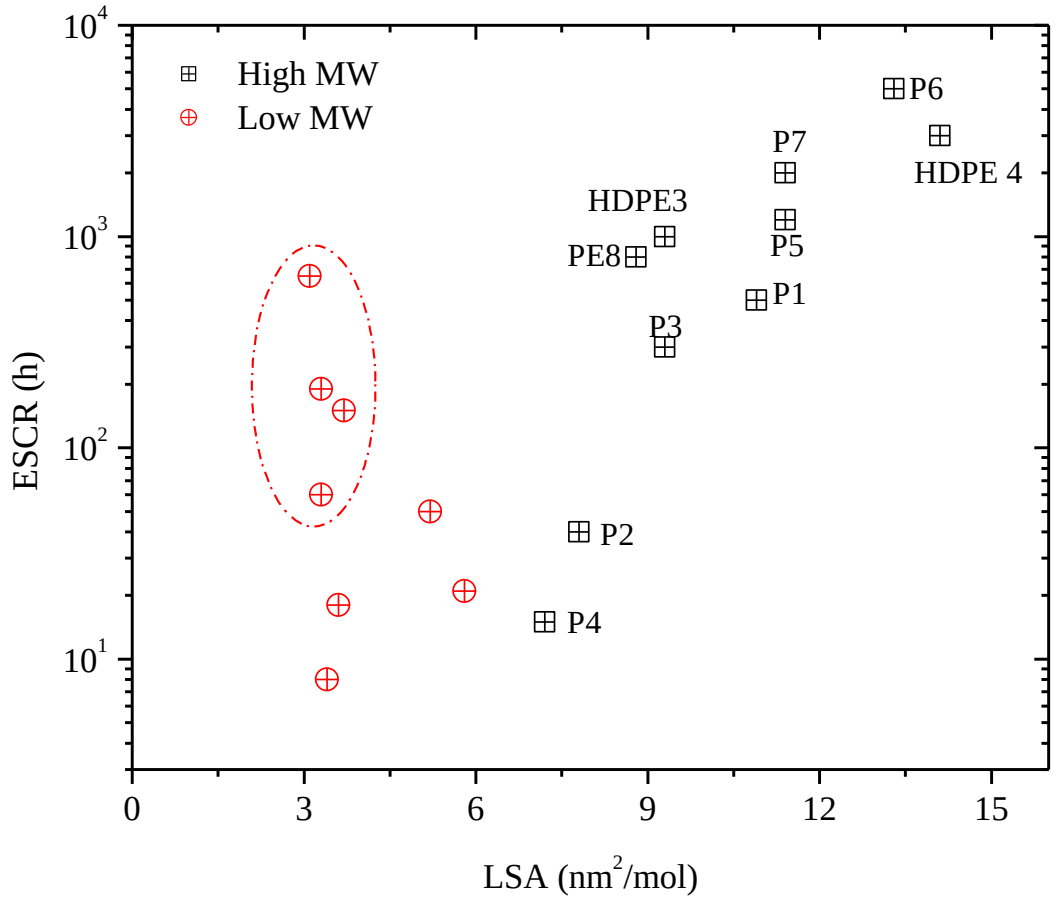

Figure 6.7: ESCR vs LSA for all PE resins

6.3.2 EFFECT OF TEMPERATURE ON CRYSTALLINE PROPERTIES

The intention here was to identify the effect of processing and post-processing temperature on the LSA, as a potential tool for modification of ESCR of PE resins. For this reason, annealing experiments (performed at different temperatures and times) and controlled cooling were conducted on HDPE 1-2, and PE 4 and PE 8. These selected resins have Mw ranging from 80 to 200 g/mole, and SCB content from 1.6 to 4.5 per 1000 carbon atoms. In addition, the chosen polyethylene resins have reasonable ESCR levels. Not all HDPE resins have measurable ESCR and some resins may have ESCR levels in the thousands of hours. In order for experiments to be completed in a reasonable amount of time, all of the HDPE resins

chosen had an ESCR of less than 800 hours. The experimental procedure required that the resins be made into sample plates using compression molding (performed at 190 ºC and 44.8 kN). Differences in PE crystalline phase structures were achieved using the annealing method, in which plates were produced, and then annealed in an oven at different temperatures for different lengths of time (refer to Table 6.2 for the design factor levels). In order to study the effect of temperature, the plates needed to be control-cooled at different cooling rates from the melt state to the solid state. PE samples were control-cooled from 190 ºC at different cooling rates (section 6.2.7). The characterization of the crystalline phase properties of sample plates was carried out using wide and small angle XRD (WAXS and SAXS, respectively). The WAXS method was used to determine the crystallinity of the resins according to Equation 6-3, and SAXS to evaluate the lamella thickness according to Equation 6-5. DSC was further utilized to verify both the percentage crystallinity and lamella thickness of the resins (for selective runs).

6.3.2.1 EFFECT OF ANNEALING ON LSA

An experimental design according to the factors in Table 6.2 was constructed and LSA was determined as described earlier. Results were analyzed using DesignExpert8 software to identify the significance of the design factors and their interactions. ANOVA (Analysis of Variance) for this D-optimal surface response design is shown in Table 6.4. It should be noted that only the significant factors are shown in this table for the sake of brevity. The model F-value of 20,200.32 implies that the model is significant. P-values less than 0.01 indicate that the model terms are significant. In this case, PE type (A), annealing temperature (B), annealing time (C), and the interactions AB and AC were found to have a significant effect on LSA. The effect of annealing temperature and time on LSA for all analyzed resins

is shown in Figure 6.8. A general decreasing trend in LSA appears as both annealing temperature (to a higher degree) and annealing time (to a lower degree) are increased. This trend suggests that post-process annealing can indeed reduce the lamella surface area, and consequently affect the ESCR (a possible reduction). That said, the degree of dependency of the polymer LSA on the annealing temperature and time varied according to molecular structure (i.e., PE type). For example, PE 8 showed 2.5-3.5 % of a decrease in LSA when subjected to different annealing times. This reduction was between 5.1-8.5 % when the annealing temperature was increased from 90 ºC to 100 ºC. HDPE 2, on the other hand, showed less sensitivity to annealing time (1-1.5 %); however, a 6-7.5 % decrease in the LSA was obtained with increasing annealing temperature. Both HDPE 1 and PE 4 showed a maximum of 3 % decrease in LSA when subjected to different annealing times, however, their LSA values were reduced by 10 % and 6.6 %, respectively, when annealing temperature was increased to 100 ºC. Based on these observations, it can be concluded that the annealing time, although statistically a significant factor, has a smaller effect on the LSA of the selected PE resins. The effect of annealing temperature on the LSA was significantly higher (also reflected in the F-value, shown in Table 6.4). PE 4 showed the lowest dependency on annealing temperature. The LSA was reduced by 3.8-6 % upon annealing at higher temperature (a 34 % lower reduction compared to HDPE 1). HDPE 1 and PE 4 both have a very similar MW and MWD, and the only molecular difference between these two resins is their comonomer content. The behaviour of LSA with annealing temperature showed that the dependency of the LSA on temperature is more apparent when SCB content is low. As SCB increased, the effect of annealing temperature on the lamella area decreased. In order to verify this postulation, lamella thickness distributions of PE 4 and HDPE 1 at different

annealing conditions were obtained. Since LSA is obtained from the crystalline lamella thickness, any changes in the lamella distribution upon annealing can be reflected on LSA. LTDs of HDPE 1 and PE 4 are shown in Figure 6.9 and Figure 6.10. It is important to note that the LTD of HDPE 1 (PE with the lowest SCB content) clearly changes with annealing time and annealing temperature. With increasing annealing conditions, LTD widens and shifts to higher values. On the other hand, analyzing the LTD of the PE 4 showed that LTD changes with annealing conditions only slightly. No major shifts in the values are obtained. This observation verified the earlier postulation that as the SCB level increases, the effect of annealing conditions on LSA becomes more subtle.

Table 6.4: ANOVA for effect of annealing time and temperature on LSA

Source	Sum of Squares	df[a]	Mean Square	F-Value	p-value
Model	1.2E+02	11	1.1E+01	20200.3	< 0.0001
A-PE Type	1.1E+02	3	3.8E+01	72513	< 0.0001
B-Annealing Temperature	5.5E-01	1	5.5E-01	1057.48	< 0.0001
C-Annealing Time	4.7E-02	1	4.7E-02	90.1152	< 0.0001
AB	1.0E-01	3	3.4E-02	65.7759	< 0.0001
AC	1.9E-02	3	6.2E-03	11.8938	0.0005
Residual	6.8E-03	13	5.2E-04		
Total	1.2E+02	24			

a: degrees of freedom.

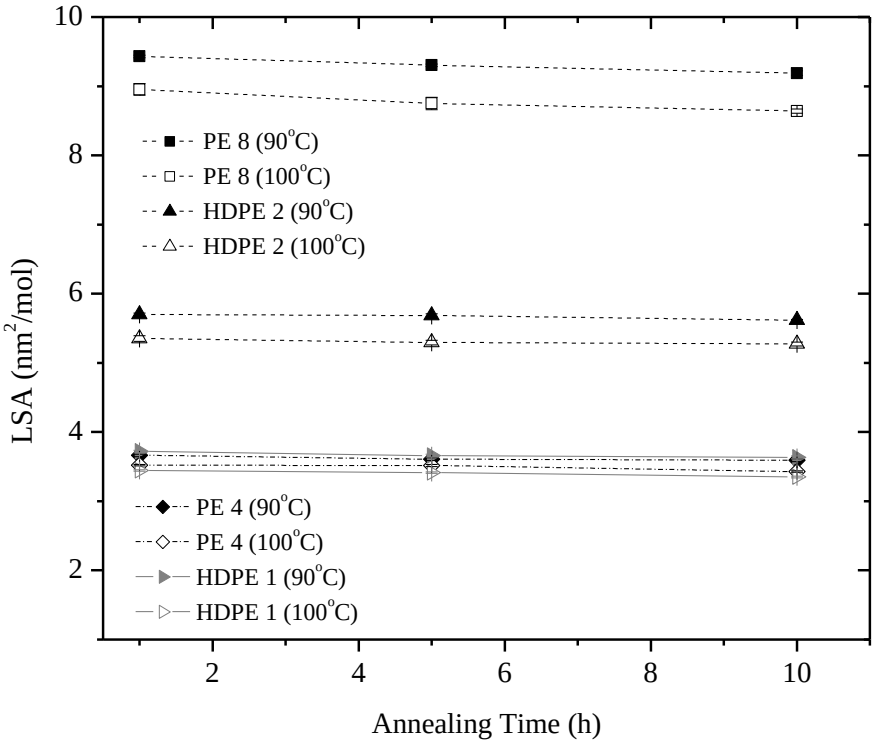

Figure 6.8: LSA at different annealing times and temperatures

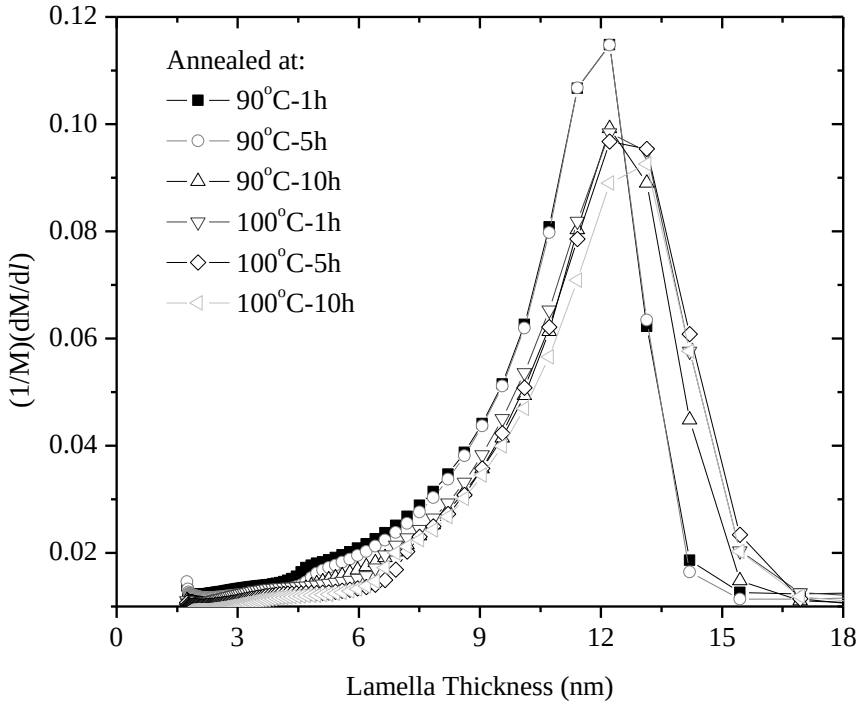

Figure 6.9: Lamella thickness distribution of HDPE 1 after annealing

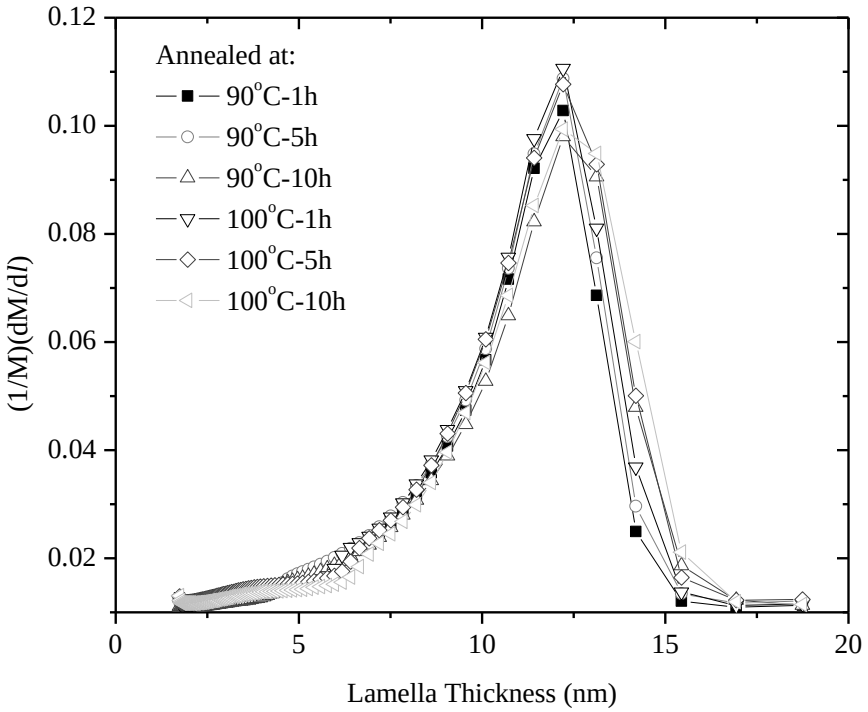

Figure 6.10: Lamella thickness distribution of PE 4 after annealing

In order to independently verify the crystallinity and lamella thickness from XRD analysis, DSC experiments were conducted on select PE samples. It was found that both crystallinity and lamella thickness from the two characterization methodologies were very similar. This can clearly be observed in Figure 6.11, where the ratios of percentage crystallinity and lamella thickness obtained from DSC and XRD are almost equal to 1.

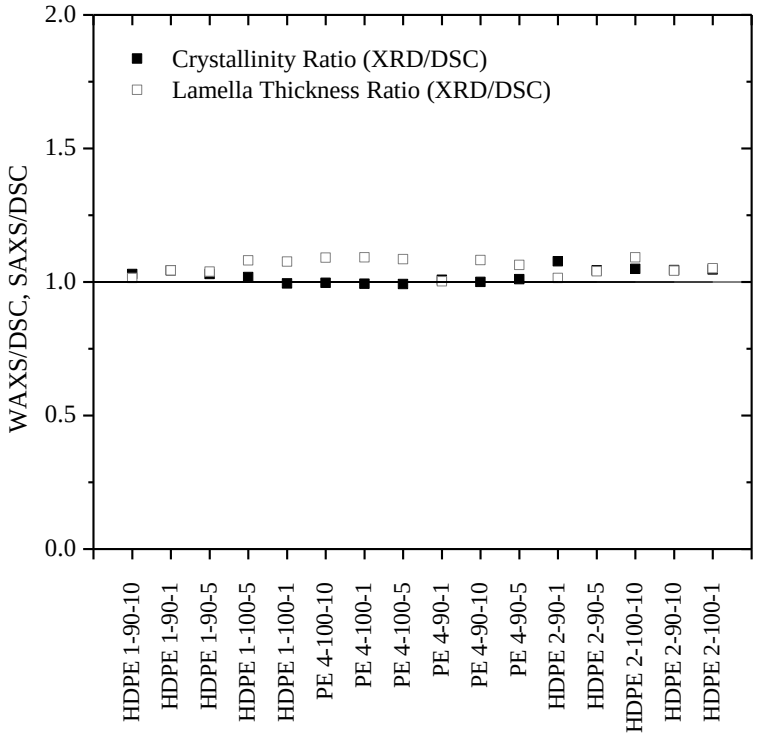

Figure 6.11: Ratio of percentage crystallinity and lamella thickness determined from XRD and DSC analyses

6.3.2.2 EFFECT OF CONTROLLED COOLING ON LSA

In order to identify the effect of cooling rate on the lamella surface area, experiments according to the second experimental design (see section 6.2.7) were conducted and the results analyzed. As found earlier in section 6.3.2.1, type of PE (A) and cooling rate (B) were observed to have a significant effect on LSA of the resins (see the ANOVA of Table 6.5). Also note that no factor interactions were significant, meaning that LSA of the selected PE resins behaves the same when subjected to different cooling rates. Figure 6.12 illustrates the results obtained for the effect of cooling rate on the LSA of representative PE resins. Quenching and air cooling both showed an unexpectedly similar effect on LSA, and the slow cooling rate (room temperature cooling) reduced LSA only marginally. Further analyses were performed to identify the effect of the cooling method on percentage crystallinity

(Figure 6.13) and lamella thickness (Figure 6.14). This was mainly performed to clarify the unexpected behaviour of LSA, when samples were exposed to controlled-cooling. The LSA is a reflection of both percentage crystallinity and crystalline lamella thickness. Therefore, the magnitude of the changes in these two properties upon cooling can change LSA to varying degrees. When PE samples were subjected to different cooling types (and, hence, rates), the obtained percentage crystallinity values caused a maximum of 14 % change in the values of the LSA. Similarly, the changes in the lamella thickness values caused a maximum of 17 % change in the values of the LSA. This observation shows that through various cooling methods, both percentage crystallinity and lamella thickness affect LSA to a similar degree. Since LSA is related to the ratio between the percentage crystallinity and the lamella thickness values, no major change in the values of LSA is obtained overall. This behaviour is reflected in Figure 6.12, where only negligible differences in the LSA through different cooling types are illustrated. This behaviour is also verified from the p-value (0.0423) for the effect of cooling type on LSA shown in Table 5 (only marginally significant). Based on this observation, it is concluded that LSA cannot be a potential indicator of changes in the crystalline phase, if PEs are subjected to different cooling rates. In this case, other crystalline properties such as X (%), "*l*", or the LTD are believed to be better indicators of structural changes in the crystalline phase. LTDs of PE 4 and HDPE 2 after quenching and air cooling were subsequently evaluated and the results are shown in Figure 6.15. There is a clear shift to lower thickness values with a faster cooling rate (quenching). It was interesting to observe that the breadth of the LTDs, however, did not change. As usual, the breadths of the LTDs were obtained from the full width at half maximum values of a Gaussian model fitted to the data points using MATLAB. The model parameters were evaluated based on a 95 %

confidence level. This methodology was utilized here because the lower and higher ends of the lamella thickness distributions were found to be very similar at different cooling rates. The breadths of the LTD of PE 4 subjected to air cooling and quenching were found to be 3.96 and 4.10, respectively. In a similar manner, HDPE 2 showed LTD breadths of 3.8 and 4.0, when subjected to quenching and air cooling, respectively.

Table 6.5: ANOVA for effect of cooling on LSA

Source	Sum of Squares	df	Mean Square	F-Value	p-Value
Model	9.6E+01	5	1.9E+01	272.25	< 0.0001
A-PE Type	9.5E+01	3	3.2E+01	448.35	< 0.0001
B-Cooling Rate	6.1E-01	2	3.0E-01	4.2757	0.0423
Residual	7.8E-01	11	7.1E-02		
Total	9.7E+01	16			

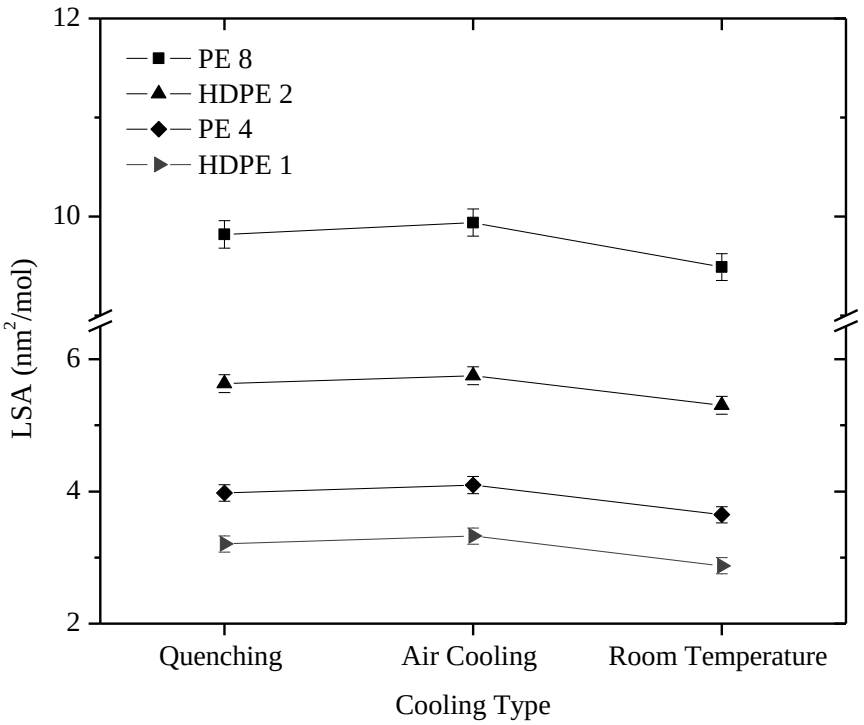

Figure 6.12: LSA vs. cooling type for representative resins

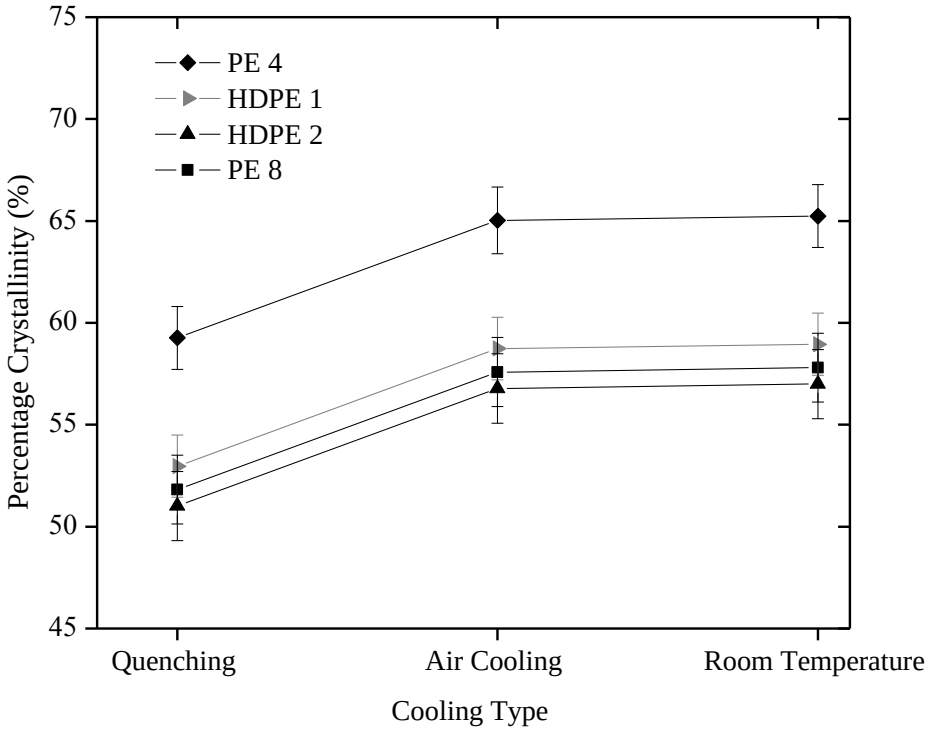

Figure 6.13: Percentage crystallinity vs. cooling type for different PE resins

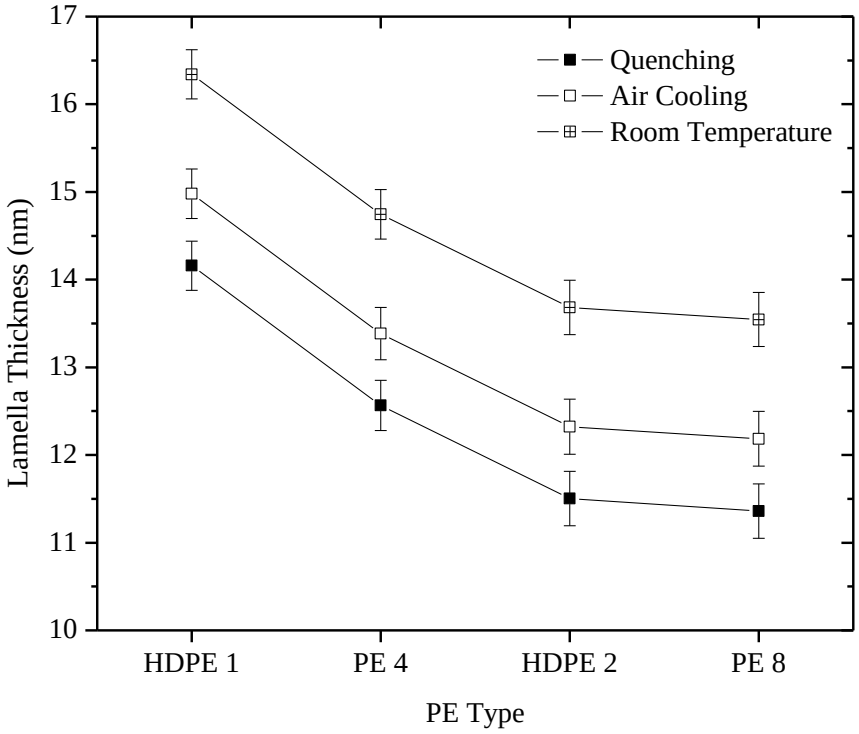

Figure 6.14: Lamella thickness vs. PE type at different cooling rates

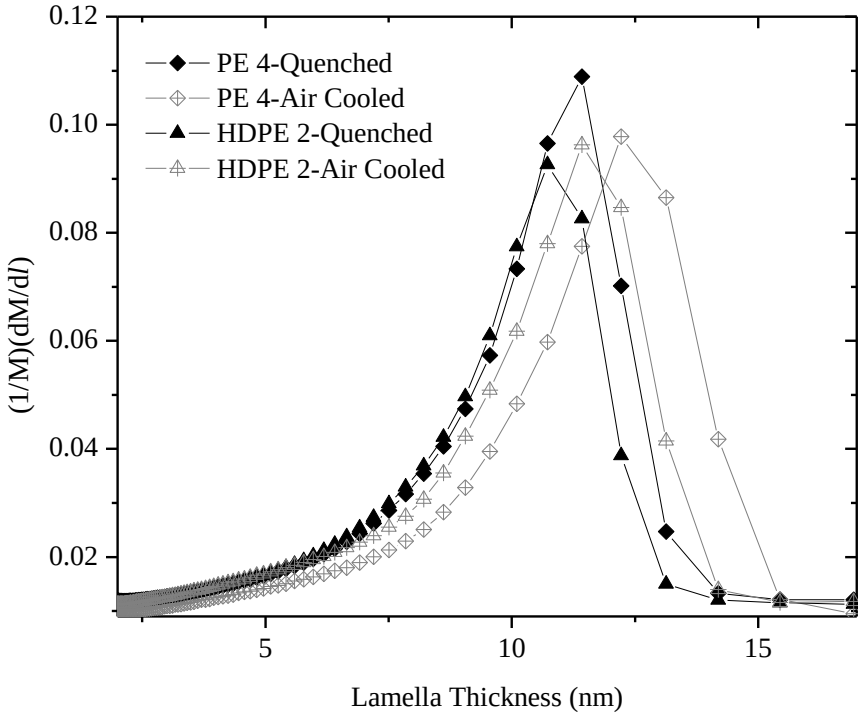

Figure 6.15: Lamella thickness distribution of PE 4 and HDPE 2 at different cooling rates

6.3.2.2.1 Controlled Cooling and cHS

In order to quantify the influence of controlled cooling on ESCR, hardening stiffness tests (20) were conducted to measure cHS values (see section 6.3.1.1, and Table 6.3). This was mainly performed to initially verify that LSA can be used as a potential factor for predicting ESCR. It was also intended to evaluate the sensitivity of a recently developed mechanical test for the measurement of ESCR (20) upon application of controlled cooling to the PE resins. Prior to any model fitting, a natural logarithmic transformation (based on the Box-Cox transformation criterion (28)) was applied on the measured cHS values. ANOVA for this factorial design based on a 95 % confidence level is shown in Table 6.6. Both PE type and cooling type were found to be significant. Figure 16 shows the summary graph, obtained based on a D-optimal factorial design on the effect of cooling rate on cHS. A decreasing trend in cHS (as representative of ESCR) was observed with decreasing the cooling rate. This trend was in line with earlier observations about the effect of cooling rate on LSA (as a result of changes in crystallinity, lamella thickness and LTD).

Table 6.6: ANOVA for the effect of controlled cooling on cHS

Source	Sum of Squares	df	Mean Square	F-Value	p-value
Model	1.23E+01	5	2.46E+00	4779.67	< 0.0001
A-PE Type	1.22E+01	3	4.08E+00	7918.82	< 0.0001
B-Cooling Type	7.29E-02	2	3.64E-02	70.6912	< 0.0001
Residual	5.67E-03	11	5.15E-04		
Total	1.23E+01	16			

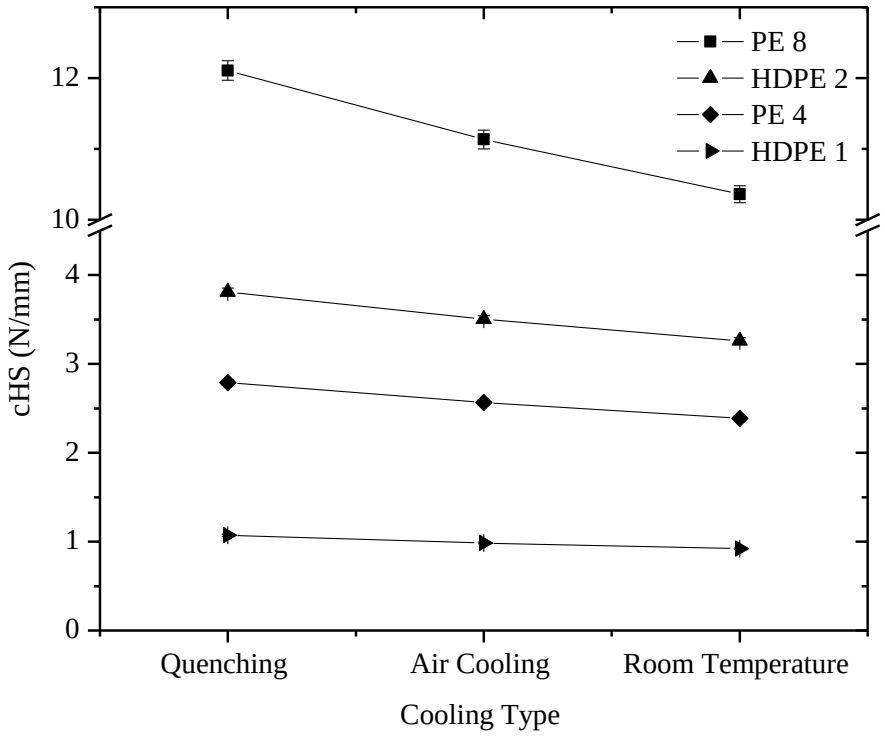

Figure 6.16: cHS vs cooling type for different resins

6.4 CONCLUDING REMARKS

The work in this chapter was aimed at resolving the ambiguity in finding a potential correlation between ESCR and the crystalline domain properties, namely, percentage crystallinity, lamella thickness, lamella thickness distribution, and lamella surface area. Moreover, the intention was to identify the effect of cooling rate and annealing conditions on the lamella surface area as an indicator of phase interconnectivity between the crystalline and amorphous regions. The experimental trials were designed so as to provide possible answers to questions posed in the introduction section of the paper. Correlations between crystalline domain properties and ESCR were found to be feasible, only if the selected PE resins were separated according to their molecular weights. In general, a decreasing trend in ESCR was

found with increasing percentage crystallinity and lamella thickness. ESCR of the low MW group was strongly affected by crystallinity as a result of high dependence of this material property on SCB. The high MW group, on the other hand, showed that if the MW is high enough (say, above 200 kg/mol), an increase in crystallinity can improve ESCR. The lamella thickness determined for LLDPE resins could distinguish their ESCR from the rest of the resins, however, no correlation between ESCR and lamella thickness could be found if comparisons were made within the LLDPE class of resins. It was concluded that for low molecular weight LLDPE resins with high SCB content, the lamella thickness distribution is a more informative tool for prediction of ESCR. LSA also was found to be a potential indicator of ESCR (based on cHS results cited in Table 6.3). Annealing experiments showed that LSA is affected by annealing temperature (to a higher degree) and annealing time (to a lower degree). The dependence of LSA on annealing conditions was found to be related to the molecular structure of the resins. It was found that the LSA values of polymers with lower SCB are more readily affected by annealing conditions. This was verified by looking into the behaviour of the LTD at different annealing conditions (breadth and shift of the distribution curves). Results based on controlled cooling showed that LSA is only marginally affected if the cooling rate is relatively slow. Both air cooling and quenching gave rise to a similar LSA. This behaviour was found to be related to the similar magnitudes of the effects of percentage crystallinity and lamella thickness on LSA, when subjected to different cooling types.

7 CHAPTER 7: REACTIVE MODIFICATION OF HIGH DENSITY POLYETHYLENE IN A UV-INITIATED PROCESS

7.1 INTRODUCTION

Modification of rheological and structural properties of polymers has always been of interest to both academic and industrial researchers. Various techniques have been developed and are currently used to tailor-make polymer properties for various end-use applications. These techniques mostly include the use of chemical modification reactions, or application of high energy irradiation prior or after the polymer is processed. High energy irradiation, including electron beams, gamma (γ) rays and ultraviolet (UV) irradiation, along with thermo-chemical reactions involving organic peroxides and vinyl-silanes are the most common modification techniques (1-6). These techniques have been used in order to induce crosslinking in the polymer, modify the rheological properties of the polymer by chain scission or create long chain branches (branches containing more than 40 carbon atoms) (7-9). Which mode predominates depends on the type of the polymer and the processing conditions (3). Among these techniques, UV radiation is highly preferred due to availability, and relatively safe and inexpensive operating conditions employed.

Structural modification of polyethylene (PE) by UV radiation has been mainly focused on crosslinking. Such work was first initiated and reported in the 1950s when crosslinking of PE was attempted (1). Crosslinking by UV was further modified by many researchers where efficient methods were developed via highly effective photocrosslinking systems in which various photoinitiators along with proper multifunctional crosslinking agents were used (10-19). These authors also looked into the effect of processing conditions (irradiation

temperature, time, intensity and depth of penetration), and types and concentration of the photoinitiator and crosslinking agent on the structure of the crosslinked polymer. In most of these techniques, in order to avoid significant crosslinking and high gel content during processing, irradiation has been applied on formed PE parts; hence, no clear understanding of the effect of irradiation on PE melt is available.

Rheological modification of various types of polymers has also been an area of interest. Modifications were conducted mainly to improve the processability and melt strength of polymers. Most of the research done in this area has been focused on polypropylene (PP) where long chain branching (LCB) was created by means of post-production irradiation (18-20, 41) or by in-situ copolymerization of propylene with dienes (21-22) or by formation of polypropylene macromonomers (22). In the case of PE, LCB was imparted on the polymer by homopolymerization of ethylene with the well-known constrained geometry catalyst (CGC) systems. These catalysts produce long chain branched polyethylene (LCBPE) with a relatively narrow molecular weight distribution (MWD) (23-24).

Ionizing irradiation methodologies have also been employed to induce LCB in PE. With these types of experiments, extra care should be given to processing factors and conditions as PE tends to favor crosslinking. Most of the studies performed in this area, focused on either using gamma rays or electron beams (9, 25-27). LCB was created by application of low irradiation doses without creating any significant amount of gel in oxygen-free or reduced oxygen environments or at temperature below the crystalline melt temperature.

Many studies have been conducted in parallel in order to identify and quantify the degree of long chain branching in polymers. This knowledge is important because long branches change the flow behaviour of the polymer. Conventional characterization methodologies

such as C-13 NMR and size exclusion chromatography (SEC) combined with viscosity and light scattering detectors have been used, but were not very successful in detecting low levels of branching (25). C-13 NMR is also not capable of clearly distinguishing LCB for copolymers of PE with 1-hexene or 1-octene comonomers as branches with more than four carbon atoms result in the same spectra pattern as the backbone PE (28). For this reason, rheological characterization is recommended as rheological characteristics are more sensitive to LCB. However, extra care should be given as both MWD and LCB have a similar effect on rheological properties. It is of great importance to be able to separate the effect of these two factors to assess their influence on processing and rheology (29). In general, the following effects are believed to be due to LCB in the structure of the polymer: increase in zero shear viscosity (η_o) at low levels of LCB and decrease in η_o at high levels of branching (i.e. low density polyethylene (LDPE)), increase in shear thinning behaviour, increase of polymer's relaxation time, and increase in extensional viscosity (indicated by enhancement of strain hardening) (18, 29-31). These general observations, however, can vary according to the type, frequency and length of the LCB.

The current study is based on a new reactive extrusion (REX) process using UV photoinitiation to modify rheological and mechanical properties of PE by inducing LCB. The work presented in this chapter had three main objectives. Firstly, design a REX process in which long branches are formed without a significant increase in molecular weight (MW) or broadening of the molecular weight distribution (MWD) of the selected resin. The second objective was to relate the effects of photoinitiatior concentration, material flow rate, and extruder screw speed with the final properties of the LCBPE. The third objective was to evaluate the extent of enhancement in the ESCR of the resins upon formation of long

branches. These effects were evaluated based on the linear viscoelastic behaviour of the modified PE resins, discussed in what follows.

7.2 EXPERIMENTAL

7.2.1 MATERIALS AND EQUIPMENT

A commercial high density polyethylene copolymer (hexene copolymer) from ExxonMobil Chemical Canada was selected for this study. Table 7.1 summarizes the material properties of the selected high density PE (HDPE) resin. All the molecular properties (excluding density) and the rheological properties (excluding MI) shown in Table 7.1 were measured in our laboratories. Other properties presented in this table were provided by the resin manufacturer. Benzophenone (BP) was used as the photoinitiator. BP crystal flakes were purchased from Fischer Scientific and were used as received.

A Haake Rheocord 90 unit equipped with a Rheomix 3000 batch mixer was used to create a BP/PE master batch prior to any reactive extrusion. The master batch mixture was ultimately ground in a 1102 Wiley mill (Arthur H. Thomas Co). The reactive extrusion experiments were carried out in a Leistritz LSM 30.34 co-rotating twin-screw extruder (L/D=40/1) with ten heating zones. The screw configuration used in the experiments is shown in Figure 7.1. The UV source used was a UV Developer kit from UV Process Supply Inc (Versa Cure). The power of the mercury lamp was 3.0 kW.

Table 7.1: Properties of selected HDPE

Molecular Properties		Rheological Properties		Mechanical Properties	
Density (g/cm^3)	0.95	MI[b] (g/ 10 min)	5.00	Yield Strength (MPa)	23
Mn (g/mol)	13,991	η_o[c] (Pa.s)	1,981	ESCR[e] (h)	10
Mw (g/mol)	51,850	Power Law Index (n)	0.50		
Mz (g/mol)	134,261	λ[d] (s)	0.05		
PDI (Mw/Mn)	3.71				
SCB[a]	1.60				

a: Short chain branching per 1000 carbon atoms, b: Melt index at 190 ºC and 2.16 kg, c: Zero shear viscosity d: Average characteristic relaxation time, e:Environmental stress cracking resistance (from a bent strip test)

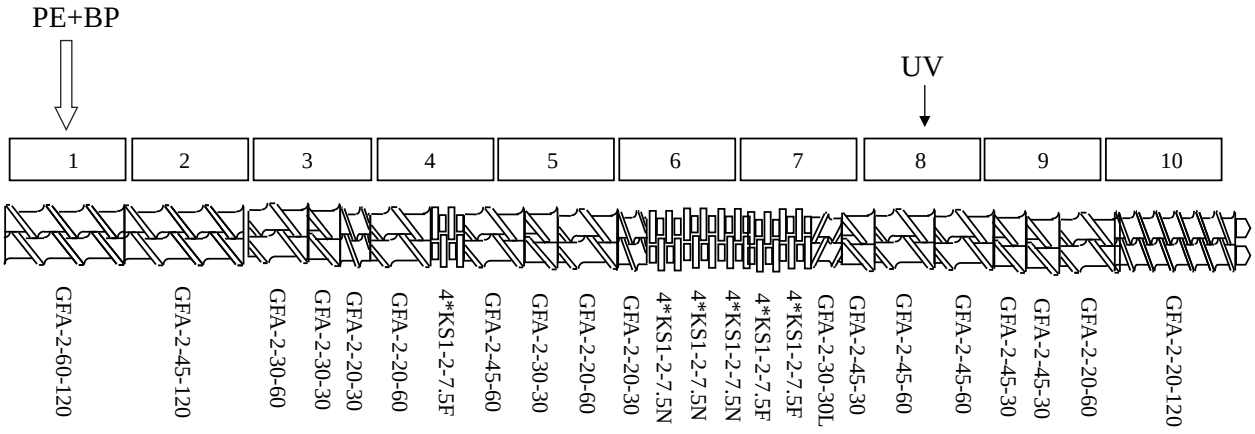

Figure 7.1: Screw configuration used in the experiments

7.2.2 PROCEDURE

To produce a homogeneous mixture of BP in the PE resin, and also to ease the addition of BP to the extruder (due to low amounts of BP needed), a master batch composed of 10 wt% of BP was prepared. PE pellets along with the proper amount of BP were combined in the batch mixer at 190 ºC and 100 rpm for 7 minutes. The mixture was subsequently ground in the Wiley mill and was combined with additional PE to produce the desired feed material for the extrusion runs. The extruder was allowed to reach preselected zone temperatures for two

hours prior to any experiments. Table 7.2 summarizes the temperature set points in the different zones of the extruder. To avoid any cross contamination between different extrusion runs and also to remove any residual material from previous experiments, the extruder was purged with fresh resin before any experiments. The feed material (combination of master batch and PE) was added to the first zone of the extruder. The UV source was used to irradiate the melt in the extruder in the eighth barrel zone which was equipped with a window of size 33x60 mm. Only one irradiation opening was chosen to reduce the extent of PE irradiation in order to prevent crosslinking. Furthermore, the irradiation opening was placed after the kneading blocks to ensure complete mixing between the components as suggested in a previous report (32).

A central composite response surface design was selected for the extrusion experiments. The variable levels used in the experiments are shown in Table 7.3. Three levels of BP concentration, flow rate, and extruder screw speed were selected. Extruder temperature (reaction temperature) and UV lamp intensity were kept constant for all the experiments at this stage. A total of 18 extrusion runs according to the coded levels shown in Table 7.4 were performed. From those, 14 runs were used for model prediction, and 4 for the evaluation of residuals (lack of fit and pure error).

Table 7.2: Extruder temperature profile

Zone Number	Temperature Set Point (ºC)
1 (feeding zone)	40
2	100
3	140
4	175
5	190
6	190
7	190
8 (irradiation)	190
9	190
10	180

Table 7.3: Variable levels for extrusion runs

Variables	-α Level	-1 Level	+1 Level	+α Level
BP (wt% [a])	0	0.1	0.5	0.64
Flow Rate [b] (g/min)	16.4	30	70	83.6
Screw Speed (rpm)	32.7	60	140	167.2

a: weight percentage, b: Flow rate of feed material into the extruder

Table 7.4: Coded levels for extrusion runs

Run #	BP (wt%)	Flow Rate (g/min)	Screw Speed (RPM)
1	-α	0	0
2	-1	-1	+1
3	-1	+1	+1
4	-1	+1	-1
5	-1	-1	-1
6	0	0	0
7	0	0	0
8	0	0	0
9	0	+α	0
10	0	0	-α
11	0	-α	0
12	0	0	0
13	0	0	+α
14	+1	-1	-1
15	+1	+1	+1
16	+1	-1	+1
17	+1	+1	-1
18	+α	0	0

7.2.3 CHARACTERIZATION

7.2.3.1 MOLECULAR CHARACTERIZATION

Molecular weight averages, molecular weight distribution, intrinsic viscosity, and radius of gyration were evaluated by high temperature gel permeation chromatography (GPC) (Polymer CHAR (Spain)), coupled with a viscometer (Viscotek 150R) and a light scattering detector. The solvent and operating temperature were 1, 2, 4 trichlorobenzene (TCB) and 140 ºC, respectively. Each GPC sample contained 15 mg PE in 9 ml of TCB. An AVANCE 500 Bruker NMR was utilized to investigate the short chain branching content of the PE resins at 120 °C. The solvent of choice was deuterated TCB.

7.2.3.2 RHEOLOGICAL EXPERIMENTS

Both oscillatory shear experiments and shear creep tests were performed on a TA Instruments AR2000 rheometer with parallel plate geometry to measure the linear viscoelastic properties of the PE samples. All PE resins were compression molded into 25 mm disks at 190 ºC and 44.5 kN, followed by quenching in cooled water. Prior to frequency sweeps, strain sweeps between 0.1-100 % strains were performed at 100 Hz and 190 ºC to identify the linear viscoelastic region of the PE samples. Further, time sweeps were conducted in order to identify any degradation or crosslinking during the frequency sweeps. The time sweeps were performed for 3 hours at 1 Hz and 1 % strain. A series of frequency sweep shear experiments were carried out at frequencies (ω) between 0.01-100 Hz under nitrogen to avoid any possible polymer degradation or crosslinking.

Shear creep tests were also conducted at 190 ºC on compression molded disks. Creep experiments were conducted at 10 Pa (linear viscoelastic region) for 3 hours. It should be noted that all the rheological experiments were independently replicated at least 3 times to ensure good reproducibility in the results.

7.2.3.3 SOLVENT EXTRACTION

Soxhlet solvent extraction in xylene was carried out to identify the gel content of the PE samples according to ASTM D2765-11. Approximately 0.3 grams of PE sample was placed inside a 120-mesh stainless steel pocket of size 40x40 mm. The pocket was immersed in 350 ml of boiling xylene (99 v-% xylene, 1 v-% antioxidant (Irganox 215 FF)). The extraction was carried out for 12 hours, followed by 12 hours of oven drying under vacuum

at 150 ºC. The weight of the sample after the drying stage was recorded and the gel content was obtained.

7.3 RESULTS AND DISCUSSION

7.3.1 SOXHLET EXTRACTION

The gel content values for selective samples are summarized in Table 7.5. Selective independent replications of the extraction experiments were also conducted to identify the variation in the reported gel content. The cited values are averages of at least three fully replicated extractions (replication indicated a standard deviation of 0.5 % in the measurement). It was concluded that the processing factors at the selected levels create negligible (for all practical purposes, no) gel. Given the noisy nature of the measurement and the fact that the linear virgin PE exhibited 0.70 % of gel, for all practical purposes the determined gel was zero (the fluctuations are simply experimental error).

Table 7.5: Gel content from Soxhlet extraction experiments

Run #	Gel Content
Virgin PE	0.70%
1	0.62%
2	0.39%
3	0.56%
4	0.82%
5	0.48%
6	0.79%
7	0.63%
11	1.62%
13	1.00%
14	1.03%
16	1.49%
17	1.00%
18	1.17%

7.3.2 RHEOLOGICAL PROPERTIES

7.3.2.1 OSCILLATORY SHEAR EXPERIMENTS

The effect of LCB on the shear properties of the modified PE samples was evaluated through oscillatory shear experiments. Long chain branches are known to significantly alter the rheological behaviour of linear PE by enhancing shear thinning behavior and increasing zero shear viscosity. The Cross model shown in equation 7-1 was fitted to the viscosity data obtained from oscillatory shear experiments. In this equation, η is the viscosity obtained from oscillatory shear experiments, η_o is the zero shear viscosity, "n" is the power law index which indicates shear thinning behaviour, lambda (λ) is a characteristic average relaxation time, and ω represents frequency. Furthermore, to verify the findings from the Cross model, a software program (NLREG) (33) was ultimately used to predict zero shear viscosities. Utilizing the

software, the oscillatory shear data in the form of storage and loss moduli (G′(ω), G″(ω)) at different frequencies were used to estimate zero shear viscosities.

$$\eta = \frac{\eta_0}{1 + (\omega\lambda)^{1-n}} \qquad 7\text{-}1$$

No significant differences between the estimated η_o from the selected techniques were found, however, for simplicity, only the values obtained from the Cross model are reported throughout this chapter. Table 7.6 summarizes the results of the estimates for η_o, λ, and "n" for all the experimental runs. Estimates of η_o from the Cross model showed an increase in zero shear viscosity of the PE resins compared to the linear virgin PE. The zero shear viscosity increased to a maximum of 11,600 Pa.s from a starting value of 1,900 Pa.s. This increase is attributed to the formation of LCB. The linear PE is a HDPE with a negligibly low amount of short chain branches and a relatively low zero shear viscosity. The overall chain entanglement in this PE is relatively low due to its low MW and the presence of untangled SCB. When long branches are created in such polymers (assuming branches are large enough and the polymer has a similar Mw), more entanglements are created, which can act as physical obstacles for deformation, and hence, can increase the zero shear viscosities.

Table 7.6: Cross model parameters

Run #	η_o (Pa.s)	λ (s)	n
Virgin PE	1,981	0.05	0.64
1	3,406	0.22	0.60
2	7,823	2.94	0.55
3	4,781	0.55	0.56
4	4,473	0.51	0.59
5	8,429	1.70	0.57
6	4,967	0.71	0.57
7	5,531	0.80	0.57
8	6,075	0.90	0.57
9	3,429	0.18	0.60
10	5,553	0.66	0.59
11	8,218	2.34	0.58
12	5,974	0.72	0.56
13	5,777	0.85	0.57
14	8,874	2.35	0.57
15	6,263	0.95	0.57
16	9,436	2.03	0.55
17	3,502	0.24	0.59
18	11,695	4.03	0.55

In order to identify the effects of all processing factors and their interactions on the zero shear viscosity of the PE resin, η_o values determined from the Cross model were analysed using DesignExpert8 software. A quadratic model was selected for this analysis as both adjusted and predicted coefficients of determination (R^2) values were higher compared to other possible models. Table 7.7 shows the ANOVA from this central composite design, based on a 95 % confidence level (only the significant terms are shown). BP, flow rate and BP^2 were the only significant terms. Both BP and BP^2 had a positive effect on η_o, whereas flow rate had a negative impact on it (shown in Figure 7.2). One interesting observation was the higher zero shear viscosity of run 1, in which no BP was added and the processing

conditions, namely, flow rate and screw speed, were selected at mid-range, compared to virgin PE. This observation suggested that creation of LCB in linear PE is even possible by UV irradiation without a photoinitiator at elevated temperatures.

Table 7.7: ANOVA of effect of design factors on zero shear viscosity (η_o)

Source	Sum of Squares	df[a]	Mean Square	F Value	p-value	
Model	68712451.94	3	22904150.65	15.42	0.0001	significant
A: BP	16807967.54	1	16807967.54	11.31	0.0046	
B: Flow Rate	40771873.92	1	40771873.92	27.44	0.0001	
A^2: BP^2	8424784.126	1	8424784.13	5.67	0.0320	
Residual	20800576.56	14	1485755.47			
Lack of Fit	20034252.06	11	1821295.64	7.13	0.0662	not significant
Pure Error	766324.5	3	255441.50			
Total	89513028.49	17				

a: degrees of freedom

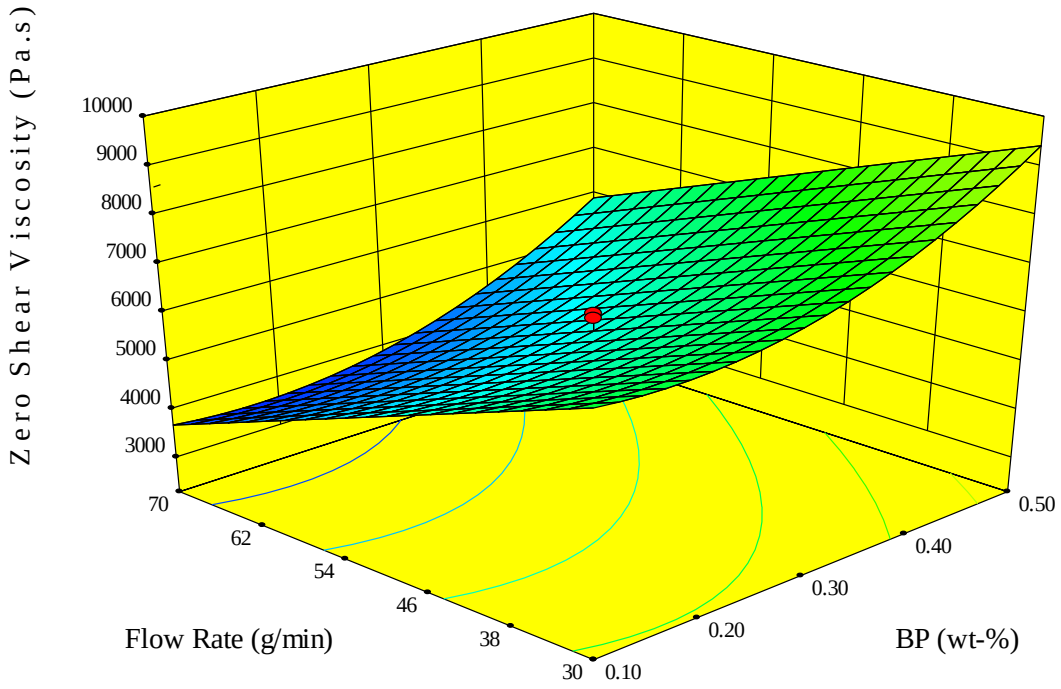

Figure 7.2: Zero shear viscosity (η_o) response surface

In order to identify the width of the transition region between the Newtonian plateau and shear thinning region, lambda values obtained from the Cross model were analysed. It is well

established that LCB increases the characteristic relaxation time of the polymer. The relaxation time increased (see Table 7.6) from a starting value of 0.05 s (virgin PE) to 4 s (run 18). As stated previously, long chained branched PE has a higher extent of entanglements, which requires longer time for the chains to fully relax. As a result, the region where this untangling/relaxation occurs moves to higher times (lower frequencies). Therefore, a broader transition region between the Newtonian plateau and shear thinning region is expected. This behaviour is reflected as an increase in the values of relaxation time, as shown in Table 7.6. Further analyses were conducted to identify the effect of processing factors on the predicted relaxation times (similar to earlier studies on η_o). Prior to any model fitting, a natural logarithmic transformation (based on a Box-Cox transformation criterion) was needed in order to enhance the normality in the predicted relaxation times. A linear model was suggested by DesignExpert8 according to the adjusted and predicted R^2. Higher order models with second order interactions and quadratic terms were also fitted to the predicted data points; however, all models were reduced to the suggested linear model. The ANOVA for this design based on a 95 % confidence level is shown in Table 7.8. Similar to η_o, only the BP content and the flow rate of PE were the significant factors. Relaxation time increased with BP content, and decreased with increasing the flow rate (lower extent of irradiation due to a thicker PE profile in the irradiation zone). This behaviour is evident in the response surface graph shown in Figure 7.3. Also, from a residence time point of view, a lower flow rate results in a longer residence time in the extruder, hence the PE is more exposed to the UV irradiation. This leads to a higher extent of radical concentration in the PE melt which potentially results in a higher degree of branching. A similar observation is

reported by He et al., (32) where at a certain BP concentration, lower throughput results in longer residence times in the extruder.

Table 7.8: ANOVA of effect of design factors on λ

Source	Sum of Squares	df[a]	Mean Square	F Value	p-value	
Model	9.08	2	4.54	14.75	0.0003	significant
A: BP	1.47	1	1.47	4.78	0.0451	
B: Flow Rate	7.61	1	7.61	24.71	0.0002	
Residual	4.62	15	0.31			
Lack of Fit	4.48	12	0.37	7.80	0.0584	not significant
Pure Error	0.14	3	0.05			
Total	13.70	17				

a: degrees of freedom

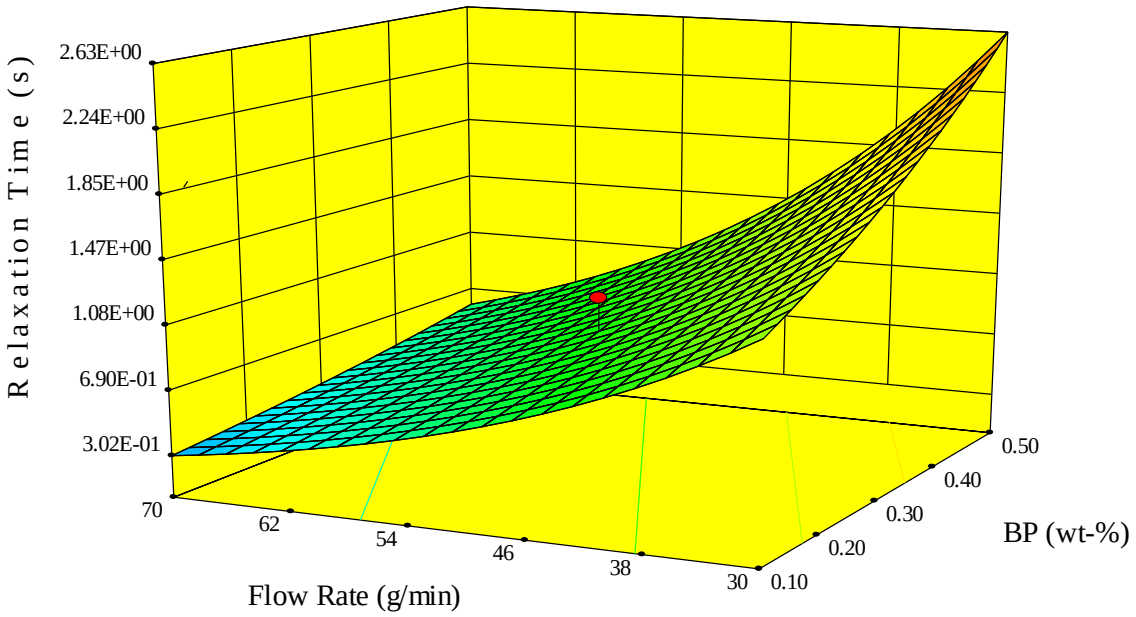

Figure 7.3: Relaxation time (λ) response surface

The analysis was repeated for the power law index (n). This property is known to be not very sensitive to processing parameters compared to relaxation time or zero shear viscosity (6). In this case, however, "n" decreased (see again Table 7.6) from a starting value of 0.64 (virgin

PE) to about 0.55 (runs 17-18). This reduction was attributed to lowering the hydrodynamic volume of the molecule with LCB (24), hence enhancing the shear thinning behaviour. A linear model was again obtained for the power law index based on the selected operating conditions. All the processing factors had a significant effect on the power law index; however, "n" was not significantly affected by the interaction between these factors in the selected operating conditions. Figure 7.4 represents the response surface graph obtained for the power law index. As was the case earlier for both η_o and λ, increasing BP content and reducing the flow rate both enhanced the shear thinning property of the PE resins. Shear thinning behaviour was further enhanced by increasing the screw speed of the extruder. It should be noted that Figure 7.4 was constructed at the lowest screw speed (60 rpm). With increasing rpm, the response surface shifts to even lower "n" values.

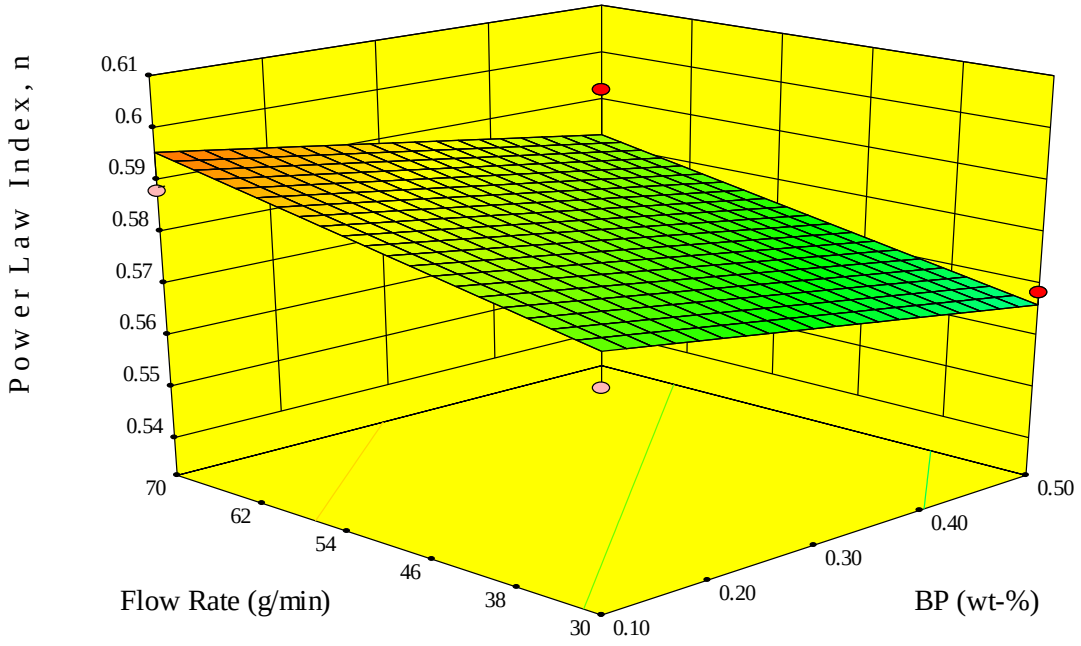

Figure 7.4: Power law index (n) response surface

To further verify the existence of LCB in the PE structure, Cole-Cole plots (G′ vs. G″) of all the experimental runs were constructed. For the sake of brevity, Cole-Cole plots of linear PE, run 1, run 2, run 16, and run 18 are presented in Figure 7.5. Separation of the curves from that of virgin PE at lower frequencies is an indication of LCB as all PE resins have similar MWD. This separation is related to the increase in G′ values with the extent of LCB (more elastic behaviour at low frequencies). As explained earlier, long branches increase the overall physical entanglement in the molecules and increase the elasticity (indicated by G′) of the molecules at low frequencies. At higher frequencies, the effect of chain topology (LCB) is considerably reduced due to the more pronounced effect of molecular weight on rheological properties.

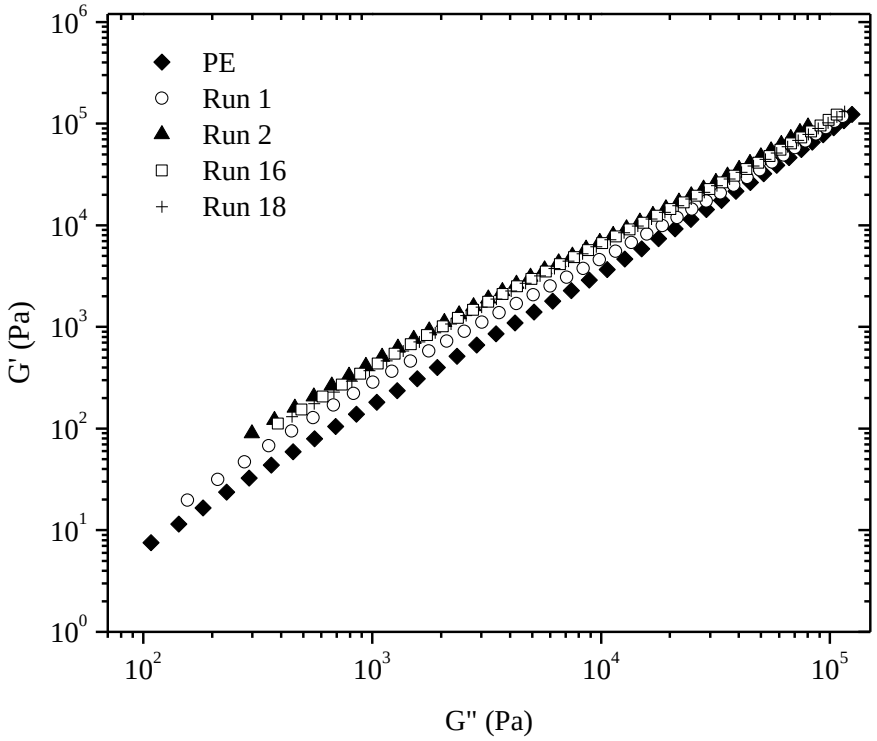

Figure 7.5: Cole-Cole plots obtained from viscoelastic properties

In addition to the Cole-Cole plots, van Gurp-Palmen plots were constructed to further verify the presence of LCB (shown in Figure 7.6). These plots were constructed due to the sensitivity of the phase angle (presented as tan (δ)) to LCB. In these plots, the phase angle is graphed against the absolute value of the complex shear modulus obtained from the oscillatory shear experiments. The van Gurp-Palmen plots are independent of molecular weight of the PE (34), hence any difference in the behaviour of the curve is attributed to MWD and LCB. The curve for the virgin PE is what is expected for a relatively narrow molecular weight HDPE resin, however, the modified resins show a different behaviour. It is evident that all the modified runs have lower loss angle values compared to the pristine PE at the same |G*| value. Since all resins have a similar MWD (see also discussion on MWD that follows), the difference in the curves is attributed to LCB. It is interesting to observe a point

of inflection that appears in the transition zone. This inflection zone becomes more enhanced as the extent of LCB increases in the modified PE resins. In cases where the degree of LCB is higher, two inflection points have been reported, creating a plateau region in the loss angle (30).

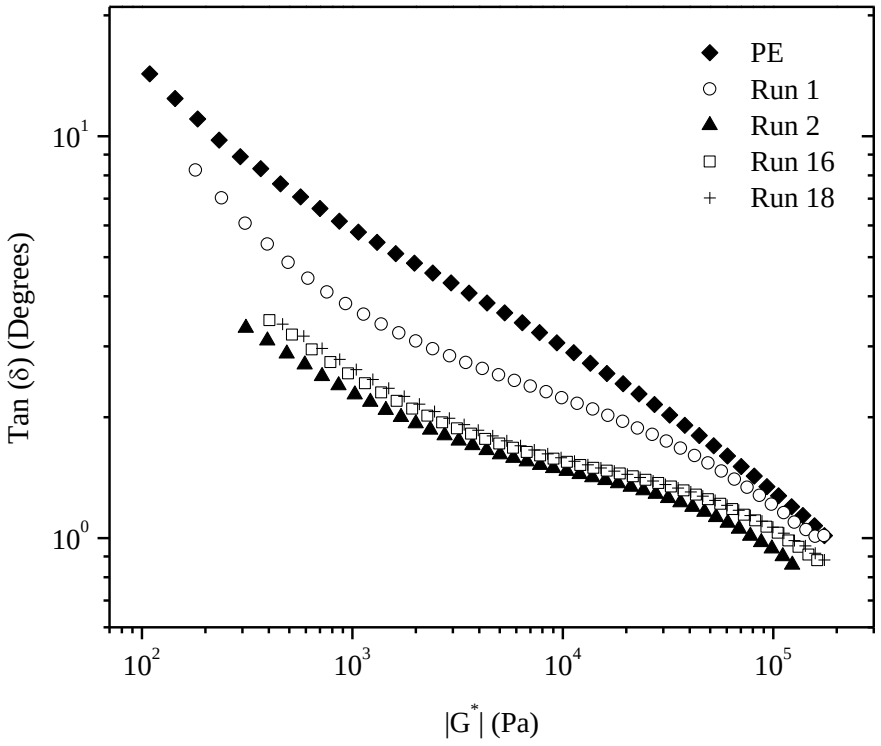

Figure 7.6: van Gurp-Palmen plot obtained from viscoelastic properties

7.3.2.2 SHEAR CREEP EXPERIMENTS

Time dependent creep experiments were conducted at 10 Pa on the five selected PE resins and the results are shown in Figure 7.7. Differences in the molecular structure (MW, MWD, and LCB) can change the creep compliance. Any increase in these molecular properties leads to a shift in the creep compliance to lower values. In this case, because all the modified PE resins have a fairly similar MW and MWD (see discussion of following section) the

difference observed in the behaviour of creep compliance can be attributed to the LCB in the samples (both content and type). The zero shear viscosity and steady state recoverable compliance (J_e^0), reported in Table 7.9, were obtained from the creep data by fitting the Maxwell model to the data. Comparing the η_o values found earlier (from fitting the Cross model to the oscillatory data points) and the values obtained from the creep experiments, it is concluded that the Cross model is capable of predicting the zero shear viscosities at low frequencies (long time region of the creep experiments) for cases where BP content is low. For run 16 and run 18 the values obtained from the creep test were slightly lower compared to the Cross model values; however the increasing trend of zero shear viscosity with BP content was apparent. Inspecting the steady state recoverable compliances, no clear conclusion could be made. With low content of LCB (the case here), it is expected to see an increase in steady state compliance as J_e^0 is highly sensitive to the MWD of the resins. Although the selected resins for the creep experiments have fairly similar MWD, the J_e^0 values obtained might still appear slightly variable.

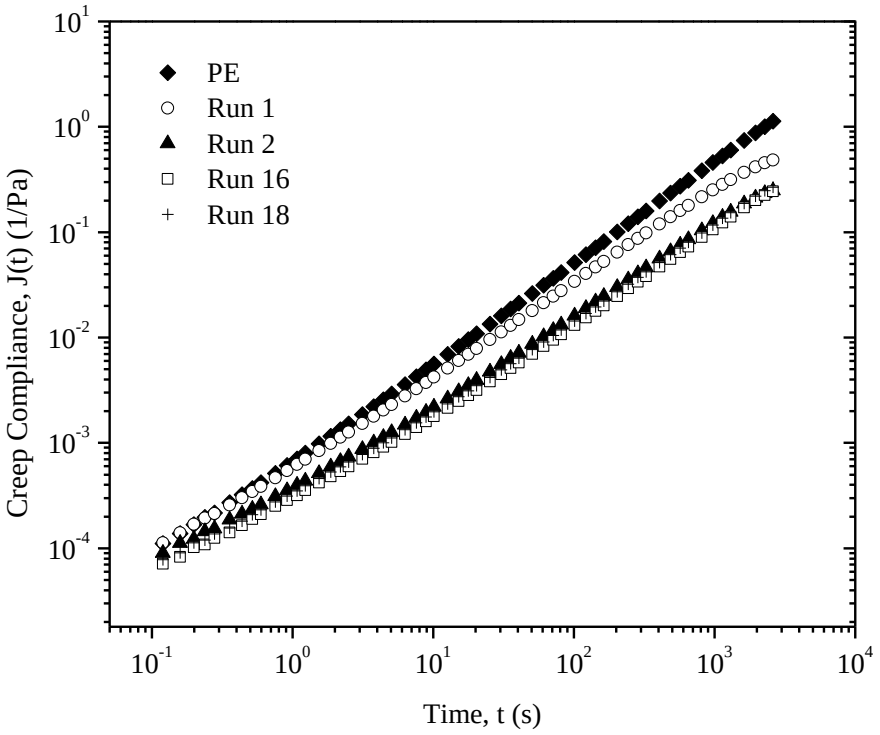

Figure 7.7: Shear creep compliance of PE resins

Table 7.9: Material properties obtained from creep experiments

Run #	η_o (Pa.s)	J_e^0 (1/Pa)
Virgin PE	2,095	0.0023
Run 1	3,436	0.0028
Run 2	7,407	0.0017
Run 16	8,333	0.0012
Run 18	9,090	0.0013

7.3.3 MOLECULAR WEIGHT PROPERTIES

GPC experiments were conducted to investigate the molecular architecture of linear and modified PE resins. Due to the high number of experimental runs, five representative samples (virgin PE, run 2, run 11, run 16, and run 18) were selected for the molecular weight characterization. This selection was made in order to illustrate the molecular weight

differences of experimental runs where higher extent of branching due to the selected processing conditions were expected (the selection was based on results obtained from rheological measurement, discussed in the previous section). The molecular weight distributions of the selected resins are displayed in Figure 7.8 and the averages are summarized in Table 7.10. It is clear that the polydispersity of the linear PE resins does not change after the modification even at the lowest selected flow rate (run 2 and run 16) where the exposure to UV is highest. The MWD of the modified PE resins, on the other hand, shifted to higher molecular weights due to the branching effect. The average molecular weight of the modified runs (see Table 7.10) also shifted to relatively higher values. It is known that GPC is not that sensitive in predicting low amounts of LCB. However, the deviation in a plot of intrinsic viscosity of virgin and modified PE at the same molecular weight averages can indicate the presence of long chain branching. Such a plot, referred to as Mark-Houwnik plot, can be used to identify structural differences in the polymer (30). LCBPE has a smaller molecular size (due to higher chain entanglement density) compared to virgin PE, and therefore, a lower intrinsic viscosity at similar molecular weights is expected. Figure 7.9 illustrates the intrinsic viscosity of the virgin and all modified PE resins versus molecular weight values. The evidence of branching in modified PE is clear, however, a direct quantification of the level of branching in different runs is not possible. Selected samples had similar intrinsic viscosity at the low MW region, and the deviation due to LCB was more apparent in the high end molecular weight region. This behaviour indicated that branching mainly occurred in the longer PE chains, as indicated earlier from the shift in MWD of the modified PE resins (branching occurred in chains with a MW higher than 250, 000 $gmol^{-1}$).

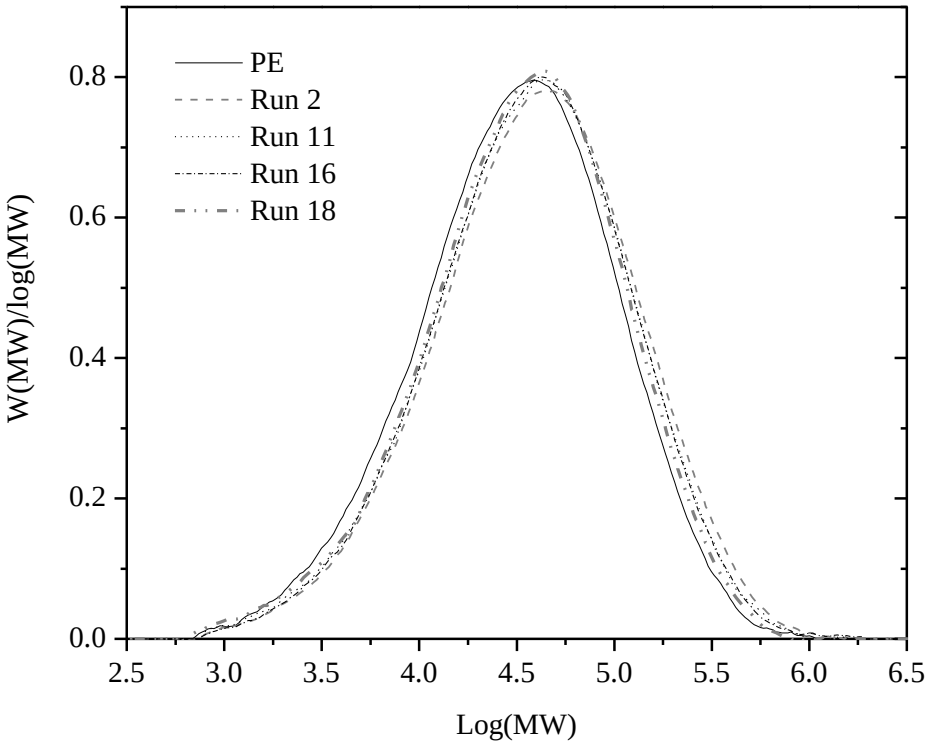

Figure 7.8: Molecular weight distributions of virgin and modified resins

Table 7.10: Molecular weight characterization of selected PE resins

Run #	Mn (g/mol)	Mw (g/mol)	Mz (g/mol)	Mw / Mn
Virgin PE	13991	51850	134261	3.71
Run 2	17192	67492	186126	3.93
Run 11	17288	67490	178438	3.9
Run 16	15888	61073	163725	3.84
Run 18	16040	57392	150599	3.58

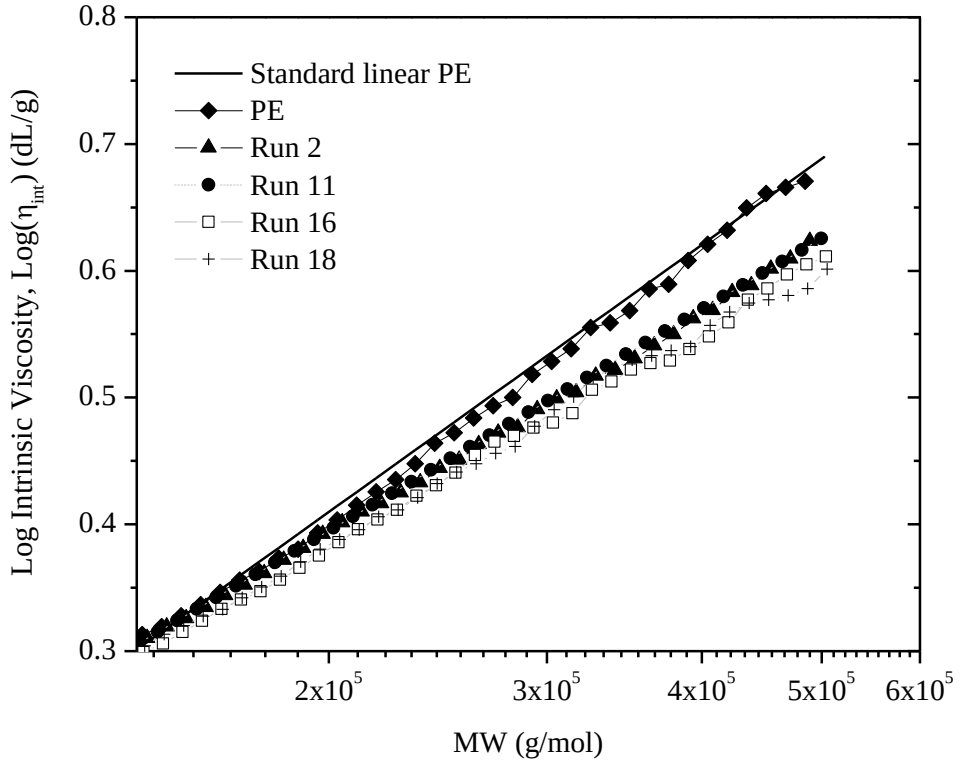

Figure 7.9: Intrinsic viscosity vs. MW

In order to quantify the decrease in the hydrodynamic size of the polymer coil due to branching, Zimm and Stockmayer developed a contraction factor (g) by comparing the mean square radius of a branched polymer to its linear (counterpart) parent polymer (35). In this work, an analogous methodology was applied. However, due to the ease of measuring intrinsic viscosity, the contraction factor was obtained by comparing the η_{int} of branched and linear PE as shown in equation 7-2):

$$g = (g')^{\frac{1}{\varepsilon}} = \left|\frac{[\eta_{int,Br}]}{[\eta_{int,L}]}\right|_{MW} \qquad 7\text{-}2$$

In this equation, $\eta_{int,Br}$ and $\eta_{int,L}$ are intrinsic viscosities of branched and linear PE obtained at the same MW value and "ε" is a parameter dependent on the GPC solvent and structure of

LCB. For a star type LCB in TCB it is reported to be 0.75 (8). The mechanism involved in our REX process includes free radical formation, followed by hydrogen abstraction and finally LCB formation. For a radiation modified PE, a random tri-functional or a tetra-functional randomly branched LCB architecture can be expected. Further calculations were carried out to obtain contraction factors for tri-functional (equation 7-3) and tetra-functional (equation 7-4) branching points. In these equations, "n" is the average number of branch points per chain. Equation 7-5 was further utilized to convert "n" to an average number of branches per 1,000 monomer units of PE, indicated by N_{LCB}. In equation 7-5, M_m is the molecular mass of the monomer, and MW is the molecular weight of the branched PE.

$$g_3 = \left[\left(1 + \frac{n}{7}\right)^{0.5} + \left(\frac{4n}{9\pi}\right)\right]^{-0.5} \quad 7\text{-}3$$

$$g_4 = \left[\left(1 + \frac{n}{6}\right)^{0.5} + \left(\frac{4n}{3\pi}\right)\right]^{-0.5} \quad 7\text{-}4$$

$$N_{LCB} = \left(\frac{M_m \times n}{MW}\right) \times 1000 \quad 7\text{-}5$$

Figure 7.10 and Figure 7.11 show the distribution of the average number of branch points (N_{LCB}) as a function of molecular weight for tri-functional (T-type) and tetra-functional (H type) branches. Both graphs were constructed for molecular weights between 150,000-500,000 g/mol, where branching was expected, and where the number of branching was relatively constant (variations in the N_{LCB} at the lower and higher MW spectrum were eliminated). A thorough explanation regarding this elimination can be found elsewhere (36).

The estimated number of branching was higher for tri-functional compared to tetra-functional. This was expected because for a particular molecular weight, a PE chain with tri-functional branching needs higher number of branching points to have a similar g value that a tetra-functional branching chain has (37). It is further believed that the tri-functional type LCB (T-type) is the major branching structure in the low molecular weight region (combination between a terminal vinyl group and a secondary alkyl radical) (38), whereas tetra-functional type branching (H-type) is the main structure for the high molecular weight region (39).

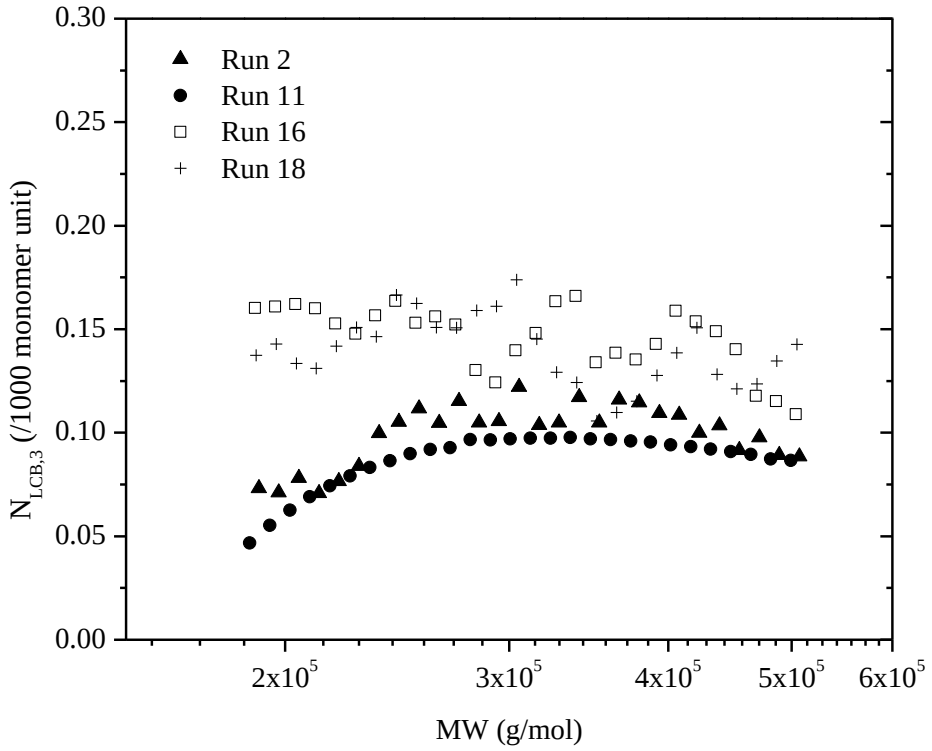

Figure 7.10: N_{LCB} for a tri-functional randomly branched structure

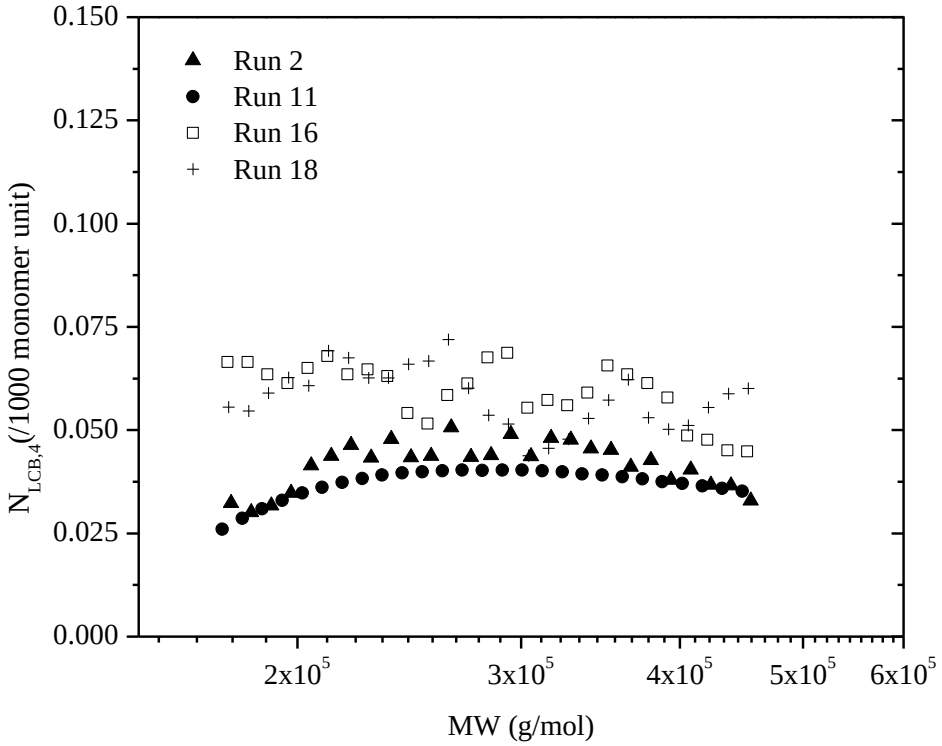

Figure 7.11: N_{LCB} for a tetra-functional randomly branched structure

Since LCB in this study is favored more in the higher molecular weight region, as indicated by the GPC measurements, it is believed that the tetra-functional type LCB is the main branching structure in our modified PE resins. The data indicated that runs 16 and 18 had a similar number of 0.055 branches per 1000 monomer units assuming tetra-functional branching. Runs 2 and 11 showed a relatively lower number of branching close to 0.038 per 1000 monomer units.

The dependence of zero shear viscosity on weight average molecular weight, number, and length of LCB has been studied. Gabriel and Münstedt have shown that low levels of LCB in metallocene catalyzed PE resulted in an increase in zero shear viscosity of a linear HDPE (39). These authors also reported a decrease in zero shear viscosities of a low density PE due to high levels of LCB as a result of high degree of branching functionality. It was further established that a graph of η_o vs. Mw can be used to identify the type of branching in polymers. A star-like LCB structure is expected to be located above the linear reference of $\eta_0 \propto Mw^{3.4}$ relation, however, a tree- or comb-like LCB structure is located below the line (18). Further studies were carried out from a theoretical point of view to find a correlation between zero shear viscosity and the molecular weight of the long chain branches (M_a) and the entanglement molecular weight (M_e) (40), as shown in equation 7-6.

$$\eta_0 \propto \left(\frac{M_a}{M_e}\right)^{\alpha} \times exp\left(\nu \frac{M_a}{M_e}\right) \qquad 7\text{-}6$$

In equation 7-6, "ν" and "α" are parameters reported to be in the order of 0.5 and 1, respectively (18). Figure 7.12 shows the zero shear viscosity data obtained from linear viscoelastic measurements (Cross model) as a function of weight average molecular weight

(Mw). The straight line represents the general relationship of $\eta_0 \propto Mw^{3.4}$ for a linear PE. It can be seen that the PE runs are located above the line, indicating that the long branches seem to have a star-type structure. As shown, presence of LCB in linear PE increases the zero shear viscosity. One interesting point observed was that, although run 16 has a higher number of branching, its Mw is lower than that of run 2. The only difference in processing these two PE samples is the amount of BP present in the formulation (rpm has no significant effect on η_o). It was postulated that a higher number of LCB in run 16 as a consequence of higher BP content (lower M_e), and similarly a higher portion of available free radicals for the reaction, results in a decrease in the effective/nominal length of branches (a lower M_a). Therefore, long branches in run 2, although fewer in number, are longer in length, which results in a higher Mw. To verify this observation, the molecular weights of the branches (M_a) were estimated by dividing the molecular weight by the number of branches for each slice of the molecular weight distribution obtained from GPC (shown in Figure 7.13). As expected, run 2 exhibited a relatively higher Ma due to its lower number of LCB compared to run 18.

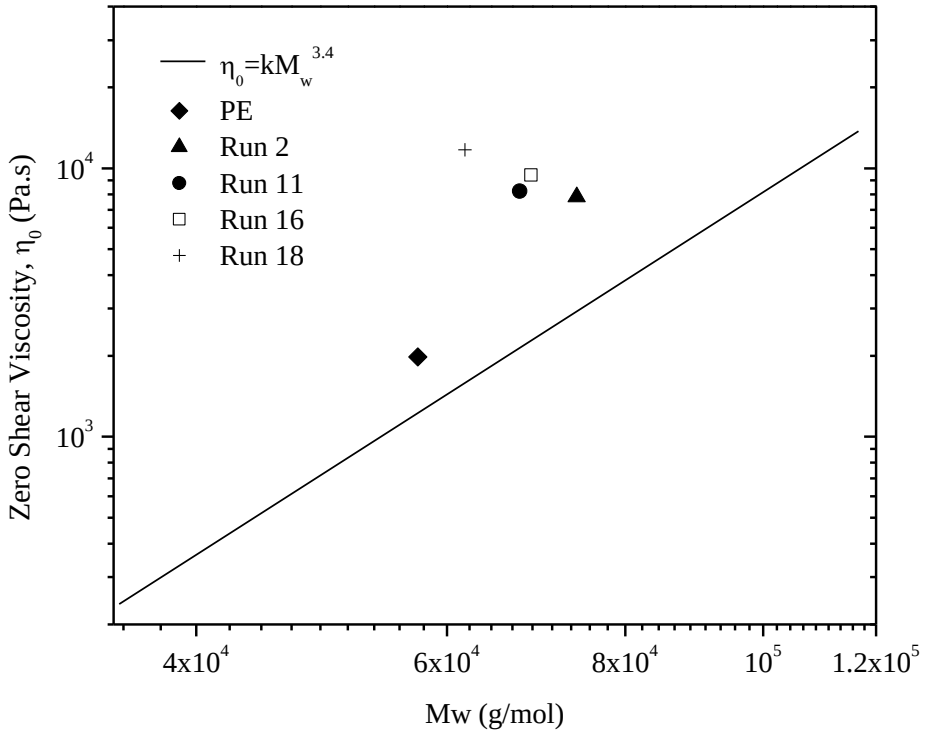

Figure 7.12: Zero shear viscosity vs. Mw

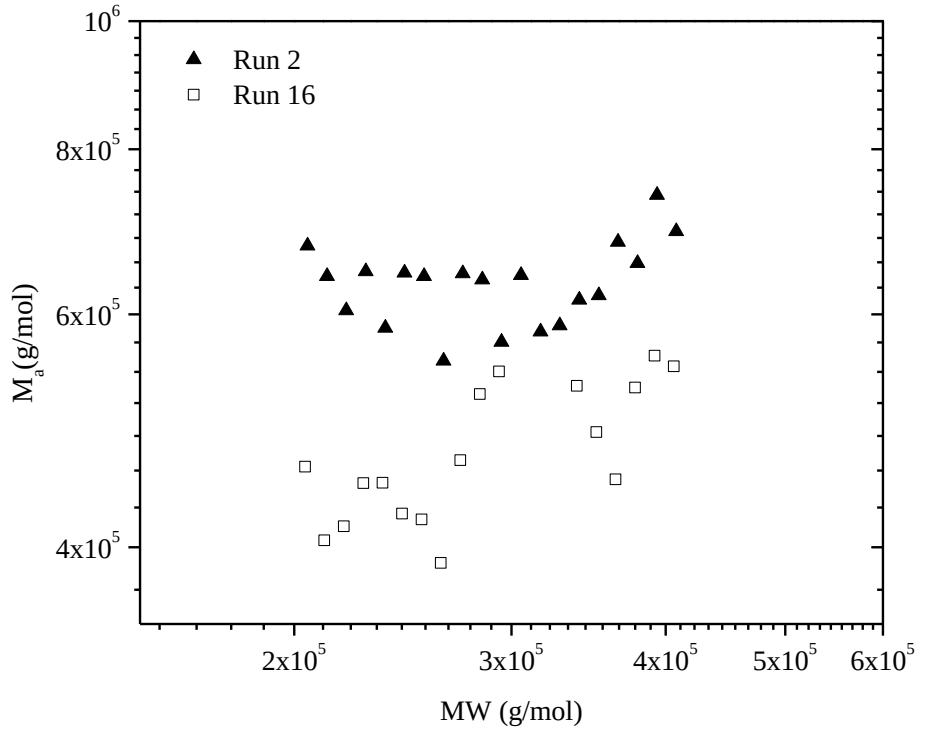

Figure 7.13: M_a vs. MW

7.3.4 EFFECT OF LCB ON ESCR

Notch constant load tests (NCLT) according to ASTM D5397 were conducted to identify the effect of LCB formation on the long-term mechanical behavior of the PE. The linear PE in this study had an ESCR value of approximately 10 h. The ESCR values of the modified PE resins are shown in Figure 7.14. An increase in ESCR, proportional to the amount of LCB, was observed for the modified PEs. Runs 16 and 18 showed a fourfold increase in ESCR, whereas the ESCR values of Runs 2 and 11 were approximately doubled. Based on the observations presented in section 7.3.3, it can be concluded that the frequency of LCB on ESCR is more dominant, compared to the length of the long branches. This can be seen from the ESCR values of Run 2, compared to those of Run 16 and Run 18. PE chains with a higher LCB frequency have a higher tendency to be located in the amorphous domain of the polymer, thus increasing the probability of creating tie-molecules, and consequently the ESCR of the resin.

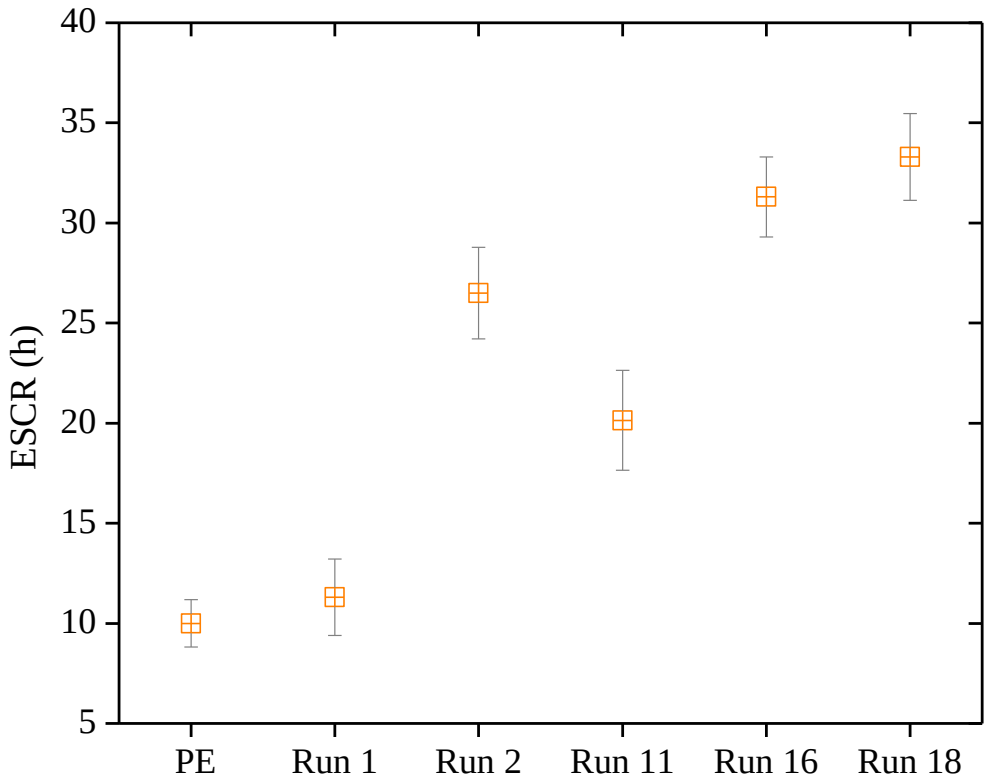

Figure 7.14: Effect of LCB on ESCR

An optimizing process map was ultimately developed at a 95 % confidence level based on the following processing condition criteria: zero shear viscosities between 4000-9000 Pa.s, relaxation times between 0.5-4 s, and screw speed of 100 rpm. This optimizing graph (see Figure 7.15) summarizes melt properties at given operating conditions for the developed REX process in this work.

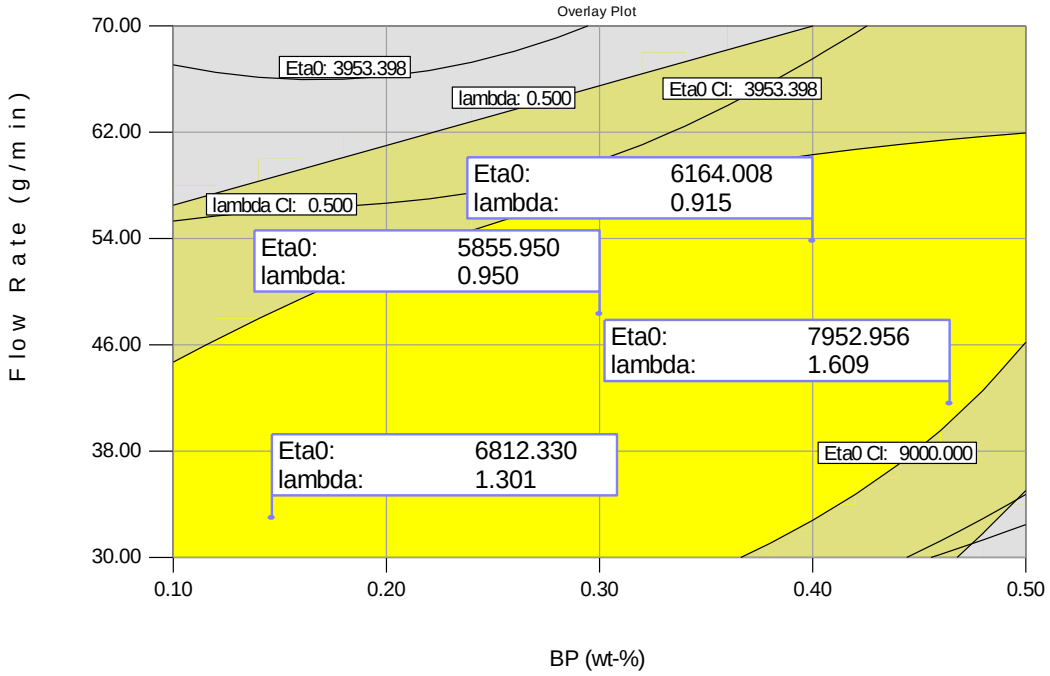

Figure 7.15: Optimizing process map from the experimental design

7.4 CONCLUDING REMARKS

A new reactive extrusion process has been designed for modification of the rheological properties of a high density polyethylene copolymer with a relatively narrow molecular weight distribution using UV photoinitiation. Modification was achieved by inducing long chain branching in the structure of the polymer without major changes in the molecular structure of PE (MW and MWD). This was achieved by a controlled exposure of the molten PE to UV radiation in order to prevent crosslinking, and instead promote branching. The modified resins were characterized in detail by various rheological and molecular methods. Linear viscoelastic properties indicated an enhancement in the zero shear viscosity and relaxation time of the modified resins with increasing BP concentration and decreasing PE

flow rate (throughput). The extruder screw speed was found to have an insignificant effect on the rheological properties at the selected operating levels. The power law constant obtained from the Cross model was not successful in identifying the effect of branching. Both Cole-Cole and van Gurp-Palmen plots were able to identify branching in the modified samples. An inflection point was observed in the van Gurp plots of the modified resins confirming the introduction of LCB in the structure of the PE. Dynamic shear creep tests were successful in predicting the zero shear viscosity of the modified resins; however, the measured steady state compliance obtained from these tests did not provide any indication of branching. GPC equipped with multiple detectors identified the expected deviation in the intrinsic viscosity of the linear PE with increasing LCB. Based on the selected operating conditions, a LCB content of up to 0.055 per 1000 monomer units was obtained. Branching occurred in the higher molecular weight end of the molecular weight distribution. Additional calculations seem to show that branching is of the random tetra-functional star-type. Ultimately, a maximum of a fourfold increase in the ESCR of the modified resins was achieved.

8 CHAPTER 8: MAPS DESCRIBING RELATIONS BETWEEN MOLECULAR PROPERTIES AND ESCR

8.1 INTRODUCTION

The major objective of this PhD thesis was to develop relationships between major molecular properties of different polyethylene resins (both in type and grade) and their environmental stress cracking resistance. Environmental stress cracking is one of the main failure mechanisms in plastics that can be extremely catastrophic and costly, especially in cases where structural integrity is needed. ESC occurs when PE resins are subjected to prolonged mechanical stresses (small tensile stresses), in the presence of an aggressive environment. The failure starts from multiple locally stress-concentrated areas (due to applied and residual stresses), generated/applied through manufacturing, processing and service/use of the polymer. Eventually these multiple zones coalesce and propagate through the bulk of PE, resulting in a sudden brittle fracture with clean crack surfaces. Efforts have been made to design processes (e.g., rotational molding) to reduce residual stresses within the polymer, but no manufacturing process is currently available to fully remove such stresses. Therefore, it is important to have a practical understanding of the structure of a polymer that is used for applications where resistance to stress cracking is crucial. This can eventually lead to innovative methods for a better understanding of structure-property relationships. In this chapter, an overview is provided to describe relationships between major molecular properties and ESCR of polyethylene. Based on these instructions and practical tips, a reliable comparison (and ranking) can be made for selecting PE's with potentially better/ higher ESCR. Essentially, this chapter is the culmination of the research of this PhD thesis.

8.2 MOLECULAR PROPERTIES VERSUS ESCR

The main molecular properties affecting the ESCR of PE are molecular weight and short chain branching content and their distributions. Crystallinity also plays an important part in controlling ESCR. A brief description of the effect of each of these molecular properties on ESCR is given below. Finally, a schematic diagram is introduced, summarizing the relationships between molecular structure characteristics and ESCR of the PEs in this study.

8.2.1 MOLECULAR WEIGHT (MW) AND MWD

The failure mechanism involved in ESCR is a disentanglement process that can take place in two main regions: (1) the interface between the amorphous and crystalline regions, and (2) the amorphous region. The disentanglement in the interface mainly involves tie-molecules that connect the crystalline lamellae to the amorphous region. Therefore, the higher the content of tie-molecules in PE, the higher is the ESCR. The rate of formation of tie-molecules is directly controlled by the MW of the polymer. PEs with higher MW, have a higher density of tie-molecules (1), hence, a higher resistance to rate of molecular disentanglement is expected. Similarly, van der Waals forces between the physical chain entanglements in the amorphous region (including inter-lamellar links, cilias and loose loops) have been shown to enhance ESCR (2). Higher molecular weights can increase the degree of such inter-lamellar connections, thus promoting ESCR. MW values in the vicinity of 150,000 g/mol are required to create a sufficiently high density of tie-molecules for an enhancement in ESCR (3).

Polyethylene resins are composed of chains with different lengths, resulting in a molecular weight distribution. MWDs can be unimodal or bimodal/multimodal. In general, PE

homopolymers with a narrow unimodal MWD have very low ESCR. Incorporation of a large amount of short chain branches can enhance the ESCR in this type of PEs, however, addition of a large amount of short branches can cause a deterioration of other mechanical properties, such as stiffness, needed for PEs in structural applications. PEs with bimodal MWD, show a relatively higher ESCR. The low molecular weight fraction of the MWD can enhance the crystalline state of the polymer and increase its fracture toughness (4), whereas the high molecular weight fraction can assist in the formation of a large number of tie-molecules, which ultimately increases ESCR. For an overall superior mechanical performance, a proper balance between the ratio of low and high molecular weight fractions is required. In general, for applications where a high ESCR is needed, a large fraction of the high molecular weight portion is preferred. PE100 pipe resins, with extremely high ESCR, have a small fraction ratio between the low and high MW fractions.

8.2.2 SHORT CHAIN BRANCHING (SCB) CONTENT AND DISTRIBUTION

Incorporation of short chain branches in PE increases ESCR. The enhancement in ESCR is directly related to the formation of a higher number of effective tie-molecules as a result of addition of short branches (both length and frequency of SCB). In addition, the distribution of SCB over the MWD is very important. For unimodal MWD PEs, most of short chain branches are formed in the lower end of the MWD spectrum. These short chain branches, although effective in increasing resistance to crack growth, are not contributing to a large enhancement of ESCR. On the other hand, in bimodal MWD PEs, addition of SCB in the high molecular weight fraction of the distribution can significantly increase ESCR.

8.2.3 CRYSTALLINITY AND DENSITY

Crystallinity and density of PE can be controlled by the amount of short chain branches. An increase in the amount of SCB generally reduces the percentage crystallinity and consequently the density of PE. However, it is still not possible to develop an equation to relate the short chain branching content to percentage crystallinity or density (5). Failure to develop such a correlation has been attributed to differences in other factors such as MW, and type and distribution of short branches. Similarly, it is not feasible to develop a simple relationship between ESCR and crystallinity/density. Assuming that MW and type/distribution of branching are constant, any decrease in crystallinity/density (as a results of an increase in short branches), would increases ESCR. On the other hand, an increase in crystallinity for PEs with relatively high MW was observed to increase ESCR (refer to Chapter 6, section 6.3.1.1). This was related to an increase in the stiffness and fracture toughness of the material, which ultimately reduced the rate of crack growth propagation. Crystallinity/density and hence their effects on ECSR can be controlled by processing temperature. Post-processing isothermal annealing at different temperatures and periods reduces the number of tie-molecules (enhancement in crystallinity/density) and reduces ESCR (refer to Chapter 6, section 6.3.2). On the other hand, fast cooling can improve ESCR.

8.2.4 SCHEMATIC DIAGRAMS RELATING MOLECULAR PROPERTIES AND ESCR

Figure 2.1 represents relationships between MW, SCB (at different MW), MWD (at different MW) and ESCR. The resins were separated into two groups, high MW and low MW, according to their weight average molecular weight, as per earlier discussions in Chapter 6,

section 6.3.1. As mentioned earlier, ESCR of HDPEs (copolymer) scales with MW. For the case of HDPE homopolymer, an increase in MW does not necessarily increase ESCR (see Figure 8.1 (a), where the lowest point of the high MW group (P 4) shows a lower ESCR compared to the low MW group members). Increasing molecular weight in HDPE homopolymers mostly adds to the crystallinity of the polymer, hence, no enhancement in ESCR is expected. Figure 8.1 (b) illustrates the effect of SCB on ESCR for PEs with different molecular weights. As shown, ESCR increases with SCB content, however, the extent of such an increase is different for PEs with different molecular weights. The low MW group, even at the highest SCB level (23/ 1000 carbon atoms), can only achieve an ESCR of around 650 h. On the other hand, the high MW group can simply reach high values of ECSR (above 1000 h), with less than 6 SCB/ 1000 carbons. This observation validated the synergistic effect of MW and SCB on enhancing ESCR. The relationship between ESCR and polydispersity index (PDI: Mn/Mw) obtained from MWD is shown in Figure 8.1 (c). It was not possible to develop a relationship between ESCR and PDI (as is usually the case with distributional properties). In both MW groups, PDI (representing the breadth of the molecular weight distribution) did not have a significant effect on ESCR. This was associated with differences in MW and SCB content (and distribution), which have a stronger influence on ESCR.

Figure 8.2 summarizes the steps involved in rationalizing a relationship between density and ESCR. Figure 8.2 (a) represents the increasing linear relationship between crystallinity and density for the low MW group. This relationship is more complicated for the high MW group (although still increasing), due to the very large differences in SCB content, SCB distribution, and the differences between the ratio of low and high MW fractions of the

MWD (most members of the high MW group are PEs with bimodal MW distributions). Figure 8.2 (b) highlights the relationship between crystallinity and MW. It was found that crystallinity scales with MW for the low MW group. It should be noted that the crystallinity of the LLDPEs (which are part of the low MW group) was completely controlled by SCB content, not MW. The relationship between crystallinity and MW, however, is reversed for the high MW group, where an increase in MW reduces crystallinity. Based on this observation, it can be concluded that the effect of short chain branches on the density/crystallinity of the high MW group is negligible. Therefore, the density of such high molecular weight PEs is mainly controlled by their MW. Figure 8.2 (c) ultimately displays the relationship between ESCR and density. Both MW groups showed a decreasing trend in ESCR with density, however, the density of the high MW group was significantly higher, representing a larger resistance to crack propagation and higher fracture toughness. The large density of the high MW group qualifies such resins for pipe applications where large fracture toughness values are required.

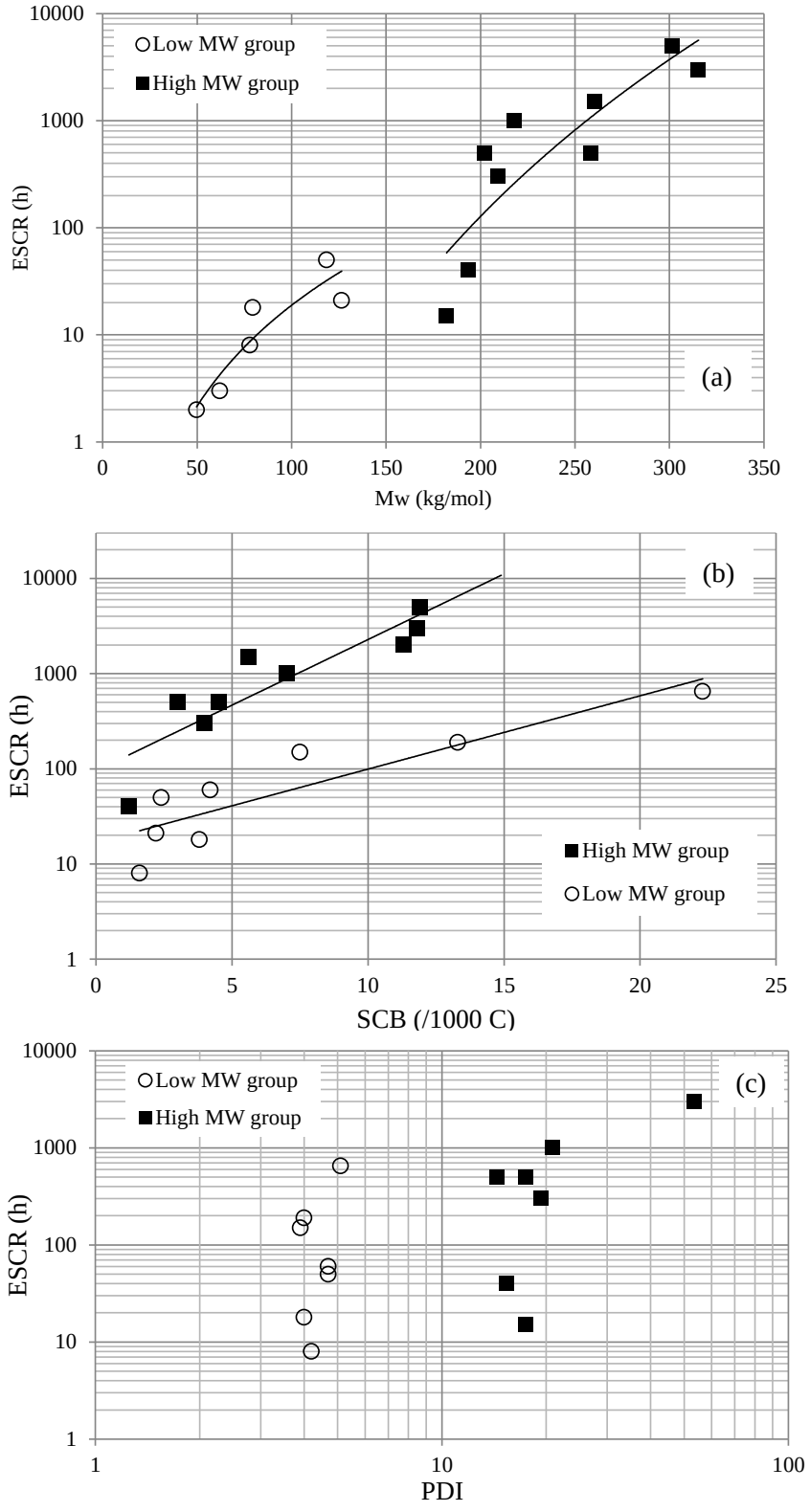

Figure 8.1: Effect of MW, SCB and MWD on ESCR

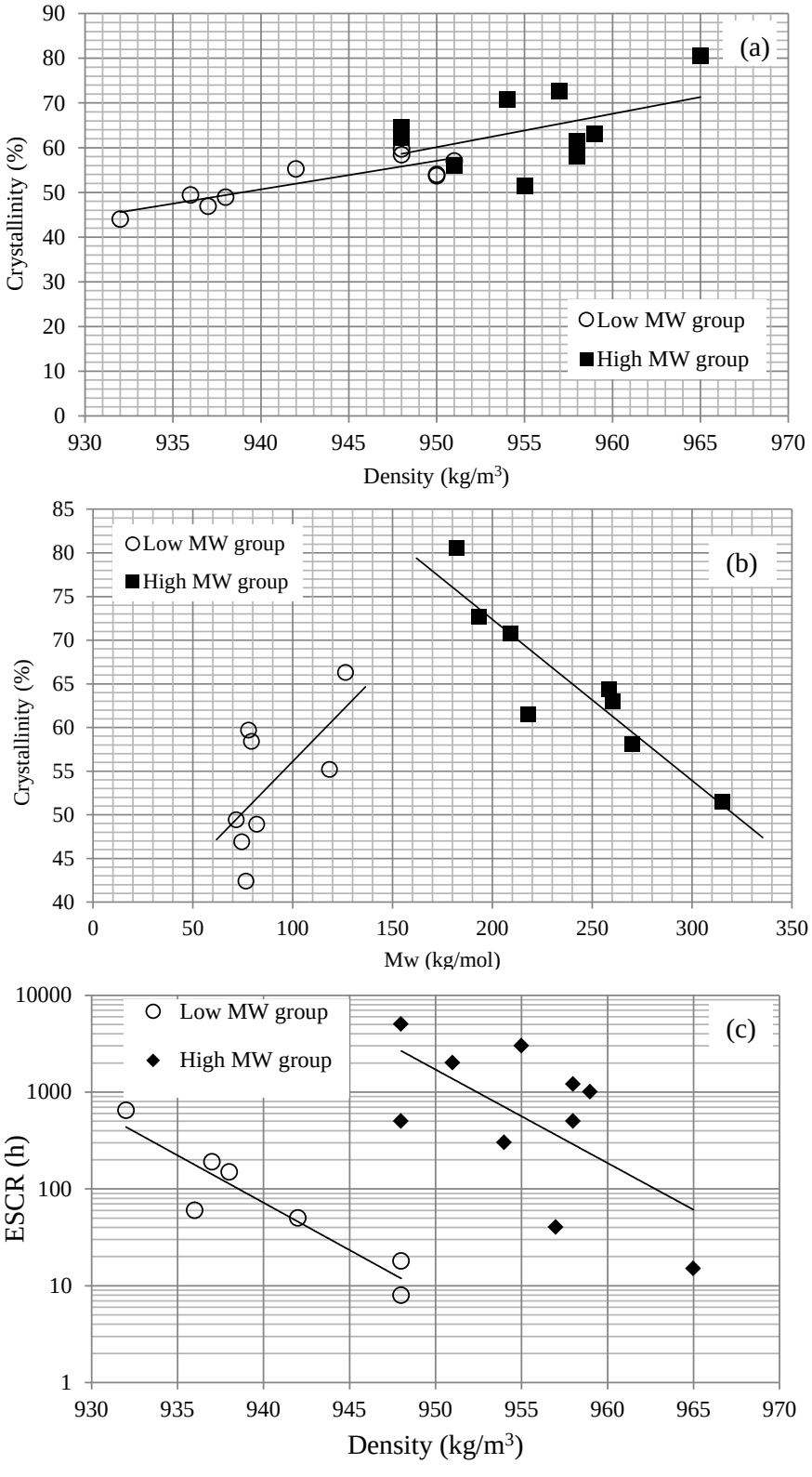

Figure 8.2: Relationship between MW, percentage crystallinity, density and ESCR

Based on these observations, several diagrams, shown in Figure 8.3, were developed for a better representation of the relationships between different molecular structure characteristics and ESCR. These diagrams were developed based on the PEs in this study, offering pathways to develop polymers with a wide range of properties and applications. This 'diagram compendium' shows the direct relationships between major molecular structure characteristics, and their possible interactions with ESCR. Another important fact is that the effect of short chain branching content is reflected on crystallinity and density. Therefore, this compendium eliminates the need for explicit inclusion of SCB content measures. It should be noted that the diagrams shown in Figure 8.3 were developed based on the resins in this study. Therefore, this compendium of plots should not be used as universal for the evaluation/estimation/prediction of ESCR, unless the molecular properties of the selected PEs fall in the same vicinity/ range as the ones used in this work.

In order to verify the reliability of Figure 8.3, diagnostic checks were conducted to identify and demonstrate the predictive capabilities of the suggested correlations, using three "unknown resins" (hence, the final check was like a 'blind' test). Molecular properties of the unknown resins were investigated and ultimately employed along with the developed diagrams to identify the "ESCR range" of the unknown resins. The first unknown resin (unknown PE 1 (uPE 1)) is an injection molding grade PE, with relatively high melt flow index. Characterization techniques according to Chapter 3, section 3.1.2, were carried out to identify the weight average molecular weight of uPE 1 (Mw=50 kg/mol). Figure 8.3 offers a crystallinity-Mw correlation (left bottom figure, low MW group) for such a low Mw PE. This correlation indicated a percentage crystallinity of 54.6 % for uPE 1. For a 54.6 % crystallinity, the correlation developed between percentage crystallinity and the density is

available in Figure 8.3 (right bottom figure, low MW group). This correlation indicated a density of around 947 kg/m^3. Ultimately, using the correlation between ESCR and density (top right figure, low MW group), suggested an ESCR value of around 7 h for uPE 1. The resin manufacturer reported an ESCR of 3 h for uPE 1, based on a bent strip test (BST). The percentage crystallinity of uPE 1, according to Chapter 3, section 3.1.1, was also evaluated and was found to be 54 %. Both ESCR and percentage crystallinity obtained from the correlation and characterization techniques were very similar, verifying the reliability of the developed correlations. Next, the second unknown resin (uPE 2), also an injection molding grade PE, was characterized and a weight average molecular weight (Mw) of 62.0 kg/mol was obtained. A similar methodology was conducted to find the resin properties from the diagrams of Figure 8.3. Mw of 62 kg/mol corresponded to a percentage crystallinity of about 56.5 % (using the low MW group correlation), a density of 950 kg/m^3 and an ESCR value of around 4 h. The BST and characterization by differential scanning calorimetry (DSC) indicated an ESCR value of 2 h and a percentage crystallinity of 57 %, once again verifying the reliability of the correlations for PEs with relatively low molecular weight and low densities. In the final blind test, the third resin had a relatively higher Mw of 127 kg/mol, corresponding to a percentage crystallinity of 66.47 % obtained from the low MW group correlation. For this resin, the crystallinity-density correlation, and ESCR-density from the high MW group is available, providing a density value of 958.4 kg/mol, and an ESCR value of close to 827 h. The company reported an ESCR of about 1000 h for this resin, which is very similar to what we found from the developed correlations in this work. However, the estimated percentage crystallinity (54 %) was significantly lower than the value obtained from the correlations. The differences between the estimated and predicted percentage

crystallinity is attributed to the lack of fit of the crystallinity-Mw curve for the low MW group. In order to enhance the predictability of this correlation, PEs with molecular weights between 120-150 kg/mol, and different short chain branching contents, should be added to fill the gap.

In addition to the mapping of typical resin structural characteristics (Figure 8.3), a "prescriptive pathway" for selecting a PE with higher ESCR is also presented in Figure 8.4. This figure is a modification of a similar diagram, originally developed by Cheng et al. (6), that contains a series of questions for a relative prediction of the extent of tie-molecules and inter-lamellar entanglements, responsible for ESCR. Steps shown in Figure 8.4 are given based on a collection of observed relationships between various molecular properties and ESCR. This diagram summarizes the efforts conducted in both the solid and melt states, through various characterization techniques, to provide a proper measure/indicator of the ESCR of PE resins.

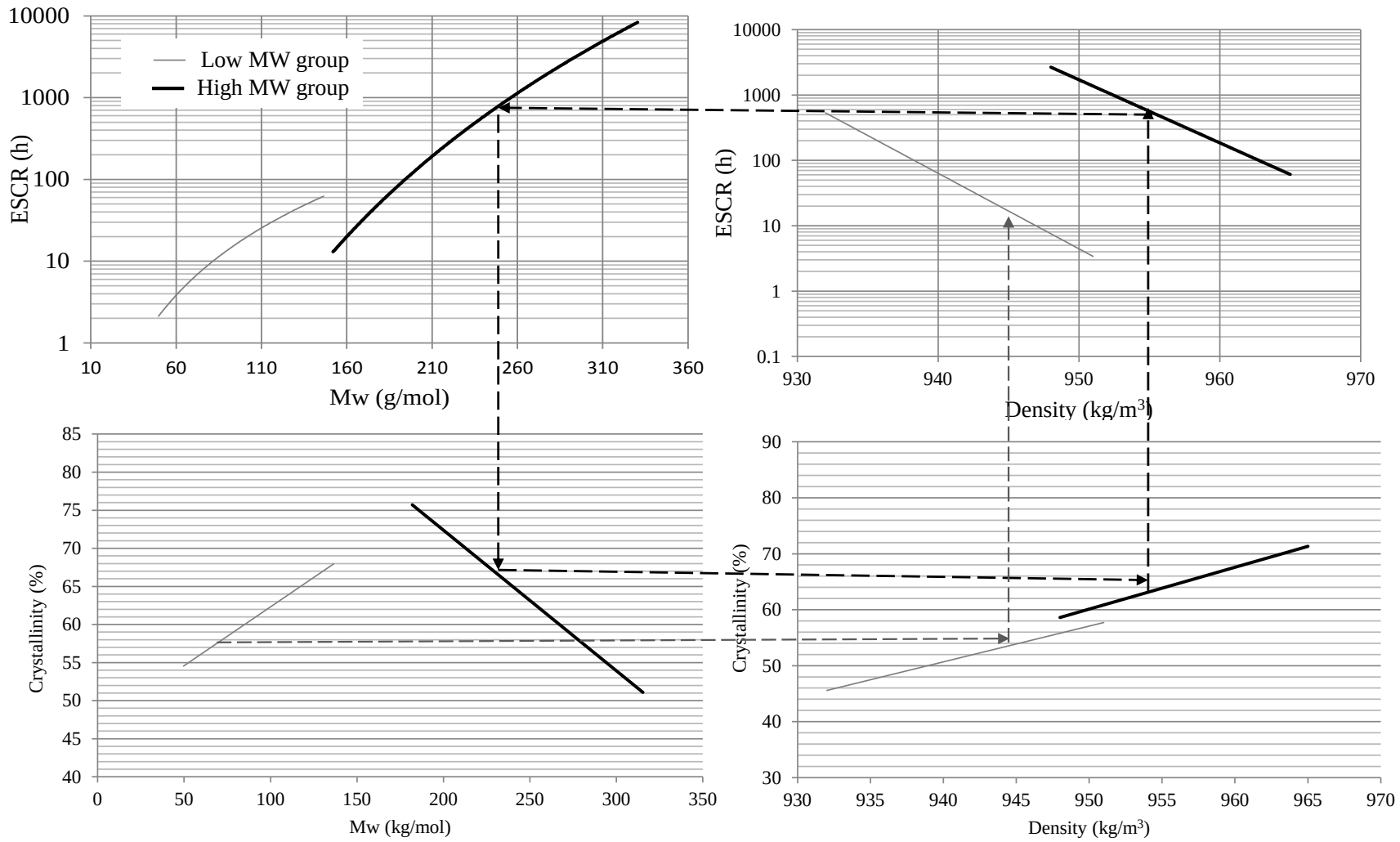

Figure 8.3: ESCR and molecular structure mapping

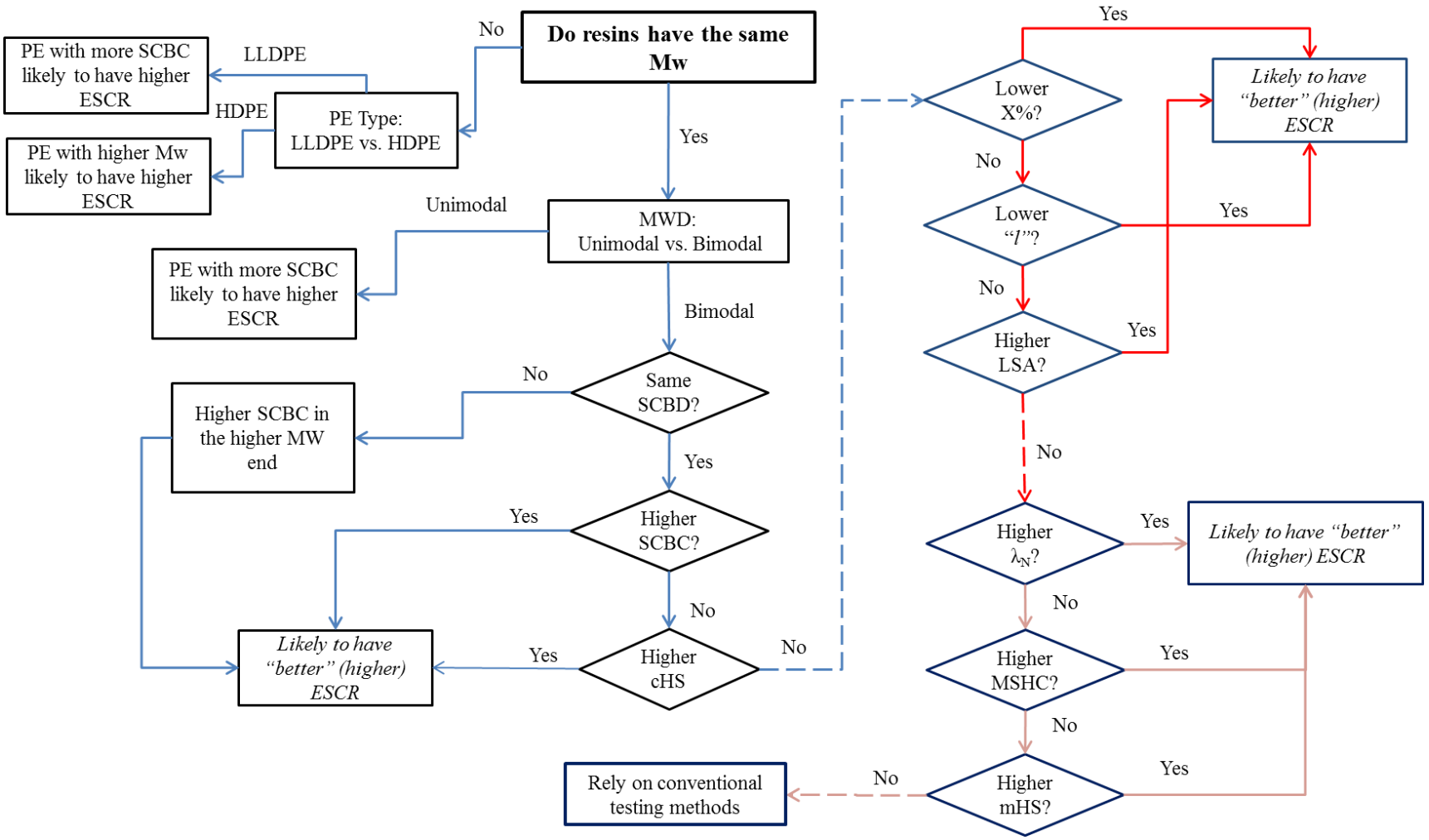

Figure 8.4: Prescriptive pathways for selecting a PE with better/higher ESCR

8.3 CONCLUDING REMARKS

A general overview of the relationship between major molecular structure characteristics and ESCR of PE resins, based on experimental characterization and published literature trends, has been provided in this chapter. In addition, relationships were developed between ESCR, Mw, percentage crystallinity and density to indicate the influence of each factor, and possibly of their interaction, on the ESCR level. Ultimately, several diagrams were developed based on all the experimental observations, displaying the developed correlations (see Figure 8.3).

Finally, a logical flowchart was suggested that offers practical prescriptions and describes pathways towards the development of PE with a better/higher ESCR (see Figure 8.4).

9 CHAPTER 9: CONCLUDING REMARKS, MAIN CONTRIBUTIONS, AND FUTURE RECOMMENDATIONS

9.1 CONCLUDING REMARKS

Environmental stress cracking resistance (ESCR) has been a subject of many studies, as it is the single largest cause of failures in plastics (1). In polyethylene, ESCR occurs through a process of chain disentanglements, in which, inter-lamellar tie-molecules (2) and physical chain entanglements (3) are fully extended, and ultimately fractured, giving rise to a sudden catastrophic brittle failure. In this PhD thesis, relationships between major molecular properties and ESCR of polyethylene were studied through various characterization techniques. In addition, studies were conducted in order to identify potential indicators for a practical and reliable indirect measure of ESCR, in both the solid and melt states. The effects of processing conditions on ESCR were further investigated to shed light on relationships between processing temperature and crystalline phase properties, controlling ESCR. Detailed concluding remarks for each topic, covered in the different chapters of this thesis, were given at the end of each corresponding chapter. In this section, the main conclusions derived from all aspects of the research are summarized.

1. The modified uniaxial tensile test is a practical and reliable test for a relative measure of ESCR of PE resins (Chapter 4).
2. The developed corrected hardening stiffness (cHS) can be used as a potential indicator of ESCR of PE (Chapter 4).
3. A normalized characteristic average relaxation time (λ_N), obtained through dynamic shear experiments, was found to be sensitive to the extent of short chain branching

content in PE. Ultimately, λ_N can be used as an indirect measure of chain entanglements in the melt (Chapter 5).

4. For PEs with very different molecular structures, the melt strain hardening coefficient (MSHC) was found to be a reliable indicator of the extent of chain entanglements. PEs with a greater MSHC have a larger number of chain entanglements, and consequently, a lower melt extensibility (or higher ESCR) (Chapter 5)
5. Investigation of the strain hardening slope from a Sentmanat extensional rheometer gave rise to the development of the melt hardening stiffness (mHS). Resins with a higher mHS were found to have higher ESCR (Chapter 5).
6. Studies conducted on the crystalline phase characteristics indicated an inverse relationship between percentage crystallinity/ lamella thickness and ESCR. This observation was related to the extent of short chain branches and molecular weight of the PEs (Chapter 6).
7. Lamella surface area (LSA) was found to be a reliable indicator of ESCR, as it is readily affected by PE's molecular structure (Chapter 6).
8. Post-processing annealing, conducted at different temperature levels and durations, was found to cause a deterioration in ESCR, as reflected on LSA values. In contrast, a faster cooling rate showed improvements in ESCR (Chapter 6).
9. Formation of long chain branches in PE, through a UV-initiated reactive extrusion, was possible over well-controlled processing conditions (Chapter 7).
10. Long chain branches increased the linear viscoelastic properties of zero shear viscosity (η_o) and characteristic relaxation time (λ). An increase in such properties

also improved the extent of chain entanglements, shown by an increase in the value of ESCR (Chapter 7).

9.2 MAIN CONTRIBUTIONS

The research in this thesis has made the following original contributions:

1. The uniaxial tensile strain hardening test developed in Chapter 4 of this thesis is an extension and improvement on previously presented tensile tests developed by Kurelec et al. (4) and Cheng et al. (5). The test proposed by Kurelec et al. (4) lacked precision and sensitivity at ambient conditions, required an extensometer for a true estimation of stress and strain, and was conducted at 0.25 mm/min. Cheng et al. (5) improved the test and found promising results, obtained from conducting a tensile test at room temperature, using engineering load-displacement data. Through the work in this thesis (Chapter 4), we developed a standard uniaxial tensile test, according to test specimen dimensions and rate of the test, for a relative measure of ESCR. In this standard tensile test, we were able to identity specimen dimensions in order to confine measurements to a small volume of the test specimen, in which a uniform deformation can be assumed. In addition, through the development of a correction factor (Chapter 4), relative measurements of ESCR were extended to other types of PE resins. This was also a considerable improvement on the prior state of the art, as described in Cheng et al (5) and Kurelec et al. (4). Discussions are underway with one of our industrial partners to initiate the steps, needed for publication of a formal standard testing protocol, in order to substitute currently used conventional testing methodologies with our uniaxial tensile test.

2. Most studies on ESCR have focused on performing mechanical tests in the solid state (6). In this thesis, we extended this work to the melt state (Chapter 5), and identified melt indicators for a relative measure of ESCR. The normalized characteristic relaxation time (λ_N), obtained from dynamic shear experiments, was established to be a valid measure of ESCR of linear low density polyethylene, where a large content of short chain branches in present. In addition, the melt strain hardening coefficient (MSHC), obtained from extensional rheological methodologies, was found to be another potential and reliable indicator of ESCR (Chapter 5). An inverse correlation between MSHC and ESCR was developed, indicating an inverse relationship between ESCR and chain extensibility in the melt. Furthermore, a new factor called "melt hardening stiffness (mHS)" was developed from the slope of a stress vs. Hencky strain obtained from a Sentmanat extensional rheometry. mHS was found to be another promising indicator of ESCR obtained from rheological studies, conducted in this thesis (Chapter 5).

3. Studies conducted in the literature about the effect of crystalline phase properties on ESCR, contain ambiguous results (7-8). In this thesis (Chapter 6), studies on crystalline phase characteristics indicated that, in order to have a clear understanding of the effect of crystalline phase on ESCR, PEs should be classified according to their weight average molecular weight. Once classified, a decreasing trend was established between percentage crystallinity/ lamella thickness and ESCR. Lamella surface area (LSA), obtained from percentage crystallinity and lamella thickness, was also found to be a reliable indicator of ESCR. Effect of processing and post-processing

temperature indicated that a faster cooling rate from the melt enhances LSA and ESCR. Annealing, on the other hand, should not be conducted, unless on PEs with relatively high molecular weights.

4. Studies on modification of polyethylene through irradiation techniques have mostly focused on crosslinking (9-10). Crosslinking was achieved by irradiating manufactured PE parts by different high energy irradiation techniques. In this thesis (Chapter 7), a state of the art reactive extrusion process was developed for the promotion of long chain branches in polyethylene. Formation of long chain branches, for the first time, was achieved by UV-irradiation of the polymer melt during extrusion, through a well-controlled process. Ultimately, enhancement in many rheological and mechanical properties (including ESCR) was obtained.

5. One of the main objectives of this research was to shed light on relationships and possible correlations between major molecular properties and ESCR. In Chapter 8 of this thesis, a schematic diagram (Figure 8.3) was provided, offering pathways to develop polymers with a wide range of properties and applications. This diagram shows the direct relationships between major molecular structure characteristics, and their possible interactions with ESCR. In addition, a series of practical prescriptions were given in Chapter 8 (Figure 8.4) for prediction of PEs with better/higher ESCR.

9.3 RECOMMENDATIONS FOR FUTURE STEPS

9.3.1 SHORT TERM RECOMMENDATIONS

- The uniaxial tensile test developed in Chapter 4 was not able to detect the effect of short chain branching content on ESCR. This issue was resolved by developing a correction factor (Chapter 4, section 4.3.3), which eventually gave rise to the development of the so-called corrected hardening stiffness (cHS). For the next stage, sample specimens according to the dimensions given in Chapter 4 of this thesis (section 4.3.2), with a lower thickness value (around 0.3 mm), should be considered. Tensile experiments should be carried out at different strain rates (0.5-10 mm/min) to identify the feasibility of designing a more fine-tuned tensile hardening stiffness test for LLDPE resins.

- Shear experiments, conducted in Chapter 5 of this thesis, provided useful information about the effect of short chain branches on melt properties. Dynamic shear experiments at lower frequencies, or shear creep experiments at longer times, are recommended to be carried out for the estimation of the plateau modulus of the resins (only for resins with a narrow molecular weight distribution). A lower plateau modulus is expected for resins with higher short chain branching content. The result from this future study can be used to further complement the findings in Chapter 5, section 5.3.1.

9.3.2 LONG TERM RECOMMENDATIONS

- It is postulated that the natural draw ratio (NDR) and material toughness obtained from a uniaxial tensile test can be used as another indirect indicator of ESCR of polyethylene in the solid state. Tests according to the developed tensile hardening stiffness test should be conducted to identify these factors. We believe that the scatter in measurements of such factors will considerably be improved through refinement of the test.

- Both melt hardening stiffness (mHS) and the melt strain hardening coefficient (MSHC) developed in Chapter 5, were found to be a reliable indicator of the extent of chain entanglements, responsible for ESCR of polyethylene. These factors, however, can only be used for a relative measure of ESCR, if long chain branches are not present in the structure of PE. Methodologies should be developed to normalize the effect of long branches on these factors, for a better representation of ESCR.

- The schematic diagram shown in Chapter 8 (Figure 8.3) has great potential in offering a broad pathway to developing polyethylene resins with a wide range of properties and applications. It is recommended to utilize more PE resins, with different molecular structures, to improve the validity and fit of the given curves, thus ultimately developing universal master curves.

- The approach in this thesis for relating major molecular structure characteristics and ESCR should be extended to other polymers. Collaborative efforts are currently

underway with Civil Engineering to apply the findings in this thesis to polypropylene for structural applications.

REFERENCES

REFERENCES FOR CHAPTER 1

(1) Jansen, J.A. E. (2004) Adv. Materials & Processes, **162**, 6, 162, 50.

(2) Strebel, J.J., Moet, A. (1992) Int. J. Fract. **54**, 21-34.

(3) Brown, N., Lu, X. (1995), **36**, 543-548.

(4) Lustiger, A., Ishikawa, N. (1991) J. of Polym. Sci. Part B: Polym. Phys., **29**, 1047-1055.

(5) Lustiger, A., Markham, R.L. (1983) Polymer, **24**, 1647-54.

(6) Lu, X., Ishikawa, N., Brown, N. (1996) J. Polym. Sci., Part B: Polym. Phys., **34**, 1809-1813.

(7) Seguela, R. J. (2005) Polym. Sci., Part B: Polym. Phys. **43**, 1729-1748.

(8) Huang, Y.L., Brown, N. (1988) J. Mater. Sci., **23**, 3648-55.

(9) Kukalyekar, N., Balzano, L., Peters, G.W.M., Rastogi, S., Chadwick, J.C. (2009). Macromol. Reaction Eng. **3**, 448-454.

(10) Cheng, J.J. *Mechanical and Chemical Properties of High Density Polyethylene Effects of Microstructure on Creep Characteristics*. University of Waterloo: Waterloo, Ont., 2008; pp. TML PUBLIC "-//W3C//DTD HTML 4.0 Transitional//EN" "http://www.w3.org/TR/REC-html40/loose.dtd">.

REFERENCES FOR CHAPTER 2

(1) Knuuttila, H., Lehtinen, A., Nummila-Pakarinen, A. (2004) Adv. Polyethylene Tech., Controlled Material Properties, **169**, 13-28.

(2) Huang, J., Rempel, G.L. (1995) Progress in Polym. Sci., **20**, 459.

(3) Cheng, J.J. *Mechanical and Chemical Properties of High Density Polyethylene Effects of Microstructure on Creep Characteristics*. University of Waterloo: Waterloo, Ont., 2008; pp. TML PUBLIC "-//W3C//DTD HTML 4.0 Transitional//EN" "http://www.w3.org/TR/REC-html40/loose.dtd">.

(4) DesLauriers, P.J., McDaniel, M.P., Rohlfing, D.C., Krishnaswamy, R.K., Secora, S.J.; Benham, E.A., Maeger, P.L., Wolfe, A.R., Sukhadia, A.M., Beaulieu, B.B. (2005) Polym. Eng. & Sci., **45**, 1203-1213.

(5) Kukalyekar, N., Balzano, L., Peters, G.W.M., Rastogi, S., Chadwick, J.C. (2009) Macromol. Reac. Eng., **3**, 448-454.

(6) Beigzadeh, D., Soares, J.B.P., Duever, T.A. (2001) Macromol. Symposia, **173**, 179-194.

(7) Severn, J.R., Chadwich, J.C., *Tailor-made Polymers: Via Immobilization of Alpha-Olefin Polymerization*. Wiley-VCH Verlag GmbH & Co. KGaA, 2008.

(8) Severn, J.R., Chadwick, J.C. (2013) Dalton Trans, **42**, 8979-8987.

(9) Kissin, Y.V., *Alkene Polymerization Reactions with Transition Metal Catalysts*, 1st ed.; Elsevier: Amsterdam, The Netherlands, 2008.

(10) D'Agnillo, L., Soares, J.B.P., Penlidis. A., (1998) Macromol. Chem. and Phy., **199**, 955-962.

(11) D'Agnillo, L., Soares, J.B.P., Penlidis, A., (1998) Polym. Int., **47**, 351-360.

(12) Lu, X., Brown, N. J. (1990) Mater. Sci., **25**, 29-34.

(13) Lu, J., Wei, G., Sue, H., Chu, J. (2000) J. Appl. Polym. Sci., **76**, 311–319.

(14) Lu, X., Brown, N. J. (1990) Mater. Sci., **25**, 411-16.

(15) Wright, D.C. Environmental Stress Cracking of Plastics. Smithers Rapra Technology, 1996.

(16) Cheng, J., Polak, M., Penlidis, A. (2009) J. Macromol. Sci., Part A: Pure and Applied Chemistry, **46**, 572-583.

(17) Lustiger, A., Markham, R.L.(1983) Polymer, **24**, 1647-54.

(18) Strebel, J.J.; Moet, A. (1992) Int. J. Fract., **54**, 21-34.

(19) Sharif, A., Mohammadi, N., Ghaffarian, S.R. (2008) J Appl. Polym. Sci., **110**, 2756-2762.

(20) Choi, B., Weinhold, J., Reuschle, D., Kapur, M. (2009) Polym. Eng. Sci., **49**, 2085-2091.

(21) Ting, S.K.M., Williams, J.G., Ivankovic, A. (2006) Polym. Eng. Sci., **46**, 763-777.

(22) Jansen, J.A. (2004) Adv. Material & Processes, **162**, 162, 50.

(23) Soares, J.B.P., Abbott, R.F., Kim, J.D. (2000) J. Polym. Sci., Part B: Polym. Phys., **38**, 1267-1275.

(24) Ward, A.L., Lu, X., Huang, Y., Brown, N. (1991) Polymer, **32**, 2172-8.

(25) Sharif, A., Mohammadi, N., Ghaffarian, S.R. (2009) J. Appl. Polym. Sci., **112**, 3249-3256.

(26) Huang, Y.L., Brown, N. (1988) J. Mater. Sci., **23**, 3648-55.

(27) Huang, Y., Brown, N. (1991) J. Polym. Sci., Part B: Polym. Phys., **29**, 129-137.

(28) Seguela, R. C. (2005) J. Polym. Sci., Part B: Polym. Phys., **43**, 1729-1748.

(29) Lu, X., Ishikawa, N., Brown, N. (1996) J. Polym. Sci., Part B: Polym. Phys., **34**, 1809-1813.

(30) Yeh, J.T., Chen, J., Hong, H. (1994) J Appl. Polym. Sci., **54**, 2171-86.

(31) Pinter, G., Haager, M., Balika, W., Lang, R.W. (2007) Polym. Test., **26**, 180-188.

(32) Kurelec, L., Teeuwen, M., Schoffeleers, H., Deblieck, R. (2005) Polymer, **46**, 6369-6379.

(33) Cheng, J., Polak, M., Penlidis, A. (2008) J. Macromol. Sci., Part A: Pure and Applied Chemistry, **45**, 599-611.

(34) Cheng, J., Polak, M., Penlidis, A. (2009) Polym. Plastics Tech. Eng., **48**, 1252-1261.

(35) Micic, P., Bhattacharya, S., Field, G. (1998) International Polym. Processing, **13**, 50-57.

(36) Micic, P., Bhattacharya, S.N. *in Proceeding, 2000 Proc. Int. Congr. Rheol., 13th*, 1, 149-157, Cambridge, United Kingdom, 2000.

(37) McGlashan, S.A., Mackay, M.E. (1999) J. Non-Newtonian Fluid Mech., **85**, 213-227.

(38) Zatloukal, M., Vlcek, J., Tzoganakis, C., Sáha, P. (2002) J. Non Newtonian Fluid Mech., **107**, 13-37.

(39) Cogswell, F.N. (1972) Polym. Eng. & Sci., **12**, 64–73.

(40) Cogswell, F.N. (1978) J. Non-Newtonian Fluid Mech., **4**, 23-38.

(41) Bersted, B.H. R. (1993) Polym. Eng. Sci., **33**, 1079-83.

(42) Binding, D.M. (1988) J. Non-Newtonian Fluid Mech., **27**, 173-89.

(43) Meissner, J. (1972) Soc. Rheol., **16**, 405-20.

(44) Padmanabhan, M., Kasehagen, L.J., Macosko, C. T. (1996) J. Rheol., **40**, 473-481.

(45) Sentmanat, M., Wang, B.N., McKinley, G.H. (2005) J. Rheol., **49**, 585-606.

(46) Muenstedt, H., Kurzbeck, S., Stange, J. (2006) Polym. Eng. Sci., **46**, 1190-1195.

(47) Sentmanat, M.L. (2004) Rheol. Acta., **43**, 657-669.

(48) Aho, J. *Rheological Characterization of Polymer Melts in Shear and Extrusion: Measurement Reliability and Data for Practical Processing*. Tampere University of Technology . Tampere, Finland, 2011.

(49) Bernnat, A., Wagner, M.H. *in Proceedings, Rheotens Experiments and Elongational Behavior of Polymer Melts.* Proceedings of the Fifth European Rheology Conference, Portorož, Slovenia, 1998.

(50) He, G., Tzoganakis, C. (2011) Polym. Eng. Sci.**, 51**, 151-157.

(51) Rideal, G.R.; Padget, J.C. T. J. (1976) Polym. Sci.: Polymer Symposia, **57**, 1-15.

(52) Wu, S.; Xu, X. (2003) J. Appl. Polym. Sci., **89**, 2966-2969.

(53) Morshedian, J., Hoseinpour, P.M. (2009) Iran. Polym. J., **18,** 103-128.

(54) Suwanda, D., Balke, S.T. (1993) Polym. Eng. Sci., **33**, 1585-91.

(55) Qing, Y., Wenying, X., Rånby, B. (1991) Polym. Eng. & Sci., **31**, 1561-1566.

(56) Kim, K.J., Ok, Y.S., Kim, B.K. (1992) European Polym. J., **28**, 1487-1491.

(57) Sarmoria, C., Vallés, E. (2004) Polymer, **45**, 5661-5669.

(58) Rabek, J.F. *Mechanisms of Photophysical Processess and Photochemical Reactions in Polymers : Theory and Applications*.; Wiley: Chichester (West Sussex) ; Toronto, 1987; pp. TML PUBLIC "-//W3C//DTD HTML 4.0 Transitional//EN" "http://www.w3.org/TR/REC-html40/loose.dtd">.

(59) Hill, D.J.T., Preston, C.M.L., Salisbury, D.J., Whittaker, A.K. (2001) Radiat. Phys. Chem., **62**, 11-17.

(60) Nield, S.A., Tzoganakis, C., Budman, H.M. (2000) Adv. Polym. Technol., **19**, 237-248.

(61) Gasparrini, G., Carenza, M., Palma, G. (1980) J. Polym. Sci., Polym. Letters, **18**, 29-33.

(62) Kim, B.K., Shon, K.H., Jeong, H.M. (2004) J. Appl. Polym. Sci., **92**, 1672-1679.

(63) Keller, A., Ungar, G. (1983) Radiat. Phys. Chem., **22**, 155-181.

(64) Qu, B.J., Rånby, B. J. (1993) Appl. Polym. Sci., **48**, 711-719.

(65) Qu, B., Qu, X., Xu, Y., Jacobsson, U., Rånby, B., Russell, K.E., Baker, W.E. (1997) Macromolecules, **30**, 1408-1413.

(66) Qu, B.J., Rånby, B. (1993) J. Appl. Polym. Sci., **48**, 701-709.

(67) Chen, Y.L., Rånby, B. (1989) J. Polym. Sci., Part A: Polymer Chemistry, **27**, 4051-4075.

(68) Chen, Y.L., Rånby, B. (1990) J. Polym. Sci., Part A: Polymer Chemistry, **28**, 1847-1859.

(69) Qing, Y., Wenying, X., Rånby, B. (1994) Polym. Eng. & Sci., **34,** 446-452.

(70) Rånby, B. (1998) Mat. Res. Innovat., **2**, 64-71.

(71) Qu, B., Xu, Y., Ding, L., Ranby, B. (2000) J. Polym. Sci., Part A: Polym. Chem., **38**, 999-1005.

(72) Cheng, S., Phillips, E., Parks, L. (2010) Radiat. Phys. Chem., **79**, 329-334.

(73) Cheng, S., Phillips, E., Parks, L. (2009) Radiat. Phys. Chem., **78**, 563-566.

(74) Dickie, B.D., Koopmans, R.J., Dow Benelix, N.V. (1990) J. Polym. Sci.: Part C: Polym. Letters, **28**, 193.

(75) Piel, C., Stadler, F.J., Kaschta, J., Rulhoff, S., Münstedt, H., Kaminsky, W. (2006) Macromol. Chem. Phys., **207**, 26-38.

(76) Randall, J.C., Zoepfl, F.J., Silverman, J. (1983) Die Makromolekulare Chemie, Rapid Communications, **4**, 149-157.

(77) Tzoganakis, C. (1989) Adv. Polym. Technol., **9**, 321-330.

REFERENCES FOR CHAPTER 3

(1) Shadfan, B., Barron, AR. *Physical Methods in Chemistry and Nano Science: A summary of the history, background and science of differential scanning calorimetry*. Chem 475. Rice University, Huston, Texas, US, 2013.

(2) Wlochowicz, A., Eder, M. (1984) Polymer, **25**, 1268-1270.

(3) Rao, B. *Size Exclusion Chromatography of Polyolefins and Evaluating Local Polydispersity*. University of Toronto, Toronto, Ontario, 1998.

(4) Zimm, B.H., Stockmayer, W.H. (1949). J. Chem. Phys., **17**, 1301-1314.

(5) Scorah, M.J., Dhib, R. Penlidis, A. *Branching level detection in polymers. Encyclopedia of Chemical Processing (ECHP)*. London: Taylor& Francis: 2005. p 251ff.

(6) Sardashti, P., Tzoganakis, C., Polak, M.A., Penlidis, A. (2013) Macromol. Reaction Eng. DOI: 10.1002/mren.201300134.

(7) Cheng, J.J. *Mechanical and Chemical Properties of High Density Polyethylene Effects of Microstructure on Creep Characteristics*.; University of Waterloo: Waterloo, Ont., 2008; pp. TML PUBLIC "-//W3C//DTD HTML 4.0 Transitional//EN" "http://www.w3.org/TR/REC-html40/loose.dtd">.

(8) Furukawa, T., Sato, H., Kita, Y., Matsukawa, K., Yamaguchi, H., Ochiai, S., Siesler, H.W., Ozaki, Y. (2006) Polym. J., **38**, 1127-1136.

(9) Jansen, J.A. (2004) Advanced Materials & Processes, **162**, 50.

(10) ASTM International. ASTM D638-10 Standard Test Method for Tensile Properties of Plastics. **2010**.

(11) ASTM International. ASTM D5397-07 Standard Test Method for Evaluation of Stress Crack Resistance of Polyolefin Geomembranes using Notched Constant Tensile Load Test. **2007**.

(12) Wright, D.C. Environmental Stress Cracking of Plastics. Smithers Rapra Technology, 1996.

(13) Ward, I.M., Sweeney, J. *Mechanical Properties of Solid Polymers*, 3rd ed.; John Wiley & Sons: United Kingdom, 2013.

(14) Dao, T.T., Ye, A.X., Shaito, A.A., Roye, N., Hedman, K. (2009). Am. Lab. (Shelton, CT, U. S.), **41**, 18-22.

(15) Cogswell, F.N. (1972) Polym. Eng. & Sci., **12**, 64–73.

(16) Morrison, F.A. *Shear Viscosity Measurement in a Capillary Rheometer*: *CM4655 Morrison Lectures*. Michigan Technological University, Houghton, Michigan, USA, 2013

(17) Sentmanat, M.L. (2004) Rheol. Acta., **43**, 657-669.

REFERENCES FOR CHAPTER 4

1. Wright, D.C. Environmental Stress Cracking of Plastics. Smithers Rapra Technology, 1996.

2. Sharif, A., Mohammadi, N. and Ghaffarian, S. R. (2008) J. Appl. Polym. Sci., **110**, 2756-2762.

3. Sharif, A., Mohammadi, N. and Ghaffarian, S. R. (2009) J. Appl. Polym. Sci., **112**, 3249-3256.

4. Ward, A. L., Lu, X., Huang, Y. and Brown, N. (1991) Polymer, **32**, 2172-2178.

5. Brown, N., Kamei, E. and Ward, I. M. *in Proceedings, 1983 International Gas Research Conference, London*, 1983, Gas Research Institute, London, 1983.

6. Seguela, R. (2005) J. Polym. Sci. Part B: Polym. Phys., **43**, 1729-1748.

7. Huang, Y. L. and Brown, N. (1988) J. Mater. Sci., **23**, 3648-3655.

8. Lu, X., Ishikawa, N. and Brown, N. (1996) J. Polym. Sci., Part B: Polym. Phys., **34**, 1809-1813.

9. Cheng, J. J. *Mechanical and chemical properties of high density polyethylene effects of microstructure on creep characteristics*, Department of Chemical Engineering, University of Waterloo, Waterloo, Ont. 2008, p. TML PUBLIC "-//W3C//DTD HTML 4.0 Transitional//EN" "http://www.w3.org/TR/REC-html40/loose.dtd">.

10. Yeh, J. T., Chen, J. and Hong, H. (1994) J. Appl. Polym. Sci., **54**, 2171-2186.

11. Lustiger, A. and Markham, R. L. (1981) Polymer, **24**, 1647-1654.

12. Cheng, J., Polak, M. and Penlidis, A. (2009) J. Macromolecular Sci., Part A: Pure and Applied Chemistry, **46**, 572–583.

13. Pinter, G., Haager, M., Balika, W. and Lang, R. W. (2007) Polym. Testing, **26**, 180-188.

14. Kurelec, L., Teeuwen, M., Schoffeleers, H. and Deblieck, R. (2005) Polymer, **46**, 6369-6379.

15. Cheng, J., Polak, M., Penlidis, A. (2009) J. Macromolecular Sci., Part A: Pure and Applied Chemistry, **45**, 599–611.

16. O'Connell, P.A., Bonner, M. J., Duckett, R.A. and Ward, I.M. (2003) J. Appl. Polym. Sci., **89**, 1663-1670.

17. Huang, Y. L. and Brown, N. (1991) J. Polym. Sci., Part B: Polymer Physics, **29**, 129-137.

REFERENCES FOR CHAPTER 5

(1) Micic, P., Bhattacharya, S.N. in Proceedings, International Congress on Rheology, 13th, Cambridge, United Kingdom, 2000, pp. 149-157.

(2) McGlashan, S.A., Mackay, M.E. (1999) J. Non-Newtonian Fluid Mech., **85,** 213-227.

(3) Zatloukal, M., Vlcek, J., Tzoganakis, C., Sáha, P. (2002) J. Non Newtonian Fluid Mech. **107**, 13-37.

(4) Zatloukal, M., Musil, J. (2009) Polym. Test., **28**, 843-853.

(5) Cogswell, F.N. (1972) Polym. Eng. Sci., **12**,64-73.

(6) Cogswell, F.N. (1978) J. Non-Newtonian Fluid Mech., **4**, 23-38.

(7) Munstedt, H. (1979) J. Rheol., **23**, 421-436.

(8) Meissner, J. (1972) Trans. Soc. Rheol., **16**, 405-20.

(9) Padmanabhan, M., Kasehagen, L.J., Macosko, C. (1996) J. Rheol., **40**, 473-481.

(10) US Patent, US6691569 B1 (2002). *Dual Windup Extensional Rheometer*. Martin Lamar Sentmanat, The Goodyear Tire & Rubber Company .

(11) Sentmanat, M.L. (2004) Rheol Acta, **43**, 657-669.

(12) Sentmanat, M., Wang, B.N., McKinley, G.H. (2005) J. Rheol., **49**, 585-606.

(13) Aho, J. *Rheological Characterization of Polymer Melts in Shear and Extrusion: Measurement Reliability and Data for Practical Processing*. Tampere University of Technology, Tampere, Finland, 2011.

(14) Cheng, J., Polak, M., Penlidis, A. (2009) J. Macromolecular Sci., Part A: Pure and Applied Chemistry, **45**, 599–611.

(15) Sardashti, P.; Tzoganakis, C.; Polak, M.A.; Penlidis, A. (2012) J. Macromolecular Sci., Part A: Pure and Applied Chemistry, **49**, 689-698.

(16) Cheng, J.; Polak, M.; Penlidis, A. (2009) Polym. Plastics Tech. & Eng., **48**, 1252-1261

(17) Willbourn, A.H. (1959) J. Polym. Sci., **34**, 569-597.

(18) Wood-Adams, P.M., Dealy, J.M., deGroot, A.W., Redwine, O.D. (2000) Macromolecules, **33**, 7489-7499.

(19) Hatzikiriakos, S.G. (2000) Polym. Eng. Sci., **40**, 2279-2287.

(20) Honerkamp, J., Weese, J. (1993) Rheol. Acta., **32**, 65-73.

(21) Scorah, M.J., Tzoganakis, C., Dhib, R., Penlidis, A. (2007) J. Appl. Polym. Sci., **103**, 1340-1355.

(22) Carreau, P.J. (1972) Trans. Soc. Rheol., **16**, 99-127.

(23) Yasuda, K., Armstrong, R.C., Cohen, R.E. (1981). Rheol. Acta., **20**, 163-178.

(24) Stadler, F., Mahmoudi, T. (2011) Korea-Australia Rheology Journal, **23**, 185-193.

(25) Munstedt, H. (2011) Soft Matter., **7**, 2273-2283.

(26) Stadler, F.J., van Ruymbeke, E. (2010) Macromolecules, **43**, 9205-9209.

(27) Cross, M.M. (1965) J. Colloid Sci., **20**, 417.

(28) Hieber, C.A., Chiang, H.H. S. (1992) Polym. Eng. & Sci., **32**, 931-938.

(29) Yan, D., Wang, W., Zhu, S.(1999) Polymer, **40**, 1737-1744.

(30) Auhl, D., Stange, J.;,Münstedt, H., Krause, B., Voigt, D., Lederer, A., Lappan, U.; Lunkwitz, K. (2004) Macromolecules, **37**, 9465-9472.

(31) Piel, C., Stadler, F.J., Kaschta, J., Rulhoff, S., Münstedt, H., Kaminsky, W. (2006) Macromol. Chem. Phys., **207**, 26-38.

(32) Stadler, F.; Piel, C., Kaschta, J., Rulhoff, S., Kaminsky, W., Munstedt, H. (2006) Rheol. Acta., **45**, 755-764.

(33) Yamaguchi, M., Suzuki, K., Maeda, S. (2002) J. Appl. Polym. Sci., **86**, 73-78.

(34) Auhl, D., Stadler, F., Munstedt, H. (2012) Rheol. Acta., **51**, 979-989.

REFERENCES FOR CHAPTER 6

1. Huang, Y., Brown, N. (1991) J. Polym. Sci. Part B: Polymer Physics, **1**, 129-137.

2. Lu, X., Ishikawa, N., Brown, N. (1996) J. Polym. Sci., Part B: Polym. Phys., **10**, 1809-1813.

3. Huang, Y. L., Brown, N. (1988) J. Mater. Sci., **10**, 3648-55.

4. Yeh, J. T., Chen, J., Hong, H. (1994) J. Appl. Polym. Sci., **13**, 2171-86.

5. Bandyopadhyay, S.; Brown, H. R. (1978) Polymer, **5**, 589-592.

6. Lu, X., Brown, N. (1990) J. Mater. Sci., **1B**, 411-16.

7. Lustiger, A., Markham, R. L. (1983) Polymer, **12**, 1647-54.

8. Hittmair, P., Ullman, R. (1962) J. Appl. Polym. Sci., **19**, 1-14.

9. Sharif, A., Mohammadi, N., Ghaffarian, S. R. (2009) J. Appl. Polym. Sci., **6**, 3249-3256.

10. Nie, M., Wang, Q., Bai, S. (2010) J. Macromolecular Sci., Part B, **4**, 640-651.

11. Strebel, J. J., Benson, M. (1996) Polym. Eng. & Sci., **9**, 1266-1271.

12. Cheng, J., Polak, M., Penlidis, (2009) A. J. Macromolecular Sci. Part A: Pure and Applied Chemistry, **46**, 572–583.

13. Marand, H., Huang, Z. (2004) Macromolecules, **17**, 6492-6497.

14. Ryousho, Y., Sasaki, S., Nagamura, T., Takahara, A., Kajiyama, T. (2004) Macromolecules, **13**, 5115-5117.

15. Loos, J., Tian, M., Rastogi, S., Lemstra, P. J. (2000) J. Mater. Sci., **20**, 5147-5156.

16. Rastogi, S., Spoelstra, A. B., Goossens, J. G. P., Lemstra, P. (1997) J. Macromolecules, **25**, 7880-7889.

17. Fischer, E. W., (1972) Pure Appl. Chem., **31**, 113-132.

18. Stadler, F.J., Piel, C., Kaschta, J., Rulhoff, S. Kaminsky, W., Munstedt, H. (2006) Rheol. Acta, **45**, 755–764.

19. Wlochowicz, A., Eder, M. (1984) Polymer, **9**, 1268-1270.

20. Sardashti, P., Tzoganakis, C., Polak, M. A., Penlidis, A. (2012) J. of Macromolecular Sci., Part A, **9**, 689-698.

21. Lu, X., Qian, R., McGhie, A. R., Brown, N. (1992) J. of Polym. Sci. Part B: Polymer Physics, **8**, 899-906.

22. Tung, L. J., Buckser, S. (1958) J. Phys. Chem., **12**, 1530-1534.

23. Shirayama, K., Kita, S., Watabe, H. (1972) Die Makromolekulare Chemie, **1**, 97-120.

24. Alberola, N., Cavaille, J. Y., Perez, J. (1990) J. Polym. Sci., Part B: Polymer Physics, **4**, 569-586.

25. Zhang, M., Lynch, D. T., Wanke, S. E. (2001) Polymer, **7**, 3067-3075.

26. Uan-Zo-li, J. T. Morphology, crystallization and melting behavior of propylene-ethylene statistical copolymers, Department of Materials Science and Engineering, Doctoral Dissertation, Virginia Polytechnic Institute, Blacksburg, Virginia, 2005.

27. van Krevelen, D. W. Properties of Polymers, 4th edition. Elsevier, 2009.

28. Box, G. E. P, Hunter, J. S., Hunter, W. G. Statistics for Experimenters: Design, Innovation, and Discovery, 2nd Edition. J. Wiley & Sons Inc., 2005.

REFERENCES FOR CHAPTER 7

(1) Qing, Y., Wenying, X., Rånby, B. (1991) Polym. Eng. & Sci., **31**, 1561-1566.

(2) Kim, K.J., Ok, Y.S., Kim, B.K. (1992) European Polym. J., **28**, December.

(3) Sarmoria, C., Vallés, E. (2004) Polymer, **45**, 5661-5669.

(4) Rabek, J.F. *Mechanisms of Photophysical Processess and Photochemical Reactions in Polymers : Theory and Applications*.; Wiley: Chichester [West Sussex] ; Toronto, 1987; pp. TML PUBLIC "-//W3C//DTD HTML 4.0 Transitional//EN" "http://www.w3.org/TR/REC-html40/loose.dtd">.

(5) Hill, D.J.T., Preston, C.M.L., Salisbury, D.J., Whittaker, A.K. (2001) Radiat. Phys. Chem., **62**, 11-17.

(6) Nield, S.A., Tzoganakis, C., Budman, H.M. (2000) Adv. Polym. Technol., **19**, 237-248.

(7) Keller, A., Ungar, G. (1983) Radiat. Phys. Chem., **22**, 155-181.

(8) Cheng, S., Phillips, E., Parks, L. (2010) Radiat. Phys. Chem., **79**, 329-334.

(9) Qu, B., Qu, X., Xu, Y., Jacobsson, U., Rånby, B., Russell, K.E., Baker, W.E. (1997) Macromolecules, **30**, March.

(10) Rånby, B. (1998) Mat. Res. Innovat., **2**, 64-71.

(11) Chen, Y.L., Rånby, B. (1989) J. Polym. Sci., Part A: Polymer Chemistry, **27**, 4051-4075.

(12) Chen, Y.L., Rånby, B. P. (1990) J. Poly. Sci., Part A: Polymer Chemistry, **28**, 1847-1859.

(13) Qing, Y., Wenying, X., Rånby, B. (1991) Polym. Eng. Sci., **31**, 1567-1571.

(14) Qing, Y., Rånby, B. (1992) Polym. Eng. Sci., **32**, 831-835.

(15) Qu, B.J., Rånby, B. (1993) J. Appl. Polym. Sci., **48**, 711-719.

(16) Qu, B.J., Rånby, B. (1993) J. Appl. Polym. Sci., **48**, 701-709.

(17) Qing, Y., Wenying, X., Rånby, B. (1994) Polym. Eng. Sci., **34**, 446-452.

(18) Auhl, D., Stadler, F., Munstedt, H. (2012) Rheol. Acta., **51**, 979-989.

(19) Auhl, D., Stange, J., Münstedt, H., Krause, B., Voigt, D., Lederer, A., Lappan, U.;, Lunkwitz, K. (2004). Macromolecules, **37**, 9465-9472.

(20) US Patent US 4916198 A (1990). High Melt Strength Propylene Polymer, Process of Making it, and use Thereof. Scheve, B.J., Mayfield, J.W., DeNicola, A.J.

(21) Walter, P., Trinkle, S., Lilge, D., Friedrich, C., Mulhaupt, R. (2001) Macromolecular Materials and Engineering, **286**, 309-315.

(22) Langston, J.A., Colby, R.H., Chung, T.C.M., Shimizu, F., Suzuki, T., Aoki, M. (2007) Macromolecules, **40**, 2712-2720.

(23) Yan, D., Wang, W., Zhu, S. (1999) Polymer, **40**, 1737-1744.

(24) Piel, C., Stadler, F.J., Kaschta, J., Rulhoff, S., Münstedt, H., Kaminsky, W.(2006) Macromol. Chem. Phys., **207**, 26-38.

(25) Dickie, B.D., Koopmans, R.J., Dow Benelux, N.V. (1990) J. Polym. Sci.,: Part C: Polymer Letters, **28**, 193.

(26) Cheng, S., Phillips, E., Parks, L. (2009) Radiat. Phys. Chem., **78**, 563-566.

(27) Cheng, S., Phillips, E."*Rheological Studies on Radiation Modified Polyethylene Resins*" (2006) Society of Plastic Engineers ANTEC Conference.

(28) US Patent 7094472 B2 (2006). Radiation Treated Ethylene Polymers and Articles made from Said Polymer. Plessis, D., Cheng, S., Suete, H.

(29) Wadud, S.E.B., Baird, D.G. (2000) J. Rheol., **44**, 1151-1167.

(30) Hatzikiriakos, S.G. (2000) Polym. Eng. Sci., **40**, 2279-2287.

(31) Wood-Adams, P.M., Dealy, J.M., deGroot, A.W., Redwine, O.D. (2000) Macromolecules, **33**, 7489-7499.

(32) Vittorias, I., Lilge, D., Baroso, V., Wilhelm, M. (2011) Rheol. Acta., **50**, 691-700.

(33) Sardashti, P., Tzoganakis, C., Polak, M.A., Penlidis, A.(2012) J. Macromol. Sci., Part A, **49**, 689-698.

(34) Honerkamp, J., Weese, J. (1993) Rheol. Acta., **32**, 65-73.

(35) Trinkle, S., Friedrich, C. (2001) Rheol. Acta., **40**, 322-328.

(36) Zimm, B.H., Stockmayer, W.H. (1949) J. Chem. Phys., **17**, 1301-1314.

(37) Krause, B., Voigt, D., Lederer, A., Auhl, D., Munstedt, H. (2004) J. Chromatography A, **1056**, 217-222.

(38) Scorah, M.J., Tzoganakis, C., Dhib, R., Penlidis, A. (2007) J. Appl. Polym. Sci., **103**, 1340-1355.

(39) Gabriel, C., Münstedt, H. I. (2002) Rheol. Acta., **41**, 232-244.

(40) Pearson, D.S., Helfand, E. (1984) Macromolecules, **17**, 888-895.

(41) US. Provisional patent application 61/854,188 (2013), Y. Amintowlieh, C. Tzoganakis, A. Penlidis.

REFERENCES FOR CHAPTER 8

1) Huang, Y.L., Brown, N. (1988) J. Mater. Sci., **23**, 3648-55

(2) Cheng, J., Polak, M., Penlidis, A. (2008) J. Macromol. Sci., Part A: Pure and Applied Chemistry, **45**, 599-611

(3) Lu, X., Ishikawa, N., Brown, N. (1996) J. Polym. Sci., Part B: Polym. Phys., **34**, 1809-1813.

(4) Sun, X., Shen, H., Xie, B. (2011) Polymer, **52**, 564-570

(5) Willbourn, A.H. (1959) J. Polym. Sci., **34**, 569-597

(6) (3) Cheng, J.J. *Mechanical and Chemical Properties of High Density Polyethylene Effects of Microstructure on Creep Characteristics*. University of Waterloo: Waterloo, Ont., 2008; pp. TML PUBLIC "-//W3C//DTD HTML 4.0 Transitional//EN" "http://www.w3.org/TR/REC-html40/loose.dtd">.

REFERENCES FOR CHAPTER 9

(1) Jansen, J.A. E. (2004) Adv. Materials & Processes, **162**, 6, 162, 50.

(2) Lustiger, A., Markham, R. L. (1983) Polymer, **12**, 1647-54.

(3) Cheng, J., Polak, M., Penlidis, A. (2009) Polym. Plastics Tech. Eng., **48**, 1252-1261.

(4) Kurelec, L., Teeuwen, M., Schoffeleers, H. and Deblieck, R. (2005) Polymer, **46**, 6369-6379.

(5) Cheng, J., Polak, M., Penlidis, A. (2009) J. Macromolecular Sci., Part A: Pure and Applied Chemistry, **45**, 599–611.

(6) Wright, D.C. Environmental Stress Cracking of Plastics. Smithers Rapra Technology, 1996.

(7) Hittmair, P., Ullman, R. (1962) J. Appl. Polym. Sci., **19**, 1-14.

(8) Sharif, A., Mohammadi, N., Ghaffarian, S. R. (2009) J. Appl. Polym. Sci., **6**, 3249-3256.

(9) (11) Chen, Y.L., Rånby, B. (1989) J. Polym. Sci., Part A: Polymer Chemistry, **27**, 4051-4075.

(10) Chen, Y.L., Rånby, B. P. (1990) J. Poly. Sci., Part A: Polymer Chemistry, **28**, 1847-1859.

APPENDICES

APPENDIX A: DEVELOPMENT OF ESCR-cHS MASTER CURVE

Evaluation of environmental stress cracking resistance (ESCR) of polymers has been a subject of many studies. Most methodologies developed for estimation of ESCR involve an application of low levels of tensile stress on notched polymer specimens. These methodologies are often carried out in the presence of an aggressive fluid, and at elevated temperatures, to accelerate the failure time of the test specimens. However, due to the implications with the notching process, and also the variability in the quality of the aggressive fluid, results are not very reliable. In addition, depending on the type of PE, such testing methodologies require a long time to be complete. For example, in case of polyethylene pipe grades, failure times (reported as ESCR) of up to 5,000 hours can be expected. The variability in the reported data and also the long testing times indicated a demand for developing new test methodologies for a practical and reliable estimation of ESCR. In Chapter 4 of this thesis, the main principles were introduced for developing a reliable and practical testing method for evaluation of ESCR of high density polyethylene (HDPE). A uniaxial tensile test, conducted at ambient conditions, was performed on HDPE test specimens. A full description, related to the design of the test specimens and the rate of the tensile test, is given in Chapter 4, section 4.3.2. Through detailed experimental designs, a test specimen shown in Figure 4.7 was suggested. It should be noted that the thickness of specimens in this study was kept around 0.6 mm, however, it is recommended to use an even lower thickness to minimize the effect of sample dimension on hardening stiffness (HS). According to our observations, shown in Chapter 4 of this thesis, as a result of the selection

of such specimen dimensions, a uniform deformation during the tensile deformation can be assumed. The slope obtained from the strain hardening region of the tensile test, called hardening stiffness (HS), was found to correlate well with the ESCR of PEs (the higher the slope of the line (HS), the higher is ESCR). In addition, studies were extended to linear low density polyethylene (LLDPE), by correcting HS using a factor ("m", see Equation 4-1), obtained from the weight average molecular weight (Mw) and short chain branching (SCB) content of the polymer (see Chapter 4, section 4.3.3). The corrected hardening stiffness (cHS) was found to be a more reliable indicator of ESCR, as it includes effects of molecular weight (MW) and branching content. Through the developed characterization technique, a relative measure of ESCR of different types of PE resin was possible.

The next logical step required verification of the developed test, for PEs with largely different molecular structure properties, compared to the resins used in Chapter 4. For this reason, all resins shown in Table 3.1 were selected to extend the studies and verify the adaptability of the developed tensile strain hardening test to PEs with different structures. In addition, it was intended to establish a standard correlation between ESCR, obtained from a Bent Strip Test (BST) and cHS, for a reliable, yet practical, estimation of ESCR. The values of ESCR and cHS for all PEs in this study are shown in Table A1. P 4 and P 11 did not show any strain hardening behavior, therefore no cHS values are reported for them (another indication of their low ESCR behavior). Figure A1 presents a master curve obtained from ESCR and cHS values. As shown, a distinct and clear relationship between ESCR and cHS is developed. Effects of molecular structure characteristics, including both MW and short branching content, are both reflected on ESCR and cHS values. The master curve shown in

Figure A1 provides a clear property mapping, and can be used as a reliable and practical measure for ranking polyethylene resins with different structural characteristics.

Table A1. ESCR and cHS values of all PEs in this study

Polymer ID	PE grade	cHS (N/mm)	ESCR[a] (h)
LLDPE 1	R.T.[1]	2.68	60
LLDPE 2	R.T.	7.38	150
LLDPE 3	R.T.	9.53	190
LLDPE 4	R.T.	18.3	650
HDPE 1	R.T.	0.95	8
HDPE 2	R.T.	3.55	50
HDPE 3	Pipe-100[2]	29.2	1000
HDPE 4	Pipe-100	73.11	3000
PE 4	I.M.[3]	2.37	18
PE 8	Pipe-80[4]	12.34	>500
P1	B.M.[5]	20.48	500
P2	B.M.	3.31	40
P3	B.M.	11.92	300
P4	B.M.	---	15
P5	Pipe-100	36.46	>1000
P6	Pipe-100	96.74	>5000
P7	Pipe-80	30.99	2000
P11	R.T.	---	21

a: ESCR obtained from a Bent Strip Test (BST), 1: Rotational molding grade PE, 2: PE100 grade pipe resin, 3: Injection molding grade PE, 4: PE80 grade pipe resin, 5: Blow molding grade PE.

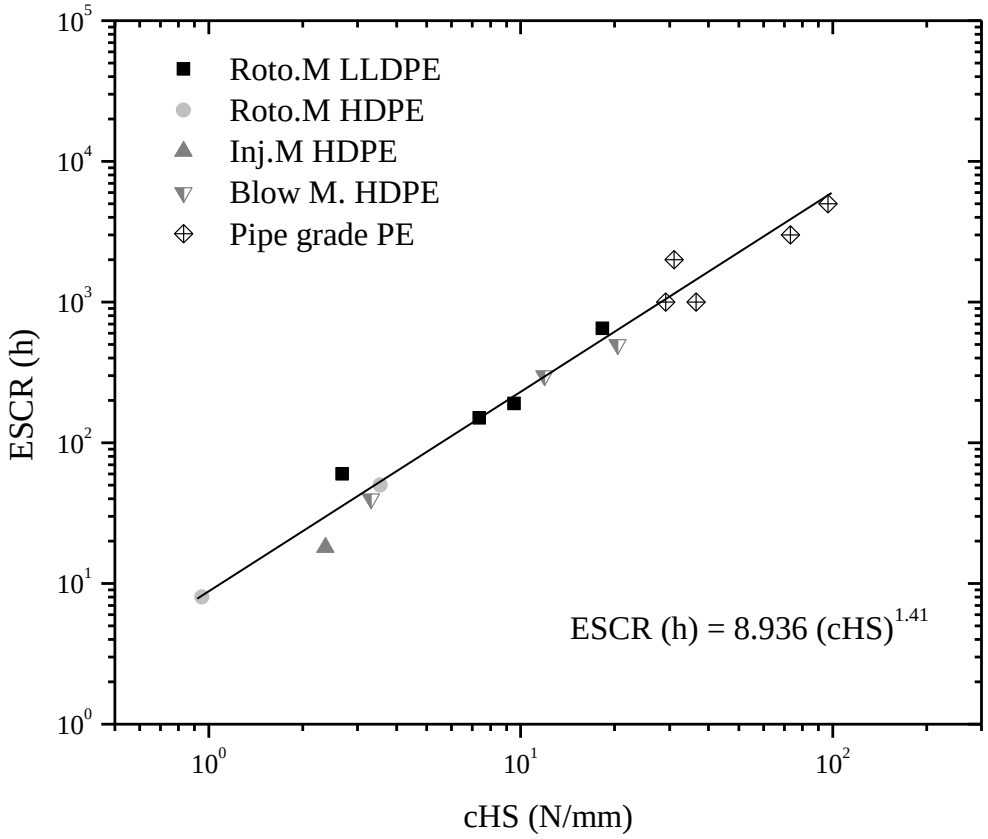

Figure A1. ESCR vs. cHS master curve

APPENDIX B: ENTRY FLOW METHODOLOGIES FOR OBTAINING EXTENSIONAL VISCOSITY

As indicated earlier in Chapter 5 of this thesis, researchers have developed indirect methods to evaluate the extensional viscosity of polymers. One of the frequently used techniques for determination of extensional viscosity is the converging flow technique. In this technique, mainly conducted by a capillary rheometer, polymer melt is forced to flow from a large reservoir through a capillary die, where the entrance pressure drop is measured as a function of flow rate (1). Cogswell (2-3) derived a solution for the estimate of extensional viscosity from simple shear flow properties. Cogswell's model was further improved by many researchers. Bersted (4) relaxed the power law index assumption and found marginal improvement in predictions of extensional viscosity, compared to Cogswell. Binding (5) further studied the converging flow field and developed a model to obtain extensional viscosity. In his analysis, Binding used an energy minimization technique to minimize the viscous energy dissipation within the flow field. Gibson (1) also used sink flow kinematics with no vortices to describe the entrance pressure drop in constrained convergence. An explanation and summary of Cogswell, Binding, and Gibson methodologies and equations are given in Appendix C of this thesis.

In this part of the study, a bench top twin bore Rosand capillary rheometer (RH2200 series) manufactured by Malvern was used to measure the shear viscosity and entrance pressure drop of all LLDPE resins (LLDPE 1-4) and HDPE 1-3, at 150 ºC. Due to the twin bore option, simultaneous measurements were made using a long die and a zero length die. The long die was used to determine shear properties, while the zero length die provided the entrance pressure drops due to the sudden barrel contraction (between the capillary reservoir

and capillary die). In order to identify the entrance pressure drop at various shear rates, three different pressure transducers were used. A 1.72 MPa and a 10.34 MPa transducer were separately attached to the bore (reference bore) equipped with the zero length die (orifice) to measure the entrance pressure drops. A 34.5 MPa transducer was attached to the sample bore, equipped with the long die, to measure the shear viscosities at various shear rates. Ultimately, the entrance pressure drops obtained from the reference bore were used to correct the applied stress data (reflected on the viscosity measurements). Table B1 summarises the instrument, orifice and die specifications.

Table B1: Specifications for the rheometer and die/orifice used for capillary measurements

Instrument Properties	Specification	Die/ Orifice Properties	Specification
Maximum Force (kN)	20	Diameter (mm)	1/1
Maximum Speed (mm/min)	600	Length (mm)	16/0.25
Bore Diameter (mm)	15	Entrance Angle (degrees)	180/180
Barrel Bore Length (mm)	250	Barrel Diameter (mm)	15/15

In order to determine the extensional properties of the resins, the entrance pressure drops (P_o) due to the orifice abrupt contraction were recorded. Throughout this section, entrance pressure drops are presented in terms of entrance viscosity (η_{ent}) according to Equation B1. This was done as it is easier to picture the dependence of viscosity on shear rate, compared to entrance pressure drop or stress. A full description regarding the reason behind presenting entrance pressure drop according to Equation B-1 is given elsewhere (1).

$$\eta_{ent} = \frac{P_o}{\dot{\gamma}_{app}} \qquad \text{B-1}$$

It should be noted that the entry flow technique is only capable of determining the extensional properties at higher shear rates. In this study, due to utilization of more sensitive pressure transducers, it was possible to measure the extensional viscosities at lower shear rate (down to 5 /s). A modified version of the Carreau-Yasuda model proposed by Zatloukal et al. (1), as shown in Equation B-2, was further employed to predict the extensional properties at the Newtonian region. The main reason for using such a model was to investigate the possibility of strain hardening behaviour of the resins. The second term proposed in Equation B-2 allows a maximum to appear in the entrance viscosity, hence giving rise to the plateau region.

$$\log(\eta_{ent}) = log\left\{\frac{\eta_{ent,o}}{1+\left(\lambda\dot{\gamma}_{app}\right)^{a}}\right\}\left[\frac{Tanh\left(\alpha\dot{\gamma}_{app}+1\right)}{Tanh(1)}\right]^{\xi} \qquad \text{B-2}$$

In Equation B-2, $\eta_{ent,o}$ is the plateau value of the entrance viscosity, and λ, a,α and ξ are fitting parameters.

The entrance viscosities of the PE resins as a function of apparent shear rate obtained from capillary rheometry and Equation B-2 are shown in Figure B1. It should be noted that entrance pressure drop is dependent on the polymer molecular structure, and the apparent shear rate. Zatloukal et al. (1) developed an effective entry length correction to better predict the extensional viscosity at lower shear rates. The idea was to find the L/D which resulted in the correct Trouton ratio (ratio of extensional viscosity in the Newtonian region to zero shear viscosity) of 3. In this work, however, the scope of the study is to investigate the feasibility

of utilizing entrance viscosity or extensional viscosity as a measure of ESCR of PE resins. Furthermore, due to the nature of the orifice die used in this study, the assumption of fluid jet flow at the downstream region of the orifice die at lower shear rates is uncertain. It is believed that the downstream region of the die is wetted with the polymer melt at low shear rates, creating higher shear flow, and hence higher entrance pressure drops/entrance viscosity. Due to this increase, it was decided not to apply the entry length correction (applying the correction factor to the entry flow methodology will have negligible/no effect on the measured extensional data). Since the same L/D was used for all PE resins, a difference in the entrance viscosity at a particular shear rate represents structural differences between the polymers, considering that all LLDPEs have similar molecular weight distributions. Once again the trend in viscosity is dominated by the effect of molecular weight, as shown in Figure B1. No strain hardening behaviour for LLDPE resins was observed as the resins have relatively low molecular weight, narrow MWD, and no long chain branches (see Table 4.1). A similar behaviour was perceived for HDPE 1 and 2, as they are both linear PE resins with no long chain branches and relatively low molecular weights. On the other hand, no conclusion could be made with respect to the strain hardening behaviour of HDPE 3. The plateau region of HDPE 3 was not attained even at the lowest achievable shear rate as a result of its highly broad molecular weight distribution (see Table 4.1).

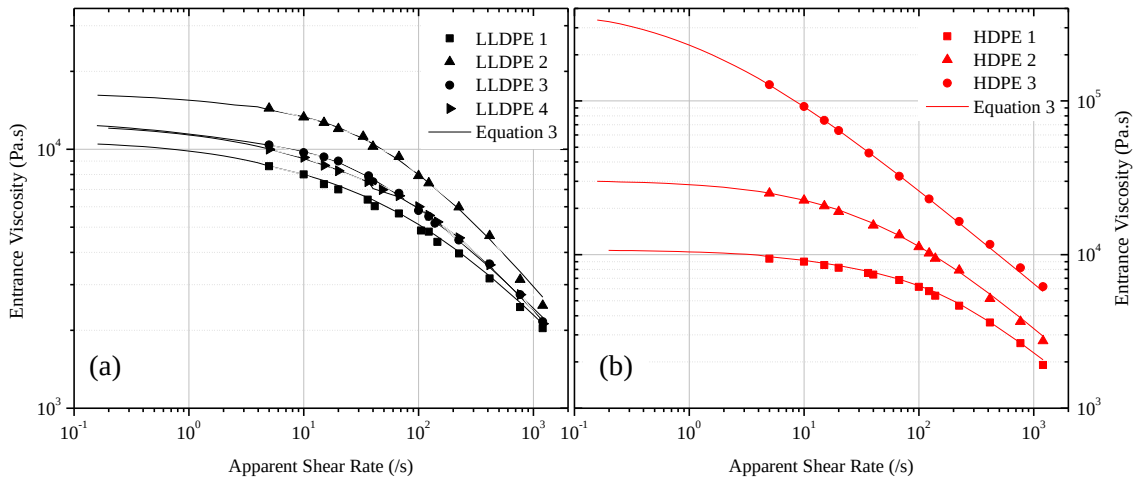

Figure B1: Entrance viscosity vs. apparent shear rate of (a) LLDPE and (b) HDPE resins at 150 ºC

The uniaxial extensional viscosities of the polymers were evaluated using entrance viscosity data along with the Cogswell, Binding and Gibson techniques. These results are shown in Figures B2 and B3. As expected, the measured extensional viscosities were higher due to the adherence of the extrudate to the downstream region of the orifice die at low shear rates. This behaviour increased the Trouton ratio of polymers as a result of higher recorded entrance pressure drops (80-100 % higher). The deviation in measured entrance pressure drops via an orifice die is common and has been reported to be high in extensional viscosity measurements of up to 100 % (6). To verify the deviation between the true and measured entrance pressure drops, a traditional Bagley correction approach was applied on LLDPE 1. Measurements were performed at 150 ºC using capillaries with L/D ratios of 6, 9, and 20. The estimated entrance pressure drops from the Bagley plot were significantly lower than those obtained from the zero length die (close to 60 % for lower shear rates). The Trouton ratio for LLDPE changed between 8-10 and 4-6 for HDPE 1-2. The Trouton ratio of HDPE 3 was not measurable as the Newtonian values of both shear and extensional viscosities were not achievable at the lowest possible shear rate. This outcome indicated the need to design

novel orifice dies to reduce the deviation caused by conventional orifice dies, as discussed in references (7-8). The observed trends in the extensional viscosities were similar to those recorded for entrance viscosities. No strain hardening was observed. LLDPE 2 showed the highest extensional properties due to its higher molecular weight. LLDPE 3-4 had very similar extensional properties reflecting similarities between their molecular structures. An analogous conclusion was made for HDPE 1-2, as extensional viscosity increased with molecular weight at lower extensional rates. Both Cogswell and Binding methodologies showed similar extensional properties for LLDPE resins at high and medium extensional rates (above 10), however, the Binding technique failed to distinguish the differences in molecular structures of the LLDPE resins at low shear rates (no difference between LLDPE 1, and LLDPE 3-4). The Gibson technique, on the other hand, was successful in distinguishing the structural differences at low and medium extensional rates. Finally, no significant differences between Binding and Cogswell techniques were found for HDPE resins, while the Gibson technique in general showed earlier thinning behaviour.

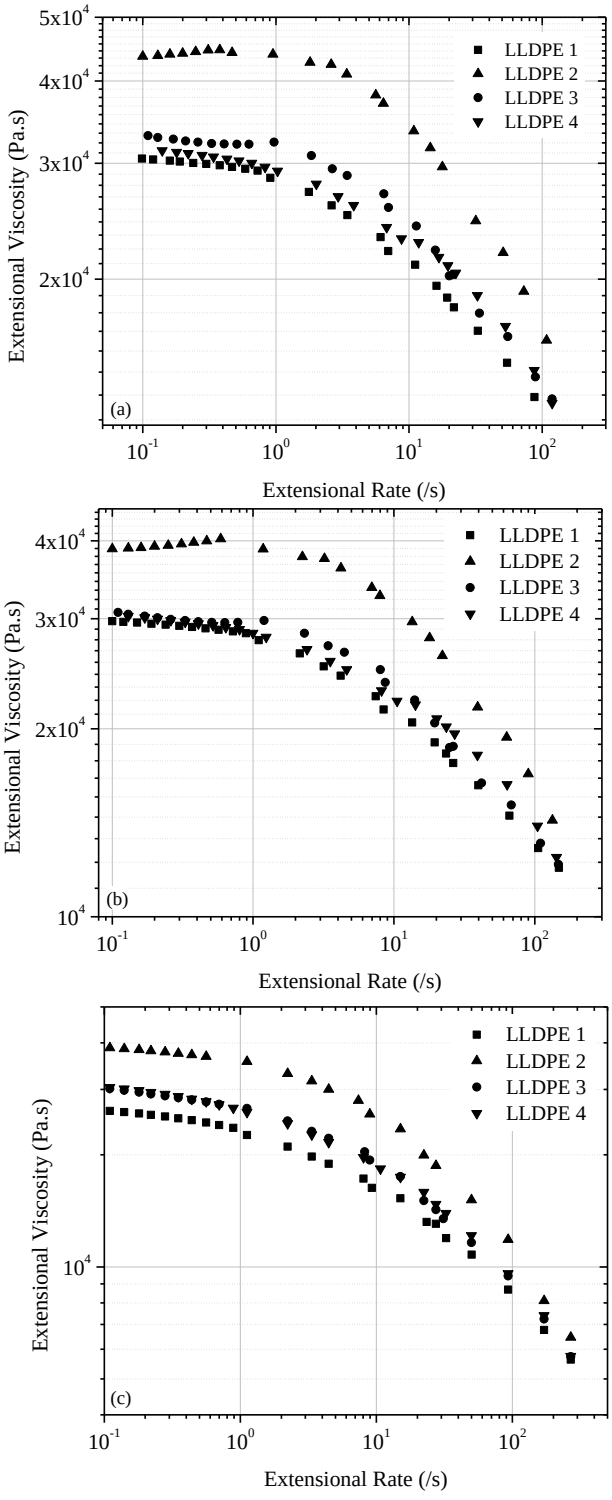

Figure B2: Extensional viscosity of LLDPE resins vs. extensional rate: (a) Cogswell, (b) Binding, and (c) Gibson methodologies

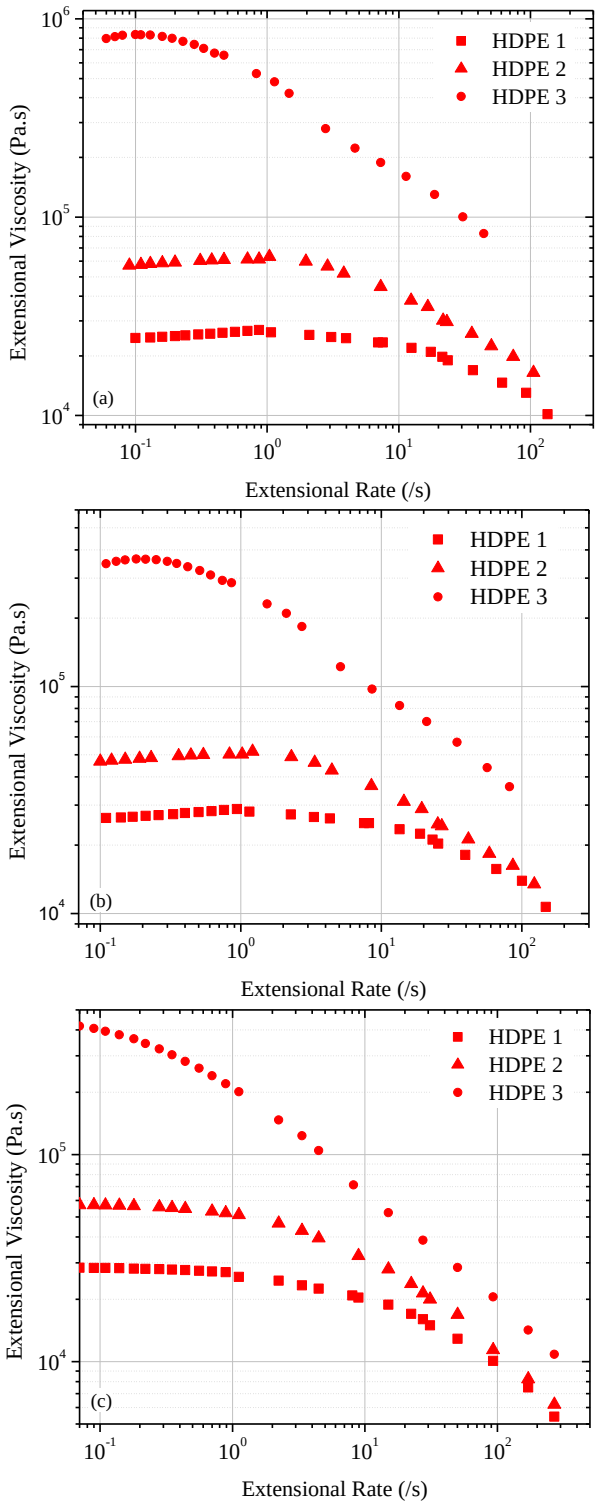

Figure B3: Extensional viscosity of HDPE resins vs. extensional rate: (a) Cogswell, (b) Binding, and (c) Gibson methodologies

References

(1) Zatloukal, M.; Vlcek, J.; Tzoganakis, C.; Sáha, P. J. (2002) Non Newtonian Fluid Mech, **107**, 13.

(2) Cogswell, F. N. (1972) Polym Eng Sci, **12**, 64.

(3) Cogswell, F. N. (1978) J Non-Newtonian Fluid Mech, **4**, 23.

(4) Bersted, B. H. (1993) Polym Eng Sci, **33**, 1079.

(5) Binding, D. M. (1988) J Non-Newtonian Fluid Mech, **27**, 173.

(6) Sunder, J.; Goettfert, A. (2001) Annu Tech Conf - Soc Plast Eng, 59th, 1036.

(7) Kim, S.; Dealy, J.M. (2001) J Rheol, **45**, 1413.

(8) Zatloukal, M.; Musil, J. (2009) Polym Test, **28**,843.

APPENDIX C: COGSWELL, BINDING, AND GIBSON METHODOLOGIES FOR OBTAINING EXTENSIONAL VISCOSITY

A brief description of Cogswell and Binding methodologies were given earlier in Chapter 2, section 2.4.1 of this thesis. In this section, more equations related to these methodologies, and equations for the Gibson model (1-2), reported by Zatloukal et al. (3), are provided.

C.1. Cogswell Model

Cogswell (1-2) developed models in terms of shear and extensional components for the estimation of extensional viscosity from shear flow. This analysis is based on the assumption that the flow is fully developed. The flow parameters are obtained by minimization of the local pressure gradient in the region. The following equations summarize the expressions, developed by Cogswell, for estimation of extensional viscosity. In these equations, P_o is the entrance pressure drop, obtained from the capillary rheometer, $\dot{\gamma}_{app}$ is the apparent applied shear rate, and η_{ENT} is the entrance pressure drop according to Equation C.1. In Equations C-2 to C-4, σ_E is the applied extensional stress, "n" is the power law index, $\dot{\varepsilon}$ is the extension rate, and τ is the corrected applied shear stress. Equations C-5 and C-6 also indicate relationships for evaluation of apparent shear rate $\dot{\gamma}_{app}$, and the power law index "n". In these equations, Q is the polymer flow rate in the capillary die, and R is the radius of the capillary die.

$$\eta_{ENT} = \frac{P_o}{\dot{\gamma}_{app}} \qquad \text{C-1}$$

$$\sigma_E = \frac{3}{8}(n+1)\ \eta_{ENT}\ \dot{\gamma}_{app} \quad \text{C-2}$$

$$\dot{\varepsilon} = \frac{4}{3(n+1)}\ \frac{\eta\ \dot{\gamma}_{app}}{\eta_{ENT}} \quad \text{C-3}$$

$$\eta = \frac{\tau}{\dot{\gamma}_{app}} \quad \text{C-4}$$

$$\dot{\gamma}_{app} = \frac{4Q}{\pi R^3} \quad \text{C-5}$$

$$n = \frac{d\ log(\eta)}{d\ log(\dot{\gamma}_{app})} - 1 \quad \text{C-6}$$

Eventually, the extensional viscosity is obtained by dividing Equation C-2 by Equation C-3 as shown below:

$$\eta_{ext} = \frac{\sigma_E}{\dot{\varepsilon}} \quad \text{C-7}$$

C.2. Binding Model

Binding (4) used an energy minimization technique to minimize the viscous energy dissipation within the flow field. The following equations were developed for the measurements of extensional rate and extensional stress, respectively.

$$\dot{\varepsilon} = \frac{(3n+1)(1+k^2)}{3k^2(1+n)^2}\ \frac{\eta\ \dot{\gamma}_{app}}{\eta_{ENT}}\ \left(\frac{3n+1}{4n}\right)^n \quad \text{C-8}$$

$$\sigma_e = \frac{2^{k-1}\, 3k\, (1+n^2)}{(3n+1)(1+k)^2}\, \frac{\eta_{ENT}\, \dot{\gamma}_{app}}{I_{nk}} \qquad \text{C-9}$$

I_{nk} and k are defined according to Equations C-10 and C-11.

$$I_{nk} = \frac{n\, ((1+n)/n)^{k+1}}{2n + (1+n)(k+1)} \qquad \text{C-10}$$

$$k = \frac{t}{1+n-t} \qquad \text{C-11}$$

In the above equations, t is defined according to Equation C-12.

$$t = \frac{dlog\, (\eta_{ENT})}{dlog(\dot{\gamma}_{app})} - 1 \qquad \text{C-12}$$

C.3. Gibson Model

In order to explain entrance pressure drop in convergence flows, Gibson (5) applied a sink flow kinematics with no vortices. Gibson assumed that the main source of the entrance pressure drop is the extensional flow. The following equations were developed according to the Gibson model for the estimation of extensional viscosity.

$$\dot{\varepsilon} = \frac{1}{4}\, \dot{\gamma}_{app} \sin(\alpha)\, (1+\cos(\alpha)) \qquad \text{C-13}$$

$$\sigma_E = \frac{\bar{\eta}_{ENT}\, \dot{\gamma}_{app}}{\frac{2}{3k'}\left[1 - \left(\frac{R}{R_b}\right)^{3k'}\right] + \left(\frac{I(k,\alpha)}{[\sin(\alpha)\, (1+\cos(\alpha))]^n}\right)} \qquad \text{C-14}$$

In Equation C-14, $\bar{\eta}_{ENT}$ and k' are defined according to Equations C-15 and C-16.

$$\bar{\eta}_{ENT} = \eta_{ENT} - \frac{2\eta(\sin(\alpha))^{3n}\left[1-\left(\frac{R}{R_b}\right)^{3n}\right]}{3n\left(\frac{\pi}{2}\right)^{3n+1}}\left(\frac{3n+1}{4n}\right)^{n} \quad \text{C-15}$$

$$k' = \frac{dlog\,(\bar{\eta}_{ENT})}{dlog(\dot{\gamma}_{app})} - 1 \quad \text{C-16}$$

References

(1) Cogswell, F.N. (1972) Polym. Eng. Sci., **12**,64-73.

(2) Cogswell, F.N. (1978) J. Non-Newtonian Fluid Mech., **4**, 23-38.

(3) Zatloukal, M., Vlcek, J., Tzoganakis, C., Sáha, P. (2002) J. Non Newtonian Fluid Mech. **107**, 13-37.

(4) Binding, D.M. (1988) J. Non-Newtonian Fluid Mech., **27**, 173-89.

(5) Gibson, A.G. (1989) Composites, **20**, 57.